ECMWF COPERNICUS REPORT

Copernicus Atmosphere Monitoring Service

Validation report of the CAMS near-real time global atmospheric composition service

March - May 2018

Issued by: KNMI

Date: 3 October 2018

Ref: CAMS84_2015SC3_D84.1.1.12_2018MAM_v1

IMPLEMENTED BY ECMWF

Validation report of the CAMS near-real-time global atmospheric composition service. Period March - May 2018

EDITORS:
H.J. Eskes (KNMI), A. Wagner (MPG), M. Schulz (MetNo),
Y. Christophe (BIRA-IASB), M. Ramonet (LSCE)

AUTHORS:
S. Basart (BSC), A. Benedictow (MetNo), Y. Bennouna (CNRS-LA),
A.-M. Blechschmidt (IUP-UB), S. Chabrillat (BIRA-IASB), H. Clark (CNRS-LA),
E. Cuevas (AEMET), H. Flentje (DWD), K. M. Hansen (AU), U. Im (AU),
J. Kapsomenakis (AA), B. Langerock (BIRA-IASB), K. Petersen (MPG),
A. Richter (IUP-UB), N. Sudarchikova (MPG), V. Thouret (CNRS-LA),
T. Warneke (UBC), C. Zerefos (AA)

REPORT OF THE COPERNICUS ATMOSPHERE MONITORING SERVICE, VALIDATION SUBPROJECT.

AVAILABLE AT:
http://atmosphere.copernicus.eu/quarterly_validation_reports

CITATION:
H.J. Eskes, A. Wagner, M. Schulz, Y. Christophe, M. Ramonet, S. Basart, A. Benedictow, Y. Bennouna, A.-M. Blechschmidt, S. Chabrillat, H. Clark, E. Cuevas, H. Flentje, K.M. Hansen, U. Im, J. Kapsomenakis, B. Langerock, K. Petersen, A. Richter, N. Sudarchikova, V. Thouret, T. Warneke, C. Zerefos,
Validation report of the CAMS near-real-time global atmospheric composition service: Period March - May 2018,
Copernicus Atmosphere Monitoring Service (CAMS) report,
CAMS84_2015SC3_D84.1.1.12_2018MAM_v1.pdf, October 2018.

STATUS:
Version 1, Final

DATE:
03/10/2018

Executive Summary

The Copernicus Atmosphere Monitoring Service (http://atmosphere.copernicus.eu, CAMS) is a component of the European Earth Observation programme Copernicus. The CAMS global near-real time (NRT) service provides daily analyses and forecasts of reactive trace gases, greenhouse gases and aerosol concentrations. This document presents the validation statistics and system evolution of the CAMS NRT service for the period up to 1 June 2018. Updates of this document appear every 3 months.

This summary is split according to service themes as introduced on the CAMS website: air quality & atmospheric composition, climate forcing, ozone layer and UV. Specific attention is given to the ability of the CAMS system to capture recent events. We focus on the 'o-suite' composition fields, which are the daily analyses and forecasts produced by the IFS (Integrated Forecast System) modelling system at ECMWF, using the available meteorological and atmospheric composition observations which are ingested in the ECMWF 4D-Var assimilation system. The model and assimilation configuration is summarised in section 2. We furthermore assess the impact of the composition observations by comparing the validation results from the 'o-suite' to a 'control' configuration without assimilation. Also, the pre-operational high-resolution forecasts of CO_2 and CH_4 are assessed in this report.

The o-suite data delivery for the period March - May 2018 (MAM 2018) was good, with an availability of 98.9% at 10 and 22 utc (two forecasts per day).

Air quality and atmospheric composition

Tropospheric ozone (O_3)

CAMS o-suite ozone is validated with surface and free tropospheric ozone observations from the GAW and ESRL networks, IAGOS airborne data and ozone sondes. For free tropospheric ozone against ozone sondes the o-suite modified normalized mean biases (MNMBs) are on average small, ±10% over the Northern Hemisphere (NH), between ±20% for stations in the Tropics, and between ±15% for the Arctic (Fig. S.1). Over Antarctica o-suite biases are observed between 0% and +20%, whereas the control run shows negative biases. For MAM 2018 good agreement is found over the NH mid latitudes in the free troposphere, which is confirmed with IAGOS evaluations over Paris and Frankfurt. In the UTLS region, the control runs shows often a better correspondence with the observations than the o-suite. Surface ozone compares well with IAGOS over Europe. Good agreements with the IAGOS free troposphere ozone profiles is also found over Western Africa and North America, the Pacific ocean and Asia, with sometimes large differences in the UTLS region (e.g. Los Angeles).

In comparison with surface observations we find a steady improvement of the o-suite over the past 5 years over European GAW stations. Biases are generally around ±10%, and within ±20% (the Arctic is discussed below). For Antarctica negative biases are observed for the control run, which is efficiently corrected by the assimilation in the o-suite.

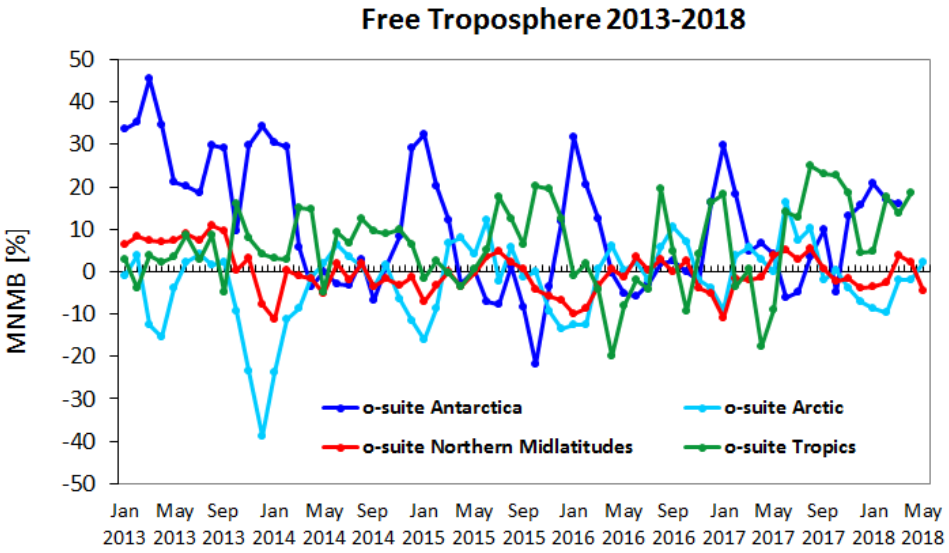

Figure S.1: Time series of MNMB of ozone in the o-suite, compared against ozone sondes, averaged over different latitude bands. The free troposphere is defined here as the layer between 750 and 300 hPa.

Tropospheric Nitrogen dioxide (NO_2)

Model validation, with respect to SCIAMACHY/Envisat NO_2 data before April 2012 and GOME-2/MetOp-A NO_2 data afterwards, shows that tropospheric NO_2 columns are well reproduced by the NRT model runs, indicating that emission patterns and NO_x photochemistry are generally well represented, although modelled shipping signals are more pronounced than in the satellite retrievals. Tropospheric NO_2 columns over some local emission hotspots (e.g. Moscow, and Red Basin in China) are overestimated, while wintertime and springtime values over Europe are underestimated. Since December 2014, the agreement between satellite retrievals and model results for time series over East-Asia and Europe is better than for previous years (Fig. S.2), as observed columns of NO_2 decreased recently, likely associated with reduced emissions, and (in contrast to the observations) simulated values show an increase over the whole timeseries available. Spring and summertime values over East-Asia are overestimated by the o-suite since 2015, a feature which did not occur for previous years. Mainly in summer and autumn the models regularly show an overestimation over several regions with fire activity (Canada, Siberia, and Nepal).

The CAMS results were compared with UVVIS DOAS observations at four sites in Europe and one site in China (Xianghe). On average a reasonable comparison was found. Differences between the o-suite analysis and forecast is sometimes substantial: at Bremen the assimilation substantially increases the concentration, leading to a positive bias. At Athens a strong negative bias is observed. It should be noted that the local variability in NO_2 may cause substantial uncertainties in these comparisons.

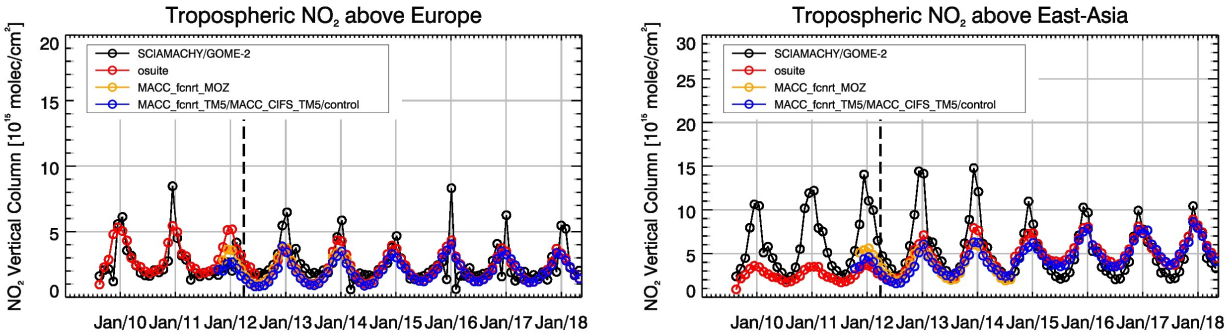

Figure S.2: Time series of tropospheric NO_2 columns from SCIAMACHY (up to March 2012), GOME-2 (from April 2012 onwards) compared to model results for Europe and East-Asia. The o-suite is in red, control is in blue (the model run without data assimilation is termed control since Sep 2014).

Tropospheric Carbon Monoxide (CO)

Model validation with respect to GAW network surface observations, IAGOS airborne data, FTIR observations (NDACC and TCCON) and MOPITT / IASI satellite retrievals reveals that the absolute values, latitude dependence and seasonality, as well as day-to-day variability of CO can be reproduced well by the CAMS-global analyses and forecasts. Biases are between -3% and -16% for European stations, and between 0 and -10% in Asia. A similar bias in Europe in the lower layers is observed by IAGOS. For stations in the southern hemisphere the comparison with NDACC and GAW measurements shows that data assimilation reduces the large positive MNMBs in the control run.

In the free troposphere the bias is close to 0, while a small positive bias of about 10% is found in the UTLS. A pronounced pollution event over Paris on 19 March is not fully captured by the CAMS-global forecasts. Other pollution episodes over North America and Asia are sometimes captured, and sometimes missed, depending on the location. Complex vertical variability observed over airports in Africa is generally captured by the o-suite, although absolute values may sometimes differ. Comparisons with NDACC-FTIR observations and with MOPITT and IASI satellite observations generally confirm the very small biases within 5% in the free troposphere, and the accurate description of seasonal and day-to-day variability. In contrast, the control run shows a pronounced positive bias in the tropics and southern hemisphere, demonstrating the positive impact of the assimilation. Prominent positive biases are only observed over East Asia and the Syberian fire region.

Formaldehyde

Model validation, with respect to SCIAMACHY/Envisat HCHO data before April 2012 and GOME-2/MetOp-A HCHO data afterwards, shows that modelled monthly HCHO columns represent well the magnitude of oceanic and continental background values and the overall spatial distribution in comparison with mean satellite HCHO columns. Compared to GOME-2 satellite retrievals, an overestimation of values regularly occurs over Australia and Central Africa, which could be both related to biogenic emissions or fire emissions. For time series over East-Asia and the Eastern US, both regions where HCHO columns are probably dominated by biogenic emissions, models and retrievals agree rather well. However, the yearly cycle over East-Asia is underestimated by the models. The CAMS results were also compared with UV-VIS DOAS observations at two sites in Europe and one site in China (Xianghe). On average an underestimation is observed. Analysis, forecast and control give the same results.

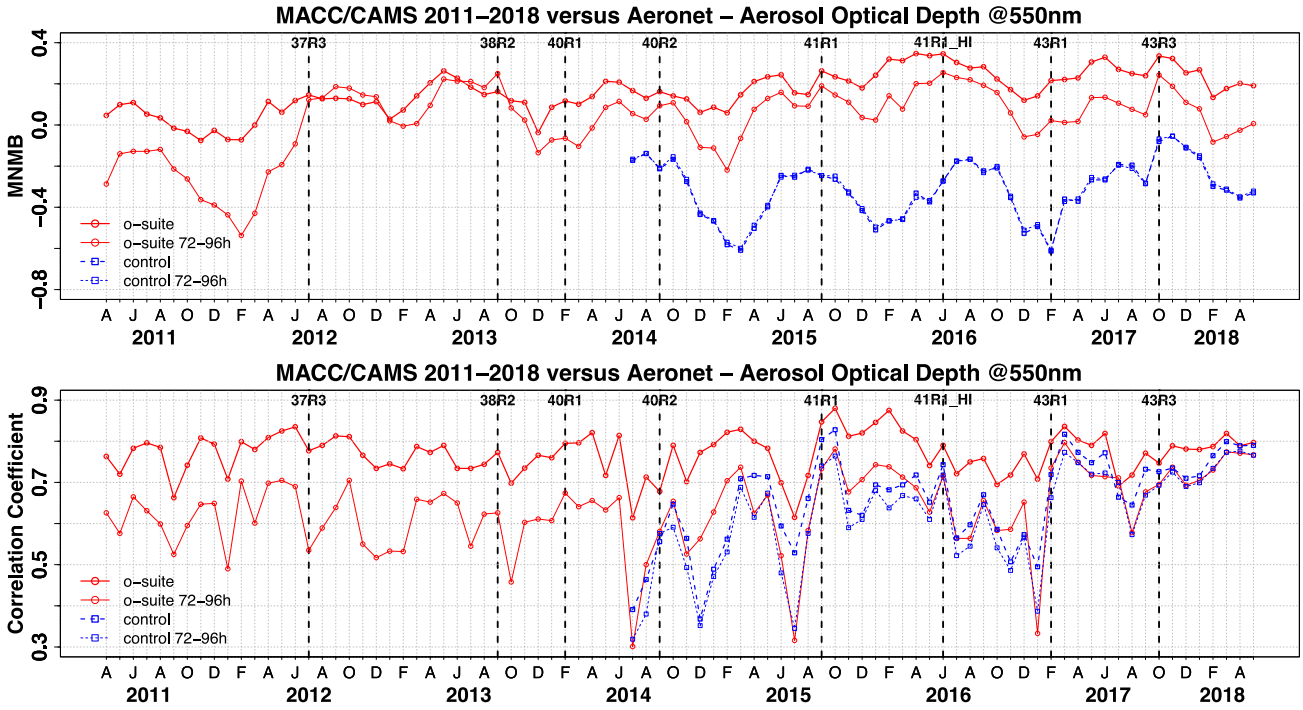

Figure S.3. Aerosol optical depth at 550nm in IFS 00Z model simulations for April 2011 – May 2018 against daily matching Aeronet Version3 level 1.5 data. a) Modified normalized mean bias (MNMB); o-suite (thick red curve); o-suite at last forecast day (light red curve); Control (blue dashed); Control at last forecast day (light blue dashed); b) Corresponding correlation coefficient. Model version changes are marked as vertical bars.

Aerosol

We estimate that the o-suite aerosol optical depth showed an average positive bias in the latest three months of +19%, measured as modified normalized mean bias against daily Aeronet (V3 level 1.5) sun photometer data. The +3 day forecasted aerosol distribution shows 18% less aerosol optical depth (AOD) than that from the initial forecast day, as shown in Figure S.3-a. The spatio-temporal correlation, shown in figure S.3-b, shows small month-to-month variation in MAM 2018 about 0.8, indicating the simulation reproduces approximately 60% of the day to day AOD variability across all Aeronet stations. We find a high AOD bias in Southern and Northern Latitudes. The o-suite forecast at +3 days shows slightly lower correlation, as a consequence of imperfect forecasted meteorology and fading impact of the initial assimilation of MODIS AOD and MODIS fire info on model performance. However, the forecast and also control experiment have improved clearly since February 2017. The second o-suite running each day at 12UTC shows almost identical performance as the o-suite starting at 00UTC.

The AOD performance of the o-suite with respect to the AERONET data exhibits no pronounced seasonal cycle since 2014. Since October 2017, global AOD is dominated by organics and sea salt.

The aerosol Ångström exponent contains information about the size distribution of the aerosol, and implicitly composition. The o-suite continues to show a positive global bias against Aeronet (V3 Level 1.5) data of +10%, indicating too fine particles in the model.

PM10 data are evaluated as defined by the IFS aerosol model. An evaluation of these PM10 surface concentrations against an average from data in the period 2000-2009 at 160 background sites in North America and Europe indicate that PM10 concentrations exhibit on average in the latest period an underestimation with MNMB bias of -10% in Europe and an overestimation of + 30% in North America. The fraction of data within factor 2 of observed values has increased compared to earlier years.

For March to May, the CAMS system reproduces the main areas of dust activity that are found over the Sahara (in the Bodelé Basin and the Mali/Mauritania border as well as in Algeria, Tunisia and Libya) and the Arabian Peninsula. The DOD observations, over Tunisia and Libya are overestimated. Higher DOD values predicted by the CAMS model are linked to an increase of the magnitude of the predicted gusts winds that consequently causes an enhancement of the dust emissions over desert dust source regions. During spring, the o-suite reproduces the daily variability of AERONET observations with a correlation coefficient of 0.81 on average for all the AERONET sites. In comparison the control run shows a correlation coefficient of 0.78. These results are comparable but slightly lower than those obtained by the SDS-WAS multi-model ensemble (0.84). Regarding mean bias (MB), both CAMS o-suite and control, as well as the SDS-WAS multi-model underestimates the AERONET observations resulting in an MB of -0.04. Otherwise, the comparison of 48h and 72h forecasts for both CAMS experiments shows that the prediction is stable during the 3-days forecasts with correlation coefficients of 0.81 (0.78), 0.80 (0.77) and 0.77 (0.75) respectively to 24, 48 and 72h forecasts for all the sites for o-suite (control).

Backscatter coefficients are low-biased in the planetary boundary layer (PBL). Possible reasons are missing of ammonia and nitrate in the model (foreseen to be activated soon), assumption of too high particle densities (too compact materials) in the mass to backscatter conversion, and the lack of a vertical transport barrier at the top of the PBL, causing dilution with free troposphere air. Free troposphere (FT) background backscatter coefficients are biased high, probably due to wrong re-distribution between PBL and FT. This is not fixed by the assimilation, which instead adds aerosol to the whole profile. The backscatter bias on a specific level thus depends on its relative position w.r.t. to the boundary layer height (BLH). The model BLH agrees reasonably (within a few 100 m) with observations under favourable measurement conditions. Very often, however, meteorological conditions prevent formation, unambiguousness or detectability of the BLH or make the latter a challenge.

System performance in the Arctic

The CAMS model runs are validated using surface ozone measurements from the ESRL-GMD and the IASOA networks (7 sites) and ozone concentrations in the free troposphere and the stratosphere are evaluated using balloon sonde measurement data.

Both runs strongly overestimates surface ozone values at most of the Arctic stations with relative biases up to +60% to +80% in March - May. This large positive model offset is related to the chemistry scheme in the CAMS global system, which does not contain the halogen reactions to capture the ozone depletion events (ODE) that occur in spring. An exception from this pattern is the results from Svalbard, where due to the position of the station on a mountaintop ODE are only rarely recorded, and Summit, at the enter of the Greenland ice sheet, where ODE does not occur. In other seasons, the CAMS ozone simulations are generally in good agreement with the observations.

Ozone concentrations in the free troposphere are in excellent agreement with observations with very low relative bias, whereas the control run underestimate concentrations up to -20%. In the stratosphere, the o-suite has a low positive bias of 3-9% for the Arctic sites, whereas the bias for the control run is 8-15%.

Comparison with FTIR observations from the NDACC network shows that the CO tropospheric columns are underestimated at the arctic sites with up to 10%, while the assimilation has a positive effect on the correlation coefficient. Comparison MOPITT versions 7 shows that modeled CO total columns are in good agreement with the satellite retrievals with low bias in the Arctic (±10%).

System performance in the Mediterranean

The model is compared to surface O_3 observations from the AirBase network. Our analysis shows that model MNMBs vary between -20% and 20% depending on the station. Temporal correlation coefficients between simulated and observed surface ozone for both the o-suite and control runs are highly significant over the entire Mediterranean from Gibraltar to Cyprus.

The CAMS o-suite reproduces the daily variability of AERONET observations, with correlation coefficients of 0.73 to 0.74, 0.79 and 0.75, respectively for Western, Central and Eastern Mediterranean. The o-suite tends to overestimated the observed AOD values by AERONET sites with a mean bias of 0.03, 0.06 and 0.04, respectively for Western, Central and Eastern Mediterranean. Higher overestimations are observed in Central Mediterranean and are linked to desert dust intrusions. At surface levels, PM10 and PM2.5 overestimations are observed in comparison with the EIONET sites, leading to an overprediction of the number of exceedances of the EU PM10 daily threshold (50 µg/m^3).

Climate forcing

Greenhouse gases

Pre-operational high-resolution forecasts of CO_2 and CH_4 have been compared to ICOS surface (20 sites) and TCCON total column (3 sites) measurements, for a one year period from January 2017 to March 2018. Most of the stations are located in Europe (14 surface and 2 TCCON sites) providing a better representativeness over this continent. The third TCCON station is located in the tropical Indian ocean, at La Réunion Island, where two surface stations are also monitoring CO_2 and CH_4 at the surface, one being installed at sea level, the other on a mountain site 2195 m asl. However the total column measurements from La Réunion are missing due to a problem with the instrument.

Several CAMS configurations exist which have been compared. This includes the cyclic (model-only) high-resolution forecasts run ghqy at 16km, the new high resolution forecast gqpe at 9km with initial conditions nudged from the GHG analysis (available from 1 January 2017 to present) and gxk8 (new test for high resolution cyclic forecast with CO_2 bug fix implemented available from 1 January to 25 March 2018), and the GHG analysis gqiq (available from 1 January 2017 to present). Apart from this also the o-suite models methane.

Both surface and total column observations show two main issues:

- an overestimation of the CO_2 seasonal cycle in North Hemisphere by about ±1%.

- a significant reduction of the bias of the new high resolution forecast experiment (gqpe).

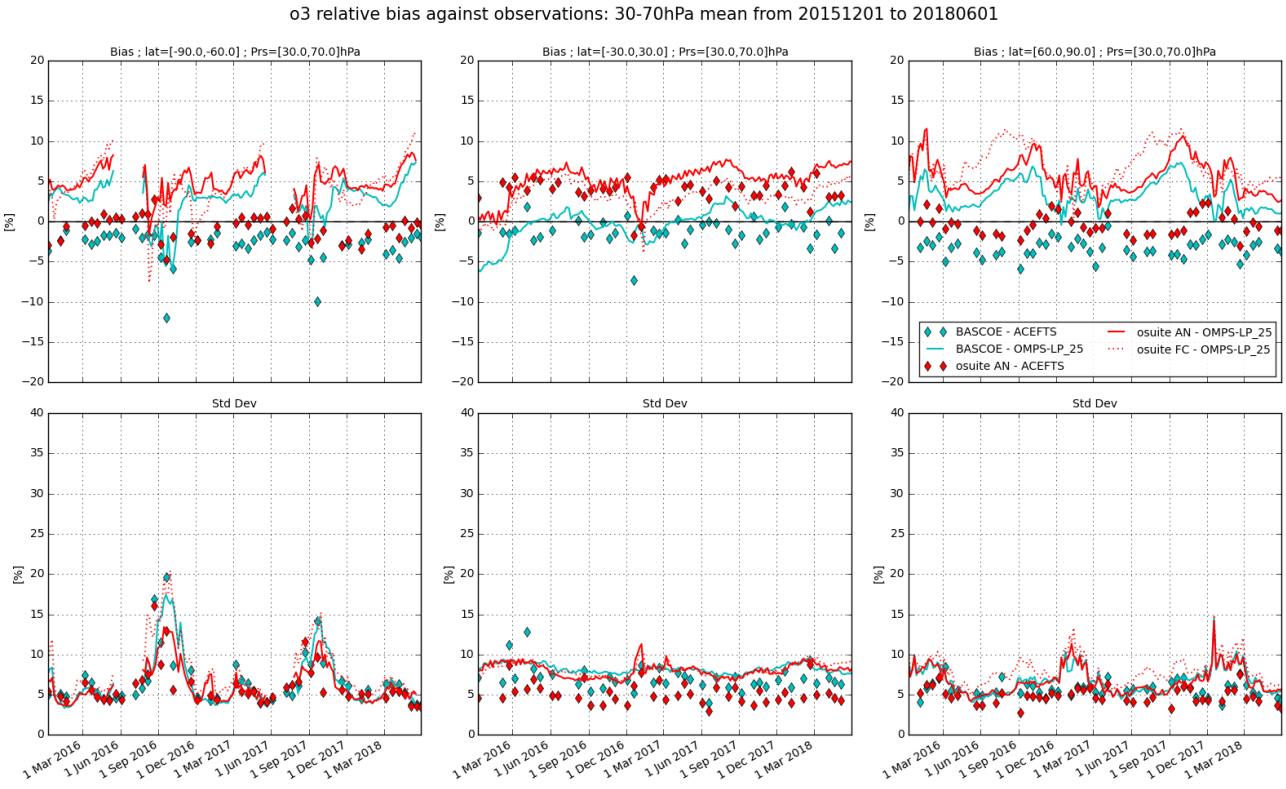

Figure S.4: Time series comparing models to observations for the period 2015-12-01 to 2018-06-01 in the middle stratosphere (30-70hPa averages): o-suite analyses vs OMPS-LP (red, solid), o-suite forecasts 4th day vs OMPS-LP (red, dotted), o-suite analyses vs ACE-FTS (red markers), BASCOE vs OMPS-LP (cyan, solid) and BASCOE vs ACE-FTS (cyan markers). Top row, normalized mean bias (model-obs)/obs (%); bottom row, standard deviation of relative differences (%).

The comparison of the high resolution forecast experiment gxk8 with gqpe shows a decrease of the wintertime CO_2 values in North Hemisphere which should contribute to improve the simulation of the seasonal cycle.

Ozone layer and UV

Ozone partial columns and vertical profiles

Ozone columns and profiles have been compared with the following observations: vertical profiles from balloon-borne ozonesondes; ground-based remote-sensing observations from the NDACC (Network for the Detection of Atmospheric Composition Change, http://www.ndacc.org); and satellite observations by two instrument (OMPS-LP, ACE-FTS). Furthermore, the o-suite analyses are compared with those delivered by the independent assimilation system BASCOE.

Compared to ozone sondes the model O_3 partial pressures are slightly overestimated in all latitude bands (MNMB between 4 and +12%) except above the Antarctic.

Comparisons with the NDACC network include 17 stations for UVVIS and FTIR stratospheric columns, microwave profiles for Ny Alesund (78.9°N) and Bern (47°N) and LIDAR profiles at

Hohenpeissenberg (47.8°N) and Observatoire Haute Provence (OHP), France (43°N). The comparison with the UVVIS stations are generally in agreement with the o-suite, while it indicates a latitudinal dependence of the biases for the control run. The result from MWR and LIDAR comparisons for the current period are in line with those of previous reports.

The comparison with independent satellite observations (Fig. S.4) is generally in good agreement for the considered period: for ACE-FTS, the NMB is mainly within 10% between 5km and 40km, and mostly within 5% between 15km and 35km except in the tropics. OMPS-LP has less regular profiles, but the NMB still remain within 15% for most parts of the 15-45 km range.

Other stratospheric trace gases

Due to the lack of stratospheric chemistry in the C-IFS-CB05 scheme, the only useful product in the stratosphere is ozone. Other species, like NO_2, have also been evaluated but the results are only indicative.

Events

Dust over the Arabian and Iberian Peninsulas: late April 2018. A dense wall of dust pushed across the Arabian Peninsula in late April 2018. The intensified north-westerly wind caused dust to rise from the Iraq Desert area and move in a south-easterly direction affecting Iraq, Kuwait, Bahrain, Qatar, Kingdom of Saudi Arabia, United Arab Emirates (UAE), and to reach Yemen the next days achieving AOD up to 7.3 and reducing drastically the visibility less than 300 m in sites in the Persian Gulf. During the same period, it is observed some hot spots of dust in Libya (on 22-23 April) and Algeria (on 25th April). These events affected the Iberian Peninsula leading to one week of high AOD (up to 1.2) and PM10/PM2.5 (up to 60 µg/m3). CAMS o-suite can timely reproduce the spatial distribution of the dust plume over the Arabian and Iberian Peninsulas in comparison with the observations despite an underestimate of the observed maximum values during the whole event.

Large number of fire events in the area of Indochina during April. IASI shows increase of CO emissions over East Asia on 11.04 with following outspread and transport of the high concentration plume to the east on 14 and 15.04. CAMS captured the locations of the emission plumes and transportation pathway. Emissions over some source regions were overestimated, e.g. over India. CO values over the Pacific ocean were underestimated along the transportation pathway.

Northern hemisphere fires: Biases in CO in the control run over the Alaska fire region are well corrected by the data assimilation in the o-suite. Most of the fire related peaks in Syberia were well described during May, apart from a large CO peak in Eastern Syberia on 12 May in the o-suite and control run which was not observed (or only partially observed) by IASI.

Table of Contents

1. Introduction

The Copernicus Atmosphere Monitoring Service (CAMS, http://atmosphere.copernicus.eu/) is a component of the European Earth Observation programme Copernicus. The CAMS global near-real time (NRT) service provides daily analyses and forecasts of trace gas and aerosol concentrations. The CAMS near-real time services consist of daily analysis and forecasts with the ECMWF IFS system with data assimilation of trace gas concentrations and aerosol properties. This document presents the system evolution and the validation statistics of the CAMS NRT global atmospheric composition analyses and forecasts. The validation methodology and measurement datasets are discussed in Eskes et al. (2015).

In this report the performance of the system is assessed in two ways: both the longer-term mean performance (seasonality) as well as its ability to capture recent events are documented. Table 1.1 provides an overview of the trace gas species and aerosol aspects discussed in this CAMS near-real time validation report. This document is updated every 3 months to report the recent status of the near-real time service. The report covers results for a period of at least one year to document the seasonality of the biases. Sometimes reference is made to other model versions or the reanalysis to highlight aspects of the near-real time products.

This validation report is accompanied by the "Observations characterization and validation methods" report, Douros et al. (2017), which describes the observations used in the comparisons, and the validation methodology. This report can also be found on the global validation page, http://atmosphere.copernicus.eu/user-support/validation/verification-global-services.

Key CAMS NRT products and their users are: Boundary conditions for regional air quality models (e.g. AQMEII, air quality models not participating in CAMS); Long range transport of air pollution (e.g. LRTAP); Stratospheric ozone column and UV (e.g. WMO, DWD); 3D ozone fields (e.g. SPARC). As outlined in the MACC-II Atmospheric Service Validation Protocol (2013) and MACC O-INT document (2011), relevant user requirements are quick looks of validation scores, and quality flags and uncertainty information along with the actual data. This is further stimulated by QA4EO (Quality Assurance Framework for Earth Observation, http://www.qa4eo.org) who write that “all earth observation data and derived products is associated with it a documented and fully traceable quality indicator (QI)”. It is our long-term aim to provide such background information. The user is seen as the driver for any specific quality requirements and should assess if any supplied information, as characterised by its associated QI, are "fit for purpose" (QA4EO task team, 2010).

CAMS data are made available to users as data products (grib or netcdf files) and graphical products from ECMWF, accessible through the catalogue on http://atmosphere.copernicus.eu/.

A summary of the system and its recent changes is given in section 2. Subsequent sections gives an overview of the performance of the system for various species, and during recent events. Routine validation results can be found online via regularly updated verification pages, http://atmosphere.copernicus.eu/user-support/validation/verification-global-services. Table 1.2 lists all specific validation websites that can also be found through this link.

Table 1.1: Overview of the trace gas species and aerosol aspects discussed in this CAMS near-real time validation report. Shown are the datasets assimilated in the CAMS analysis (second column) and the datasets used for validation, as shown in this report (third column). Green colors indicate that substantial data is available to either constrain the species in the analysis, or substantial data is available to assess the quality of the analysis. Yellow boxes indicate that measurements are available, but that the impact on the analysis is not very strong or indirect (second column), or that only certain aspects are validated (third column).

Species, vertical range	Assimilation	Validation
Aerosol, optical properties	MODIS Aqua/Terra AOD PMAp AOD	AOD, Ångström: AERONET, GAW, Skynet, MISR, OMI, lidar, ceilometer
Aerosol mass (PM10, PM2.5)	MODIS Aqua/Terra	European AirBase stations
O_3, stratosphere	MLS, GOME-2A, GOME-2B, OMI, SBUV-2, OMPS	Sonde, lidar, MWR, FTIR, OMPS, ACE-FTS, OSIRIS, BASCOE and MSR analyses
O_3, UT/LS	MLS	IAGOS, ozone sonde
O_3, free troposphere	Indirectly constrained by limb and nadir sounders	IAGOS, ozone sonde
O_3, PBL / surface		Surface ozone: WMO/GAW, NOAA/ESRL-GMD, AIRBASE
CO, UT/LS	IASI, MOPITT	IAGOS
CO, free troposphere	IASI, MOPITT	IAGOS, MOPITT, IASI, TCCON
CO, PBL / surface	IASI, MOPITT	Surface CO: WMO/GAW, NOAA/ESRL
NO_2, troposphere	OMI, partially constrained due to short lifetime	SCIAMACHY, GOME-2, MAX-DOAS
HCHO		GOME-2, MAX-DOAS
SO_2	GOME-2A, GOME-2B (Volcanic eruptions)	
Stratosphere, other than O_3		NO_2 column only: SCIAMACHY, GOME-2
CO_2, surface, PBL		ICOS
CO_2, column	GOSAT	TCCON
CH_4, surface, PBL		ICOS
CH_4, column	GOSAT, IASI	TCCON

Table 1.2: Overview of quick-look validation websites of the CAMS system.

Reactive gases – Troposphere
GAW surface ozone and carbon monoxide: http://macc.copernicus-atmosphere.eu/d/services/gac/verif/grg/gaw/gaw_station_ts!CIFS/TM5 AN IAGOS tropospheric ozone and carbon monoxide: http://www.iagos.fr/cams/ Surface ozone from EMEP (Europe) and NOAA-ESRL (USA): http://www.academyofathens.gr/cams Tropospheric nitrogen dioxide and formaldehyde columns against satellite retrievals: http://www.doas-bremen.de/macc/macc_veri_iup_home.html Tropospheric CO columns against satellite retrievals: http://cams.mpimet.mpg.de
Reactive gases - Stratosphere
Stratospheric composition: http://www.copernicus-stratosphere.eu NDACC evaluation in stratosphere and troposphere (the NORS server) http://nors-server.aeronomie.be
Aerosol
Evaluation against Aeronet stations: http://aerocom.met.no/cams-aerocom-evaluation/ More in-depth evaluations from the Aerocom website: http://aerocom.met.no/cgi-bin/aerocom/surfobs_annualrs.pl?PROJECT=CAMS&MODELLIST=CAMS-VALreports&FULL=explicit&INFO=nohover&PERFORMANCE=ind&YEARFILTER=ALLYEARS&PSFILTER=ALLVARS&Type0=SCATTERLOG&Ref0=AERONETSunNRT&Run0=ECMWF_OSUITE&Parameter0=OD550_AER&St WMO Sand and Dust Storm Warning Advisory and Assessment System (SDS-WAS) model intercomparison and evaluation: http://sds-was.aemet.es/forecast-products/models
Satellite data monitoring
Monitoring of satellite data usage in the Reanalysis and Near-Real-Time production: http://copernicus-atmosphere.eu/d/services/gac/monitor/

Naming and color-coding conventions in this report follow the scheme as given in Table 1.3.

Table 1.3. Naming and color conventions as adopted in this report.

Name in figs	**experiment**	**Color**
{obs name}	{obs}	black
o-suite D+0 FC	0001	red
Control	gsyg	blue
High-resolution greenhouse gas	ghqy	orange

2. System summary and model background information

The specifics of the different CAMS model versions are given below (section 2.1) including an overview of model changes. Other systems used in CAMS are listed in section 2.2. An overview of products derived from this system is given in section 2.3. Timeliness and availability of the CAMS products is given in section 2.4.

2.1 System based on the ECMWF IFS model

Key model information is given on the CAMS data-assimilation and forecast run o-suite and its control experiment, used to assess the performance of the assimilation. The forecast products are listed in Table 2.1. Table 2.2 provides information on the satellite data used in the o-suite. Further details on the different model runs and their data usage can be found at http://atmosphere.copernicus.eu/documentation-global-systems.
Information on older MACC experiment types, including MACC_fcnrt_MOZ and MACC_CIFS_TM5 can be found in older Validation reports available from http://www.gmes-atmosphere.eu/services/aqac/global_verification/validation_reports/.

Table 2.1: Overview of model runs assessed in this validation report.

Forecast system	**Exp. ID**	**Brief description**	**Upgrades (e-suite ID)**
o-suite	0001	Operational CAMS DA/FC run	20180626-present 20170926-20180625 20170124-20170926 20160621-20170124 20150903-20160620 20140918-20150902
Control	gzhy gsyg gnhb gjjh geuh g4o2	control FC run without DA	20180626-present (gzhy) 20170926-20180625 (gsyg) 20170124-20170926 (gnhb) 20160621-20170124 (gjjh) 20150901-20160620 (geuh) 20140701-20150902 (g4o2)
GHG run	ghqy gf39	High resolution T1279, NRT CO_2 and CH_4 without DA	20160301-20170621 (ghqy) 20150101-20160229 (gf39)
	gqpe	High resolution Tco1279 (~9km) NRT CO_2, CH_4 and linCO forecast, initialized from GHG analysis gqiq and CAMS operational CO analysis	20170101-present
	gqiq	GHG analysis Tco399 (~25km)	20170101-present

Table 2.2: Satellite retrievals of reactive gases and aerosol optical depth that are actively assimilated in the o-suite.

Instrument	Satellite	Provider	Version	Type	Status
MLS	AURA	NASA	V3.4	O3 Profiles	20130107 -
OMI	AURA	NASA	V883	O3 Total column	20090901 -
GOME-2A	Metop-A	Eumetsat	GDP 4.7	O3 Total column	20131007 -
GOME-2B	Metop-B	Eumetsat	GDP 4.7	O3 Total column	20140512 -
SBUV-2	NOAA-19	NOAA	V8	O3 21 layer profiles	20121007 -
OMPS	Suomi-NPP	NOAA / EUMETSAT		O3 Profiles	20170124 -
IASI	MetOp-A	LATMOS/ULB	-	CO Total column	20090901 -
IASI	MetOp-B	LATMOS/ULB	-	CO Total column	20140918 -
MOPITT	TERRA	NCAR	V5-TIR V7-TIR	CO Total column	20130129 - 20160124 -
OMI	AURA	KNMI	DOMINO V2.0	NO2 Tropospheric column	20120705 -
OMI	AURA	NASA	v003	SO2 Tropospheric column	20120705-20150901
GOME-2A/2B	METOP A/B	Eumetsat	GDP 4.7	SO2 Tropospheric column	20150902 -
MODIS	AQUA / TERRA	NASA	Col. 5 Deep Blue Col. 6, 6.1	Aerosol total optical depth, fire radiative power	20090901 - 20150902 - 20170124 -
PMAp	METOP-A METOP-B	EUMETSAT		AOD	20170124 - 20170926 -

2.1.1 o-suite

The o-suite consists of the IFS-CB05 chemistry combined with the CAMS bulk aerosol model. The chemistry is described in Flemming et al. (2015) and Flemming et al. (2017), aerosol is described in Morcrette et al. (2009). The forecast length is 120 h. The o-suite data is stored under **expver '0001'** of **class 'MC'**. On 21 June 2016 the model resolution has seen an upgrade from T255 to T511, and forecasts are produced twice per day. The latest upgrade of the system is based on IFS version cy45r1_CAMS (https://confluence.ecmwf.int/display/COPSRV/Current+global+production+suites) and took place on 26 June 2018, see. The validation for this upgrade is described in Eskes et al., 2018. The update relevant for this report (for MAM-2018) is the 26 September 2017 upgrade, https://confluence.ecmwf.int/pages/viewpage.action?pageId=79955183. The performance of this upgrade is discussed in Eskes et al., 2017. A summary of the main specifications:

- The modified CB05 tropospheric chemistry is used (Williams et al., 2013), originally taken from the TM5 chemistry transport model (Huijnen et al., 2010)
- Stratospheric ozone during the forecast is computed from the Cariolle scheme (Cariolle and Teyssèdre, 2007) as already available in IFS, while stratospheric NOx is constrained through a climatological ratio of HNO_3/O_3 at 10 hPa.

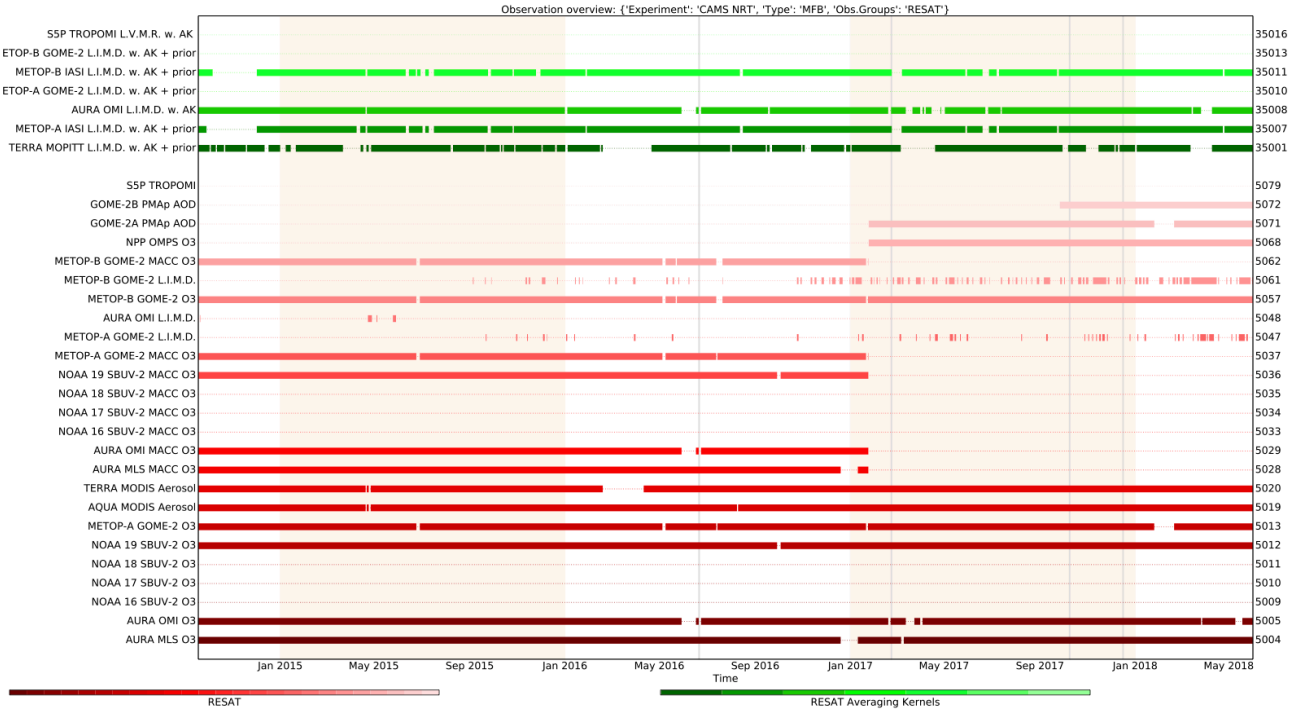

Figure 2.1: Satellite observation usage in the real-time analysis, for ozone, CO, aerosol AOD, from October 2014 onwards. Top four rows: products assimilated with averaging kernels. New assimilated products since the 24 January 2017 upgrade are the PMaP AOD including GOME-2B and OMPS ozone profile observations. Note that the lines mentioning "MACC O3" should be discarded.

- Monthly mean dry deposition velocities are based on the SUMO model provided by the MOCAGE team.
- Data assimilation is described in Inness et al. (2015) and Benedetti et al. (2009) for chemical trace gases and aerosol, respectively. Satellite data assimilated is listed in Table 2.2 and Fig. 2.1.
- Anthropogenic and biogenic emissions are based on MACCity (Granier et al., 2011) and a climatology of the MEGAN-MACC emission inventories (Sindelarova et al., 2014)
- NRT fire emissions are taken from GFASv1.2 (Kaiser et al. 2012).

The aerosol model includes 12 prognostic variables, which are 3 bins for sea salt and desert dust, hydrophobic and hydrophilic organic matter and black carbon, sulphate aerosols and its precursor trace gas SO_2 (Morcrette et al., 2009). Aerosol total mass is constrained by the assimilation of MODIS AOD (Benedetti et al. 2009). A variational bias correction for the MODIS AOD is in place based on the approach used also elsewhere in the IFS (Dee and Uppala, 2009).

New source scheme for Secondary Organic Aerosols (part of the Organic Matter), based on scaled CO emissions. This is a change form the current AEROCOM-based emissions. The impact is an increase of organic matter aerosol concentrations. The upgrade of 24 January 2017 introduced the following adjustments: 1. Reduced dust emissions over Taklamakan desert and India. 2. Dust emissions adjusted towards more larger particles. 3. Reduction in sulphate aerosol. 4. Mass fixer for aerosols.

A history of updates of the o-suite is given in Table 2.4, and is documented in earlier MACC-VAL reports:
http://www.gmes-atmosphere.eu/services/aqac/global_verification/validation_reports/.

A list with changes concerning the assimilation system can be found at
http://atmosphere.copernicus.eu/user-support/operational-info/global-system-changes.
The CAMS o-suite system is upgraded regularly, following updates to the ECMWF meteorological model as well as CAMS-specific updates such as changes in chemical data assimilation. These changes are documented in e-suite validation reports, as can be found from the link above. Essential model upgrades are also documented in Table 2.4.

On 26 September 2017 the system has been upgraded to cy43r3. A validation report for this upgrade (Eskes et al., 2017) is available here:
https://atmosphere.copernicus.eu/sites/default/files/repository/CAMS84_2015SC2_D84.3.1.3_201706_esuite_v1_0.pdf

2.1.2 Control

The control run (relevant expver = **gsyg** since 26/11/2017) applies the same settings as the respective o-suites, based on the coupled IFS-CB05 system with CAMS aerosol for cy41r1/cy40r2, except that data assimilation is not switched on. The only two exceptions with regard to this setup are:

- at the start of every forecast the ECMWF operational system is used to initialise *stratospheric* ozone, considering that stratospheric ozone, as well as other stratospheric species are not considered to be a useful product of this run. The reason for doing so is that this ensures reasonable stratospheric ozone as boundary conditions necessary for the tropospheric chemistry.
- The full meteorology in the control run is also initialized from the ECMWF operational NWP analyses. Note that this is different from the o-suite, which uses its own data assimilation setup for meteorology. This can cause slight differences in meteorological fields between o-suite and control, e.g. as seen in evaluations of upper stratospheric temperatures.

2.1.3 High-resolution CO_2 and CH_4 forecasts and delayed-mode analyses

The pre-operational forecasts of CO_2 and CH_4 use an independent setup of the IFS as the osuite, at a resolution of TL1279, i.e. ~16 km horizontal, and with 137 levels. This system runs in NRT, and does not apply data assimilation for the greenhouse gases.

The land vegetation fluxes for CO_2 are modelled on-line by the CTESSEL carbon module (Boussetta et al., 2013). A biogenic flux adjustment scheme is used in order to reduce large-scale biases in the net ecosystem fluxes (Agusti-Panareda, 2015). The anthropogenic fluxes are based on the annual mean EDGARv4.2 inventory using the most recent year available (i.e. 2008) with estimated and climatological trends to extrapolate to the current year. The fire fluxes are from GFAS (Kaiser et al., 2012). Methane fluxes are prescribed in the IFS using inventory and climatological data sets, consistent with those used as prior information in the CH_4 flux inversions from Bergamaschi et al. (2009). The anthropogenic fluxes are from the EDGAR 4.2 database (Janssens-Maenhout et al, 2012) valid for the year 2008. The biomass burning emissions are from GFAS v1.2 (Kaiser et al., 2012). The high resolution forecast experiments also included a linear CO scheme (Massart et al., 2015).

Table 2.4: Long-term o-suite system updates.

Date	o-suite update
2009.08.01	Start of first NRT experiment f7kn with coupled MOZART chemistry, without aerosol. Also without data assimilation.
2009.09.01	Start of first MACC NRT experiment f93i, based on meteo cy36r1, MOZART v3.0 chemistry, MACC aerosol model, RETRO/REAS and GFEDv2 climatological emissions, T159L60 (IFS) and 1.875°×1.875° (MOZART) resolution.
2012.07.05	Update to experiment fnyp: based on meteo cy37r3, MOZART v3.5 chemistry, where changes mostly affect the stratosphere, MACCity (gas-phase), GFASv1 emissions (gas phase and aerosol), T255L60 (IFS) and 1.125°×1.125° (MOZART) resolution. Rebalancing aerosol model, affecting dust.
2013.10.07	Update of experiment fnyp from e-suite experiment fwu0: based on meteo cy38r2, no changes to chemistry, but significant rebalancing aerosol model. Assimilation of 21 layer SBUV/2 ozone product
2014.02.24	Update of experiment fnyp from e-suite experiment fzpr: based on meteo cy40r1. No significant changes to chemistry and aerosol models.
2014.09.18	Update to experiment g4e2: based on meteo cy40r2. In this model version IFS-CB05 is introduced to model atmospheric chemistry.
2015.09.03	Update to experiment g9rr: based on meteo cy41r1.
2016.06.21	Update to experiment 0067: based on meteo cy41r1, but a resolution increase from T255 to T511, and two production runs per day
2017.01.24	Update to cycle 43R1_CAMS, T511L60
2017.09.26	Update to cycle 43R3_CAMS, T511L60
2018.06.26	Update to cycle 45R1_CAMS, T511L60

The experiments analyzed in this report are:

- "**ghqy**" from March 2016. The initial conditions used in ghqy on 1st of March 2016 are from the GHG analysis (experiment gg5m). Furthermore, the meteorological analysis used to initialize the ghqy forecast changed resolution and model grid in March 2016. Note that the CO_2, CH_4 and linear CO tracers are free-running.
- "**gqpe**" from January 2017 to present. It runs with a TCO1279 Gaussian cubic octahedral grid (equivalent to approximately 9km horizontal resolution). Note that the CO_2, CH_4 and linear CO tracers are initialized with the GHG analysis (gqiq) for CO_2 and CH_4 and the CAMS operational analysis for CO.
- The greenhouse gas analysis experiment "**gqiq**" runs on a TCO399 grid (equivalent to around 25km) and 137 vertical levels, and is available from January 2017. This experiment runs in

delayed mode (4 days behind real time) and makes use of observations from TANSO-GOSAT (methane and CO_2) and MetOp-IASI (methane).

A new forecast experiment, "gxk8" is available from January 2018 to 25 March 2018 to test a bug fix in CO_2.

2.2 Other systems

2.2.1 BASCOE

The NRT analyses and forecasts of ozone and related species for the stratosphere, as delivered by the Belgian Assimilation System for Chemical ObsErvations (BASCOE) of BIRA-IASB (Lefever et al., 2014; Errera et al., 2008), are used as an independent model evaluation of the CAMS products. The NRT BASCOE product is the ozone analysis of Aura/MLS-SCI level 2 standard products, run in the following configuration (version 05.07):

- The following species are assimilated: O_3, H_2O, HNO_3, HCl, HOCl, N_2O and ClO.
- It lags by typically 4 days, due to latency time of 4 days for arrival of non-ozone data from Aura/MLS-SCI (i.e. the scientific offline Aura/MLS dataset).
- Global horizontal grid with a 3.75° longitude by 2.5° latitude resolution.
- Vertical grid is hybrid-pressure and consists in 86 levels extending from 0.01 hPa to the surface.
- Winds, temperature and surface pressure are interpolated in the ECMWF operational 6-hourly analyses.
- Time steps of 20 minutes, output every 3 hours

See the stratospheric ozone service at http://www.copernicus-stratosphere.eu/. It delivers graphical products dedicated to stratospheric composition and allows easy comparison between the results of o-suite, BASCOE and TM3DAM. The BASCOE data products (HDF4 files) are also distributed from this webpage. Other details and bibliographic references on BASCOE can be found at http://bascoe.oma.be/. A detailed change log for BASCOE can be found at http://www.copernicus-stratosphere.eu/4_NRT_products/3_Models_changelogs/BASCOE.php.

2.2.2 TM3DAM and the multi-sensor reanalysis

One of the MACC products was a 30-year reanalysis, near-real time analysis and 10-day forecast of ozone column amounts performed with the KNMI TM3DAM data assimilation system, the Multi-Sensor Reanalysis (MSR) system (van der A et al., 2010, 2013),
http://www.temis.nl/macc/index.php?link=o3_msr_intro.html.
The corresponding validation report can be found at
http://www.copernicus-atmosphere.eu/services/gac/global_verification/validation_reports/.

The NRT TM3DAM product used for the validation of the CAMS NRT streams is the ozone analysis of Envisat/SCIAMACHY (until April 2012), AURA/OMI, and MetOp-A/GOME-2, run in the following configuration:

- total O_3 columns are assimilated
- Global horizontal grid with a 3° longitude by 2° latitude resolution.
- Vertical grid is hybrid-pressure and consists in 44 levels extending from 0.1 hPa to 100 hPa.
- Dynamical fields from ECMWF operational 6-hourly analysis.

An update of the MSR (MSR-2) was presented in van der A et al. (2015), which extended the record to 43 years based on ERA-interim reanalysis meteo and with an improved resolution of 1x1 degree.

2.2.3 SDS-WAS multimodel ensemble

The World Meteorological Organization's Sand and Dust Storm Warning Advisory and Assessment System (WMO SDS-WAS) for Northern Africa, Middle East and Europe (NAMEE) Regional Center (http://sds-was.aemet.es/) has established a protocol to routinely exchange products from dust forecast models as the basis for both near-real-time and delayed common model evaluation. Currently, twelve regional and global models (see the complete list in the following link https://sds-was.aemet.es/forecast-products/forecast-evaluation/model-inter-comparison-and-forecast-evaluation/at_download/file) provides daily operational dust forecasts (i.e. dust optical depth, DOD, and dust surface concentration).

Different multi-model products are generated from the different prediction models. Two products describing centrality (multi-model median and mean) and two products describing spread (standard deviation and range of variation) are daily computed. In order to generate them, the model outputs are bi-linearly interpolated to a common grid mesh of 0.5º x 0.5º. The multimodel DOD (at 550 nm) Median from nine dust prediction models participating in the SDS-WAS Regional Center is used for the validation of the CAMS NRT streams.

2.3 CAMS products

An extended list of output products from the NRT stream o-suite are available as 3-hourly instantaneous values up to five forecast days. These are available from ECMWF (through ftp in grib2 and netcdf format, http://atmosphere.copernicus.eu/global-near-real-time-data-access).

2.4 Availability and timing of CAMS products

The availability statistics provided in Table 2.6 are computed for the end of the 5-day forecast run. The CAMS production KPI is defined as the percentage of cycles in which all the general data dissemination tasks are completed before the deadlines: 10 UTC for the 00:00 and 22 UTC for the 12:00 UTC run. This was in part based on requirements from the regional models. We note that at present most regional models can still provide their forecasts even if the global forecast is available a bit later. Note that since 21 June 2016 two CAMS forecasts are produced each day.

For the period March - May 2018, 98.9% of the forecasts were delivered on time. two model cycles were late: 2018032812 - started late due to power failure; 2018041300 - finished late due to fire in Computer Hall

Table 2.6: Timeliness of the o-suite from Dec 2014 to the end of May 2018. From June 2016 onwards CAMS has produced two forecasts per day.

Months	**On time, 22 utc**	**80th perc**	**90th perc**	**95th perc**
Dec-Feb '14-'15	97%	D+0, 19:43	D+0, 20:28	D+0, 21:13
Mar-May 2015	96%	D+0, 19:38	D+0, 21:03	D+0, 21:40
Jun-Aug 2015	95%	D+0, 20:24	D+0, 20:53	D+0, 21:54
Sept-Nov 2015	95%	D+0, 19:44	D+0, 20:55	D+0, 21:51
Dec-Feb '15-'16	100%	D+0, 18:39	D+0, 18:57	D+0, 19:43
Mar-May 2016	98%	D+0, 19:32	D+0, 19:47	D+0, 20:00
Jun-Aug 2016 (00 and 12 cycle)	100%	D+0, 08:53 D+0, 20:55	D+0, 09:04 D+0, 21:01	D+0, 09:18 D+0, 21:18
Sep-Nov 2016	98.9%	D+0, 08:44 D+0, 20:44	D+0, 08:51 D+0, 20:48	D+0, 08:52 D+0, 20:51
Dec 2016 - Feb 2017	99.4%	D+0, 09:02 D+0, 21:01	D+0, 09:11 D+0, 21:02	D+0, 09:18 D+0, 21:04
Mar-May 2017	100%	D+0, 09:08 D+0, 21:07	D+0, 09:14 D+0, 21:09	D+0, 09:19 D+0, 21:11
Jun-Aug 2017	100%	D+0, 09:05 D+0, 21:05	D+0, 09:07 D+0, 21:08	D+0, 9:09 D+0, 21:10
Sep-Nov 2017	100%	D+0, 09:02 D+0, 21:00	D+0, 09:05 D+0, 21:04	D+0, 9:09 D+0, 21:07
Dec 2017 - Feb 2018	98.33%	D+0, 08:55 D+0, 20:54	D+0, 08:59 D+0, 20:59	D+0, 09:01 D+0, 21:02
Mar-May 2018	98.9%	D+0, 09:00 D+0, 21:00	D+0, 09:06 D+0, 21:03	D+0, 09:08 D+0, 21:06

3. Tropospheric Ozone

3.1 Validation with sonde data in the free troposphere

Model profiles of the CAMS runs were compared to free tropospheric balloon sonde measurement data of 38 stations taken from the NDACC, WOUDC, NILU and SHADOZ databases for May 2017 to May 2018 (see Fig. 3.1.1 - 3.1.2). Towards the end of the period, the number of available soundings decreases, which implies that the evaluation results may become less representative. The figures contain the number of profiles in each month that are available for the evaluation. The methodology for model comparison against the observations is described in Douros et al., 2017. The free troposphere is defined as the altitude range between 750 and 200hPa in the tropics and between 750 and 300hPa elsewhere.

In all zonal bands MNMBs for the o-suite are mostly within the range ±25%, for all months, see Fig. 3.1.1.-3.1.2. The control run generally shows larger negative MNMBs, (up to -40%).

Over the Arctic, the o-suite mostly shows slightly positive MNMBs during summer and spring (MNMBs up to 16%), while during the winter season the MNMBs get negative (within -10%) see, Fig. 3.1.1.

Over the NH mid-latitudes MNMBs for the o-suite are on average close to zero all year round (maxima are -4% to +6%), which is generally a clear improvement compared to the control run, which shows larger negative MNMBs during the respective period.

Over the Tropics and over Antarctica, ozone mixing ratios are mostly overestimated by the o-suite (up to 25%) by the o-suite, see Fig. 3.1.2. The control run sows large negative MNMBs for Antarctica.

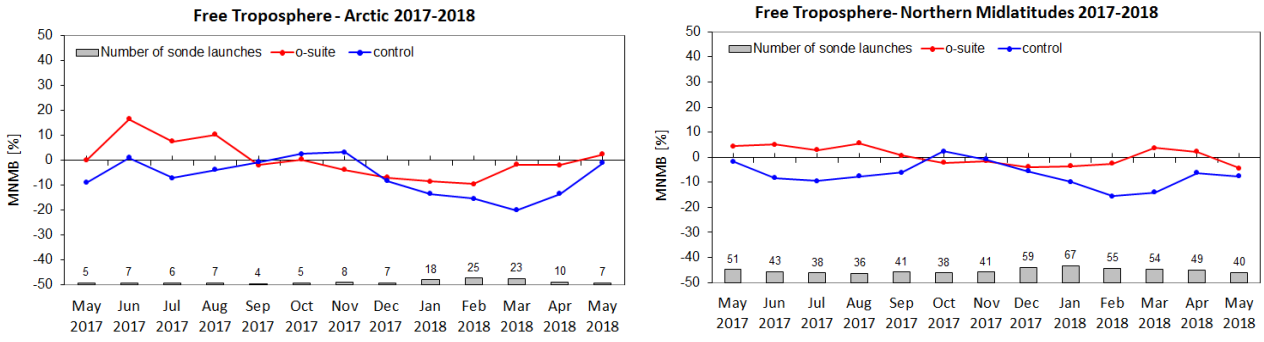

Figure 3.1.1: MNMBs (%) of ozone in the free troposphere (between 750 and 300 hPa) from the IFS model runs against aggregated sonde data over the Arctic (left) and the Northern mid latitudes (right). The numbers indicate the amount of individual number of sondes.

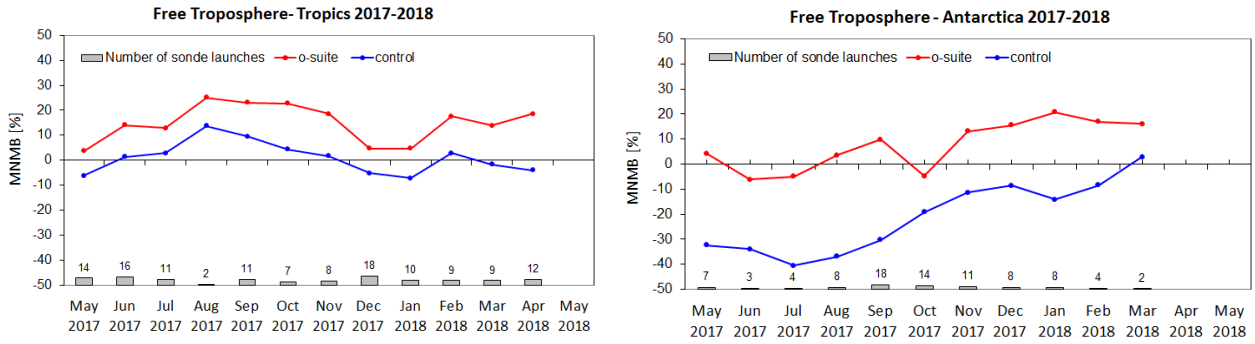

Figure 3.1.2: MNMBs (%) of ozone in the free troposphere (between 750 and 200hPa (Tropics) / 300hPa) from the IFS model runs against aggregated sonde data over the Tropics (left) and Antarctica (right). The numbers indicate the amount of individual number of sondes.

3.2 Ozone validation with IAGOS data

The daily profiles of ozone measured at airports around the world, are shown on the website at http://www.iagos.fr/macc/nrt_day_profiles.php. For the period from March - May 2018, the data displayed on the web pages and in this report include only the data as validated by the instrument PI. The available flights and available airports are shown in Fig. 3.2.1 top and bottom respectively. Performance indicators have been calculated for different parts of the IAGOS operations.

Six aircrafts were operating during this period. With these aircrafts, operating fully over the three month period, we can expect a total of about 1260 flights. The actual number of flights within the period was 626 (1252 profiles) giving a performance of 49 %. These flights are shown in Fig. 3.2.1 (top). Sixty one percent (40%) of the operational flights had usable measurements of ozone and 61% of flights had usable CO. Delivering these O_3 and CO data were two aircraft from Lufthansa operating from Frankfurt, two aircraft operated by Air France based in Paris, one from China Airlines based in Taipei and one from Hawaiian Airlines since mid-October 2017, with flight operations from Honolulu. Fig. 3.2.1 (bottom) shows the available airports, with a plotting circle scaled to the highest number of flights at an airport.

Europe

Fig. 3.2.2 presents ozone timeseries at Paris and Frankfurt during March – May 2018. Ozone is well represented throughout the profiles until the UTLS region when ozone is generally overestimated by o-suite and underestimated by control run as clearly seen in Fig. 3.2.3. Some examples of individual profiles are presented in Fig. 3.2.4.

As mentioned in the regional report for MAM 2018, in France the month of April 2018 has been characterized the hottest April since 1900 (http://www.meteofrance.fr/actualites/61725131-une-semaine-d-avril-memorable), with an exceptional warm weather during the week from 18 to 24 April. Europe has also recorded high temperatures around the same period and also a little earlier in the month for some places.

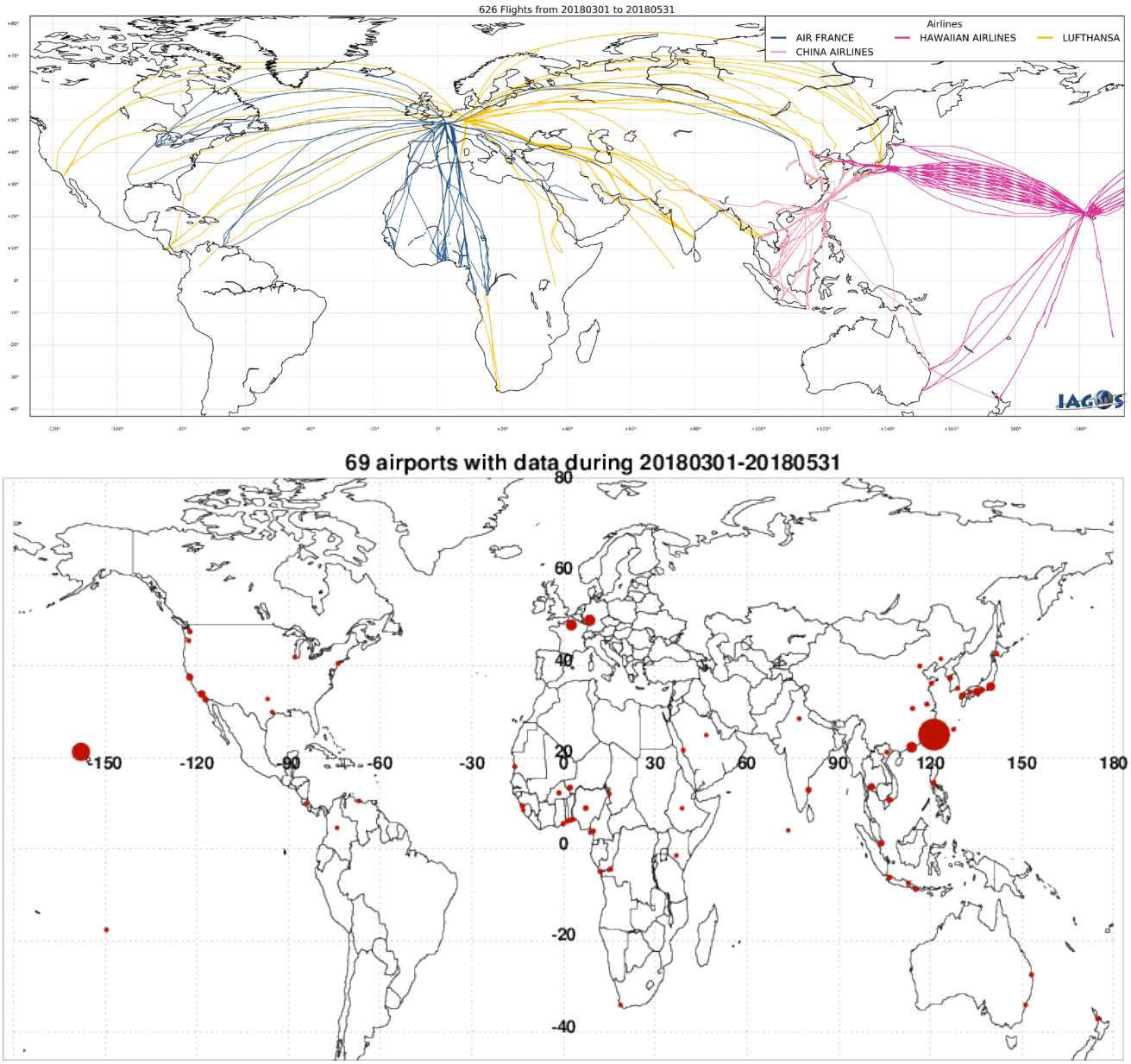

Figure 3.2.1. Map of the flights (top) and the visited airports (bottom) during the period March - May 2018, by the IAGOS-equipped aircraft. The size of the plotting circle represents the number of profiles available.

In the time series at Frankfurt (Fig 3.2.2), an increase in ozone is observed in the surface and boundary layer at the end of April around day 20. This can also be seen in the individual profiles at Frankfurt on 21 April, ozone values present about 80 ppbv in the boundary layer. The results of CAMS-global and control run are similar except in the upper layers where control run performs better.

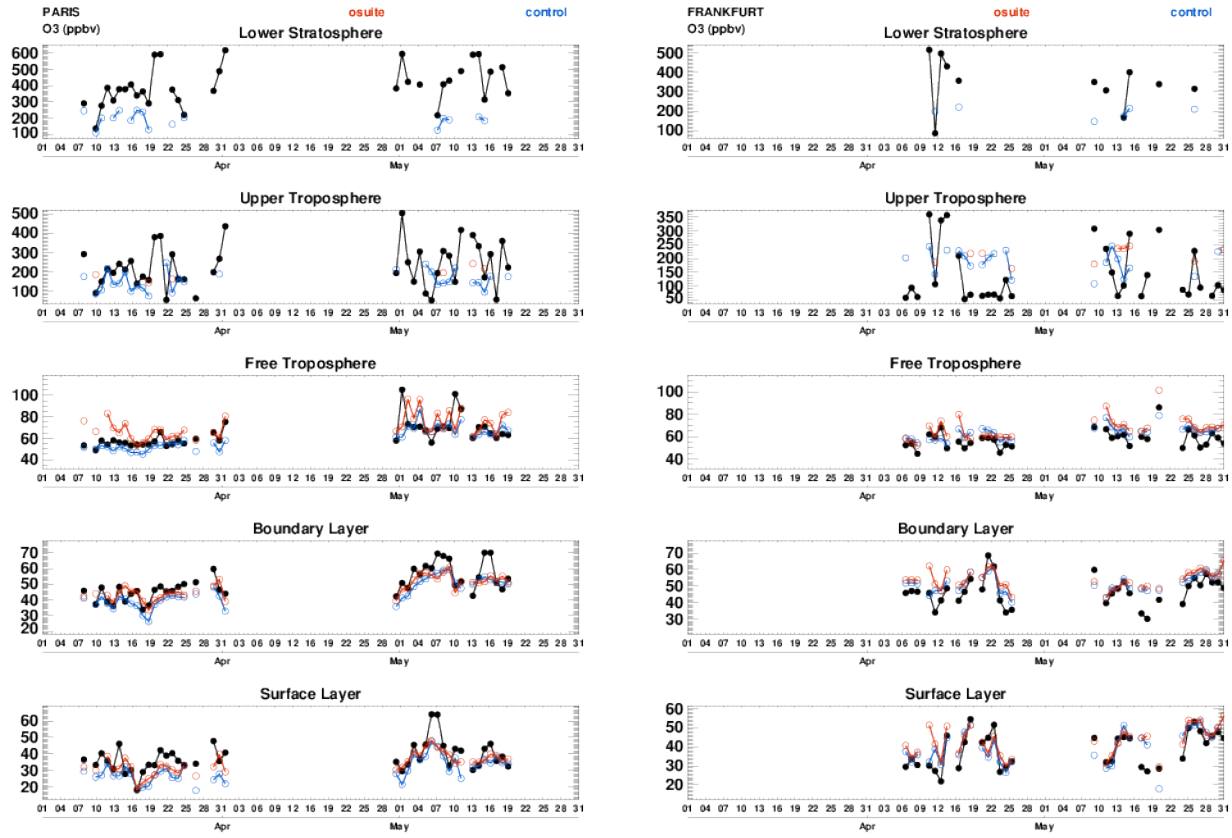

Figure 3.2.2. Time series of daily mean ozone over Paris and Frankfurt during March – May 2018 for 5 layers, Surface, Boundary layer, Free Troposphere, Upper Troposphere and Lower Stratosphere.

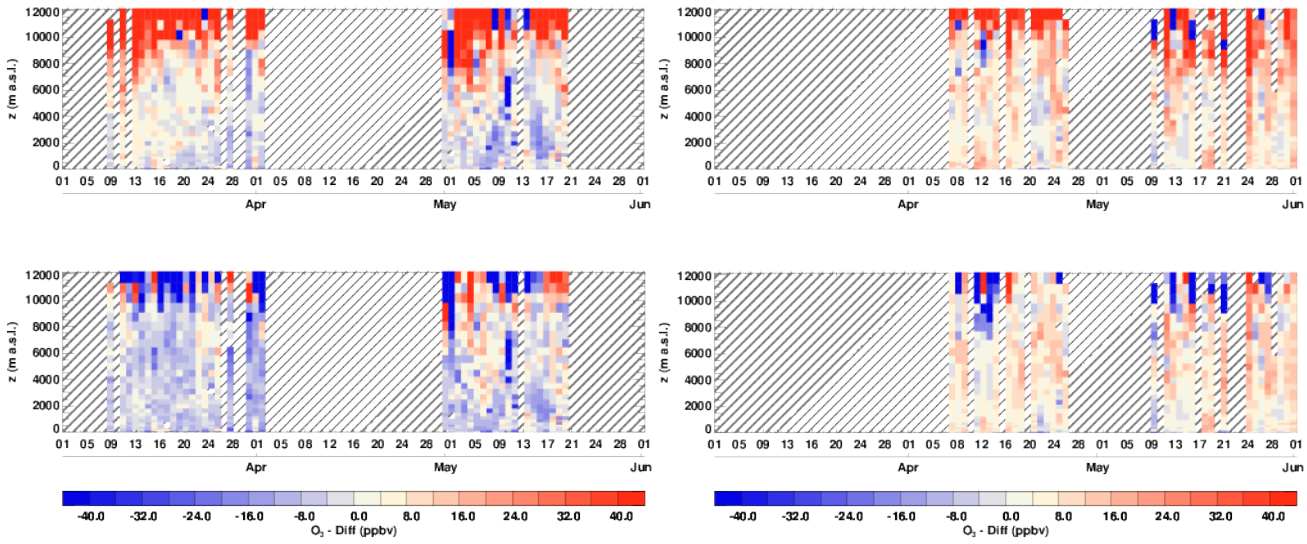

Figure 3.2.3 Time series of the absolute differences (model - observations) in daily profiles for ozone over Paris (left) and Frankfurt (right) during March – May 2018. Top panels correspond to o-suite and bottom panels to control run.

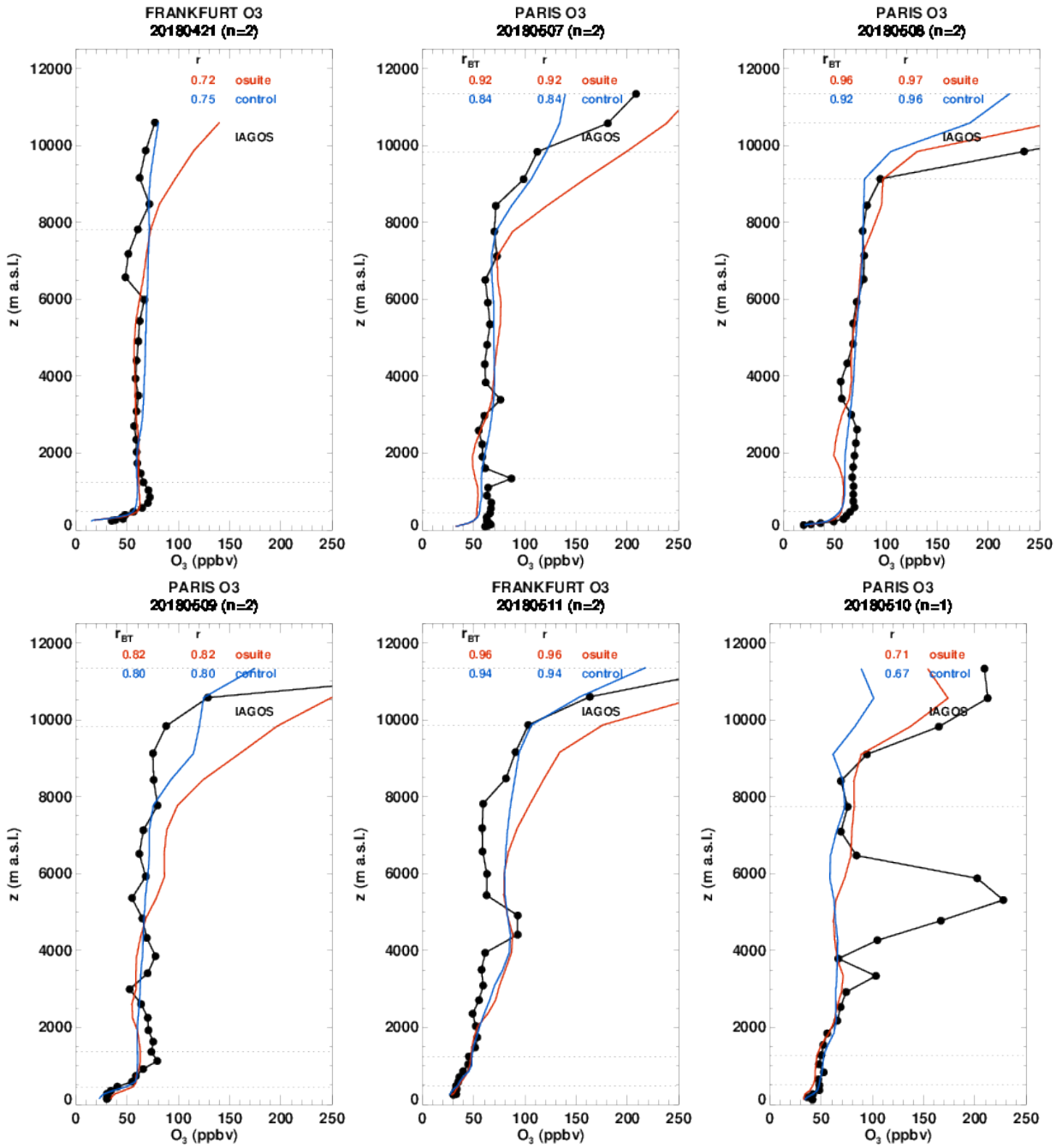

Figure 3.2.4. Selection of daily profiles for ozone from IAGOS (black) and the two NRT runs (o-suite:red, control: blue) over Europe during March – May 2018.

As also mentioned in the regional report, during the first half of May, France is splitted by a north-south weather divide, with anticyclonic conditions in the northern half of the country, and fresh and instable conditions in the southern half. Large positive anomalies have been recorded in sunshine duration in the northernmost stations, and conversely negative anomalies in the south. Between 4 and 9 May, an increase in ozone is observed in the surface and boundary layer at Paris. This is shown on some profiles for the 7, 8 and 9 May (Fig. 3.2.4). These profiles are well reproduced by

both models from the surface up to the mid-troposphere. Above 6000 m the models start to deviate from the observations with a slightly better performance from the control run.

On 10 May, another episode in ozone is observed at Paris with a wide peak located between the altitudes of 4000 and 6000m, and reaching the value of about 220 ppbv at 5000 m (Fig. 3.2.4). This peak is not detected by the models. One day later (11 May) a peak in ozone is also observed at the same altitude in Frankfurt but with a much smaller magnitude of about 100 ppbv. In the case of Frankfurt, although the profiles of the models do not present a clear peak, a increase in ozone values is produced by the models with a mixing ratio of 80 ppbv between the altitudes of 2000 m and 6000 m.

West Africa

Several destinations across West Africa have been visited during the period March – May 2018. These include some situated on the Gulf of Guinea (Cotonou, Conakry, Lome, Douala) where pollution from oil industries has effects on the profiles all year round, some situated inland (Ouagadougou, Abuja), and some in the southern hemisphere (Brazzaville). All these cities are subject to anthropogenic emissions from vehicles and to biomass burning during the dry season, from December to March and from June to October in the northern and southern hemisphere respectively. We do not therefore expect to see a big influence of biomass burning on the profiles shown here for MAM. In Fig. 3.2.5.a-b examples of ozone profiles sampled in this region are shown. These ozone profiles present anomalies in the boundary layer and/ or in the free troposphere likely related to forest fires as they are often correlated with peaks in CO (see section 4.2). In the examples presented here, the results from the o-suite and control run are very similar at all locations. The increases in ozone are in general detected by the both models, but the magnitudes are often underestimated throughout the free troposphere and in the boundary layer.

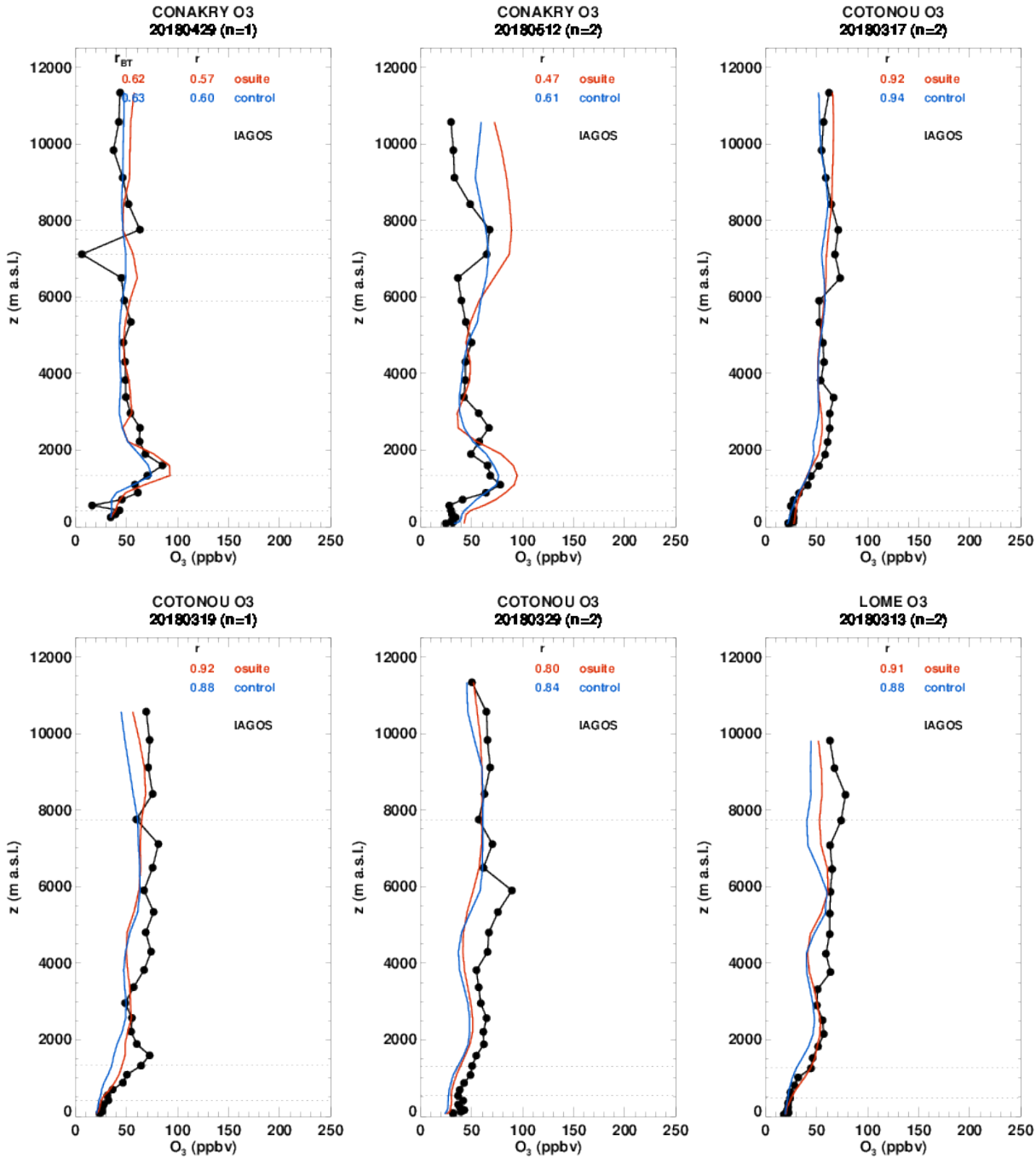

Figure 3.2.5.a Selection of daily profiles for ozone from IAGOS (black) and the two NRT runs (o-suite: red, control: blue) over West Africa during March – May 2018.

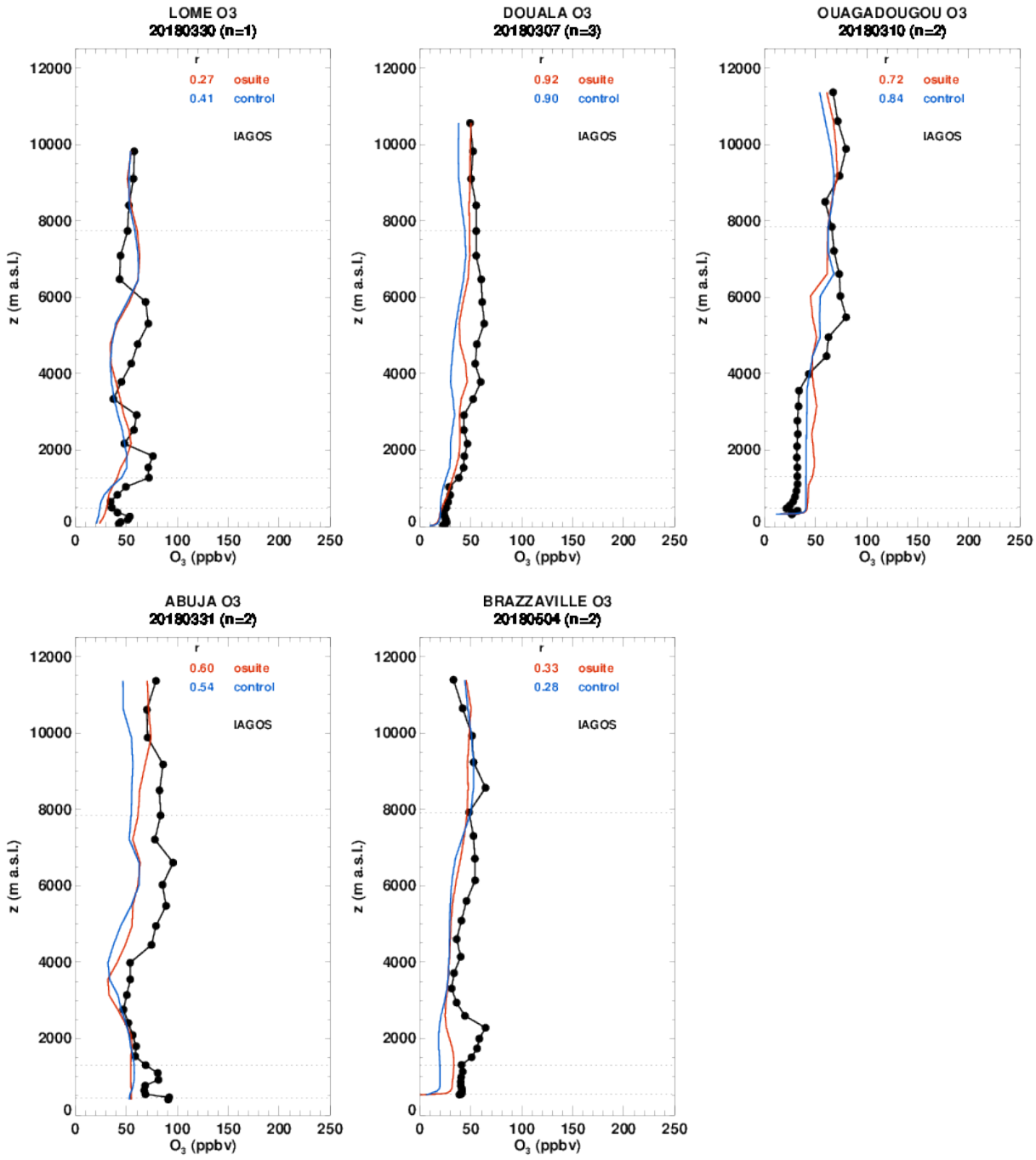

Figure 3.2.5.b Selection of daily profiles for ozone from IAGOS (black) and the two NRT runs (o-suite: red, control: blue) over West Africa during March – May 2018.

North America

During the period March May 2018, most available profiles in North America are at Californian airports: Los Angeles, San Francisco and San Diego (Fig. 3.2.6.a-b). At these airports ozone is in general well reproduced in the lower part of the troposphere. In San Diego on 12 May, two peaks in ozone are observed near 5000m and 7000 m, reaching about 120 ppbv. The presence of these peaks is likely related to the transport of smoke from forest fires in Mexico. The o-suite detects a

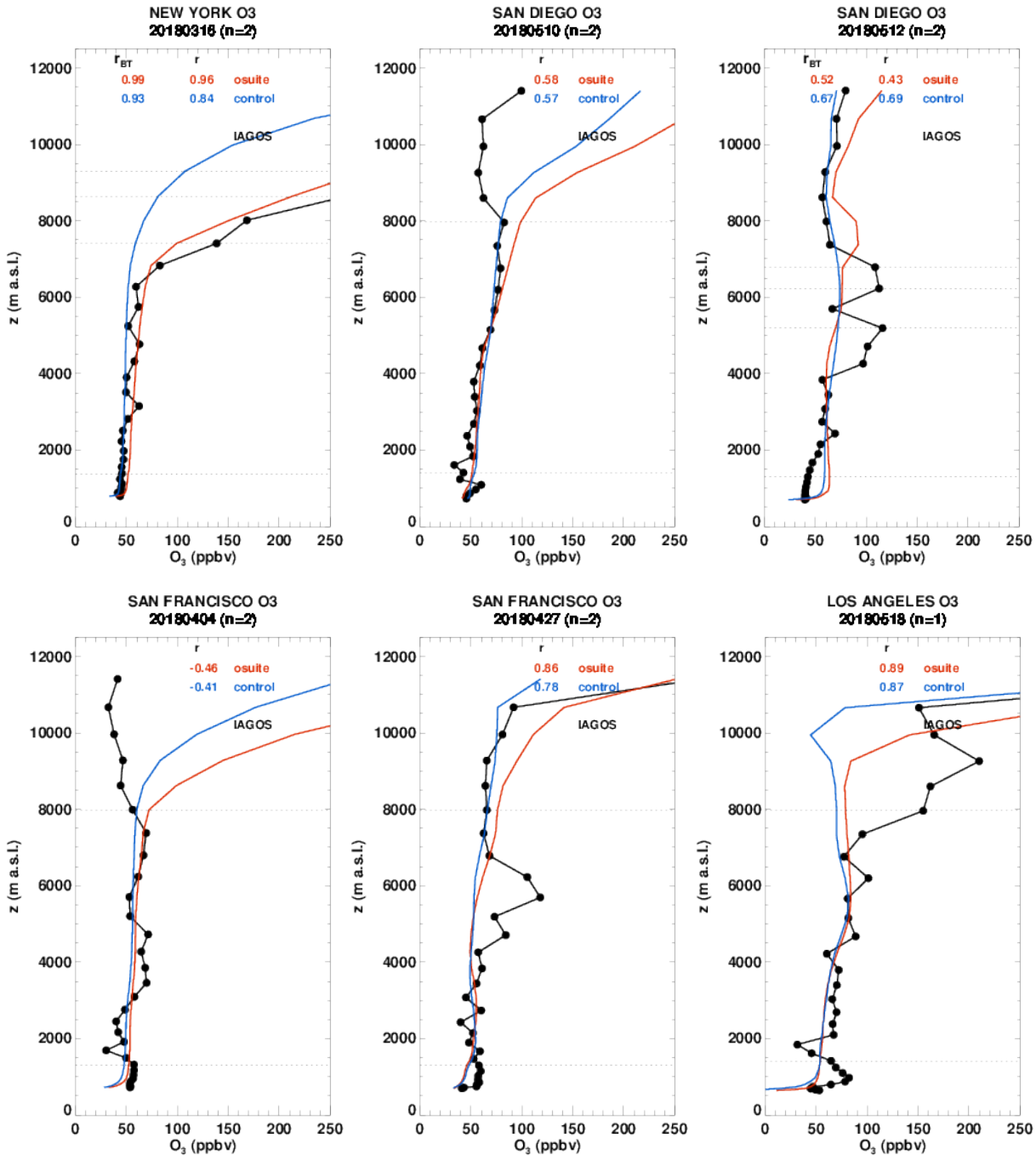

Figure 3.2.6.a Selection of daily profiles for ozone from IAGOS (black) and the two NRT runs (o-suite: red, control: blue) over North America during March – May 2018.

single peak but at a higher altitude of about 8000 m and with a magnitude of nearly 90 ppbv, while the control run is not detecting any peak. At San Francisco on 27 April, an ozone peak of 120 ppbv is observed near 6000 m. In this case none of the models is detecting an increase in ozone in the free troposphere. At most locations, the largest discrepancies between models and observations are found in the UTLS where the results can be very different. This can be seen in particular on the profiles of New York on 16 March, San Diego on 10 May, San Francisco on 4 April, Los Angeles on 1st April and 6 May.

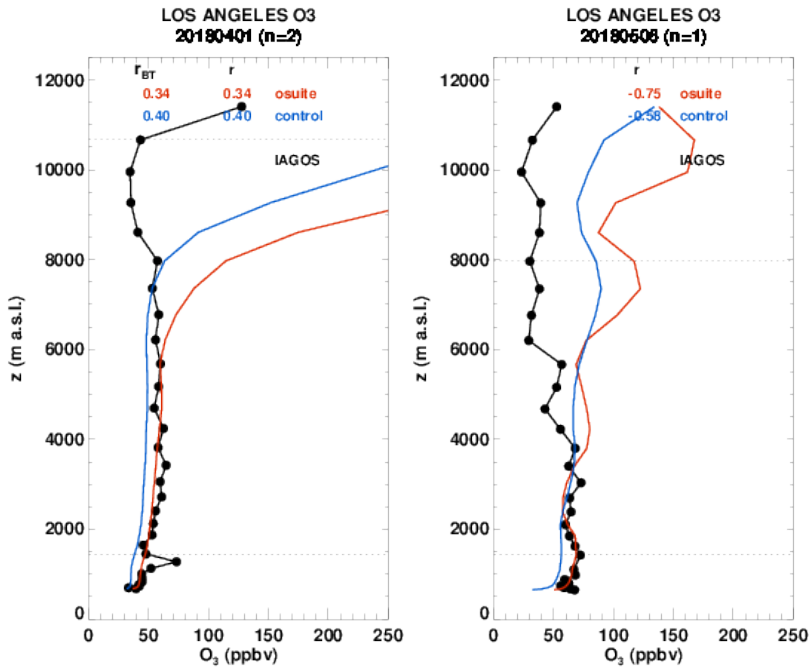

Figure 3.2.6.b Selection of daily profiles for ozone from IAGOS (black) and the two NRT runs (o-suite: red, control: blue) over North America during March – May 2018.

Northeastern Asia

In Fig. 3.2.7, several profiles are presented for the airports of: Qingdao (China), Tokyo (Japan) and Seoul (Corea). For these airports of Northeastern Asia, the models are generally in good agreement with the observation or slightly overestimate ozone in the surface and boundary layer. In the mid-troposphere, control run is mostly in good agreement with observations, while CAMs-global present large overestimations.

India

Very few profiles are available at Indian airports for the period between March and May 2018. In Fig. 3.2.8 two profiles are presented: at Madras on 7 and 23 April. These two profiles present similar shapes and ozone magnitudes. Ozone values are low in the surface and boundary layer, and the profile is nearly constant in the free troposphere up to the UTLS with ozone mixing ratio of 50 ppbv. Both the o-suite and the control run show a good correspondence with the observations with slight overestimations in the surface and boundary layer.

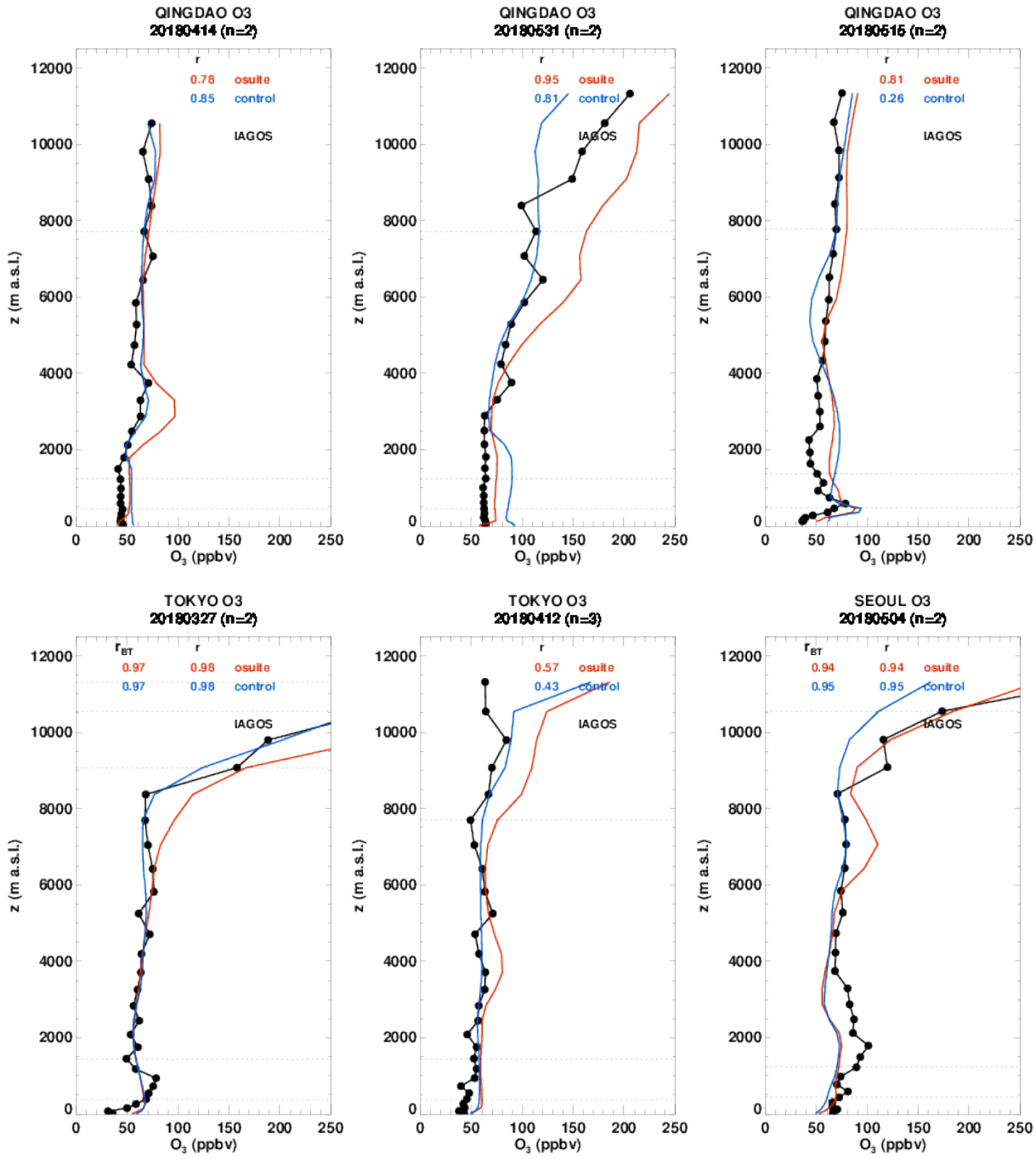

Figure 3.2.7 Selection of daily profiles for ozone from IAGOS (black) and the two NRT runs (o-suite:red, control: blue) over Northeastern Asia during March – May 2018.

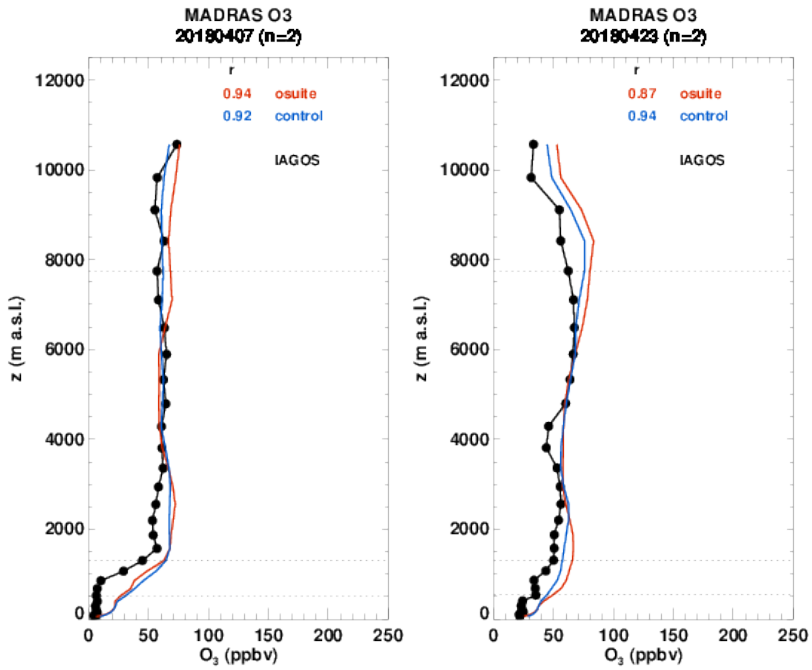

Figure 3.2.8. Selection of daily profiles for ozone from IAGOS (black) and the two NRT runs (o-suite: red, control: blue) over India during March – May 2018.

Pacific

As aforementioned, the Hawaiian aircraft started monitoring operations in October 2017. The pristine environment of the Island makes Hawaii a key location for addressing air quality and climate change issues, and for the validation of models. During the period March – May 2018, the airport of Honolulu has been sampled continuously (Fig. 3.2.9). As it can be seen on the time series the models agree well with the observations in the surface and boundary layer, with a slightly better agreement from the control run as compared to CAMS-global. This is also shown on Fig. 3.2.10 with the time series of the absolute differences (model-observations). In the UTLS the results from the control run are significantly better than those of CAMS-control which present large overestimations.

In Fig. 3.2.11 several profiles at Honolulu which present anomalies at different altitudes are shown. The profiles of 1st April, 6 May and 27 May present a complex shape with a major ozone maximum of about 80 ppbv in the free troposphere at an altitude of 5000 m, 4000 m and 3000 m respectively. The complex shape is in general well reproduced by both models except in the UTLS for the profile of the 6 May where both models largely overestimate ozone. The aforementioned major maxima in the free troposphere are well detected by the models at a similar altitude as observations. The magnitude of the modelled maxima is also in well agreement with observations, except in the case of the 1st April where control run present good results but CAMS-global is overestimating the magnitude of the peak with a value of 100 ppbv. The profile for the 25 March shows an anomaly in the UTLS with a peak in ozone reaching 200 ppbv which might be related to a stratospheric intrusion. This peak is not detected by the models which present a constant profile in the UTLS with an ozone mixing ratio of about 50 ppbv.

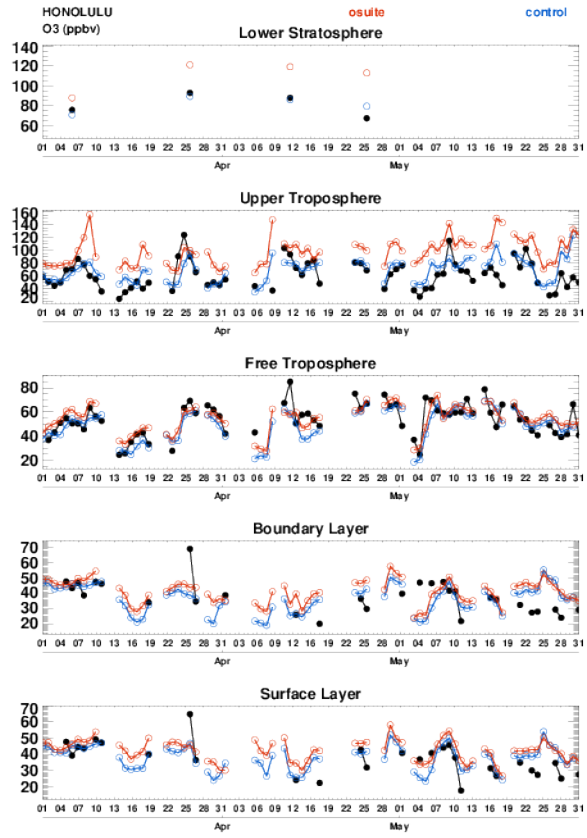

Figure 3.2.9. Time series of daily mean ozone over Honolulu during March – May 2018 for 5 layers, Surface, Boundary layer, Free Troposphere, Upper Troposphere and Lower Stratosphere.

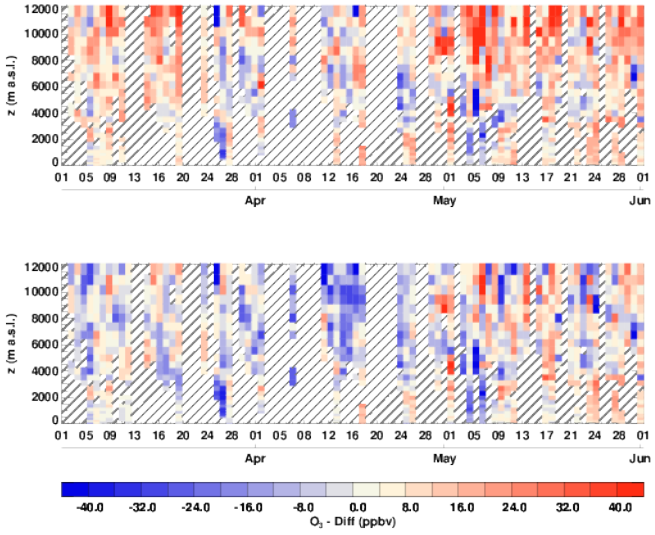

Figure 3.2.10. Time series of the absolute differences (model - observations) in daily profiles for CO Honolulu during March – May 2018. Top panel corresponds to o-suite and bottom panel to control run.

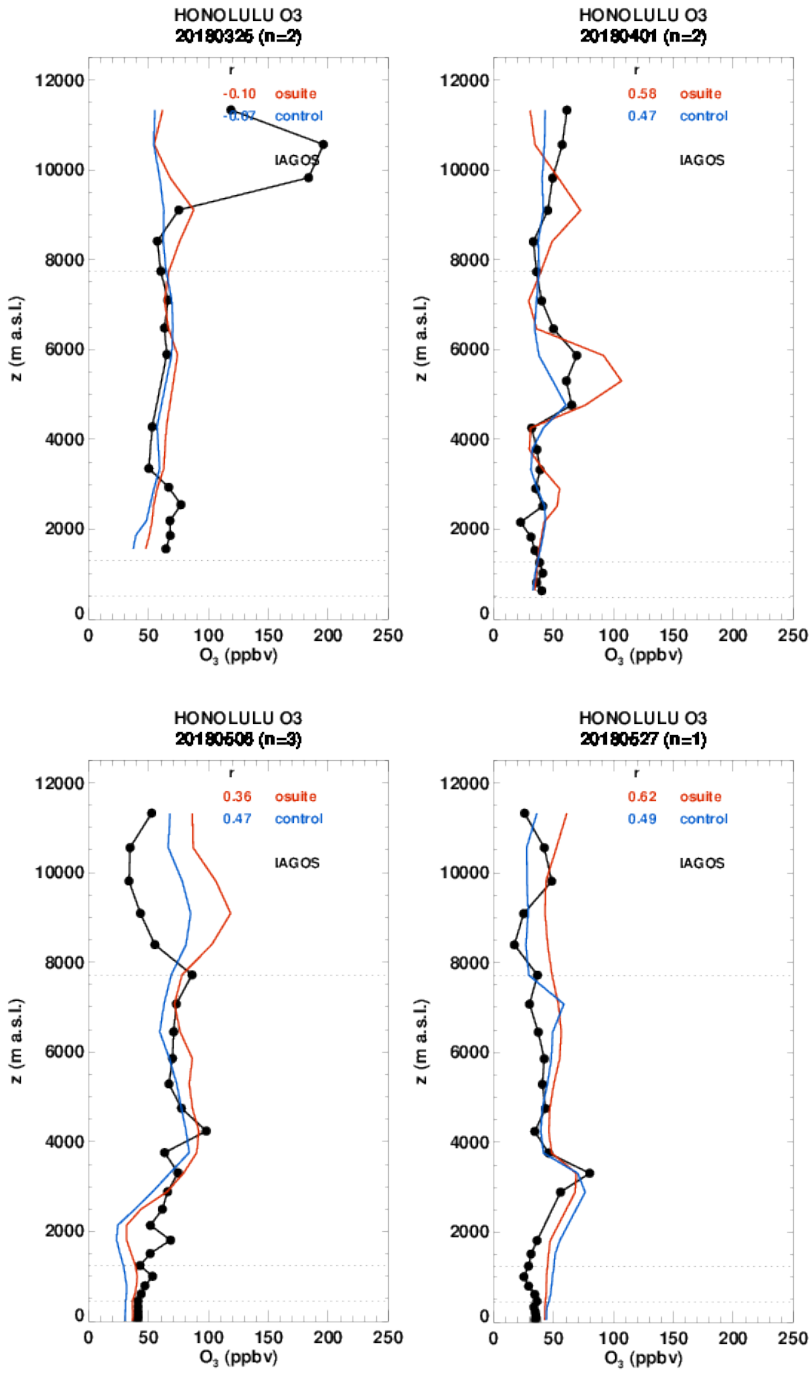

Figure 3.2.11 Selection of daily profiles for ozone from IAGOS (black) and the two NRT runs (o-suite: red, control: blue) over the Pacific during March – May 2018.

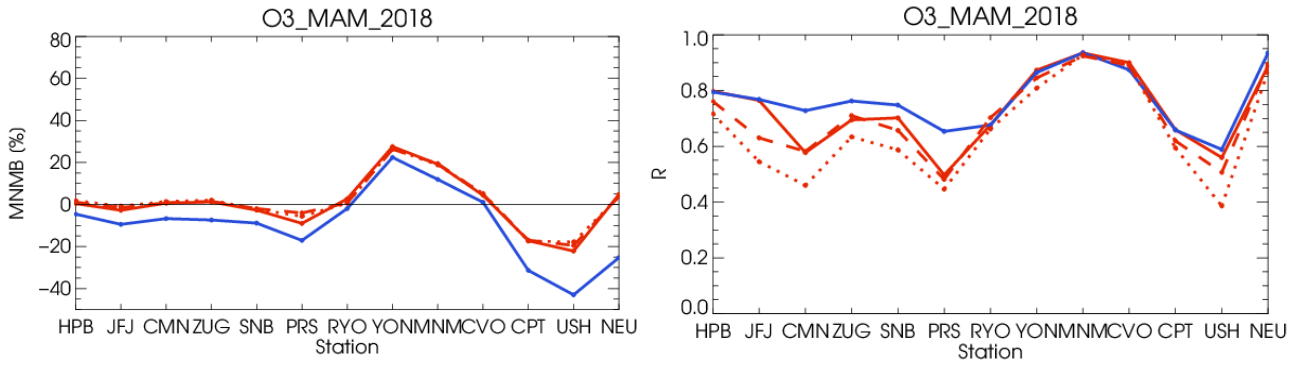

Figure 3.3.1: Modified normalized mean bias in % (left) and correlation coefficient (bottom right) of the NRT model runs compared to observational GAW data in the period March 2018 to May 2018 (o-suite: solid red, D+0: red-dashed, D+4: red-points, and control: blue).

3.3 Validation with GAW and ESRL-GMD surface observations

For the Near Real Time (NRT) validation, 14 GAW stations and 8 ESRL stations are currently delivering O_3 surface concentrations in NRT, and the data are compared to model results. In the following, a seasonal evaluation of model performance for the 2 NRT runs (o-suite and control) has been carried out for the period from March to May 2018. The latest validation results based on GAW stations can be found on the CAMS website, http://www.copernicus-atmosphere.eu/d/services/gac/verif/grg/gaw/, and based on ESRL on http://www.academyofathens.gr/kefak/cams/index.html.

Modified normalized mean biases in % (left, panel) and correlation coefficients (right, panel) for different forecasts days (D+2, red-dashed and D+4, red- pointed) with respect to GAW observations are shown in Figs. 3.3.1 and 3.3.2. It indicates that MNMBs for both o-suite and control run mostly remain stable up to D+4 (forecast run from 96h to 120h). Correlations between simulated and observed surface ozone values remain almost stable up to D+2 (forecast run from 48h to 72h), but then drop (correlations for D+4 are lower than correlations for D+2 and D+0), see Fig. 3.3.1 and 3.3.2, right graph).

A comparison of the seasonal-mean MNMB over Europe (Fig. 3.3.3) from December 2012 to present shows that the MNMB over European GAW stations is minimal during the winter season, and tends to increase in other months. Also on average the MNMB for the o-suite shows a slight improvement over the years, while it remains higher, and more variable for the consecutive control runs. Temporal correlation is consistently better for control than for the o-suite.

Results are summarized in Figs 3.3.1 and 3.3.3.

Looking at different regions, for European stations (HPB, JFJ, ZUG, SNB, CMN, PRS), observed O_3 surface mixing ratios are very close to the observations. The control run shows lower O_3 mixing ratios and thus a slight negative bias. MNMBs are between 1 and -8% for the o-suite, see Fig. 3.3.1. Correlations for the European stations are between 0.49 and 0.79 for the o-suite and between 0.65 and 0.79 for the control run, see Fig. 3.3.1.

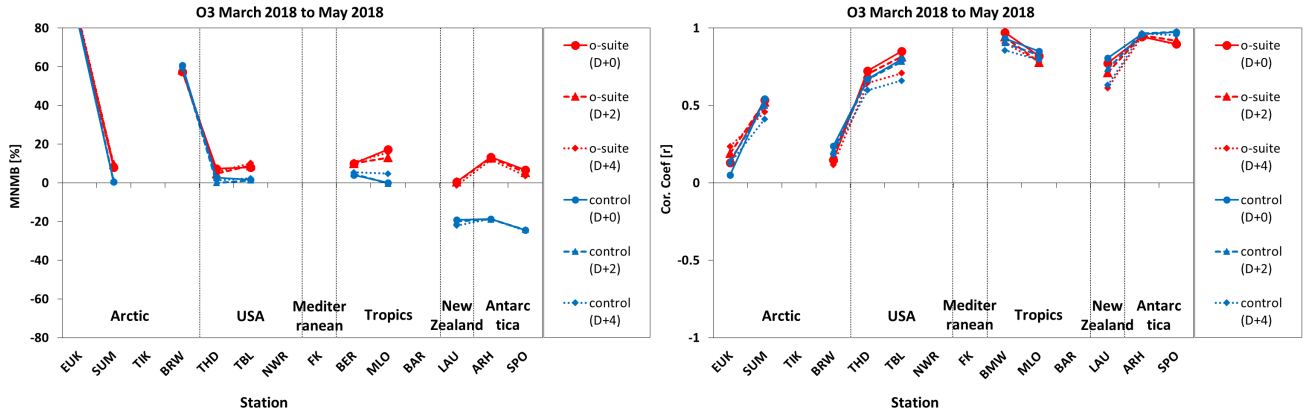

Figure 3.3.2: Modified normalized mean bias in % (left) and correlation coefficient (right) of the NRT forecast runs compared to observational ESRL data in the period March 2018 to May 2018. Circles correspond to D+0, triangles to D+2 and rhombs to D+4 metrics respectively.

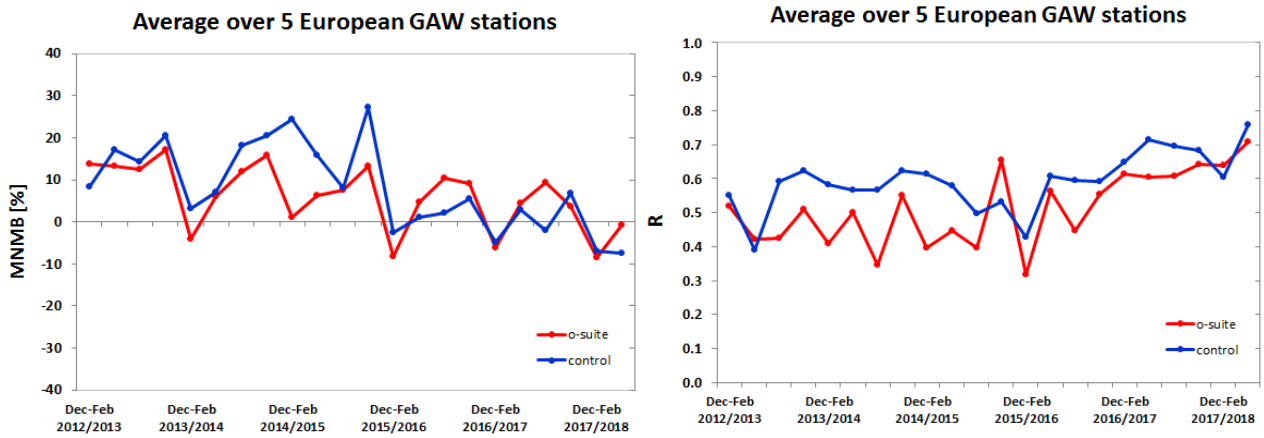

Figure 3.3.3: Long term (Dec. 2012 – May 2018) evolution of seasonal mean MNMB (left) and correlation (right), as averaged over 5 GAW stations in Europe, for o-suite (red) and control (blue).

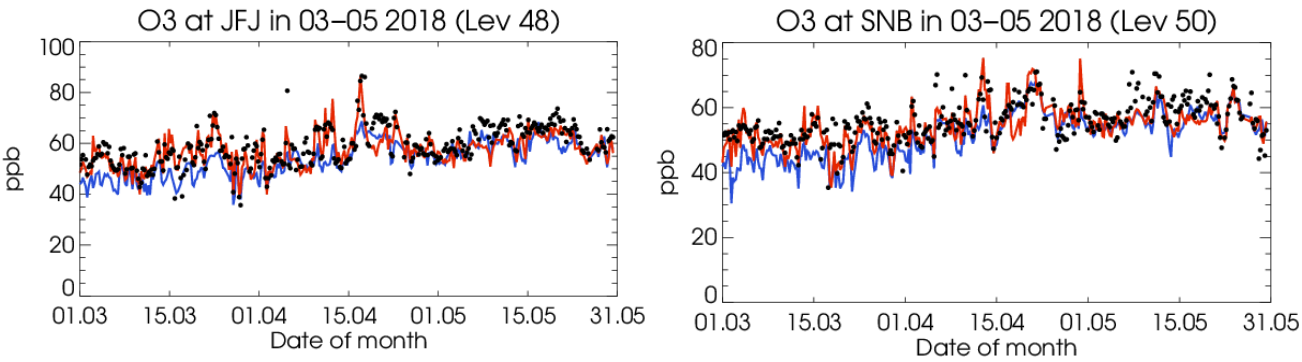

Figure 3.3.4: Time series for the o-suite (red) and control (blue) compared to GAW observations at Jungfraujoch (39.03°N, 141.8°E) and Sonnblick (47.05°N, 12.96°E)

Over Arctic stations (EUK, BRW and SUM), both runs strongly overestimates surface ozone values at Point Barrow and at Eureka (EUK) stations ($MNMB_{EUK}$≈80%, $MNMB_{BRW}$≈60%) while at SUM o-suite slightly overestimate surface ozone and the control run reproduces well the surface ozone mean concentrations. The large positive model offsets at point Barrow and Eureka is because Cams global simulations cannot capture ozone depletion events in March – May 2018 (see Figure 3.3.5 left graph). These events are related to halogen chemistry reactions that are not represented in the model simulations. This has also as result low correlations between simulated and observed surface ozone at EUK and BRW (r≈0.10 at EUK and r≈0.15 at BRW) while over Summit where ozone depletion events does not occure during spring 2018 correlations are high for both runs (r≈0.55).

For stations located in Asia (RYO, YON, MNM) both runs overestimate the minimum concentrations MNMBs between 2 and 22%, see Fig 3.3.6. Correlation coefficients range between 0.67 and 0.93.

For USA stations (TBL and THD), the observed ozone mixing ratios are overestimated by 10% from the o-site run while the control run has almost zero bias. Correlations between o-suite and observations are 0.70 at THD and 0.82 at TBL and slightly lower for the control run (0.65 at THD and 0.77 at TBL).

The observed ozone mixing ratios are overestimated by 10% from the o-site run while the control run has almost zero bias also at Bermuda (BER) and at Mauna Loa (MLO) station in the Tropics. Correlations between simulated and observed surface ozone are high for both the o-suite and the control run over Bermuda (r>0.9) and Mauna Loa stations (r>0.8).

O_3 mixing ratios of the southern hemispheric stations (CPT, USH) are underestimated with MNMBs between -17 and -22% by the osuite. The control run shows larger underestimations between -31% and 43%, see Fig 3.3.8. Correlation coefficients range around 0.55 and 0.65. At Lauder (LDR) station in New Zealand the o-suite reproduces well O_3 mixing ratios (MNMB≈0%) while the control run underestimate it by -20%. Correlation between simulated and observed surface ozone values are 0.8 for both runs.

For the South Pole station in Antarctica (SPO), the data assimilation almost corrects the negative offset in the control run (o-suite MNMBs= 6%, control MNMB= -25%), see Fig 3.3.7 (right panel). For Neumayer station (NEU) the MNMB is 4% for the o-suite and -25% for the control, Fig. 3.3.8. At Arrival Heights station (ARH) the o-suite overestimates surface ozone values by 10% while the control run underestimates it by -20%. Correlations between simulated and observed surface ozone are very high for both runs at both ARH and SPO stations (r>0.9).

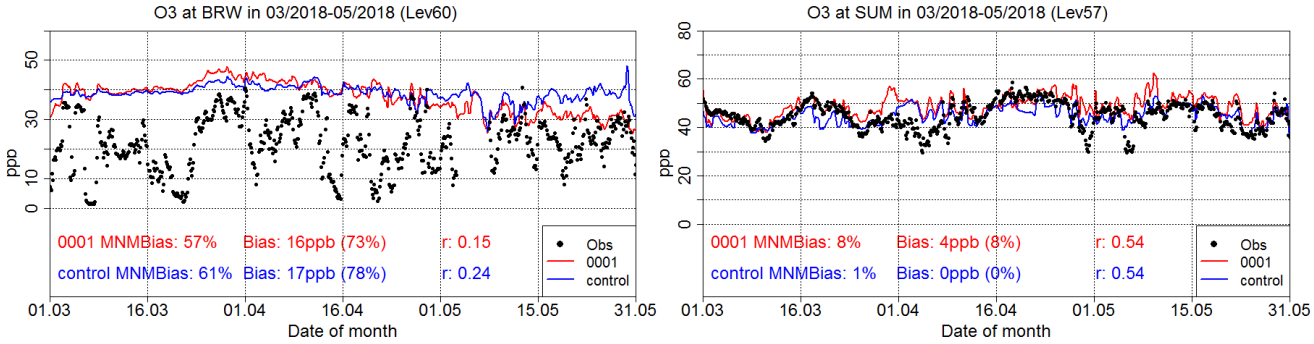

Figure 3.3.5: Time series for the o-suite (red) and control (blue) compared to ESRL observations at Summit, Greenland station (72.57°N, 38.48°W, left) and at Point Barrow, Alaska station (71.32°N, 156.51°W, right)

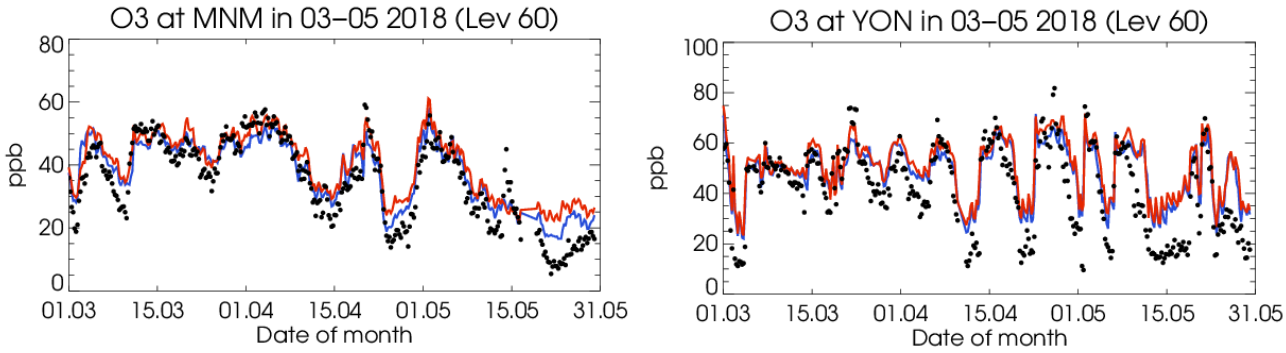

Figure 3.3.6: Time series for the o-suite (red) and control (blue) compared to GAW observations at Minamitorishima (24.29°N, 153.98°E) and Yonagunijima (24.47°N, 123.02°E).

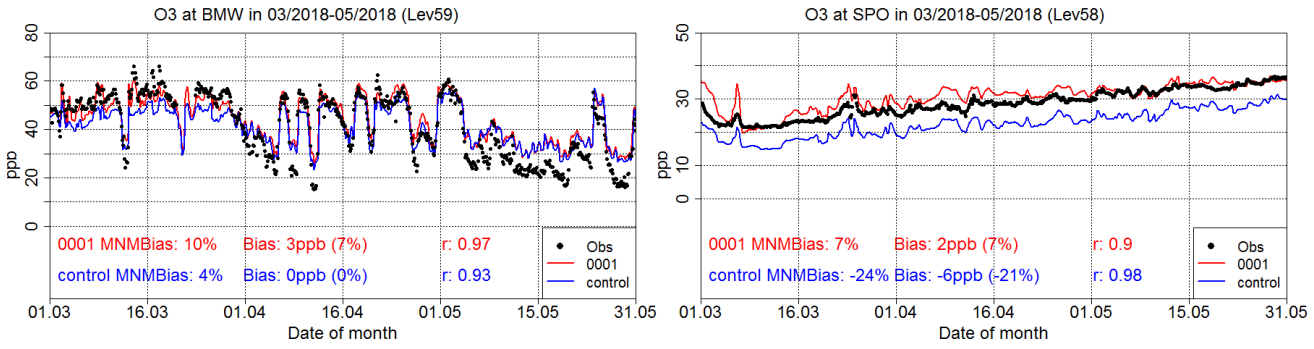

Figure 3.3.7: Time series for the o-suite (red) and control (blue) compared to ESRL observations (black dots) Tudor Hill, Bermuda station (32.27°N, 64.88°W) and at South Pole, Antarctica station (90.00°S, 24.80°W).

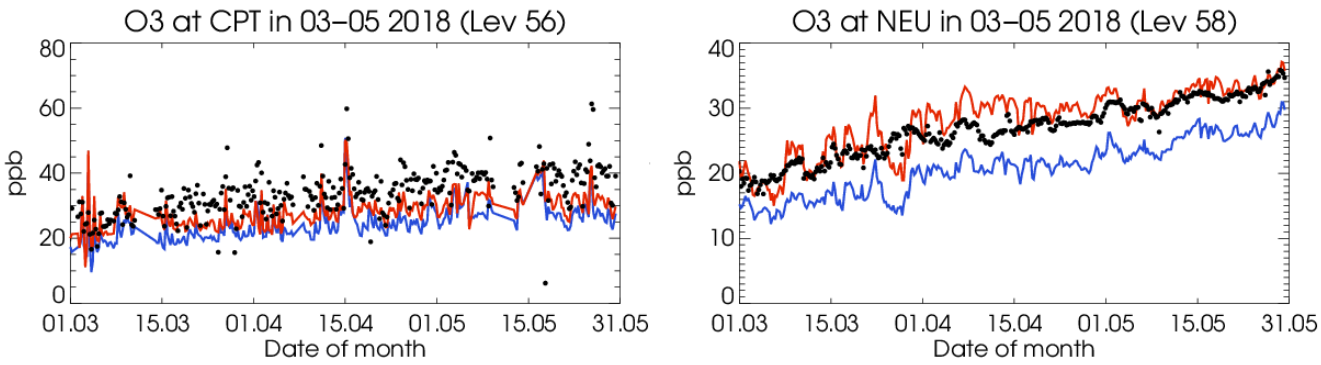

Figure 3.3.8: Time series for the o-suite (red) and control (blue) compared to GAW observations (black dots) at Cape Point (34.55°S, 18.48°W) and GAW observations at Neumayer (70.65°S, 8.25°W).

3.4 Validation with AirBase observations in Mediterranean

The surface ozone validation analysis over the Mediterranean is based on an evaluation against station observations from the Airbase Network (http://acm.eionet.europa.eu/databases/airbase/). In addition, 2 stations from the Department of Labour Inspection - Ministry of Labour and Social Insurance, of Cyprus (http://www.airquality.dli.mlsi.gov.cy/) are used in the validation analysis. For the validation analysis, stations in the Mediterranean located within about 100 km from the shoreline of the Mediterranean shore are used. Table 3.4.1 shows the names, coordinates, elevation and the MNMBs and correlations obtained with the 2 forecast runs (o-suite and control). It indicates that the variance explained by each station of both the o-suite and control is high and correlations are highly significant over Western, Central and Eastern Mediterranean. It should be noted that the o-suite reproduces slightly better than the control run the surface ozone day to day variability over Western Mediterranean (see Table 3.4.1).

In terms of biases, o-suite MNMBs vary between -20% and 20% depending on the stations. The Control MNMBs are on average -7% lower than o-suite MNMBs. Over the stations Plan Aups/Ste Baume in France and Gharb in Malta the o-suite and overestimate surface ozone concentrations by 9% and 1% respectively. Again the Control MNMBs are -7% lower than o-suite MNMBs. Over Agia Marina station in Cyprus the control run accurately reproduce surface ozone mean concentrations (MNMBs≈0%) while the o-suite overestimate it by 7%. Finally at Oros Troodos high altitude station both runs significantly overestimate surface ozone concentrations (MNMBs≈30% see also 3.4.1, lower graphs).

The spatial distribution of MNMBs and the correlation coefficients of the o-suite over the Mediterranean are shown in 3.1.4.2, where it is evident that correlations over the entire Mediterranean from Gibraltar to Cyprus are highly significant.

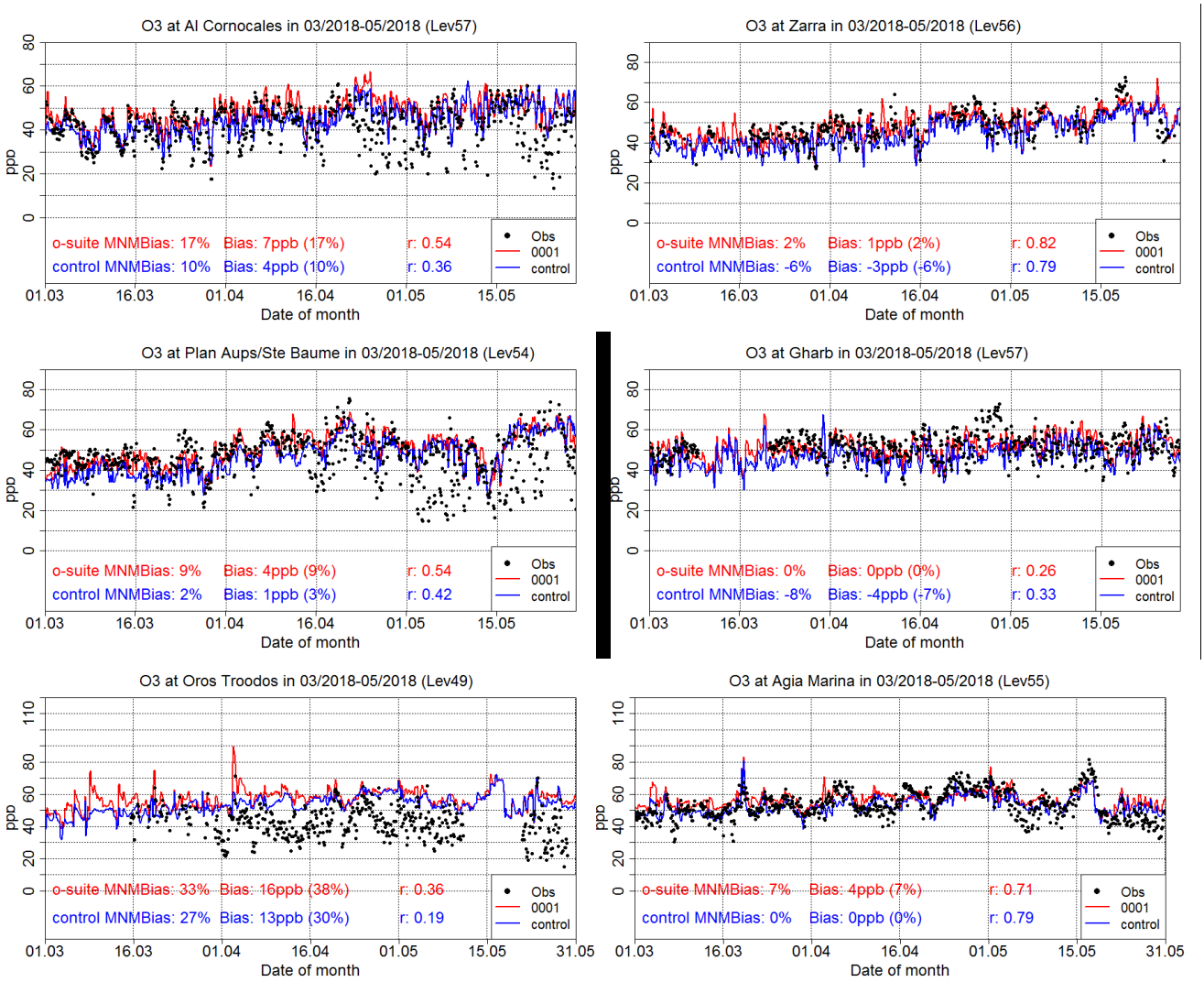

Figure 3.4.1: Time series for the o-suite (red) and Control (blue) compared to Airbase observations at Al Cornocales, Spain station (36.23°N, 5.66 °W, top left), at Zarra, Spain station (39.08°N, 1.10°W, top right), at Plan Aups/Ste Baume, France station (43.34°N, 5.73°E, center left), at Gharb, Malta station (36.07°N, 14.20°E, center right and compared to observations provided by the Department of Labour Inspection - Ministry of Labour and Social Insurance of Cyprus), at Oros Troodos (34.95°N, 32.86°E, low right) and at Agia Marina, Cyprus station (35.04°N, 33.06 °E, low right).

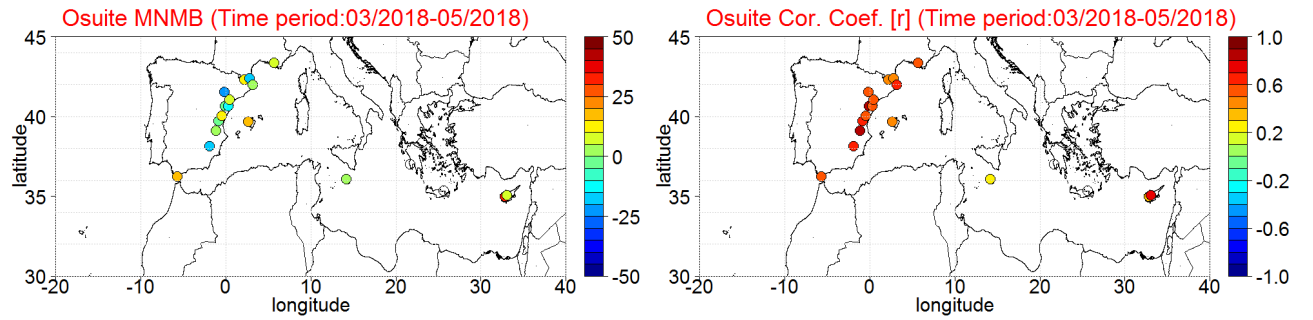

Figure 3.4.2: Spatial distribution of MNMB in % (left) and correlation coefficient (right) of the o-suite run compared to observational data during the period from 1 March 2018 to 31 May 2018.

Table 3.4.1: Coordinates, elevation, corresponding model level (level 60 is the surface level), as well as validation scores (MNMBs and correlations for the period MAM 2018) obtained with the 2 forecast runs (o-suite and control), for each one of the selected Mediterranean stations. MNMBs and correlations with blue denote stations where control run performs better while with red are denoted stations where o-suite performs better.

						Distance from the	MNMB		Cor. Coef	
Station Name	Stat_ID	Lon	Lat	Alt (m)	Level	shore (km)	o-suite	control	o-suite	control
Al Cornocales	ES1648A	-5.66	36.23	189	57	16	16.8	10.1	0.54	0.36
Caravaka	ES1882A	-1.87	38.12	1	60	73	-17.4	-25.5	0.61	0.66
Zarra	ES0012R	-1.10	39.08	885	56	70	1.9	-6.4	0.82	0.79
VIillar Del Arzobispo	ES1671A	-0.83	39.71	430	60	48	-0.8	-8.6	0.62	0.62
Cirat	ES1689A	-0.47	40.05	466	60	37	13.1	5.0	0.59	0.51
Bujaraloz	ES1400A	-0.15	41.51	327	60	60	-21.2	-29.4	0.58	0.58
Morella	ES1441A	-0.09	40.64	1150	53	51	-3.7	-11.6	0.83	0.79
Bc-La Senia	ES1754A	0.29	40.64	428	59	21	-10.0	-18.2	0.57	0.54
Ay-Gandesa	ES1379A	0.44	41.06	368	58	15	6.4	-1.5	0.53	0.53
Ak-Pardines	ES1310A	2.21	42.31	1226	57	81	12.6	4.9	0.44	0.31
Hospital Joan March	ES1827A	2.69	39.68	172	57	3	18.8	11.2	0.42	0.34
Al-Agullana	ES1201A	2.84	42.39	214	60	25	-15.6	-22.8	0.48	0.44
Av-Begur	ES1311A	3.21	41.96	200	56	9	1.8	-5.7	0.64	0.63
Plan Aups/Ste Baume	FR03027	5.73	43.34	675	54	21	9.0	2.5	0.54	0.42
Gharb	MT00007	14.20	36.07	114	57	31	0.2	-7.5	0.26	0.33
Aliartos	GR0001R	23.11	38.37	110	59	18	NA	NA	NA	NA
NEO	-	21.67	37.00	50	60	2	NA	NA	NA	NA
Finokalia	GR0002R	25.67	35.32	250	57	4	NA	NA	NA	NA
Oros Troodos	-	32.86	34.95	1819	49	11	32.7	26.8	0.36	0.19
Agia Marina	CY0002R	33.06	35.04	532	55	14	7.1	0.5	0.71	0.79

3.5 Validation with IASOA surface observations

Model results were compared to O3 observations from the Villum Research Station, Station Nord in north Greenland (81.6oN 16.7oW), Alert Nunavut, Canada (82.5oN 62.5oW), Eureka, Nunavut, Canada (80.1oN 86.4oW), Zeppelin Mountain, Svalbard (78.9oN 11.9oE), and Tiksi, Russia (71.6oN 128.9oE) from the IASOA network, Fig. 3.5.1.

The data from Svalbard and VRS are covering the period from December 2014 to May 2018. Data from Eureka covers the period August 2016 – May 2018, data from Alert covers the period January 2016 – December 2017 and data from Tiksi covers the period September 2016 – February 2018. Ozone depletion events in March – June in 2015 – 2018 are not captured by the model simulations during spring at any of the sites. These events are related to halogen chemistry reactions that are not represented in the model simulations. The simulations are on average in good agreement with the observations apart from the spring depletion events.

For the period March – May 2018 the measurements are not quality controlled. Due to the ozone depletion events the model simulations overestimate measured concentrations, except for the few days without depletion events, where the predicted model levels are in a fair agreement with observations at the sites. This results in large positive bias and low correlation coefficients for the period (Table 3.1.2). One exception from this pattern is the results from Svalbard. Due to the position of the station on a mountaintop depletion events are only rarely recorded and the predicted levels are generally in good agreement with the measurements.

Table 3.5.1. Normalised Mean Bias (NMB) and correlation coefficient (r) of the Control and the O-suite simulations for the sites Alert, Eureka, Svalbard, Tiksi and Villum Research Station (VRS) for the period March – May 2018.

		NMB	R
Alert	o-suite	0.50	0.34
	control	0.49	0.21
Eureka	o-suite	1.15	0.11
	control	1.12	0.03
Svalbard	o-suite	-0.03	0.28
	control	-0.03	0.37
Tiksi	o-suite	0.46	0.47
	control	0.40	0.41
VRS	o-suite	0.18	0.31
	control	0.16	0.20

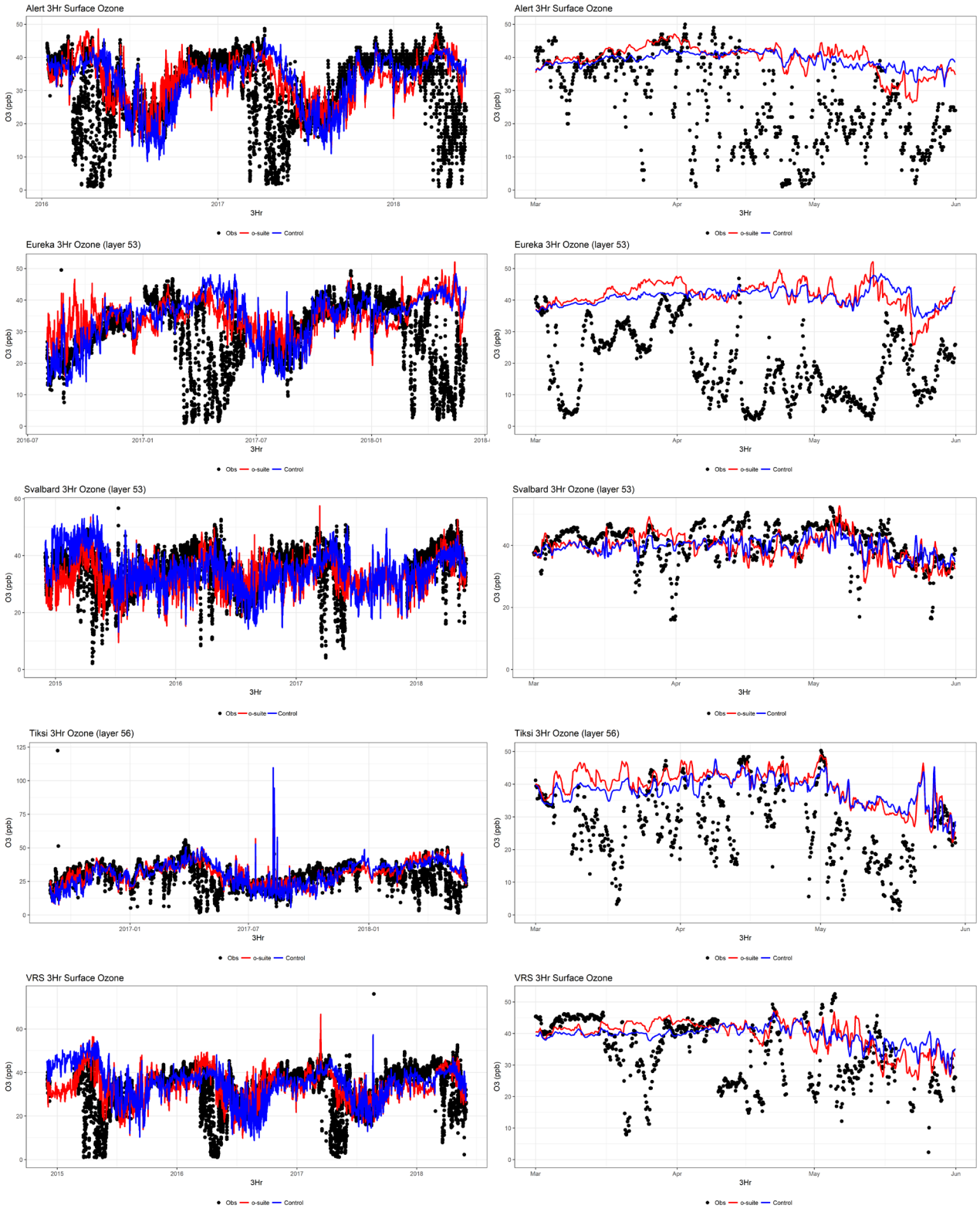

Figure 3.5.1: Time series for o-suite (red) and Control (blue) compared to observations (black dots) at Alert, Nunavut, Canada (Top row) Eureka, Nunavut, Canada (second row), Svalbard (third row), Tiksi, Russia (fourth row) and the Villum Research Station, Station Nord, Greenland (bottom row) for the full period (left) and for December-February (right).

4. Carbon monoxide

4.1 Validation with Global Atmosphere Watch (GAW) Surface Observations

For the Near-Real-Time (NRT) validation, 11 GAW stations have delivered CO surface mixing ratios in NRT and data is compared to model results as described in Douros et al (2017) and is used for CAMS model evaluation for March – May 2018. The latest validation results can be found on the CAMS website: http://www.copernicus-atmosphere.eu/d/services/gac/verif/grg/gaw/

For stations in the Northern Hemisphere, both runs mostly show slightly negative MNMBs. For the stations located in the Southern Hemisphere, the control shows a strong positive offset, which is corrected by the data assimilation for the o-suite.

For stations in Europe, and the Southern hemisphere, the MNMBs and correlation coefficients indicate that the forecast remains stable till the D+4 (forecast run from 96h to 120h).

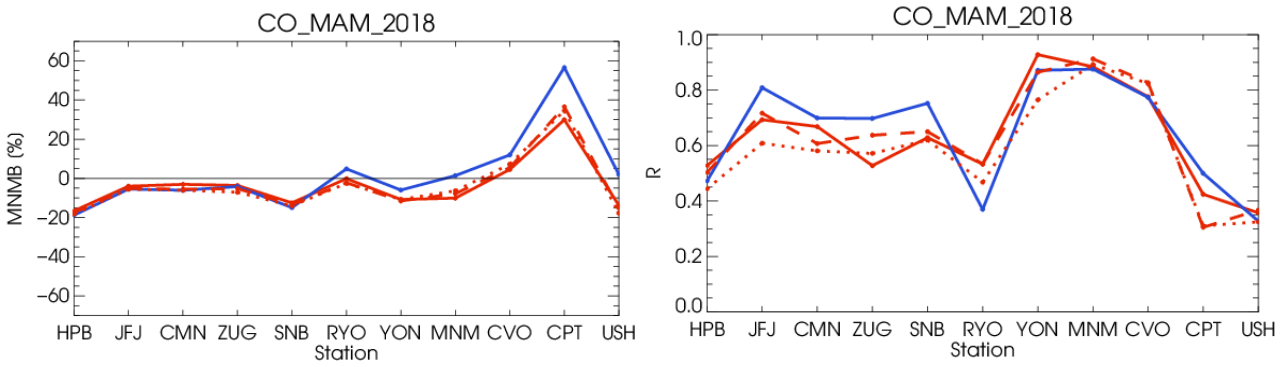

Figure 4.1.1: Modified normalized mean bias in % (left) and correlation coefficient (bottom right) of the NRT model runs compared to observational GAW data in the period March 2018 to May 2018 (o-suite: solid red, D+0: red-dashed, D+4: red-points, and control: blue).

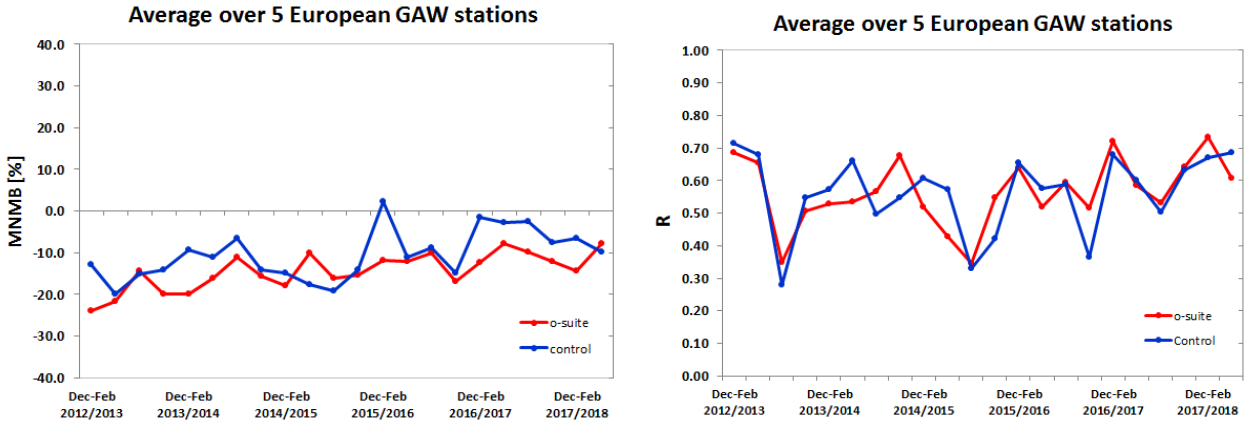

Figure 4.1.2: Long term (Dec. 2012 – May 2018) evolution of seasonal mean MNMB (left) and correlation (right), as averaged over 5 GAW stations in Europe, for o-suite (red) and control (blue).

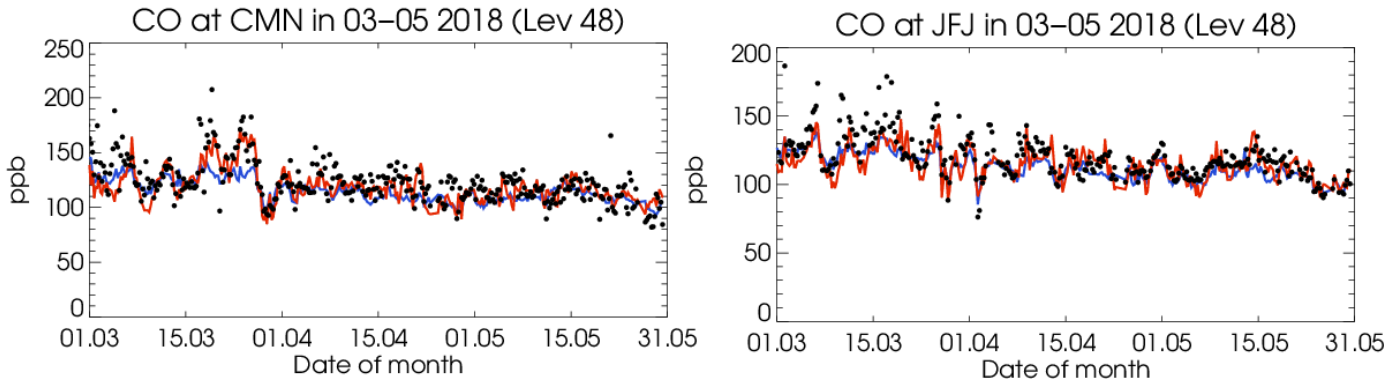

Figure 4.1.3: Time series for the o-suite (red) and control (blue) compared to GAW observations at, Jungfraujoch (46.5°N, 7.9°E) and Monte Cimone (44.18°N, 10.70°E)

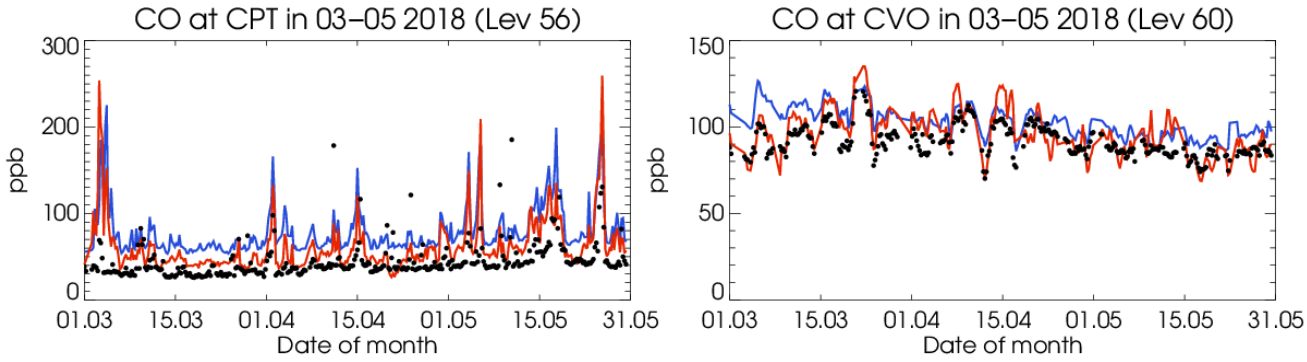

Figure 4.1.4: Time series for the o-suite (red) and control (blue) compared to GAW observations at Cape Point (34.35°S, 18.5°E) and Cape Verde (16.9°N, 24.9°W).

A comparison of the seasonal-mean MNMB over Europe (Fig. 4.1.2) from December 2012 to present shows a slowly improving MNMB from about -20% in 2013 to -10% for more recent periods. Temporal correlation remains relatively constant at r=0.6 on average.

For European stations, the o-suite shows an underestimation of observed CO mixing ratios, with MNMBs between -3% and -16%. The control shows higher CO mixing ratios for European stations with MNMBs between -4% and -18%. Correlation coefficients are between 0.52 and 0.69 for the o-suite and between 0.47 and 0.80 for the control run.

For stations in Asia (RYO, YON, MNM) the o-suite and control are accurately reproducing the observations with MNMBs between 0 and -10% for the o-suite and between 4% and 1% for the control run, see Fig. 4.1.5. Correlation coefficients range between 0.53 and 0.92.

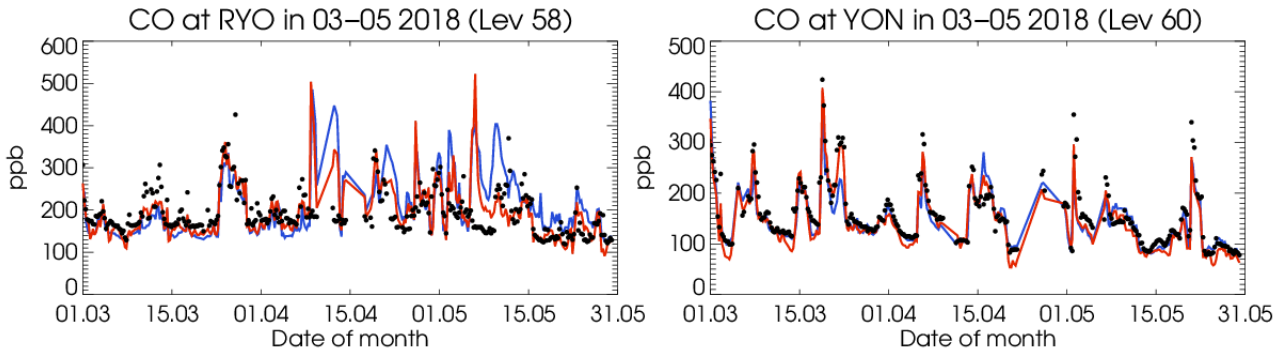

Figure 4.1.5: Time series for the o-suite (red) and control (blue) compared to GAW observations at Ryori (39.03°N, 141.82°E) and Yonagunijima (24.47°N, 123.02°E).

4.2 Validation with IAGOS Data

The daily profiles of ozone and CO measured at airports around the world are shown on the website at http://www.iagos.fr/macc/nrt_day_profiles.php. For the period March to May 2018, data from several aircraft have been validated, as discussed in Sec. 3.2.

Figure 4.2.1 shows the time series of daily mean values in different atmospheric layers over Paris and Frankfurt. At Paris and Frankfurt, the models underestimate CO in both the boundary and surface layer with the largest underestimations in Frankfurt (Fig. 4.2.2). This behavior is more obvious in the individual profiles over Europe (Fig. 4.2.3). In the low stratosphere, models in general overestimate the amount of CO. The best agreement between models and observations is found in the free and upper troposphere.

As mentioned in regional report, the last 10 days of March have been characterized by cold weather in North and Western Europe with temperature below seasonal (see also section 3.2). Around 19 March, times series at Paris shows an increase in CO in surface and boundary layers (Fig. 4.2.1). The profile for 19 and 20 March at Paris are also shown in Fig. 4.2.3. On 19 March, CO mixing ratio is almost constant with 250 ppbv from the surface to the top of the boundary layer. On 20 March, the CO mixing ratio at the surface reaches 300 ppbv. These episodes are likely due to cold weather and increase in CO emissions. For these profiles, the results of CAMS-global and control run are similar, the profiles from the models are nearly constant and both strongly underestimate CO mixing ratios in surface and boundary layers.

As shown in the ozone section; an increase in ozone is observed at Frankfurt in the surface and boundary layer at the end of April around day 20. This increase might be related to the exceptional warm weather in Europe at this period. The CO profile of at Frankfurt on 21 April is correlated to that of ozone with large CO values at the same levels (Fig. 4.2.3). The results of CAMS-global and control run are similar and this increase in CO is not detected by the models.

On 8 May, a strong anomaly in CO is observed in the surface layer with mixing ratio reaching more than 400 ppbv. This CO anomaly is correlated with that of ozone (profiles of the 7, 8 and 9 May) during a period of warm weather (see section 3.2).

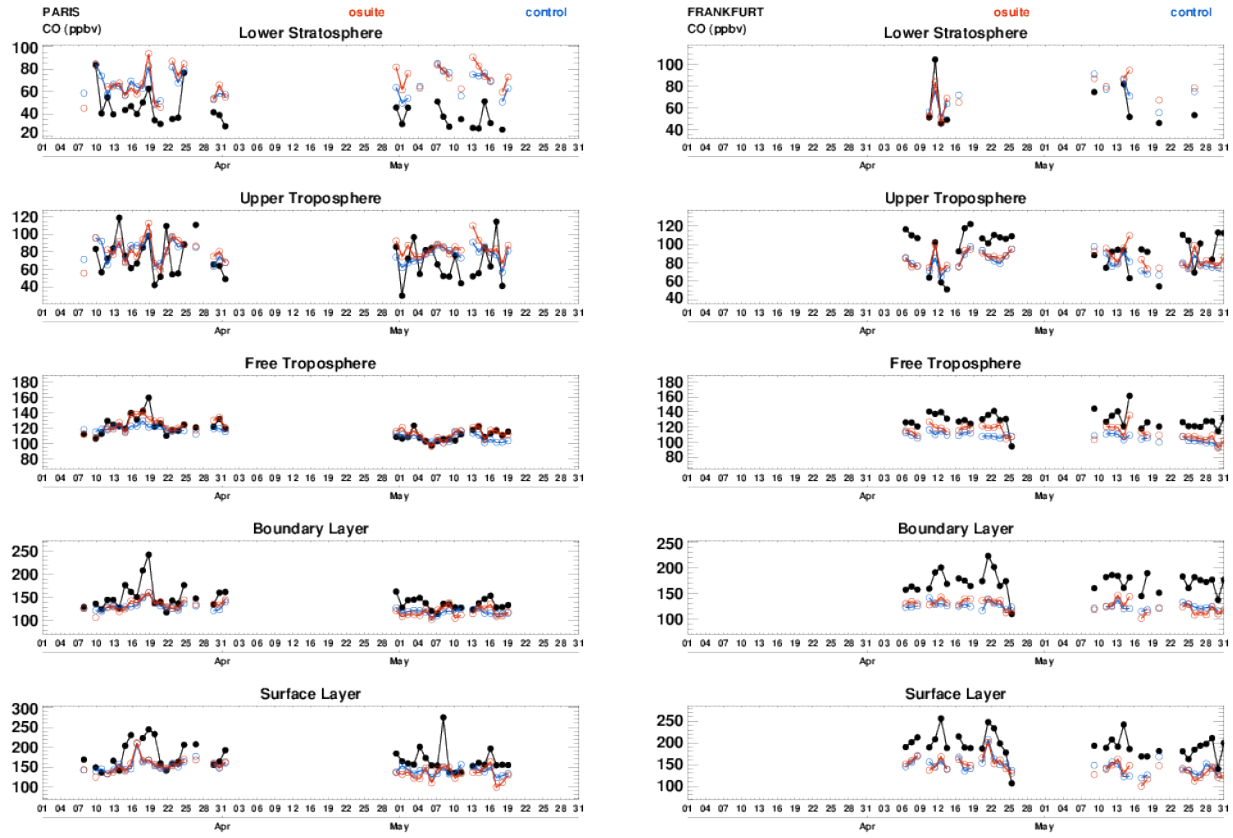

Figure 4.2.1. Time series of daily mean CO over Paris during March – May 2018 for 5 layers, Surface, Boundary layer, Free Troposphere, Upper Troposphere and Lower Stratosphere.

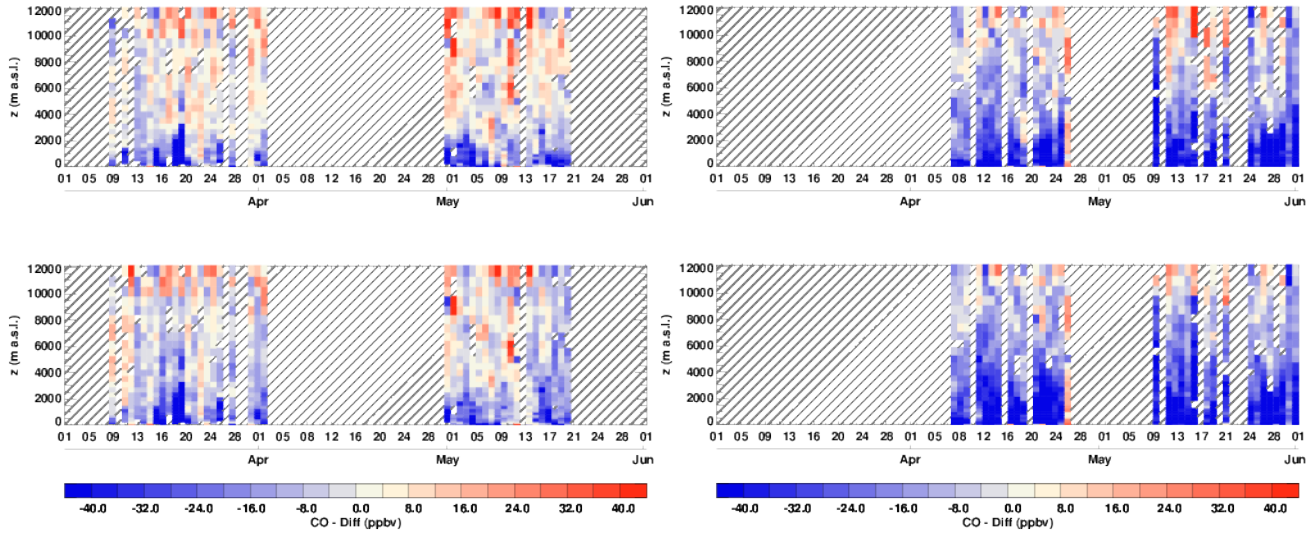

Figure 4.2.2. Time series of the absolute differences (model - observations) in daily profiles for CO over Paris (left) and Frankfurt (right) during March – May 2018. Top panels correspond to o-suite and bottom panels to control run.

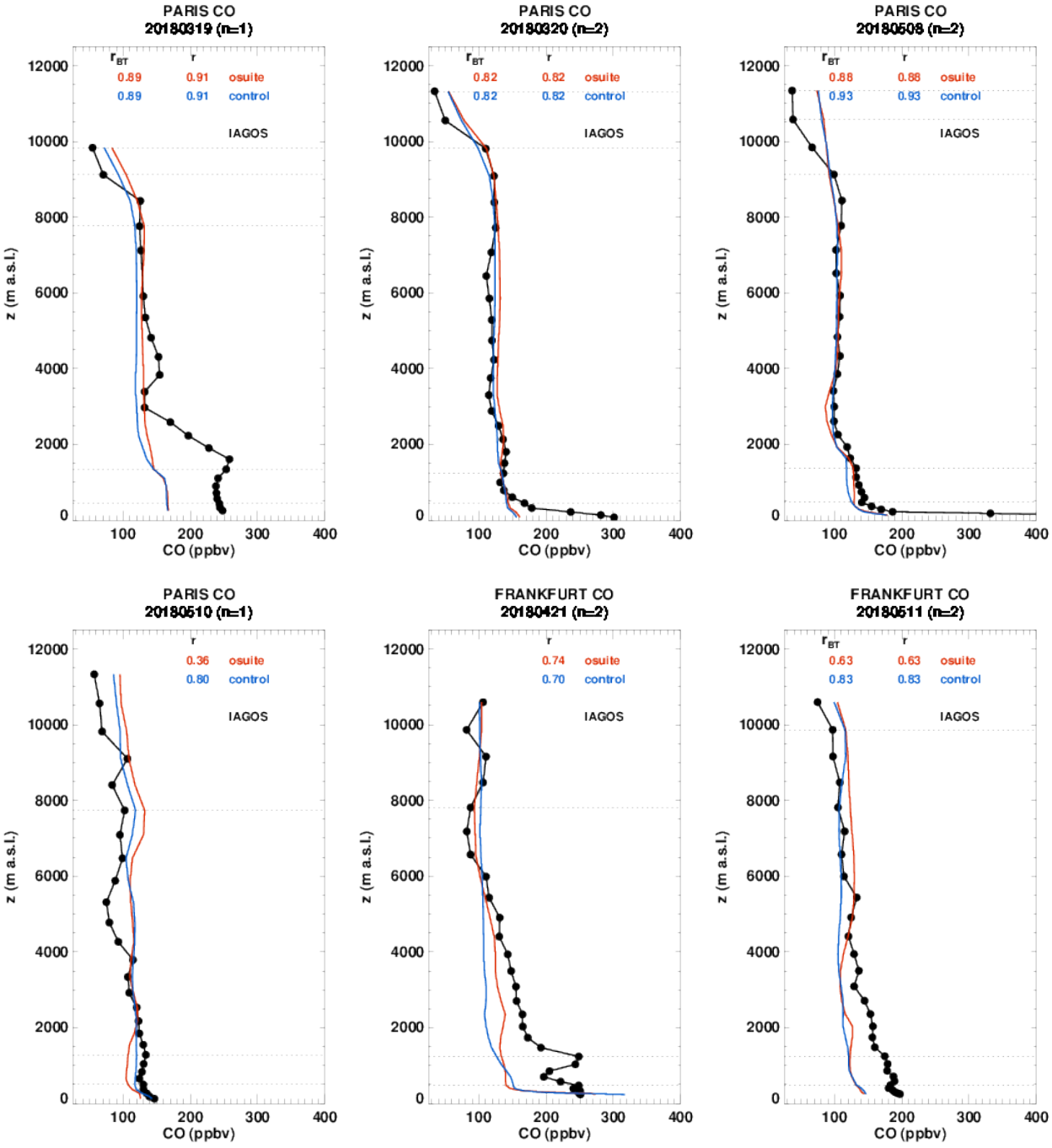

Figure 4.2.3 Selection of daily profiles for ozone from IAGOS (black) and the two NRT runs (o-suite: red, control: blue) over Europe during March – May 2018.

On 10 May, the ozone profile at Paris presented a strong peak between 4000 m and 6000 m (see section 3.2). On Fig. 4.2.3, it can be seen that CO profile on the same day shows a clear decrease in CO values near the same range of altitudes. This is a checkpoint that reinforces the hypothesis of a stratospheric intrusion event. It was also noted that a peak in ozone has been observed at the same altitude a day after in Frankfurt (see section 3.2). Unlike in the case of Paris, the CO profile at Frankfurt on 11 May is not presenting a decrease in CO at the associated altitude and therefore no conclusion can be drawn.

West Africa

Fig. 4.2.4-a-b highlights some examples of profiles for CO over West Africa sampled by Air France aircraft during March – May 2018. The profiles presented here are for airports of Cotonou, Douala , Lome, Brazaville, N'djamena, Niamey and Ouagadougou. These cities are affected by anthropogenic emissions from vehicles, oil industries, and from biomass burning which stretches across Africa just north of the equator from December to March and south of the equator from June to October. The MAM season is outside the period of most intense burning, however at the end of March intense fires occurred in the countries neighbouring the Ivory Coast and peaks in CO were seen in Cotonou, Lome. At the beginning of March, there were also fire in Cameroun and Nigeria, and a peak is observed in Douala. For these peaks, the two models present similar results. The increases in CO are generally seen at the correct altitudes by both o-suite and control run, showing some underestimations in the lower part of the free troposphere (near 2000 m) where the peaks are observed and also in the surface and boundary layer. The pollution at Ouagadougou is significant with levels of CO reaching more than 400 ppbv, which are not always reproduced by the models. With level of CO pollution around 200 ppbv in Brazzaville, N'djamena and Niamey, both models present large overestimations near the surface.

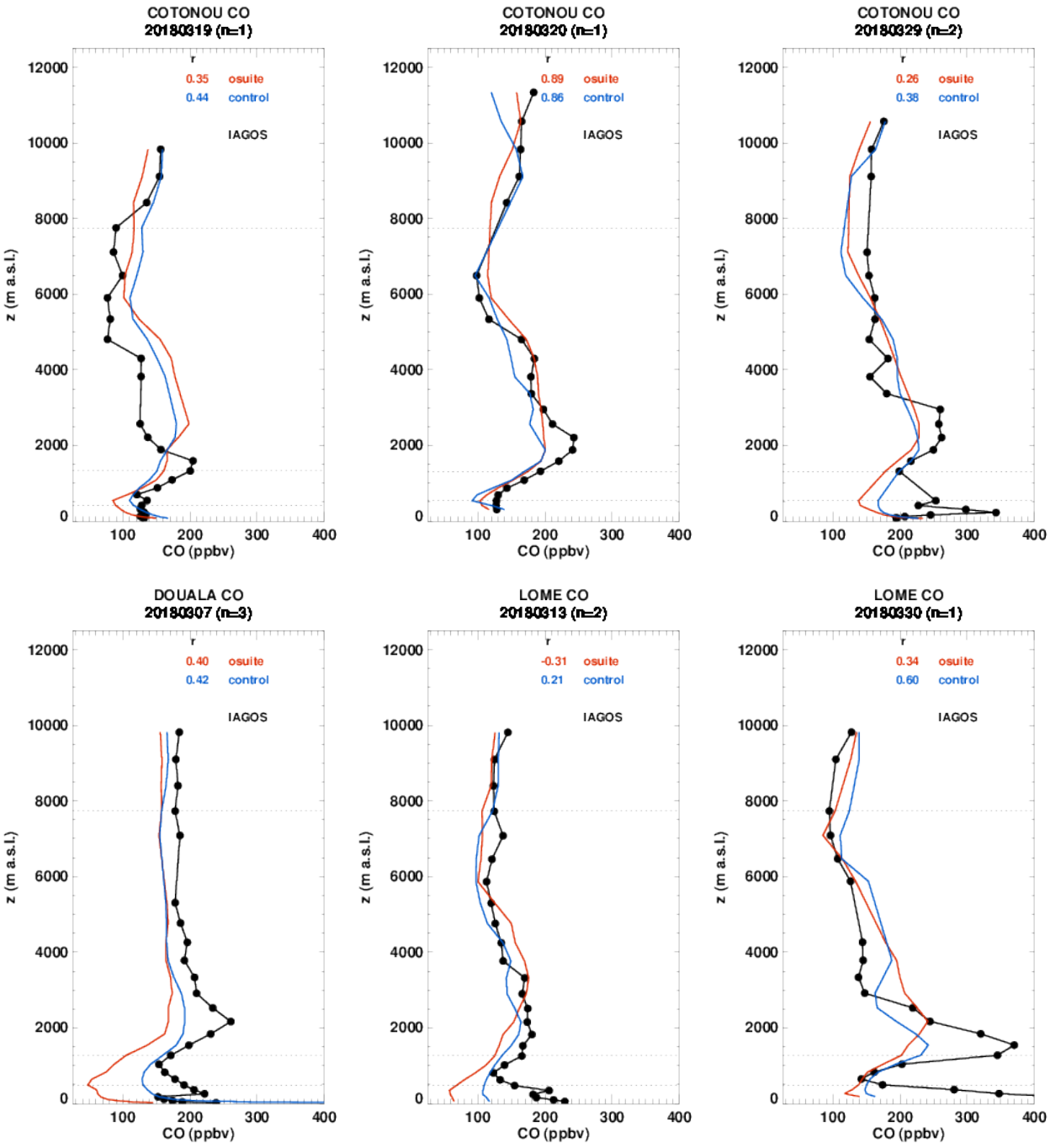

Figure 4.2.4-a Profiles of CO from IAGOS (black) and the two NRT runs over West Africa during March – May 2018.

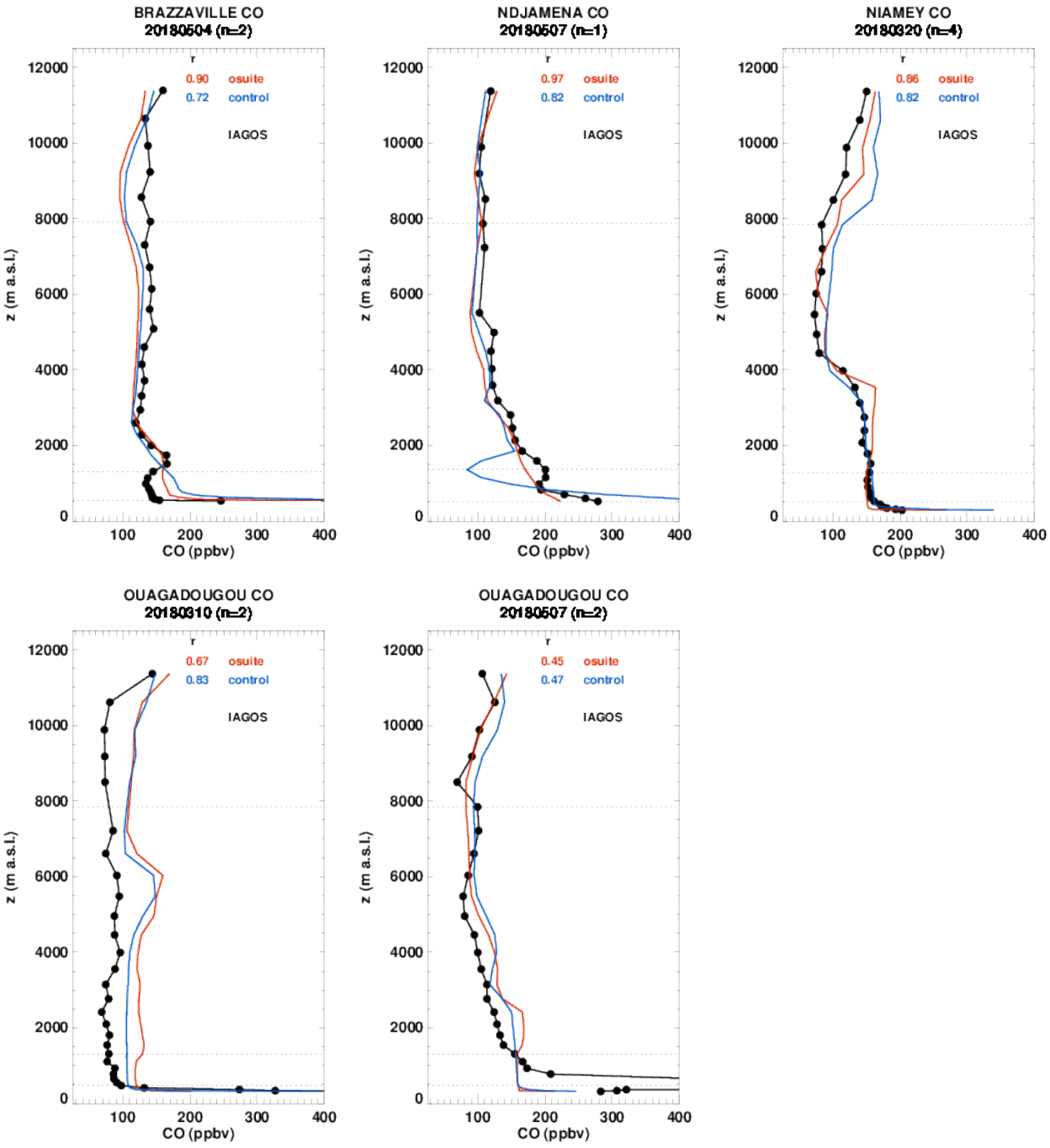

Figure 4.2.4-b Profiles of CO from IAGOS (black) and the two NRT runs over West Africa during March – May 2018.

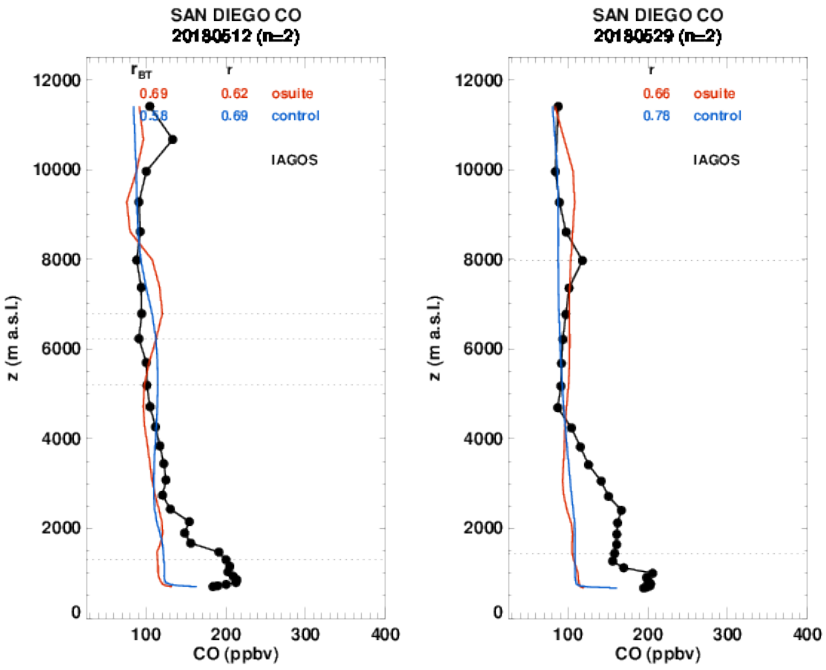

Figure 4.2.5. Profiles of CO from IAGOS (black) and the two NRT runs over North America during March – May 2018.

North America

In North American airports similarly to Europe, it has been shown in previous reports that CO is usually underestimated in the surface and boundary layer by the two runs, while there is a good agreement in the free troposphere. In Fig. 4.2.5, two profiles at San Diego are presented on 12 and 29 May (Fig. 4.2.5). On 12 May, CO mixing ratios reach 200 ppbv in the surface and boundary layers, and are strongly underestimated by both models which behave similarly, with a nearly constant profile of 100 ppbv. On 29 May, the same type of profile is observed and with higher mixing ratios extending up to 3000 m. The results of the models again strongly underestimate the values of CO mixing ratios in the lowest layers. The results in the UTLS are similar for both models and there is good agreement with the observations.

Northeastern Asia

Fig. 4.2.6 highlights profiles at several locations in China, Japan and Thailandia. It should be noted that the worst performance of the models is obtained at Hong Kong and Ho Chi Minh City airport where the profiles of the models are nearly constant with height with small mixing ratios of CO while strong CO peaks are observed by IAGOS in the free troposphere. At the other airports (Qingdao, Osaka, Nagoya, Bangkok and Taipei), the complex shapes of the profiles are rather well reproduced by both models with sometimes shifts in the altitude of the maxima. Regarding the magnitude, no systematic behavior (underestimation/overestimation) can be found here. However, in general the results from the o-suite are often better than those of control run.

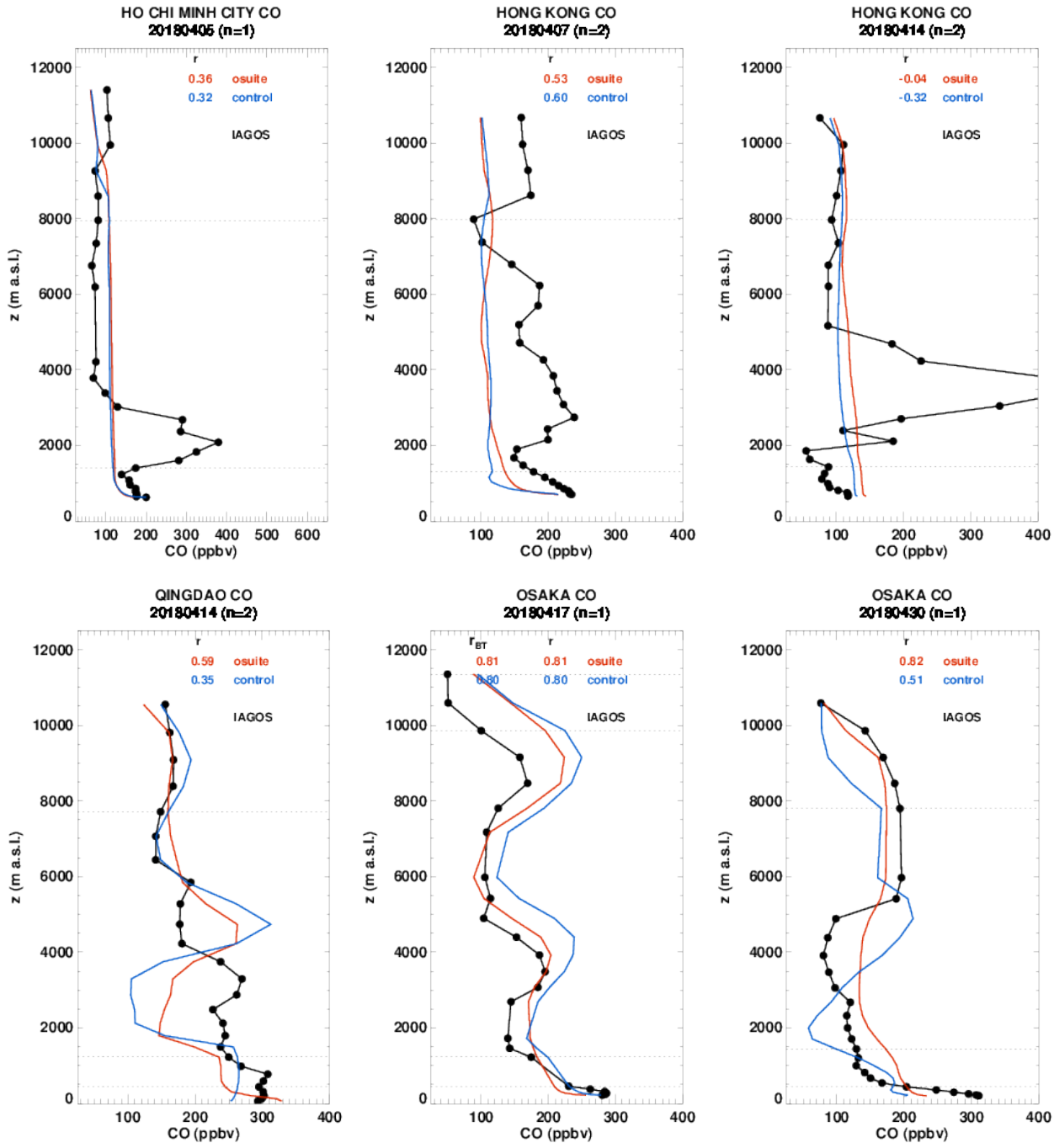

Figure 4.2.6.a Profiles of CO from IAGOS (black) and the two NRT over North Eastern Asia during March – May 2018.

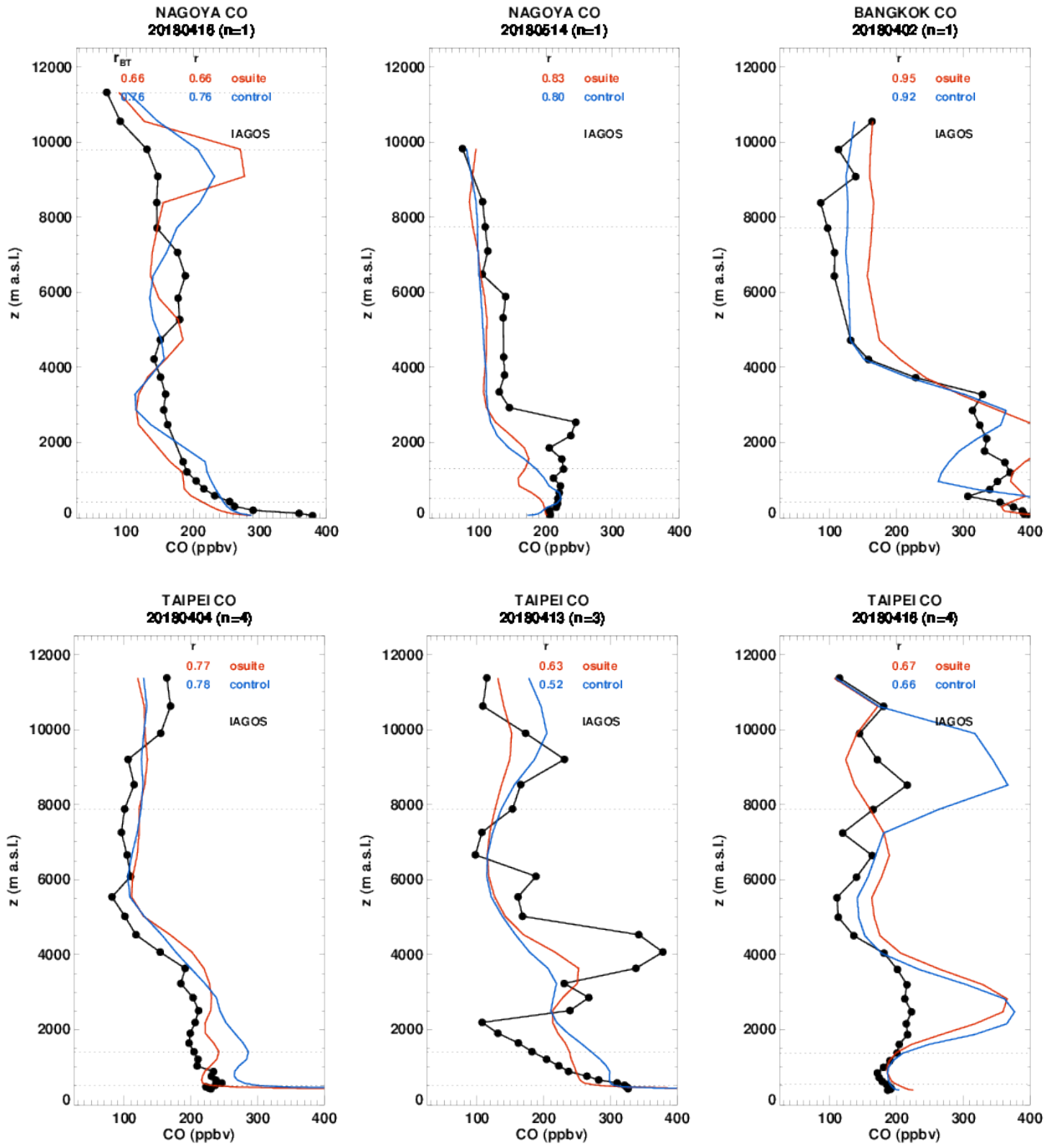

Figure 4.2.6.b Profiles of CO from IAGOS (black) and the two NRT over North Eastern Asia during March – May 2018.

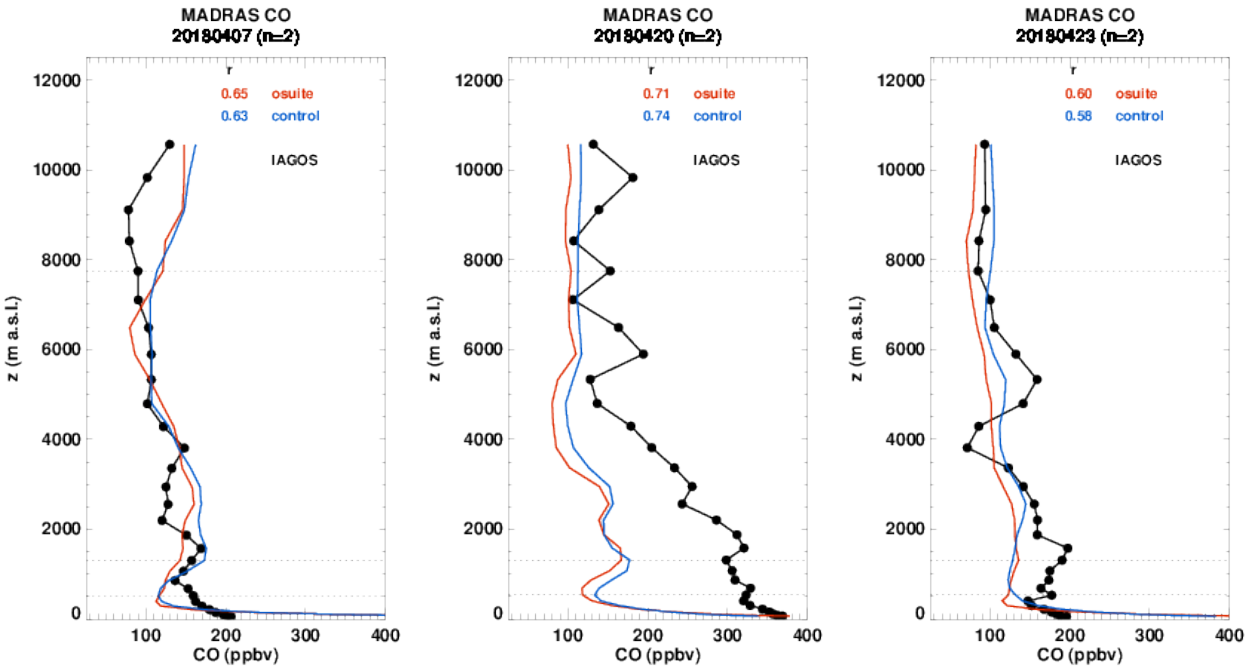

Figure 4.2.7: Profiles of CO from IAGOS (black) and the two NRT over India during March – May 2018.

India

In addition to urban emissions, air quality is also affected by agricultural fires, in particular in northern India particular during the period April to May (pre-monsoon period) and October to November (post-monsoon). Three profiles at Madras are presented in Fig. 4.2.7 for the 7, 20 and 23 May. For all the profiles the results of CAMS-global and control run are similar in all layers of the atmosphere. The overall shape of the profiles is reproduced by the models, but the magnitude of the maxima is often underestimated. These underestimations are largest in the lowest layers of the atmosphere and in the case of extremely high CO mixing ratios such as it is the case for the profile of the 20 April.

Indonesia

In Fig. 4.2.8, three profiles at Jakarta are presented for 11 April, 5 May and 28 May. In all profiles the behavior of the models is similar. The best agreement is found in the UTLS. In the surface, boundary layers and free troposphere the discrepancies between the models and the observations are large. The CO peaks observed in lower troposphere on 5 May are not detected by the models, whereas on 28 May the peak modeled near 1500 m is not present in the observations.

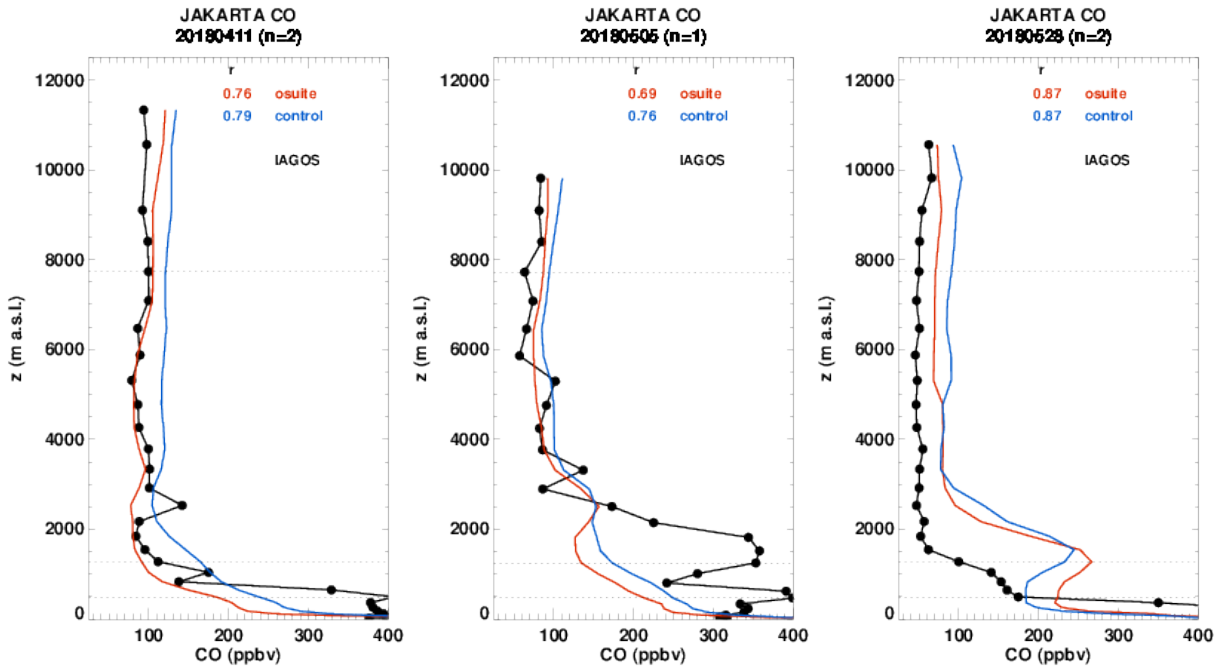

Figure 4.2.8. Selection of daily profiles for ozone from IAGOS (black) and the two NRT runs (o-suite: red, control: blue) over Indonesia during March – May 2018.

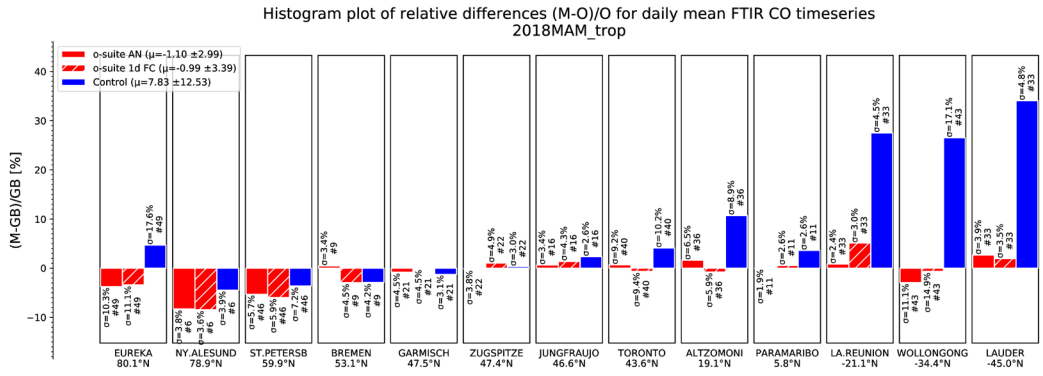

Figure 4.3.1: Seasonal relative mean bias for tropospheric CO columns (MB, %), standard deviation (STD, %) and number of observations used for the considered period MAM 2018, compared to NDACC FTIR observations. The overall uncertainty for the CO measurements is approximately 5%. Stations are sorted with decreasing latitude (northern to southern hemisphere).

4.3 Validation against FTIR observations from the NDACC network

In this section, we compare the CO profiles of the CAMS models with FTIR measurements at different FTIR stations within the NDACC network. These ground-based, remote-sensing instruments are sensitive to the CO abundance in the troposphere and lower stratosphere, i.e. between the surface and up to 20 km altitude. Tropospheric CO profiles and columns are validated. A description of the instruments and applied methodologies can be found at http://nors.aeronomie.be.

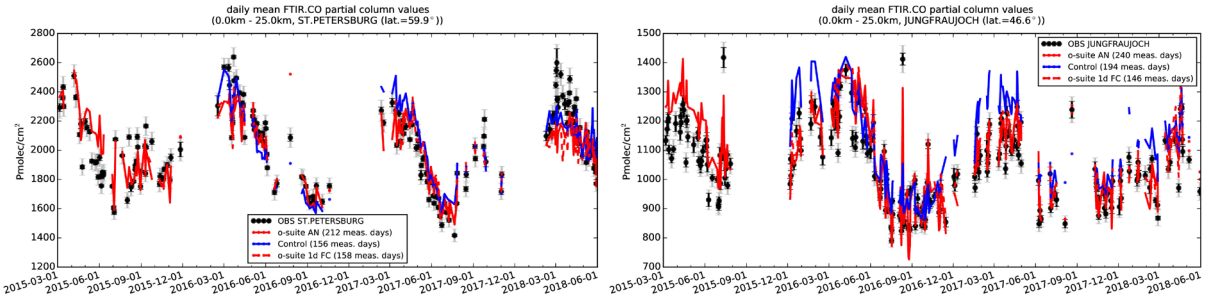

Figure 4.3.2: Daily mean values of tropospheric CO columns by the o-suite (AN and 1d FC, red) and the Control run (blue) compared to NDACC FTIR data at St Petersburg and Jungfraujoch for the period March 2015-May 2018.

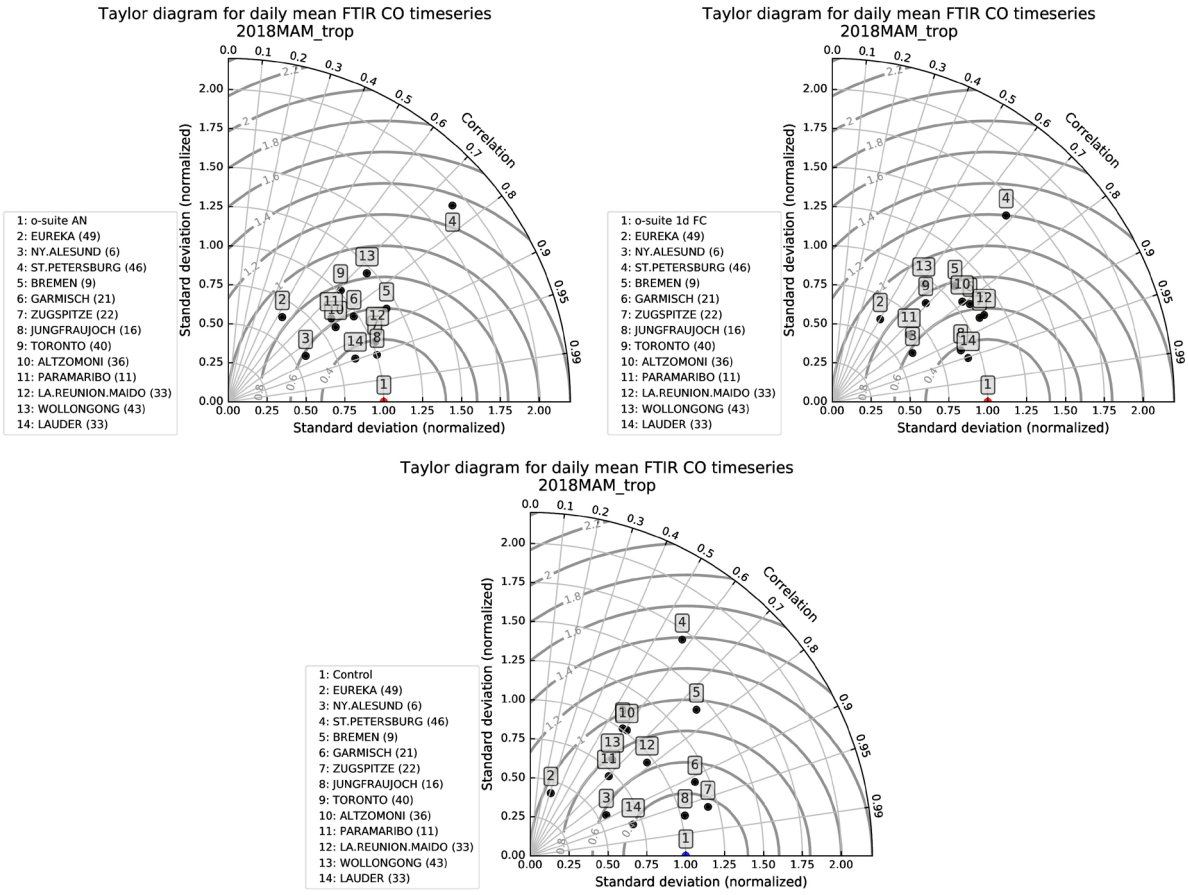

Figure 4.3.3: Taylor diagrams relating the standard deviations for the model and GB time series and their correlation. All time series are normalized such that the std of the model is 1. For the arctic sites (Eureka and Ny Alesund) the variability of the FTIR measurements differs from the variability of the o-suite AN with a factor below 0.5. At St – Petersburg the reverse is observed.

Figure 4.3.1 show that the o-suite tropospheric columns of CO agree well. All biases for the o-suite AN and 1d FC are within the measurements uncertainty.

For all stations in the southern hemisphere, the control run overestimates the CO with MBs up to 20%-30%.

The Taylor diagrams in Figure 4.3.3 provide information on the correlation of all three models under consideration with the FTIR time series. Leaving out the sites with few measurements, the assimilation has a positive effect on the correlation coefficient. Looking at the correlation values, the o-suite 1d FC seems to perform slightly worse compared the o-suite AN. The variability in the FTIR tropospheric columns is in general smaller than the variability of the corresponding model columns (approximately by a factor of 0.75). At St. Petersburg the opposite is observed: the FTIR signal is more variable than the model (see Figure 4.3.2).

4.4 Evaluation with MOPITT and IASI data

In this section, modeled CO total columns are compared to MOPITT versions 6 and 7 (thermal infrared radiances) (Emmons et. al., 2009, Deeter et al., 2010) and IASI satellite retrievals (Clerbaux et al., 2009). Figure 4.4.1 shows the global distribution of CO total columns retrieved from MOPITT V7 (top left) and IASI (top right) and the relative biases of the model runs with respect to MOPITT V7, averaged for April 2018.

Both, MOPITT and IASI show high CO values over East Asia, Thailand, India, the Siberian fire region and the biomass burning area in central Africa, with IASI values being higher than MOPITT in these regions. The modeled CO geographical distribution and magnitude of values show that the model performs reasonably well. The relative difference between the model runs and MOPITT shows that both model runs have positive biases over East Asia and the Siberian fire region of up to 50%. The control run shows overestimations also in the Indonesian region and in biomass burning regions in South America and Africa of up to 40 %. In general, the o-suite performs better than the control run without data assimilation, with some overestimations (up to 20%) in the equatorial region and tropics in the Northern Hemisphere with some regional exceptions and underestimations (up to -20%) in mid-latitudes. The control run shows overestimations in the Southern Hemisphere by about 20-30% and in the tropics in the Northern Hemisphere (up to 20%) and underestimations in the northern mid-latitudes (up to -20%).

Figure 4.4.1 shows no significant difference between the o-suite analysis and 2nd and 4th forecast days. Figure 4.4.2 shows time series of CO total column for MOPITT V6 and V7, IASI and the model runs over the eight selected regions. For the comparison with MOPITT, the modelled CO concentrations were transformed using MOPITT V7 averaging kernels (Deeter, 2004). Both, MOPITT and IASI CO total columns are assimilated in the o-suite run, while a bias correction scheme is applied to IASI data to bring it in line with MOPITT. MOPITT and IASI CO total columns show a relatively similar variability over different regions. IASI CO values were lower compared to MOPITT over most regions with some seasonal exceptions till the year 2016. Since then IASI and MOPITT are more consistent with each other over Europe, US and East Asia regions. Significant difference between MOPITT and IASI are observed over the Alaskan and Siberian fire regions in winter seasons, with IASI CO total column values lower up to 30 %. In North and South Africa, deviations become larger since 2016 with IASI values being higher than MOPITT by to 20%.

The modelled seasonality of CO total columns is in relatively good agreement with the retrievals. In general, the comparison between the o-suite and control runs shows that assimilation of satellite CO has a more positive, pronounced impact on model results over East and South Asia, South Africa, and since the end of 2016 over the US region in winter and spring seasons, and smaller impact over the other regions. Since June 2016 the o-suite shows very good agreement with the satellite

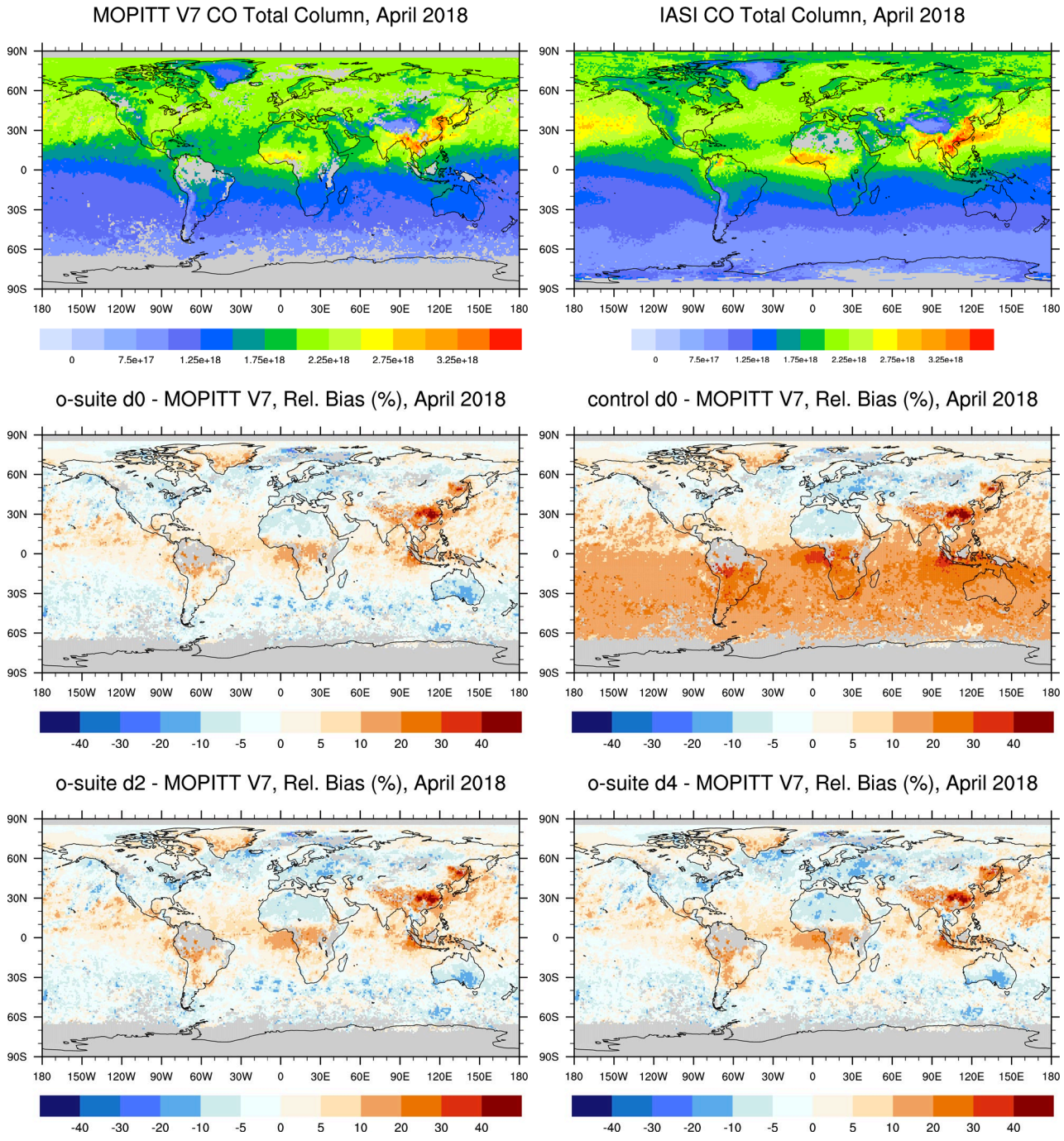

Fig. 4.4.1: CO total columns for MOPITT V7 (top left) and IASI (top right) satellite retrievals and relative difference between the model runs and MOPITT for April 2018: o-suite (middle left), control run (middle right), o-suite 2nd forecast day (bottom left), o-suite 4th forecast day (bottom right). Grey color indicates missing values.

retrievals over Europe and the US region with biases of less than 5 %. In May 2018 Siberian and Alaskan fire regions show a rapid increase of the modelled CO total columns which is inconsistent with the satellite data (except for o-suite run in Alaskan fire region). More details will be shown in the case studies section.

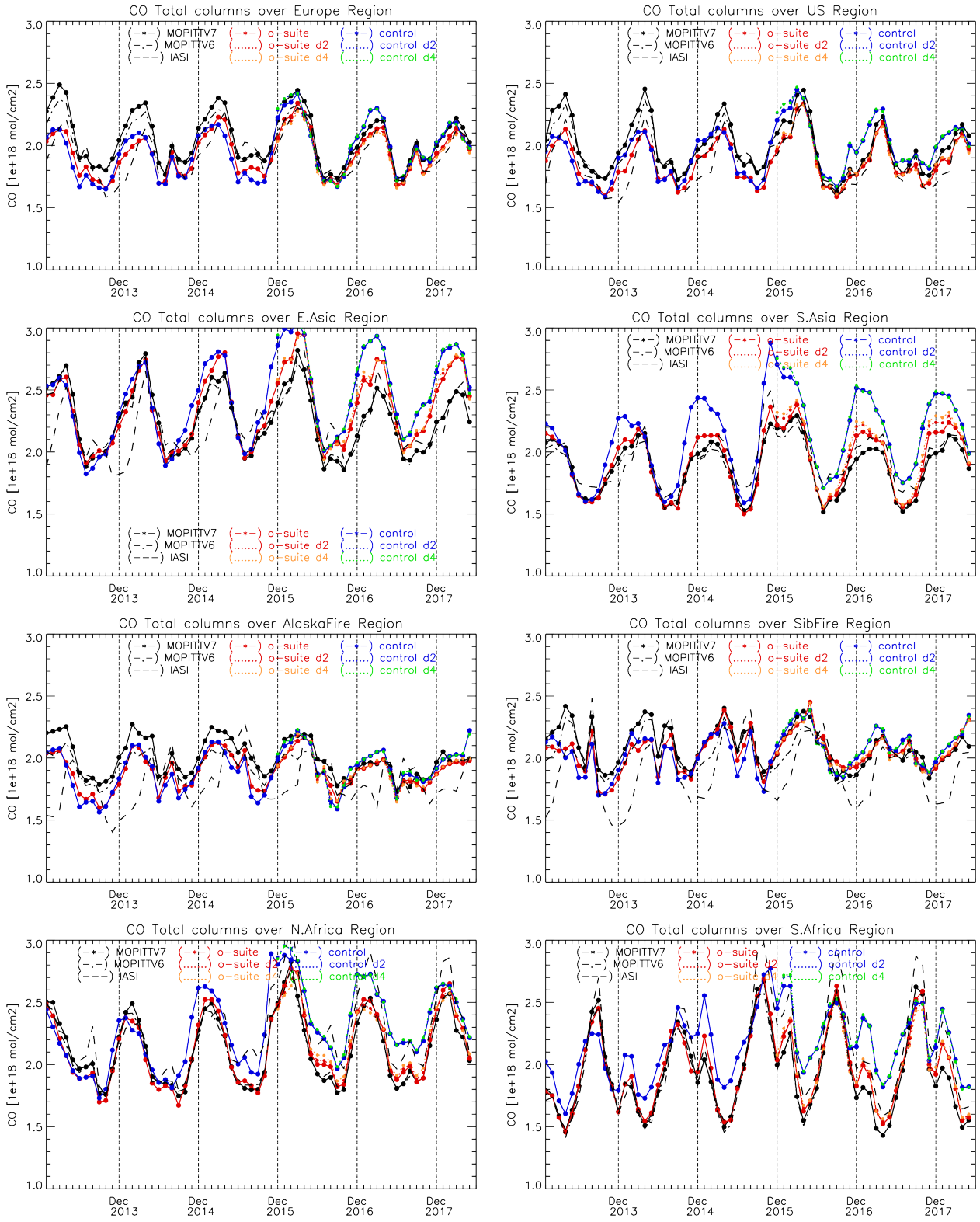

Fig. 4.4.2: Time series of CO total columns for satellite retrievals MOPIT V6 and V7, IASI (black) and the model runs over the selected regions: o-suite (red, solid), control (blue, solid), o-suite 2nd forecast day (red, dotted), o-suite 4th forecast day (orange, dotted), control 2nd forecast day (blue, dotted), control 4th forecast day (green, dotted).

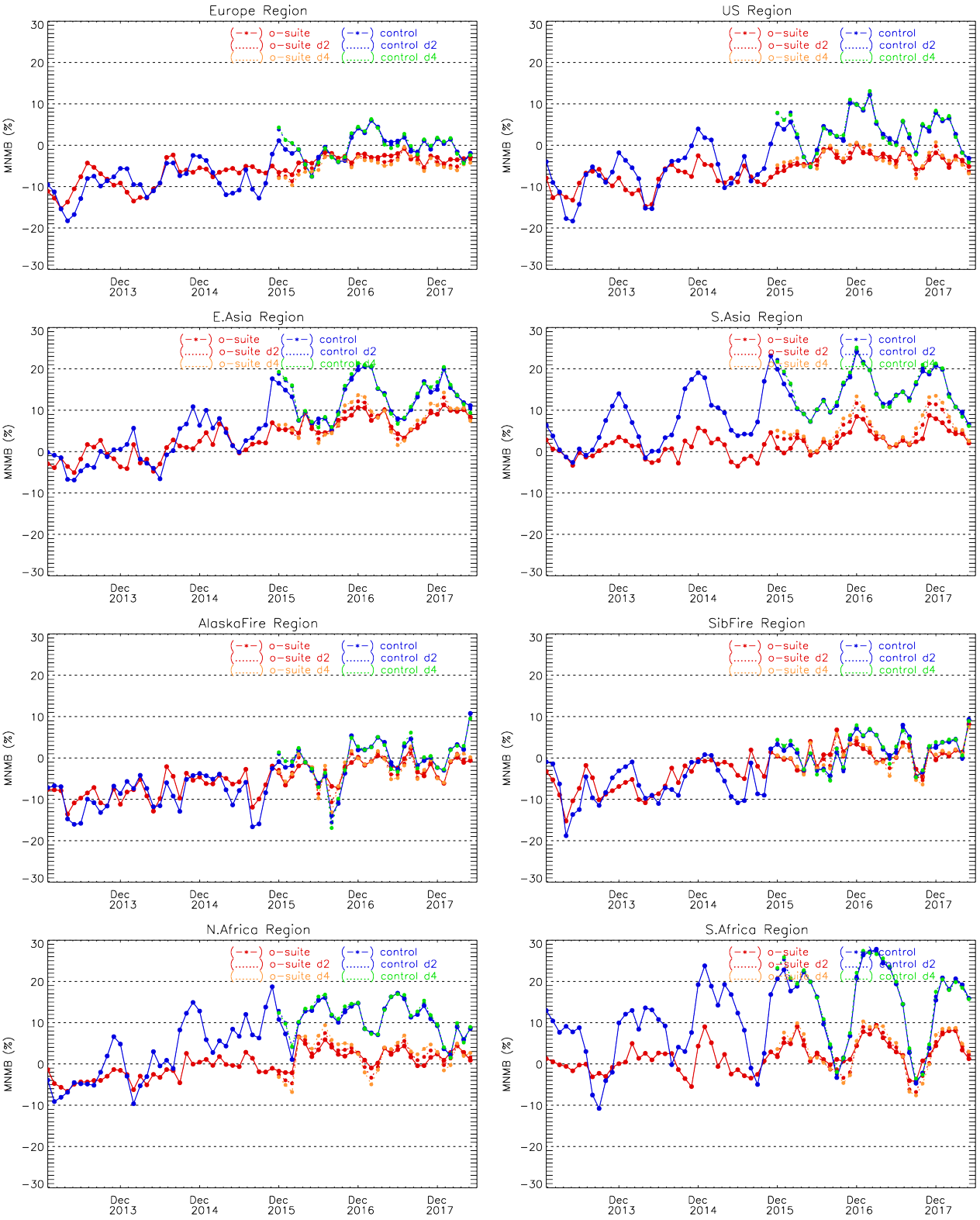

Fig. 4.4.3: Modified normalized mean bias (%) for CO total columns from the model simulations vs MOPITT V7 retrievals over selected regions. O-suite (red, solid), control run (blue, solid), o-suite 2nd forecast day (red, dotted), o-suite 4th forecast day (orange, dotted), control 2nd forecast day (blue, dotted), control 4th forecast day (green, dotted).

The modified normalized mean bias (MNMB) of the model runs compared to MOPITT V7 (Fig. 4.4.3) allows quantifying the impact of the assimilation on the model performance. The o-suite model run shows negative biases over Europe, the US and Alaskan fire regions with some seasonal exceptions. The control run shows a systematic positive bias of up to 20% over South Asia in November-December 2014, 2015, 2016, and 2017. Over southern Africa the control run overestimates satellite retrieved values by up to 25% in the seasonal maximum in winter and spring 2015, 2016, and 2017. In general, the o-suite is within +/- 10% in all regions, while the control run shows larger biases in East and South Asia and North and South Africa, as well as a stronger seasonal cycle. For the control run, d0, d2 and d4 forecast days are almost similar. For the o-suite run, d2 and d4 forecast days show growing positive/negative biases of up to 5 % compared to the analysis d0 in East and South Asia and North and South Africa. In spring 2018 the o-suite run shows better agreement with the satellite observations than the control run over the Asian and African regions with biases within 10%. In May 2018, o-suite performs reasonably over the Alaskan fire region while the control run overestimates satellite data by 10%. Over Siberian fire regions both runs overestimate observations by 10%. The o-suite shows a systematic growing positive bias within 5% for d2 and d4 in autumn-winters in East and South Asia and in summer-autumns in North Africa and a negative growing bias within 5% in winters in North Africa and autumns in South Africa.

5. Tropospheric nitrogen dioxide

5.1 Evaluation against GOME-2 retrievals

In this section, model columns of tropospheric NO_2 are compared to SCIAMACHY/Envisat NO_2 satellite retrievals (IUP-UB v0.7) [Richter et al., 2005] for model data before April 2012, and to GOME-2/MetOp-A NO2 satellite retrievals (IUP-UB v1.0) [Richter et al., 2011] for more recent simulations. This satellite data provides excellent coverage in space and time and very good statistics. However, only integrated tropospheric columns are available and the satellite data is always taken at the same local time, roughly 10:00 LT for SCIAMACHY and 09:30 LT for GOME-2, and at clear sky only. Therefore, model data are vertically integrated, interpolated in time and then sampled to match the satellite data. GOME-2 data were gridded to model resolution (i.e. 0.4° deg x 0.4° deg). Model data were treated with the same reference sector subtraction approach as the satellite data. Uncertainties in NO_2 satellite retrievals are large and depend on the region and season. Winter values in mid and high latitudes are usually associated with larger error margins. As a rough estimate, systematic uncertainties in regions with significant pollution are on the order of 20% – 30%.

Figure 5.1.1 shows global maps of GOME-2 and model monthly mean tropospheric NO_2 columns as well as differences between retrievals and simulations for April 2018 as an example of the maps for spring 2018. The overall spatial distribution and magnitude of tropospheric NO_2 is well reproduced by both model runs, indicating that emission patterns and NO_x photochemistry are reasonably represented. Some differences are apparent between observations and simulations, with generally larger shipping signals simulated by the models. For example, shipping signals are much more pronounced in model simulations to the south of India. Springtime emissions over central European pollution hotspots are underestimated . However, other local maxima of values observed over anthropogenic emission hotspots in East Asia (e.g. over the heavily populated Sichuan Basin; 30°N, 105°E), India and others such as Teheran, Mecca, Helsinki and Moscow are overestimated. NOx Fire emissions around Sierra Leone/Guinea (West Afrrica), Nepal (South Asia) and over East Russia seem to be overestimated by both model runs (see www.gmes-atmosphere.eu/d/services/gac/nrt/fire_radiative_power/ to compare to satellite based fire radiative power), features known from previous NRT reports. Note that the overestimation in East Russia also occurs for HCHO, mixed results are found around Sierra Leone, while for Nepal HCHO values are in better agreement (see chapter 5.1). This may indicate that fire emission factors are probably more reasonable for HCHO than for NO_2 for some some regions compared to others.

Closer inspection of the seasonal variation of tropospheric NO_2 in some selected regions (Fig. 5.1.2) reveals significant differences between the models and points to some simulation problems. Over regions where anthropogenic emissions are major contributors to NO_x emissions, models catch the shape of the satellite time series rather well. However, over East-Asia absolute values and seasonality were in previous years strongly underestimated by all model runs (most likely due to an underestimation of anthropogenic emissions), with the o-suite showing the best results since an upgrade in July 2012. As NO_2 column retrievals decreased since 2014, model simulated values are in better agreement with the satellite retrieved ones for recent years. However, this decrease in values is not reproduced by the simulations which in contrast to satellite observations show an

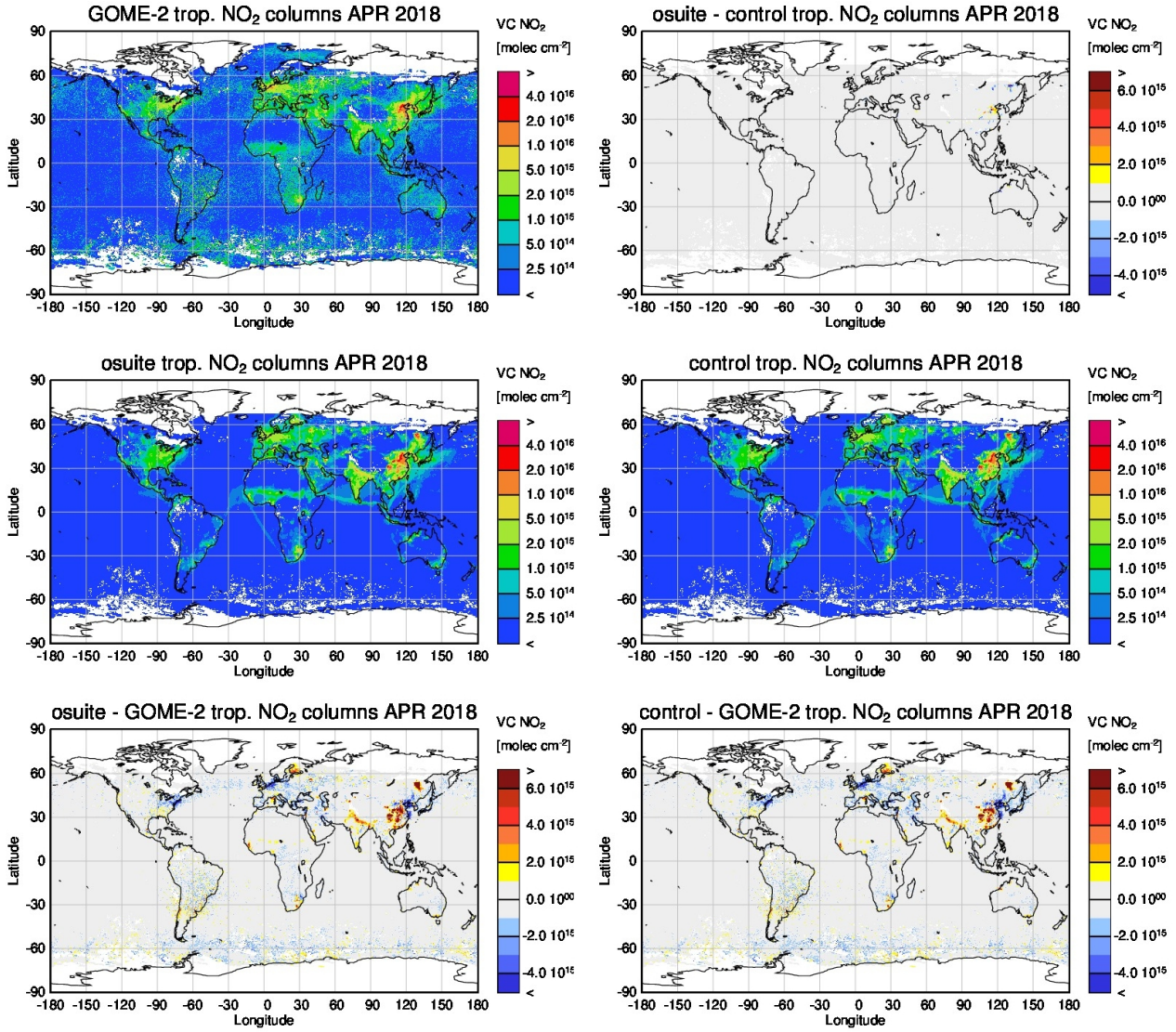

Figure 5.1.1: Global map comparisons of satellite retrieved and model simulated tropospheric NO_2 columns [molec cm^{-2}] for April 2018. The top row shows monthly mean tropospheric NO_2 columns retrieved by GOME-2 as well as the difference between o-suite and control, the second row shows the corresponding tropospheric NO_2 columns for model simulated averages. The third row shows differences of monthly means between models and GOME-2. GOME-2 data were gridded to model resolution (i.e. 0.4° deg x 0.4° deg). Model data were treated with the same reference sector subtraction approach as the satellite data.

increase over the complete timeseries of simulations available and as such, the better agreement for more recent years cannot be attributed to an improvement of the simulations. Springtime and summertime model values increased in 2015 compared to previous years, which is in contrast to the satellite retrievals, so that the simulated values for the summers since 2015 are about 50% larger than satellite retrieved ones. As for East-Asia, a decrease in satellite retrieved values also occurs in 2015 over Europe where a peak is usually found around January, which is, as a result, only slightly underestimated by the models for January 2015. The underestimation of tropospheric NO_2 columns over Europe may be caused to some extent by a change of emission inventories in 2012. However, the situation changed over the last three winter periods, for which GOME-2 shows (compared to previous years) a strong increase in January peak values, combined with a decrease in values for

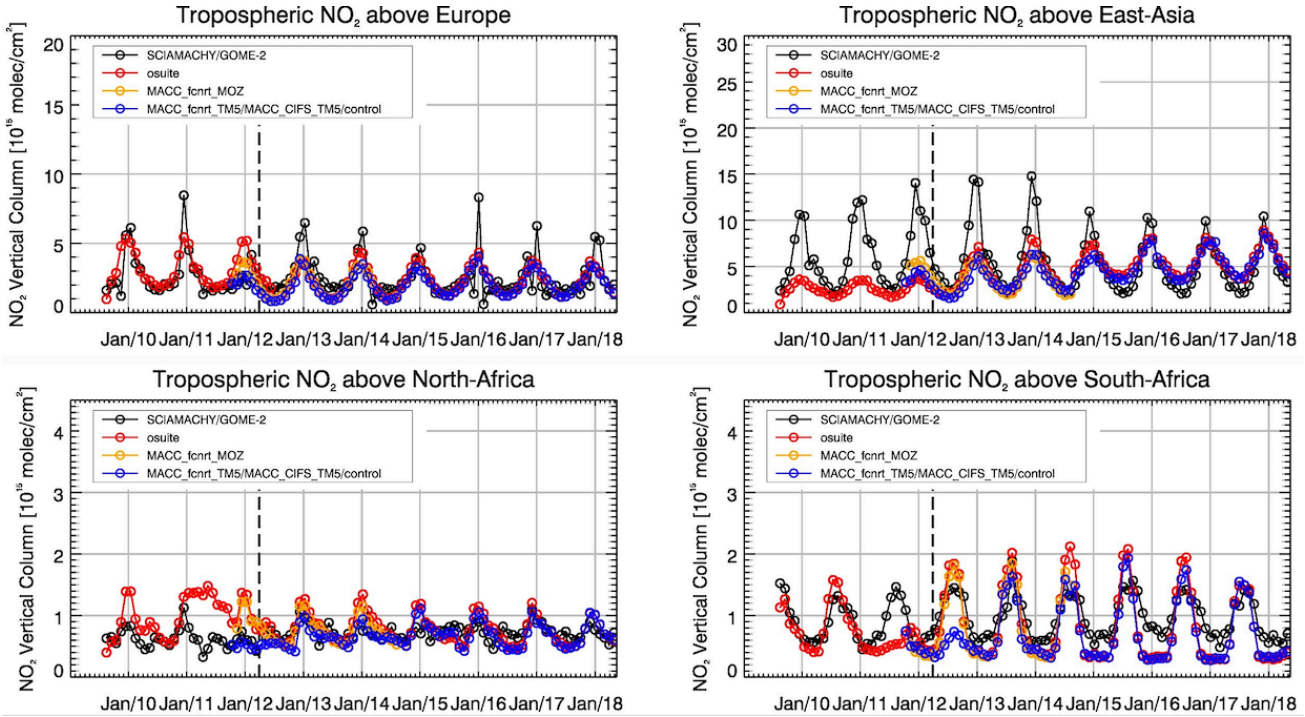

Figure 5.1.2: Time series of average tropospheric NO_2 columns [10^{15} molec cm^{-2}] from SCIAMACHY (up to March 2012) and GOME-2 (from April 2012 onwards) compared to model results for different regions (see Annex 2 for definition of regions). Upper panels represent regions dominated by anthropogenic emissions, lower panels represent those dominated by biomass burning. The blue line shows MACC_fcnrt_TM5 from November 2011 to November 2012, MACC_CIFS_TM5 results from December 2012 to August 2014 and control results from September 2014 onwards (the model run without data assimilation is termed control since Sep 2014). Vertical dashed black lines mark the change from SCIAMACHY to GOME-2 based comparisons in April 2012.

December and February, which is not reproduced by the models. It is not clear if the GOME-2 observations are realistic here, although a first inspection of daily GOME-2 satellite images did not point to problems regarding the retrieval.

Over regions where biomass burning is the major contributor to NO_x emissions, seasonality and amplitude of model columns are determined by fire emissions. The seasonality for the two regions in Africa is simulated reasonably well for 2010 and after October 2011. In the time period in between, a bug in reading fire emissions lead to simulation errors for all MOZART runs. Over North-Africa, the o-suite shows improved results since an update in July 2012 and the change to IFS-CB05 in September 2014. However, tropospheric NO_2 columns around December are still overestimated by the models. Summertime NO_2 columns over North-Africa are underestimated compared to the satellite data from 2015 onwards. The models (especially the o-suite) strongly overestimate the seasonal cycle for South-Africa for 2014 -2016 with an overestimation of the seasonal maximum which usually occurs around August of each year (e.g. by a factor of 1.4 larger compared to GOME-2 retrievals in August 2016). However, summertime values are in better agreement with the upgrade of the o-suite in 2017. For 2014 model runs without data assimilation agree much better with satellite observations, in contrast to more recent CB05-based o-suite runs since 2015.

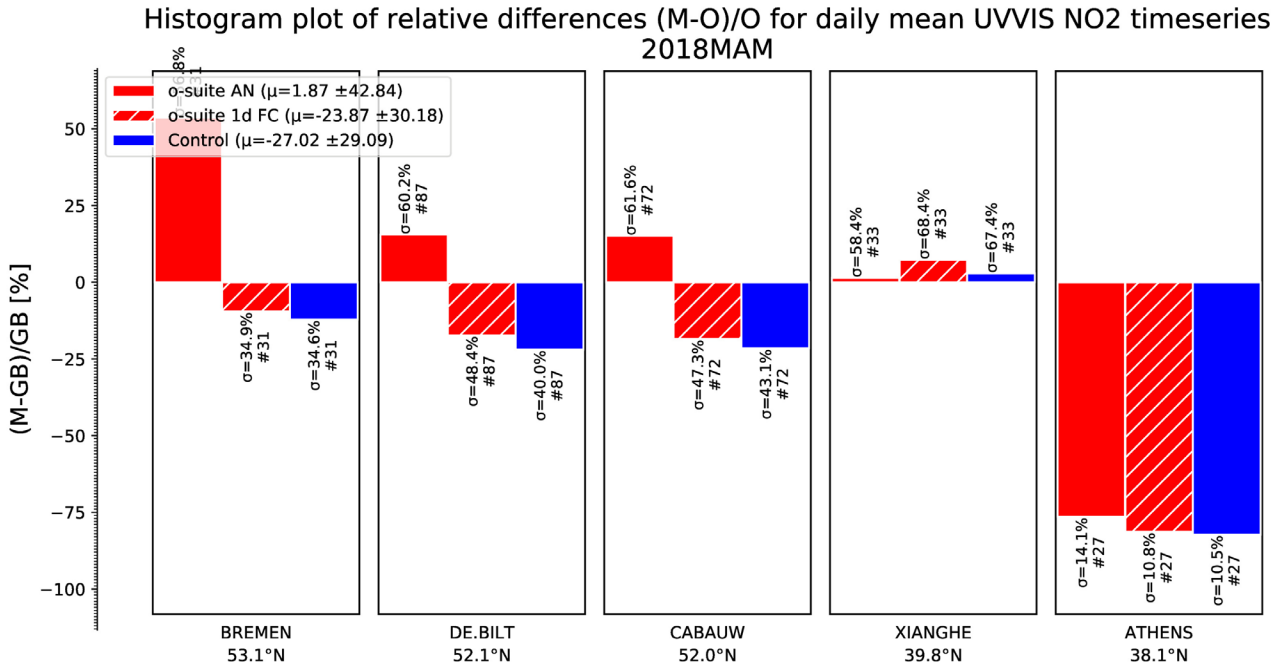

Figure 5.2.1: Table diagram showing the seasonal bias (March –May 2018) for five stations, sorted by latitude.

For November 2015 and November 2016, satellite retrieved values over South-Africa do not decrease below 1x10^{15} molec/cm^2, a feature which did not show up in the time series before. However, this changed again in November 2017.

Details on the NO_2 evaluation can be found at:
http://www.doas-bremen.de/macc/macc_veri_iup_home.html.

5.2 Evaluation against ground-based DOAS observations

In this section, we compare the NO_2 columns of the CAMS models with UVVIS DOAS measurements at Xianghe (39.8°N, 117°E, station near Beijing, altitude 92m) and column data from the other stations.[1] This ground-based, remote-sensing instrument is sensitive to the NO_2 abundance in the lower troposphere, up to 1km altitude with an estimated uncertainty of 8%. Tropospheric NO_2 profiles and columns are validated (up to 3.5km or 10km). A description of the instruments and applied methodologies is the same all DOAS OFFAXIS measurements, see http://nors.aeronomie.be. It is important to mention here that the model partial column values are calculated from the smoothed model profiles. This guarantees that the model levels where the measurement is not sensitive do not contribute to the observed bias. We should mention that the measurement data is still catalogued as rapid delivery and not in the consolidated NDACC database.

[1] No contribution from Reunion and OHP due to instrument failure.

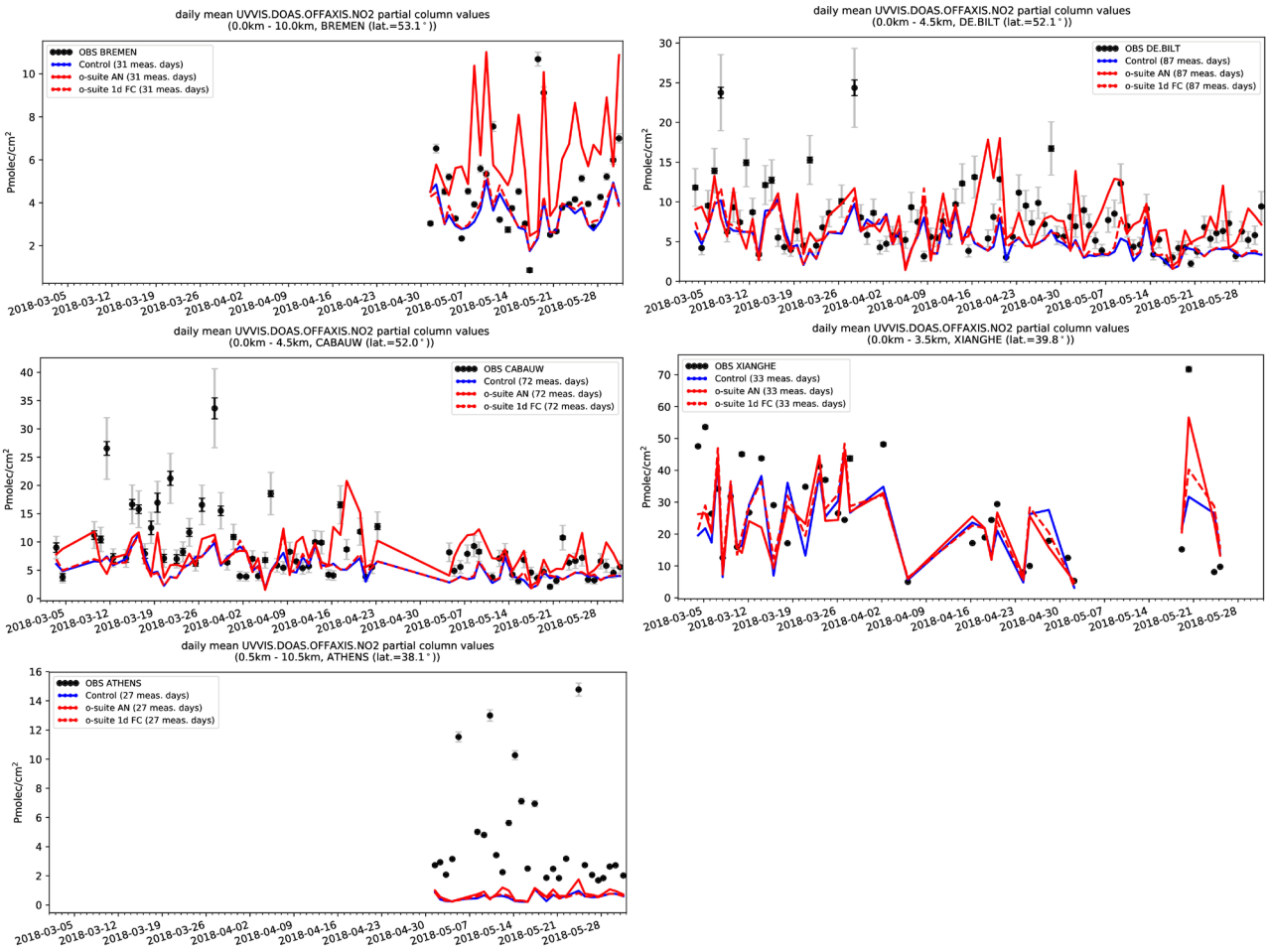

Figure 5.2.2: Time series of NO_2 partial columns at the five different sites. For all sites except Athens, background concentrations are well captured by the model and the o-suite AN sees some of the high pollution days.

Fig. 5.2.1 shows the biases for March-May 2018 at the different sites. Both Bremen and Athens are outliers (both stations cover the time period only partially Fig 5.2.2). For all sites except Athens, the o-suite AN overestimates the NO_2 concentrations. At Athens a strong underestimation is observed. The o-suite is able to capture some of the high pollution events.

6. Formaldehyde

6.1 Validation against satellite data

In this section, simulations of tropospheric formaldehyde are compared to SCIAMACHY/Envisat HCHO satellite retrievals (IUP-UB v1.0) [Wittrock et al., 2006] for model data before April 2012 and to GOME-2/MetOp-A HCHO data (IUP-UB v1.0) [Vrekoussis et al., 2010] afterwards. As the retrieval is performed in the UV part of the spectrum where less light is available and the HCHO absorption signal is smaller than that of NO_2, the uncertainty of monthly mean HCHO columns is relatively large (20% – 40%) and both noise and systematic offsets have an influence on the results. However, absolute values and seasonality are retrieved more accurately over HCHO hotspots.

In Figure 6.1.1, monthly mean satellite HCHO columns are compared to model results for April 2018. The magnitude of oceanic and continental background values and the overall spatial distribution are well represented by the o-suite and control. The models overestimate values over Northern Australia and Central Africa which could be fire or biogenic emissions. The same is true for fire emissions over East Russia, where an overestimation was also found for tropospheric NO_2 (see chapter 3.2). However, the overestimation over fire regions around Nepal reported for tropospheric NO_2 does not occur for HCHO, indicating that emission factors for HCHO are probably more reasonable here than for NO_2.

Time series in Fig. 6.1.2 highlight three cases:

- East-Asia and the Eastern US, where HCHO is dominated by biogenic emissions. Model results and measurements generally agree rather well. However, all model runs underestimate the yearly cycle over East-Asia since 2012. In contrast to MOZART runs, MACC_CIFS_TM5 overestimates satellite values for the Eastern US since the middle of 2013. However, the newer IFS-CB05 runs perform well for Eastern US since 2015. For recent years and both regions, there is virtually no difference between the most recent o-suite run with IFS-CB05 chemistry and the corresponding control run without data assimilation. The variability or “ups and downs” in HCHO columns observed by GOME-2 since December 2014 is due to the lack of data (caused by instrument degradation) for these regions during Northern Hemisphere winter months (see Fig. 6.1.1 for the spatial coverage of HCHO data in December 2017). This also explains the negative values in the GOME-2 time series for Eastern US which occur in the time series since December 2015 and is a likely reason for the relatively large underestimation of values during DJF 2016/2017 by the models compared to the retrievals. Summertime maxima are still underestimated by the now higher resolution runs over East-Asia for 2016 and 2017.
- North-Africa, where biomass burning as well as biogenic sources largely contribute to HCHO and its precursors. Satellite observations over North-Africa are generally overestimated by IFS-CB05 chemistry model runs and also the latest higher resolution model versions since July 2016.

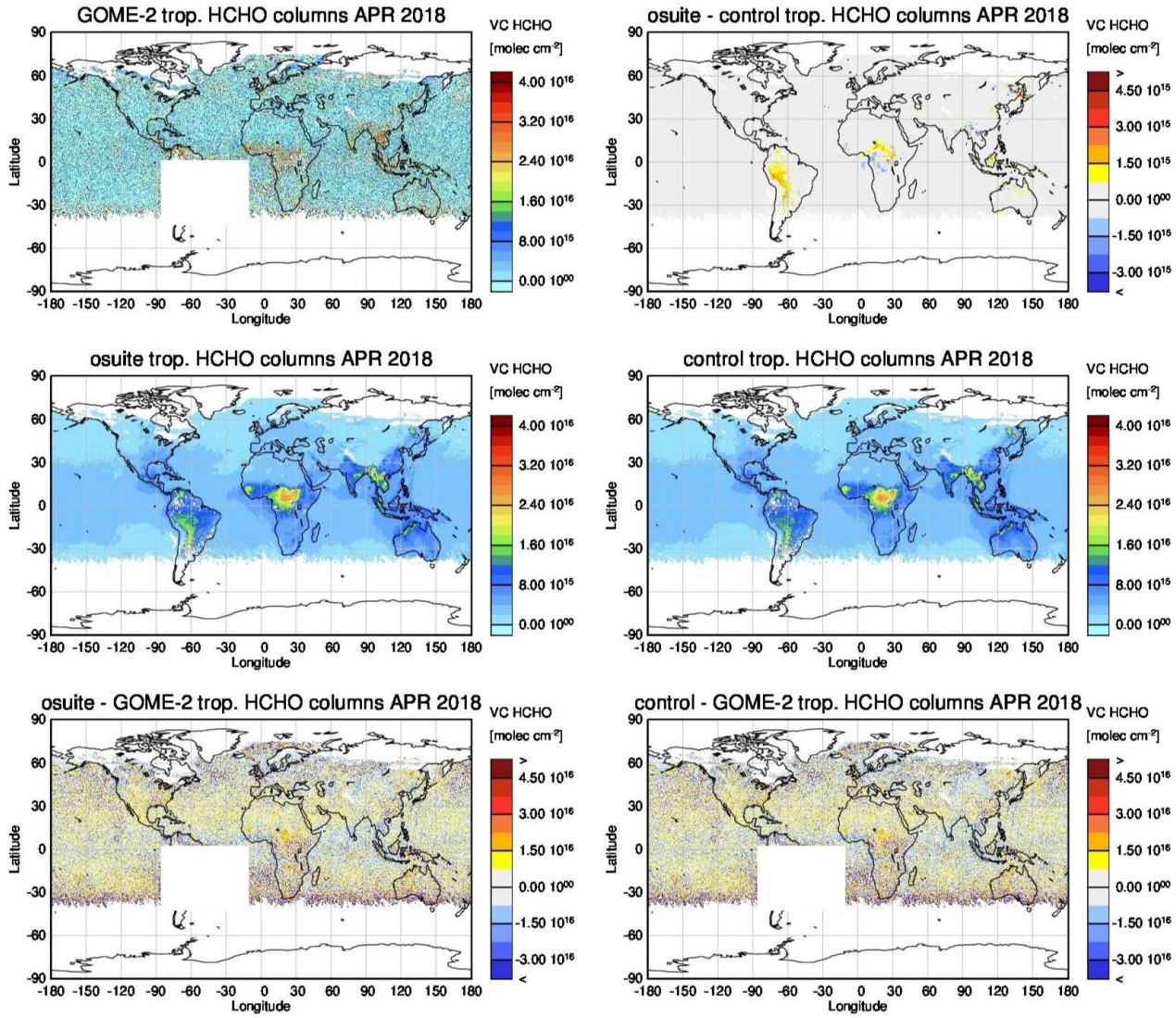

Figure 6.1.1: Global map comparisons of satellite retrieved and model simulated tropospheric HCHO columns [molec cm^{-2}] for April 2018. The top row shows monthly mean tropospheric HCHO columns retrieved by GOME-2, the second row shows the same but for model simulated averages. The third row shows differences of monthly means between models and GOME-2. GOME-2 data were gridded to model resolution (i.e. 0.4° deg x 0.4° deg). Model data were treated with the same reference sector subtraction approach as the satellite data. Satellite retrieved values in the region of the South Atlantic anomaly are not valid and therefore masked out (white boxes in all images except those which show model results only).

- Indonesia, where HCHO is also dominated by biogenic sources and biomass burning. Old MOZART based model versions generally overestimate satellite values here (by a factor of 3 – 4 in the second half of 2010) and fail to reproduce the observed seasonality. This may be due to the use of fire emissions including El Nino years which experience much larger fire activities. MOZART simulations and observations agree much better since late 2012. IFS-CB05 runs agree very well with satellite retrieved ones for December 2014 to August 2015. For September and October 2015, satellite retrieved HCHO columns show a pronounced maximum. 2015 was a strong El Nino year, which caused droughts and higher fire activity in Indonesia. As for previous

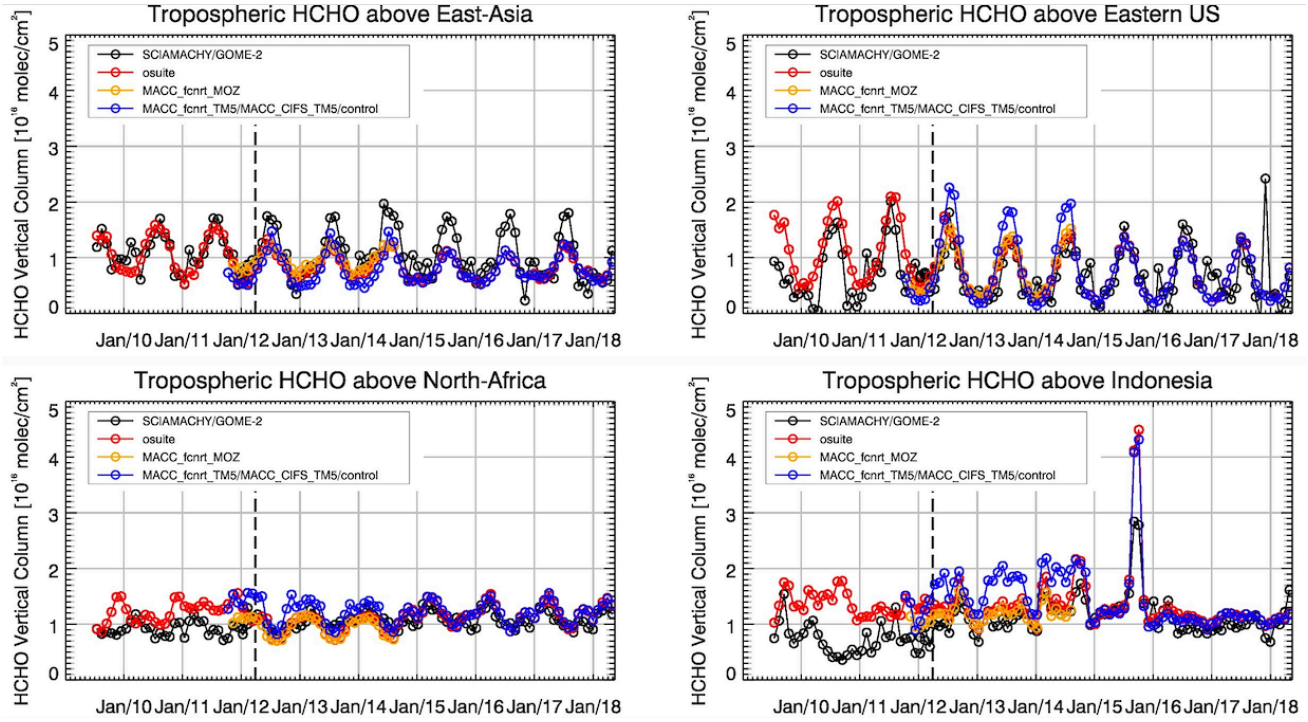

Figure 6.1.2: Time series of average tropospheric HCHO columns [10^{16} molec cm^{-2}] from SCIAMACHY (up to March 2012) and GOME-2 (from April 2012 onwards) compared to model results for different regions. The blue line shows MACC_fcnrt_TM5 from November 2011 to November 2012, MACC_CIFS_TM5 results from December 2012 to August 2014 and control results from September 2014 onwards (the model run without data assimilation is termed control since Sep 2014). The regions differ from those used for NO_2 to better focus on HCHO hotspots: East-Asia (25-40°N, 110-125°E), Eastern US (30-40°N, 75-90°W), Northern Africa (0-15°N, 15°W-25°E) and Indonesia (5°S-5°N, 100-120°E). Negative satellite retrieved values over Eastern US are due to a lack of data (caused by instrument degradation) during Northern Hemisphere winter months for this region. Vertical dashed black lines mark the change from SCIAMACHY to GOME-2 based comparisons in April 2012.

El Nino years, fire emissions used by IFS-CB05 seem to be largely overestimated, resulting in model simulated HCHO columns which are almost twice as large as those retrieved by GOME-2. Further investigations (see previous reports) show that this is not caused by cloud flagging applied to the satellite and model data. The recent higher resolution runs in general overestimate values over Indonesia as well. There is little variation from one month to another in both, satellite observations and model simulations since middle of 2016, apart from a decrease in retrieved HCHO columns for Dec 17/ Jan 18 which is not reproduced by the simulations.

Details on the HCHO evaluation can be found at:
http://www.doas-bremen.de/macc/macc_veri_iup_home.html.

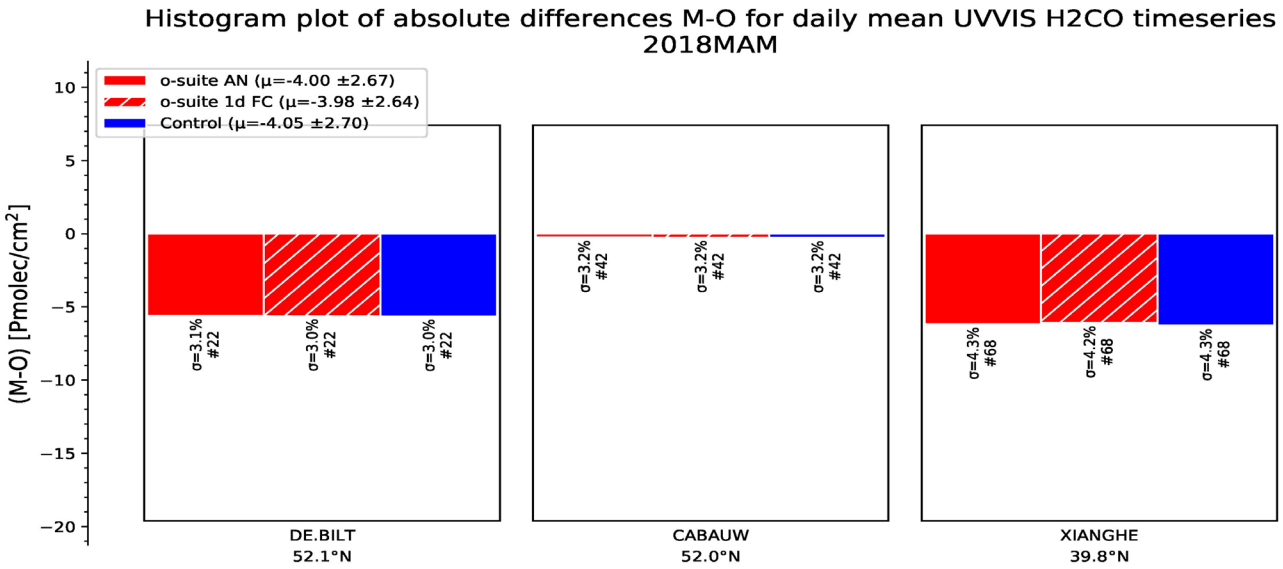

Figure 6.2.1: Table diagram showing the seasonal absolute bias (March –May 2018) for three stations, sorted by latitude.

6.2 Evaluation against ground-based DOAS observations

In this section, we compare the H2CO columns of the CAMS models with UVVIS DOAS measurements at Xianghe, Cabauw and De Bilt.[2] These ground-based, remote-sensing instruments are sensitive to the HCHO abundance in the lower troposphere. Tropospheric HCHO profiles and columns are validated (up to 3.5km (Xianghe) or 10km (Cabauw and De Bilt)). A description of the instruments and applied methodologies is the same as for the MWR O_3 and FTIR O_3 and CO validations see http://nors.aeronomie.be. It is important to mention here that the model partial column values are calculated for the smoothed model profiles. This guarantees that the model levels where the measurement is not sensitive do not contribute to the observed bias. We should mention that the measurement data is still catalogued as rapid delivery and not in the consolidated NDACC database.

Fig. 6.2.1 shows the absolute biases for March-May 2018 at the different sites, which shows an underestimation of all models at all sites. From Fig. 6.2.1 and 6.2.2 we see little difference between the o-suite and the control run. Although the background column values are well captured by the models, the high emission events are not.

[2] No contribution from Reunion and OHP due to instrument failure.

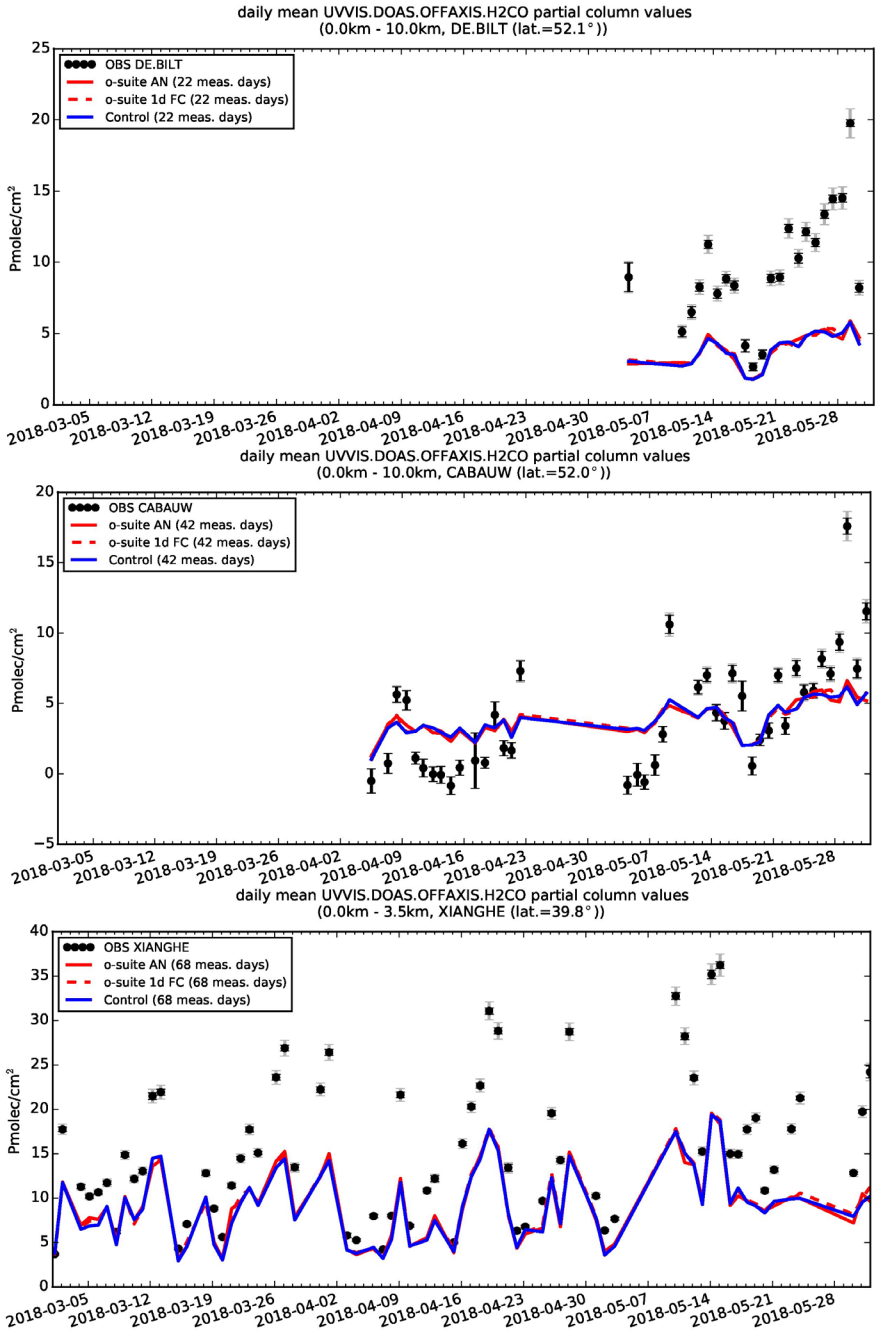

Figure 6.2.2: Time series of HCHO partial columns at the five different sites. All models underestimate the HCHO concentrations.

7. Aerosol

7.1 Global comparisons with Aeronet and EMEP

The comparison of the CAMS simulation of time series of aerosol optical depth can be compared for all Aeronet stations via: http://aerocom.met.no/cams-aerocom-evaluation/

More detailed evaluation including scores, maps, scatterplots, bias maps and histograms illustrating the performance of the aerosol simulation in the IFS system are made available through the AeroCom web interface. The model run can be compared here to eg the CAMS interim and other models, such as the AeroCom Median model.

Correlation, based on daily aerosol optical depth and NRT Aeronet observations, has been rather stable recently. The o-suite forecast at +3 days shows only slightly lower correlation. See figure S3.

Part of the month-to-month variation in correlation is due to the varying quality and coverage of the Aeronet network. This has been improved by the version 3 from Aeronet. We use therefore version 3 level 1.5 for all global comparison to Aeronet.

The regional performance of the o-suite model exhibits some seasonal variation in AOD depending on region (Fig. 7.1.1-a). For instance, the model performance in the North American winter season with respect to correlation seemed to be worst in 2011-2013 but seems to be more balanced now. Noteworthy is the persistent AOD overestimation over North America (Fig. 7.1.1-b), but also the change from underestimation to overestimation in East Asia since February 2017. The latitudinal display of model and Aeronet AOD in the period investigated here (Fig. 7.1.2) shows the positive bias against Aeronet NRT in the Southern but also Northern Hemisphere.

The simulated aerosol size distribution may be validated to first order using the wavelength dependent variation in AOD, computed as Ångström exponent, with higher Ångström exponents indicative of smaller particles. Figure 7.1.3-a shows the temporal evolution of simulated and observed mean Ångström exponent, while the correlation is found in figure 7.1.3-b. We find in MAM 2018 a positive bias of +10%. Temporal and spatial variability is rather high and correlation is lower than for AOD (Figure 7.1.3-b). Figure 7.1.4 shows that the Oct 2017 model changes are responsible for a shift in Ångström exponent. More organic matter seems to shift the size distribution to smaller sizes. The latest model upgrade with a bugfix for sea salt and improved parameterisations for SO4 lead to sea salt increased with 45% while sulphate further decreased a bit. Dust AOD on average has increased from DJF to MAM, but this increase was found also in earlier years and reflects increased source strength in N-Africa in spring.

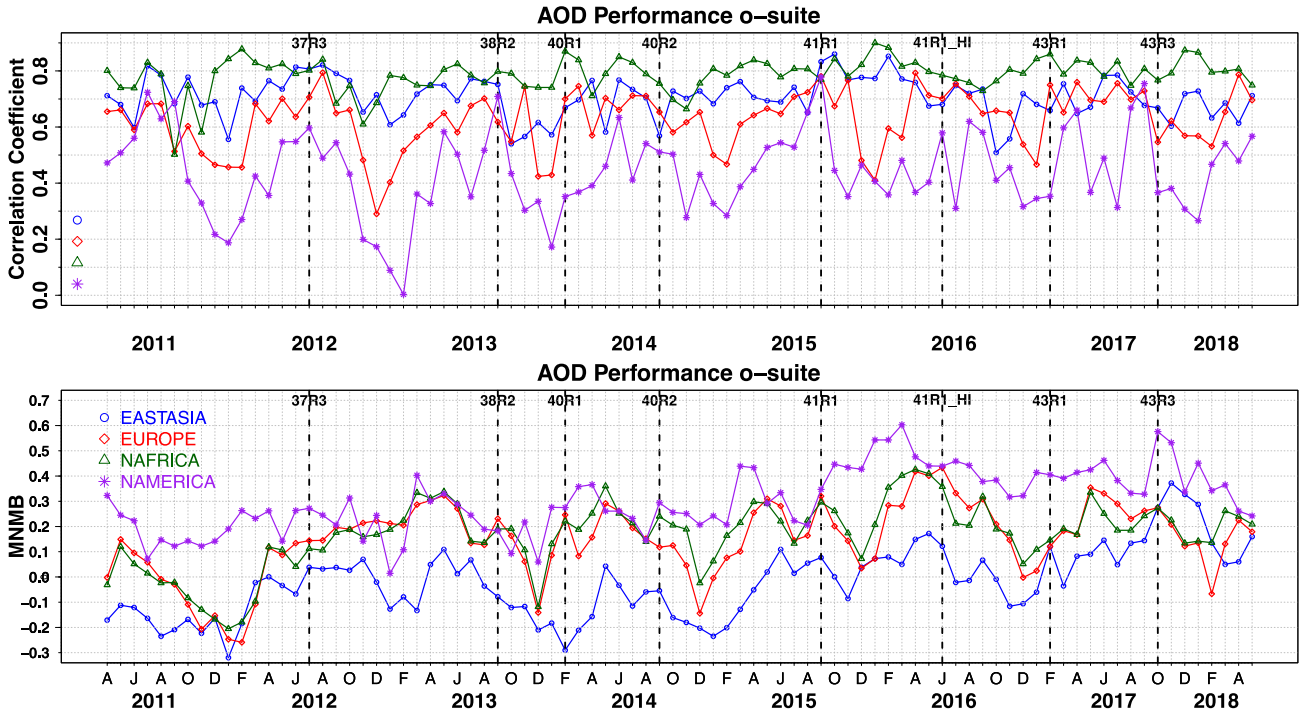

Figure 7.1.1. (top) Correlation coefficient and (bottom) modified normalized mean bias (MNMB) in AOD, since 2011, based on daily AOD comparison (Aeronet V3 level 1.5 data) in four world regions [Eastasia (blue); Europe (red); NAfrica (green); NAmercia (purple)] for the o-suite.

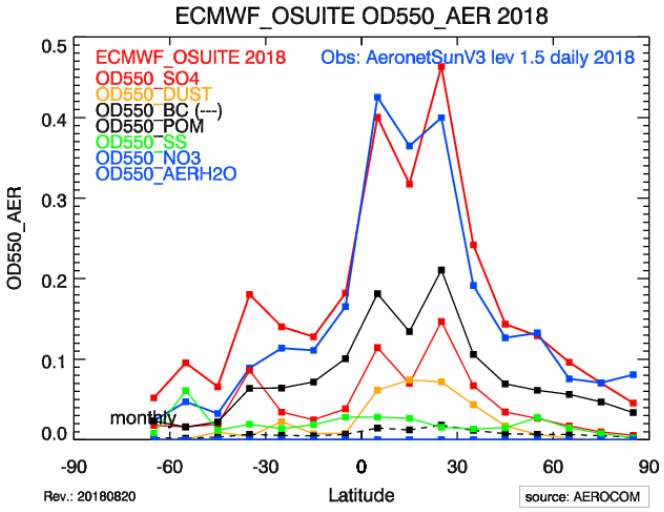

Figure 7.1.2. Aerosol optical depth of o-suite (red) compared to latitudinally aggregated Aeronet V3 level 1.5 data (blue) for the three months covered by this report.

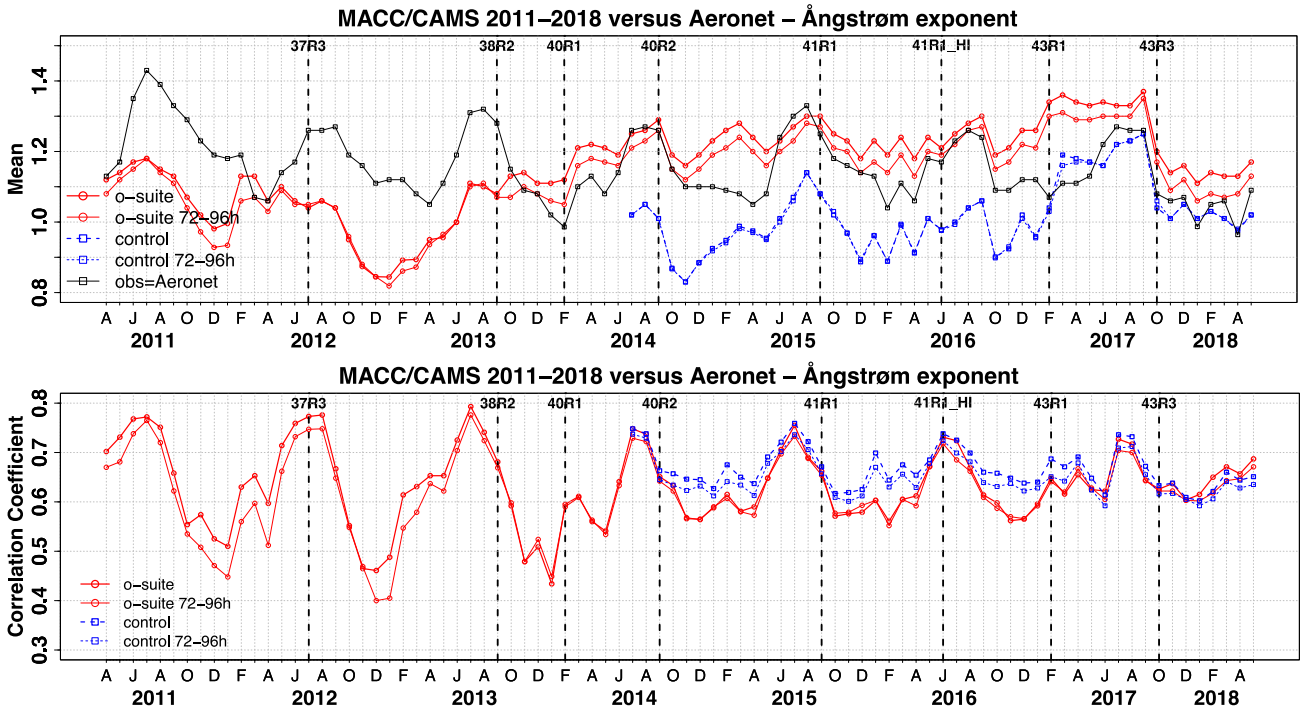

Figure 7.1.3. a) (top) Evolution of mean Ångström exponent in o-suite and control at Aeronet sites (Aeronet V3 level 1.5 data), based on matching monthly mean values. o-suite (thick red curve); o-suite at last forecast day (light red curve); control (blue dashed curve); control at last forecast day (light blue dashed curve). b) (bottom) Correlation using daily matching Ångström exponent.

The o-suite uses data assimilation to obtain a first guess aerosol field. In the forecast period, however, a-priori model parameterisations and emissions (except fire emissions, which are kept in the forecast equal to the latest GFAS emission values) determine more and more the shape and amplitude of the aerosol fields. The performance of the day three forecasted AOD fields as compared to the first guess is shown in Figure S3 in the summary of this report. Table 7.1.1 shows an average global decrease in total aerosol optical depth by 18% during the first four forecast days, dominated by sulphate and organics. The control run with no assimilation shows significant less AOD (-33% compared to o-suite, see figure S3). All this supports the conclusion that either a-priori IFS aerosol and aerosol precursor sources are too small or sinks are too effective in the IFS model.

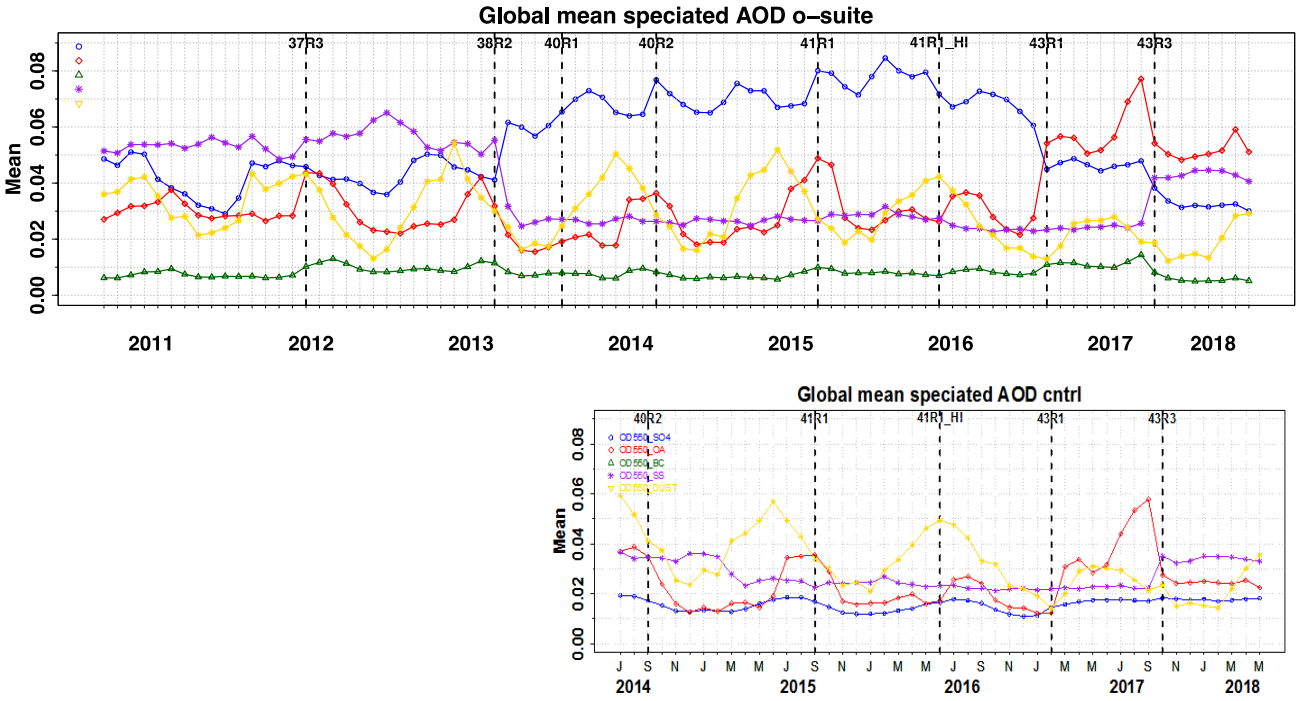

Figure 7.1.4. Evolution of the aerosol components of total AOD@550nm [OD550_SO4 = sulphate(blue); OD550_OA = organics(red); OD550_BC = black carbon(green); OD550_SS = sea salt(purple); OD550_DUST = dust(yellow)] in o-suite and control simulation.

Table 7.1.1. Mean global total and speciated AOD in the o-suite for the last two periods covered by the VAL report and change after 3 forecast days.

	o-suite		o-suite	
	Mean DJF 2017/18 0-24h	Change wrt to first day on day 4	Mean MAM 2018 0-24h	Change wrt to first day on day 4
AOD@550	0.145	-19%	0.160	-18%
BC-OD@550	0.005	-25%	0.005	-43%
Dust-OD@550	0.014	5%	0.026	-46%
OA-OD@550	0.049	-25%	0.054	-39%
SO4-OD@550	0.031	-25%	0.032	-31%
SS-OD@550	0.044	-15%	0.043	-14%

Surface concentration of particulate matter below 10 µm (PM10) from the o-suite experiment have been validated against data from 160 background IMPROVE and EMEP stations. A climatological average has been constructed from data in the period 2000-2009 as available in the EBAS database hold at NILU. The data availability is not the same at all stations, and sometimes covers only a few years. All time series used are documented via the CAMS-AeroCom web interface. In earlier evaluations the bias maps showed that both in North America and Europe a high bias appears at a few stations located in regions close to the coastlines. This is an indication that simulated PM10

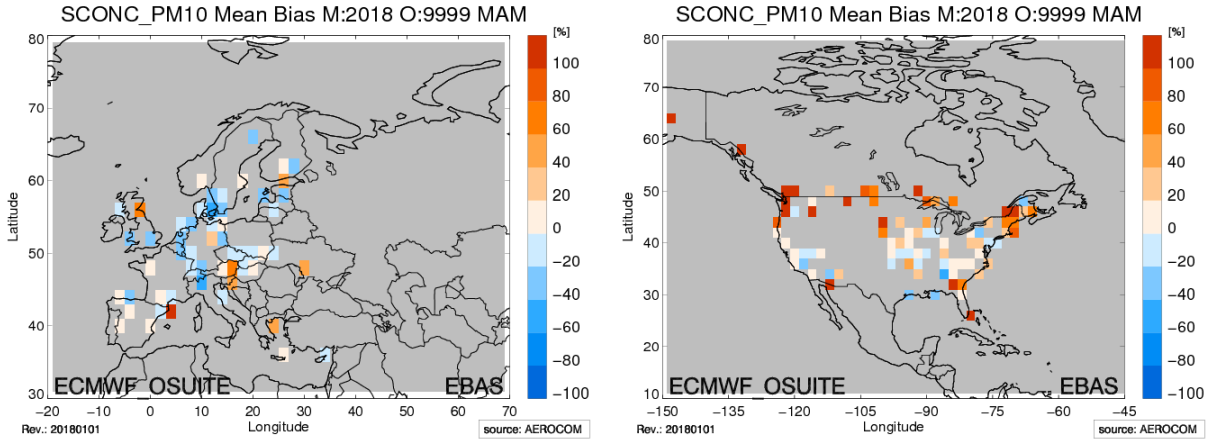

Figure 7.1.5. Bias [%] map of monthly mean PM10 concentrations at EMEP (Europe) and IMPROVE sites (North America); simulated o-suite versus EMEP/IMPOVE derived climatological average (2000-2009).

concentrations are high due to sea salt aerosols. This has changed with the implementation of recent model versions. Regional models using the sea salt concentrations as boundary condition should look into the PM10 data as produced by the IFS aerosol module.

A negative MNMB bias of -10% both in Europe and a +30% overestimate in North America appears (figure 7.1.5). Figure 7.1.6 is showing the evolution of mean observed and simulated PM10. The biggest change appeared in July 2017, the bias of both o-suite and control now becoming positive overall. Shown is also the statistics of being within factor 2, a more robust metrics for a comparison to climatological data. This statistics has clearly improved over time, indicating best PM10 performance in summer months for the o-suite. O-suite is also better most of the times than the control simulation.

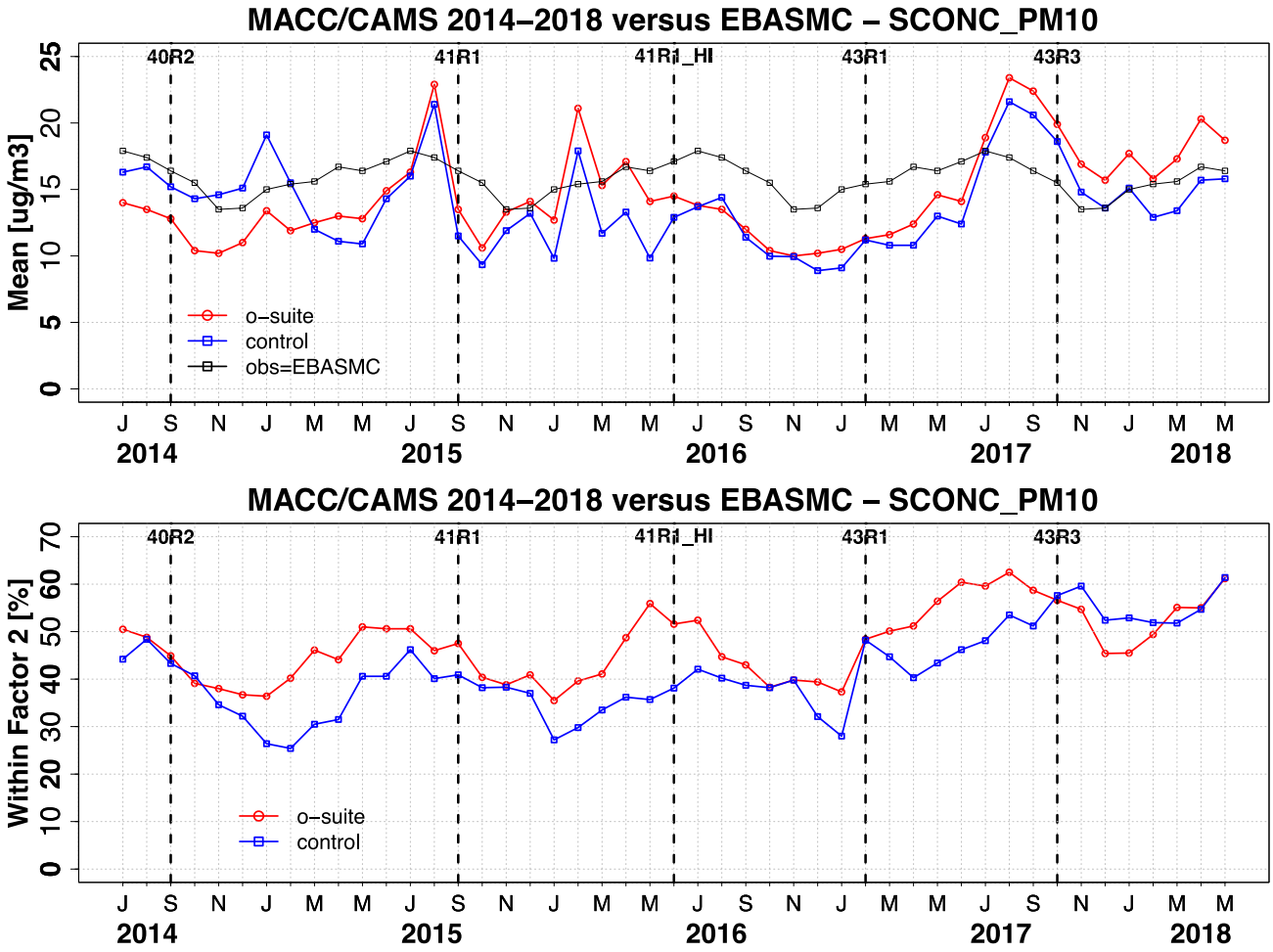

Figure 7.1.6. Temporal evolution of monthly mean average PM 10 concentrations at EMEP (Europe) and IMPROVE sites (North America) and data fraction within a factor 2 of observed; ca 160 sites, observed data averaged from data available in EBAS from 2000-2009.

7.2 Dust forecast model intercomparison: Validation of DOD against AERONET, and comparisons with Multi-model Median from SDS-WAS

72-hour forecasts (on 3-hourly basis) dust aerosol optical depth (DOD) from CAMS o-suite and control experiments have been validated for the period 1 December 2017 – 28 February 2018 against AERONET direct-sun cloud-screened observations, MODIS/Terra and Aqua Collection 6.1 Level 3 (1º x 1º) and compare with the SDS-WAS Multi-model Median DOD. The SDS-WAS Multi-model Median DOD is obtained from twelve dust prediction models participating in the Sand and Dust Storm Warning Advisory and Assessment System (SDS-WAS) Regional Center for Northern Africa, Middle East and Europe (http://sds-was.aemet.es/).

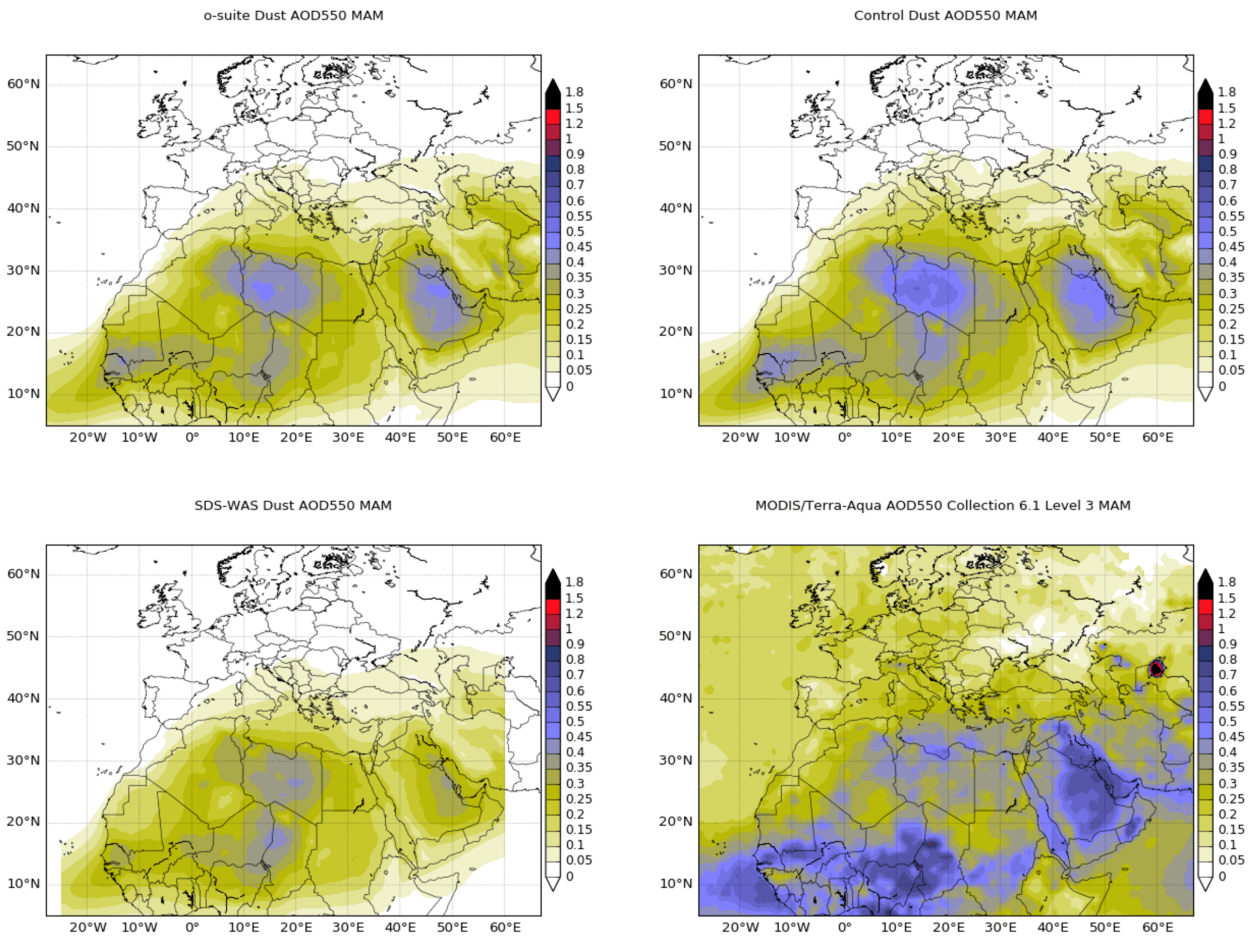

Figure 7.2.1: Averaged DOD 24h forecast from o-suite (top left) and control (top right), DOD of the multi-model SDS-WAS Median product (bottom left) as well as AOD from MODIS/Terra-Aqua Collection 6.1 Level 3 combined Dark target and Deep Blue product (bottom right) for the study period.

For spring, major dust activity is concentrated over the Sahara (in the Bodelé Basin and the Mali/Mauritania border as well as in Algeria, Tunisia and Libya) and the Arabian Peninsula as it is shown by satellites (see MODIS in Figure 7.2.1). CAMS model can simulate the main areas of dust activity in comparison with MODIS, although o-suite and control show higher DOD values particularly, over the Tunisia and Libya as well as areas of northern Iran and Turkmenistan (see Figure 7.2.1) in which also the SDS-WAS Multi-model product presents a lower signal. In the Middle East, both CAMS experiments show maximum DOD concentrations over the whole Arabian Peninsula in agreement with MODIS observations. Higher DOD values predicted by the CAMS model are linked to an increase of the magnitude of the predicted gusts winds that consequently causes an enhancement of the dust emissions over desert dust source regions. The current IFS operational version (that provides the meteorological fields to the C-IFS model) started on 26 September 2017 (cycle 43r3).

For March to May, o-suite is the model can reproduce the daily variability of AERONET observations with a correlation coefficient of 0.81 in average for all the AERONET sites in comparison with control with a correlation coefficient of 0.78. These results are slightly lower to those obtained by the SDS-

WAS Multi-model of 0.84. Regarding MB, both CAMS experiments (o-suite and control) as well as the SDS-WAS Multi-model underestimate the AERONET observations resulting in an MB of -0.04 for all these experiments.

Tropical North Atlantic (see Dakar in Figure 7.2.2 and Table 7.2.1) region presents the best results of the AERONET comparison in terms of correlation. Both experiments can reproduce the daily variability with correlation coefficients of 0.89 (0.88) respectively for o-suite (control). Over the Sahara (see Tamanrasset in Figure 7.2.2 and Table 7.2.1), o-suite shows better results than control with an increase of the correlation coefficient from 0.84 (control) to 0.87 (o-suite) although o-suite present higher underestimation (MB of -0.10) than control experiment (MB of -0.04). The SDS-WAS Median Multi-model presents similar results than o-suite with a correlation coefficient of 0.88 for Sahara although it underestimates the observations with an MB of -0.10. In the Sahel, o-suite presents strong underestimations (MB of -0.26, slightly higher than control with MB of -0.22) despite that the model can reproduce the observed daily variability (with a correlation value of 0.72 for o-suite and 0.65 for control).

In the North-Western Maghreb, CAMS experiments present underestimations (MB of -0.07) in comparison with the AERONET observations and lower correlation coefficients in comparison with the SDS-WAS Median Multi-model (0.67 for o-suite, 0.69 for control and 0.81 for the SDS-WAS Median Multi-model).

In the Middle East (see Table 7.2.1 as well as Shagaya Park and Mezaira AERONET sites in Figure 7.2.3), o-suite and control shows similar performance scores than o-suite with a correlation coefficient of 0.84 for o-suite and 0.83 for control although underestimations in control (MB of -0.06) are increased in o-suite (MB of -0.10). These results are close than the SDS-WAS Multi-model (with a correlation coefficient of 0.84 and MB of -0.10).

Over long-range transport regions, the performance of o-suite is better than in the previous season. The model results are limited over sub-Tropical North Atlantic region with correlation values of 0.70 (see Table 7.2.1 as well as Santa Cruz de Tenerife AERONET sites in Figure 7.2.2). Both CAMS models present lower correlation coefficients in the Iberian Peninsula and Western Mediterranean (between 0.71 and 0.73 for o-suite and between 0.73 and 0.76 for control) in comparison with Central-Eastern Mediterranean (between 0.80 and 0.82 for o-suite and between 0.77 and 0.81 for control) as it is shown in Table 7.2.1. The worth scores in the Iberian Peninsula and Western Mediterranean are directly linked to the dust activity over the Maghreb and northern Sahara.

Otherwise, the comparison of 48h and 72h forecasts for both CAMS experiments shows that the prediction is stable during the 3-days forecasts with correlation coefficients of 0.81 (0.78), 0.80 (0.77) and 0.77 (0.75) respectively to 24, 48 and 72h forecasts for all the sites for o-suite (control). In the Sahara region, the correlation coefficient (r) is better at 48h and 72h than forecast (see Table 7.2.2).

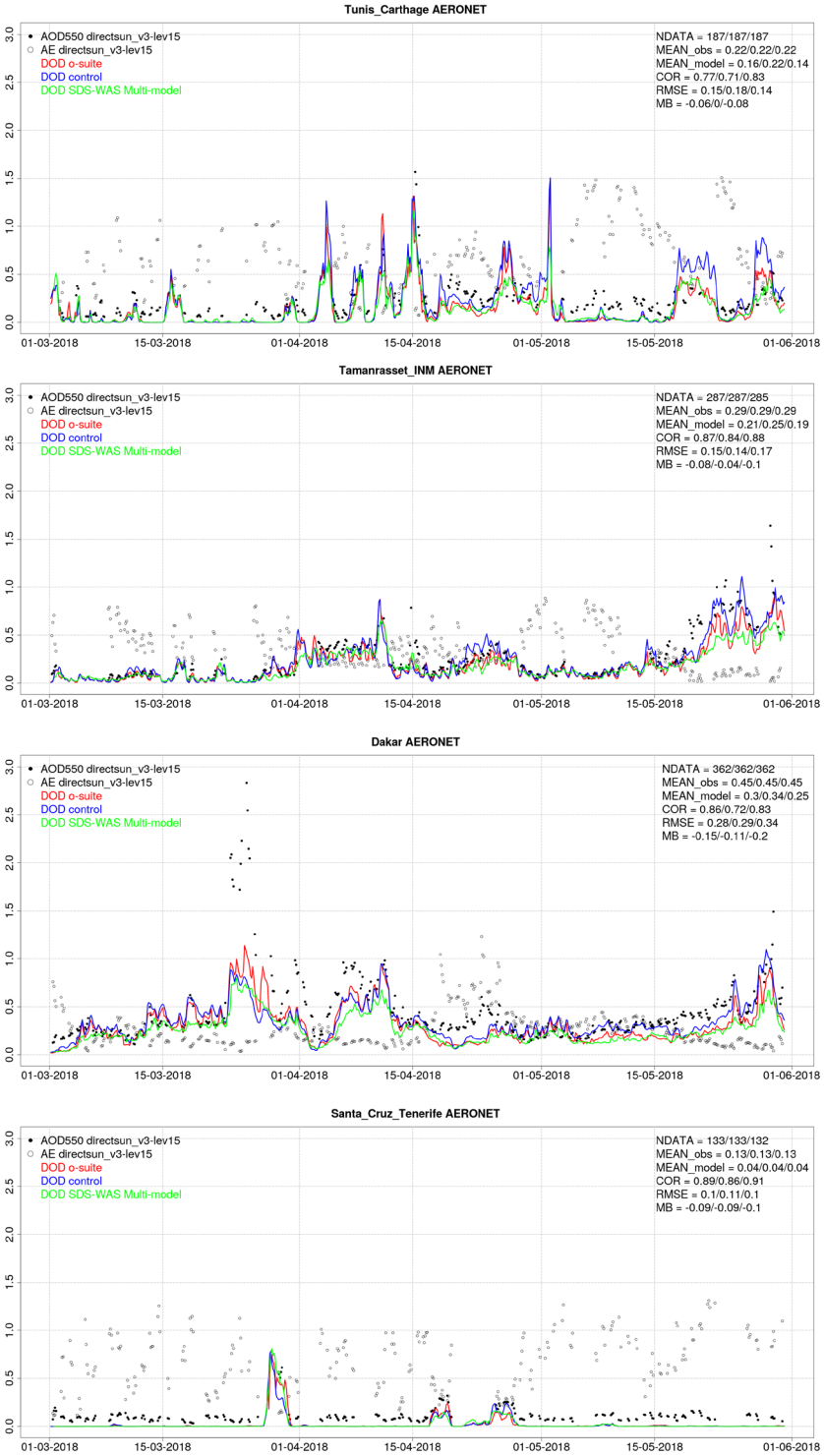

Figure 7.2.2: AOD from AERONET (black dots), DOD o-suite (red line), DOD control (blue line) and DOD Multimodel SDS-WAS Median (green line) for the study period over Tunis Carthage (North Western Magrebh), Tamanrasset (Sahara), Dakar (Sahel) and Santa Cruz de Tenerife (sub-Tropical North Atlantic). Skill scores per each individual site and model (o—suite/control/SDS-WAS Multi-model) are shown in the upper right corner (NDATA: available 3-hourly values used for the calculations, MEAN observations, MEAN_model, COR, RMSE, MB).

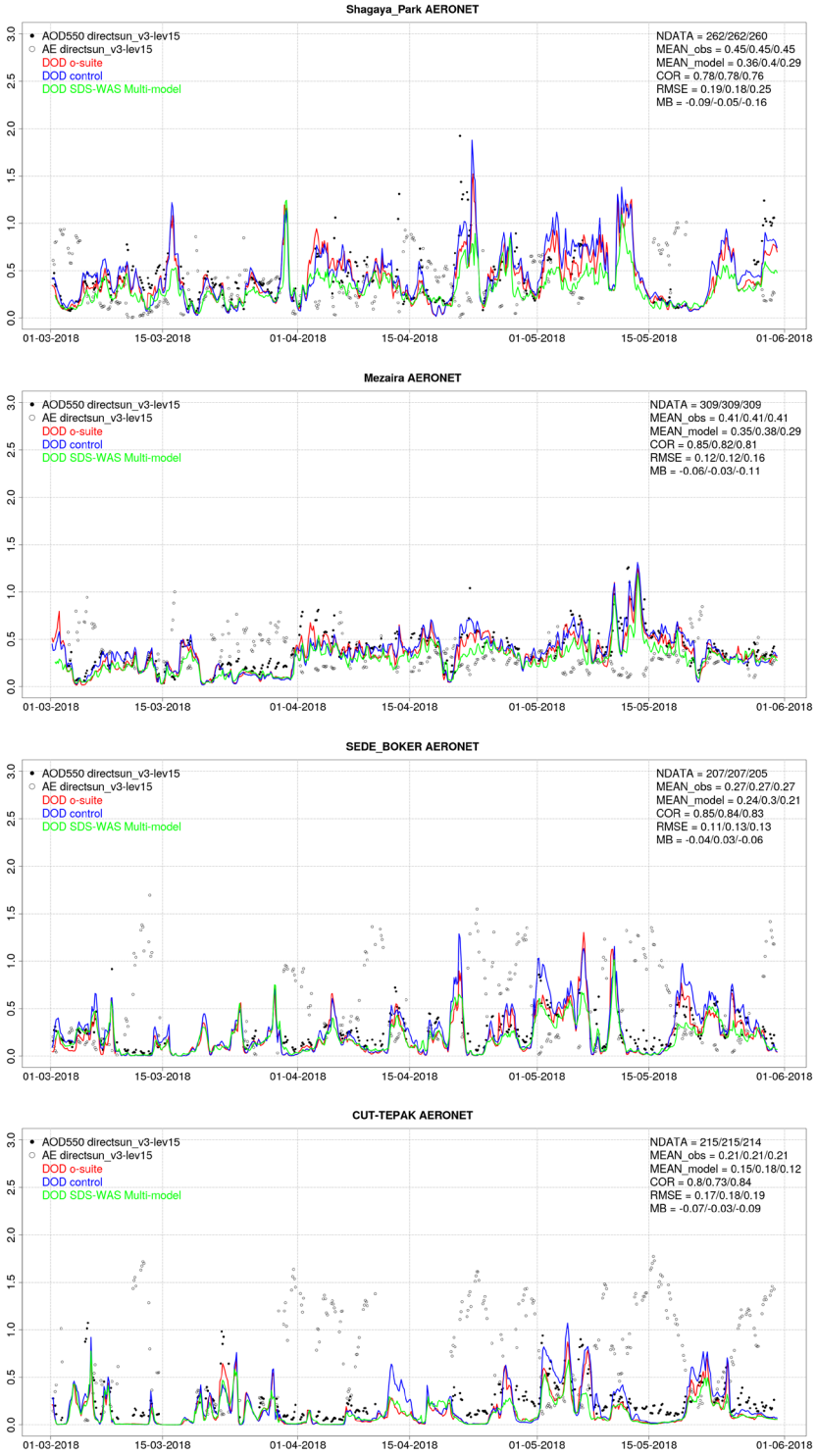

Figure 7.2.3: AOD from AERONET (black dots), DOD o-suite (red line), DOD control (blue line) and DOD Multimodel SDS-WAS Median (green line) for the study period over Shagaya Park (Middle East), Mezaira (Middle East), SEDE BOKER and CUT-TEPAK (Eastern Mediterranean). Skill scores per each individual site and model (o—suite/control/ SDS-WAS Multi-model) are shown in the upper right corner (NDATA: available 3-hourly values used for the calculations, MEAN observations, MEAN_model, COR, RMSE, MB).

Table 7.2.1: Skill scores (MB, FGE, RMSE and r) of 24h forecasts for CAMS o-suite, CAMS control and SDS-WAS Multi-model Median for the study period, and the number of data (NDATA) used. Dust AOD (DOD) from AERONET is the reference.

		control				o-suite DOD				SDS-WAS Median DOD			
	NDATA	MB	FGE	RMSE	r	MB	FGE	RMSE	r	MB	FGE	RMSE	r
Sahara	287	-0.04	-0.18	0.14	0.84	-0.08	-0.30	0.15	0.87	-0.10	-0.35	0.17	0.88
Sahel	1010	-0.22	-0.43	0.38	0.65	-0.26	-0.57	0.38	0.72	-0.27	-0.57	0.40	0.72
Tropical North Atlantic	98	-0.09	-0.93	0.12	0.88	-0.10	-0.95	0.12	0.89	-0.12	-1.17	0.15	0.91
Subtropical North Atlantic	263	-0.04	-0.22	0.08	0.69	-0.04	-0.21	0.08	0.70	-0.04	-0.27	0.08	0.72
North Western Maghreb	126	-0.07	-0.40	0.13	0.69	-0.07	-0.38	0.13	0.67	-0.08	-0.23	0.13	0.81
Western Iberian Peninsula	410	-0.04	-0.14	0.12	0.73	-0.06	-0.17	0.11	0.71	-0.06	-0.19	0.10	0.74
Iberian Peninsula	590	-0.03	0.50	0.10	0.73	-0.04	0.44	0.10	0.73	-0.05	0.44	0.10	0.77
Western Mediterranean	1409	-0.03	0.33	0.09	0.76	-0.04	0.28	0.09	0.77	-0.04	0.29	0.09	0.80
Central Mediterranean	1421	0.01	0.28	0.15	0.81	-0.04	0.11	0.14	0.82	-0.05	0.11	0.13	0.85
Eastern Mediterranean	1320	-0.02	0.48	0.16	0.77	-0.06	0.34	0.16	0.80	-0.08	0.31	0.17	0.85
Eastern Sahara	173	-0.02	0.09	0.15	0.85	-0.09	-0.07	0.18	0.83	-0.10	-0.08	0.19	0.85
Middle East	681	-0.06	-0.10	0.17	0.83	-0.10	-0.19	0.18	0.84	-0.15	-0.28	0.24	0.80

Table 7.2.2: Skill scores (MB, FGE, RMSE and r) of 48h and 72h forecasts for CAMS o-suite and CAMS control for the study period, and the number of data (NDATA) used. Dust AOD (DOD) from AERONET is the reference.

		48h control				48h o-suite				72h control				72h o-suite			
	NDATA	MB	FGE	RMSE	r	MB	FGE	RMSE	r	MB	FGE	RMSE	r	MB	FGE	RMSE	r
Sahara	282	-0.03	-0.12	0.14	0.84	-0.06	-0.22	0.14	0.86	-0.02	-0.08	0.14	0.84	-0.04	-0.17	0.14	0.85
Sahel	1001	-0.22	-0.43	0.38	0.65	-0.25	-0.53	0.39	0.68	-0.23	-0.46	0.39	0.66	-0.26	-0.54	0.40	0.67
Tropical North Atlantic	95	-0.10	-0.90	0.13	0.85	-0.10	-0.89	0.14	0.82	-0.10	-0.90	0.13	0.85	-0.11	-0.95	0.14	0.83
Subtropical North Atlantic	259	-0.04	-0.20	0.09	0.63	-0.04	-0.18	0.08	0.68	-0.04	-0.21	0.08	0.74	-0.04	-0.19	0.08	0.73
North Western Maghreb	122	-0.07	-0.34	0.13	0.67	-0.08	-0.34	0.14	0.64	-0.08	-0.33	0.13	0.68	-0.08	-0.33	0.13	0.70
Western Iberian Peninsula	408	-0.05	-0.12	0.11	0.72	-0.06	-0.15	0.11	0.70	-0.05	-0.12	0.10	0.77	-0.05	-0.14	0.10	0.77
Iberian Peninsula	588	-0.03	0.52	0.10	0.74	-0.04	0.46	0.10	0.74	-0.02	0.51	0.11	0.74	-0.03	0.47	0.10	0.75
Western Mediterranean	1403	-0.03	0.34	0.09	0.77	-0.04	0.28	0.09	0.77	-0.03	0.36	0.09	0.76	-0.04	0.32	0.09	0.77
Central Mediterranean	1418	0.01	0.27	0.16	0.78	-0.03	0.14	0.14	0.81	-0.01	0.24	0.17	0.68	-0.04	0.15	0.16	0.71
Eastern Mediterranean	1305	-0.02	0.49	0.17	0.77	-0.06	0.38	0.16	0.80	-0.01	0.47	0.19	0.72	-0.05	0.40	0.18	0.73
Eastern Sahara	169	-0.01	0.10	0.18	0.81	-0.07	-0.04	0.19	0.80	-0.02	0.08	0.19	0.79	-0.06	-0.01	0.19	0.78
Middle East	681	-0.07	-0.12	0.18	0.82	-0.10	-0.19	0.19	0.83	-0.07	-0.12	0.18	0.80	-0.10	-0.18	0.19	0.81

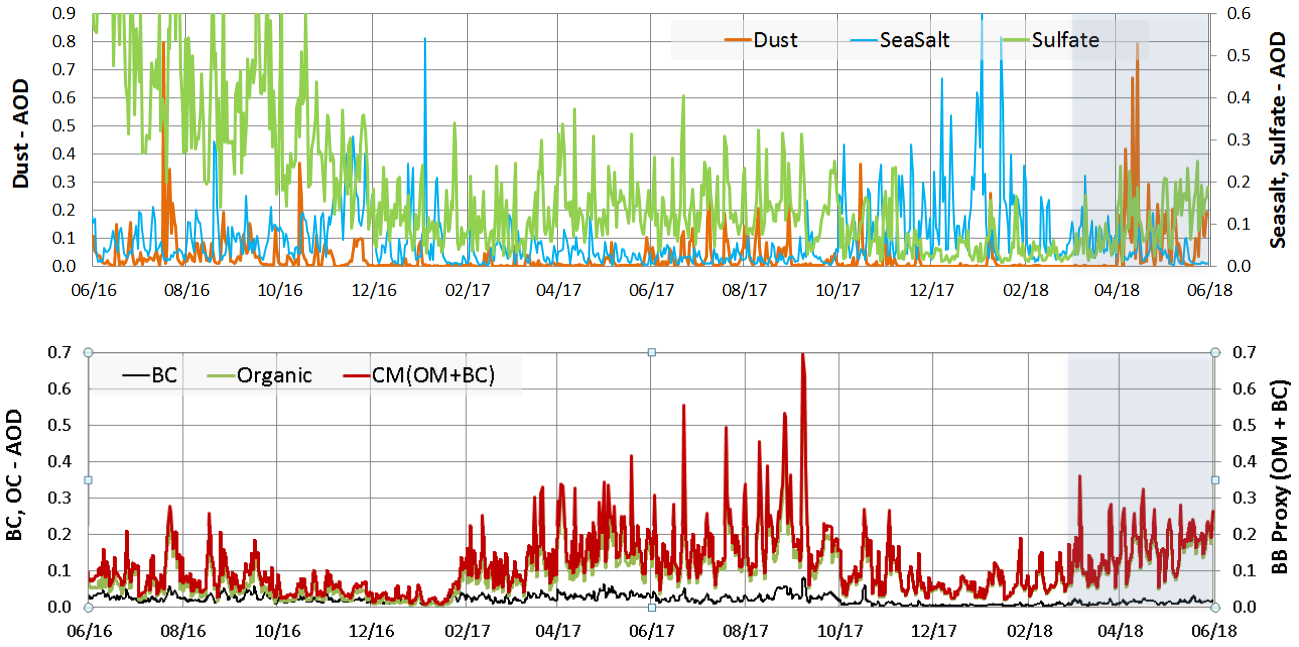

Figure 7.3.1: Maximum daily AOD over Germany for aerosols included in the IFS model from 06/2016 - 05/2018: sea salt (blue), dust (orange), sulfate (light green), black carbon (BC, black), organic matter (green), proxy for 'biomass burning' (as OC+BC - red). Note the different y-axes for the aerosol species.

7.3 Backscatter profiles

Technical specifications of data sources, evaluated parameters and methods are described in the report CAMS-84 D8.1. In this section, the temporal and vertical variation of the backscatter coefficient (bsc) profiles are evaluated, statistically as bias, correlation, and standard deviation of o-suite '0001' and control run gsyg' vs ceilometers, and summarized in Taylor plots. Second topic is the reproduction of the planetary boundary layer (PBL), and thirdly, the representation of individual aerosol types is considered. Covariance plots of daily 2-D time-height sections serve for case studies and for development of a fractional skill score. The vertically integrated bsc is not in focus, because it reveals similar but less accurate information like AOD. As several case studies have confirmed the reliability of the methodology, we focus towards evaluation metrics and interpretations of aerosols representation in the model versions.

Period Overview

The model aerosol optical depth (AOD) and ceilometer overviews exhibit periods with significant aerosol plumes over Germany. Figure 7.3.1 shows the maximum AOD over Germany, separately for contributions of mineral dust (SD), sea salt (SS), carbonaceous matter (CM), black (BC) and organic carbon (OC), as well as sulfate (SU). More prominent SD events than in the previous years occurred in the MAM 2018 period, starting in April 2018. The other components follow their usual seasonality.

Table 7.3.1: Correlation r, relative bias rb (bsc_{model}/bsc_{ceilo}) and modified normalized mean bias mnmb of osuite and control run vs ceilometer observations for JFMAM 2018.

	r_{L41}	r_{L46}	r_{L51}		rb_{L41}	rb_{L46}	rb_{L51}		$mnmb_{41}$	$mnmb_{46}$	$mnmb_{51}$
osuite	0.42	0.67	0.40		0.6	1.3	0.8		28	52	-25
control	0.25	0.67	0.29		0.4	1.1	0.7		-37	3	-45

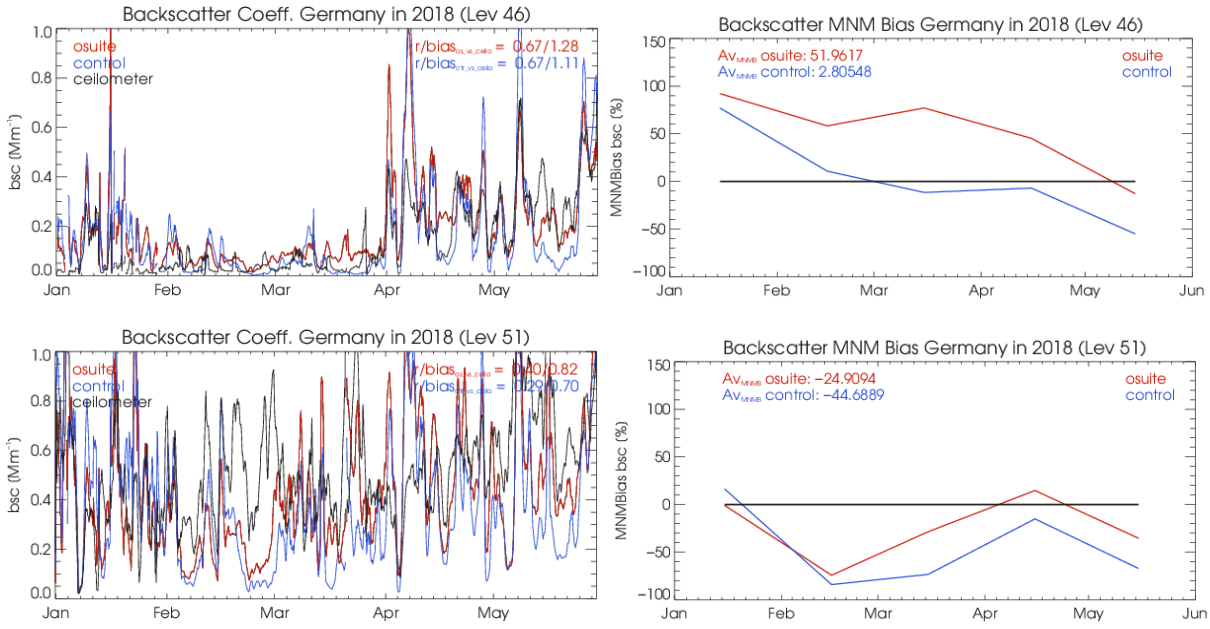

Figure 7.3.2: Variation of bsc at L41 (~3.9 km a.g.), L46 (~2.0 km a.g.), L51 (~0.8 km a.g.) during 2017. Each is averaged over 21 German ceilometer stations. The numbers are given in table 7.3.1.

Temporal variation at selected model levels:

Fig. 7.3.2 and Table 7.3.1 show the temporal variation of bsc at different model levels (L41, L46, L50), averaged over 21 German ceilometer sites. The corresponding mean heights above ground are 3.9 km (L41), 2.0 km (L46), 0.8 km (L51). Pearson's r, relative bias (RB) as well as modified normalized mean biases (MNMB) at these model levels over the JFMAM 2018 period are given in Table 7.3.1. Both runs exhibit a higher bias in the FT and lower bias in the PBL, except for April. Owing to this opposite behavior, the best agreement is found near the top of the PBL, and the seasonal variation of the PBL height reflects in seasonal variations of the metrics. Similar information, in a transposed way, is contained in the average vertical backscatter profiles in Figure 7.3.3. They also show that the assimilation (AOD) does not consistently improve the shape of the vertical profile.

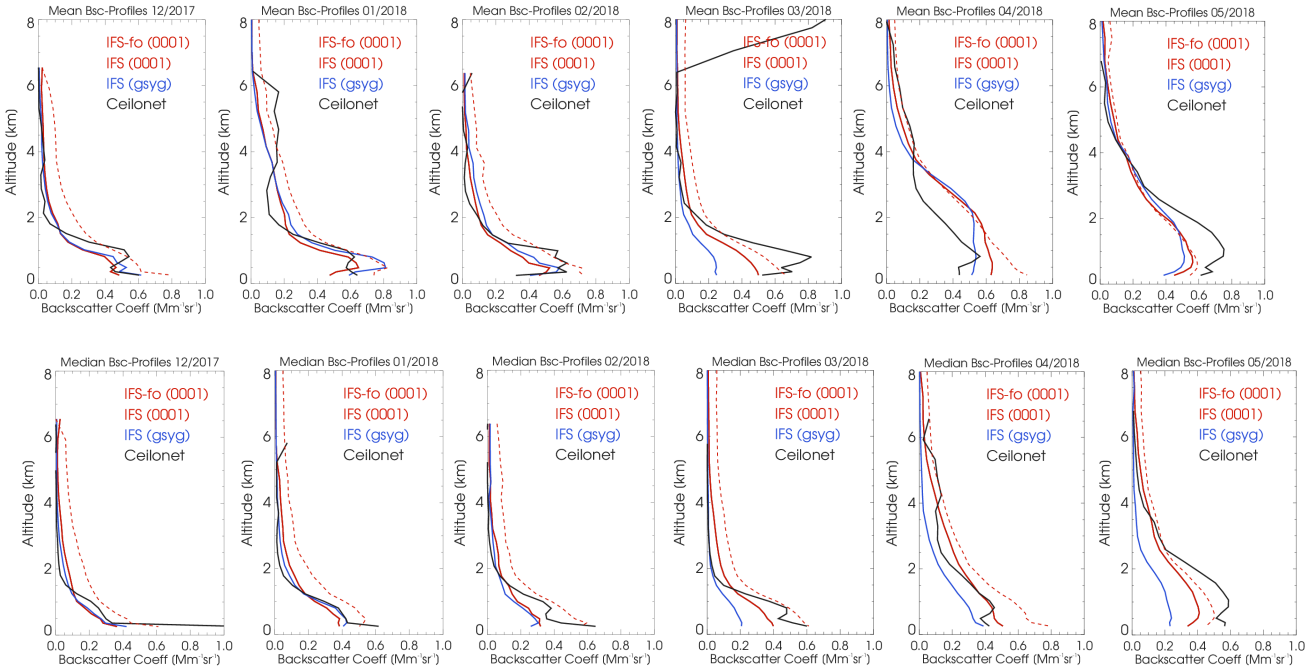

Figure 7.3.3: Monthly mean (upper panel) and median (lower panel) profiles of backscatter coefficients from osuite (red), control run gsyg (blue), and ceilometers (black) combined from 21 German stations in Dec 2017 to May 2018. The profiles are partly contaminated by remaining cloud artefacts.

Mean profiles:

Model bsc in the PBL are on average lower than observed (cf. Tab. 7.3.1). In April 2018, however, this was different due to high dust loadings in the model. While enhanced emissions of organic matter (OM) have been introduced in Jan 2017, and parametrizations of SO_2/SO_4 conversion/deposition were improved, nitrate and ammonia are still missing in the current model version, which contribute roughly 10-30% of aerosol mass (as NO_3NH_4 or $(NH_4)_2SO_4$) in the rural central European PBL. (According to pers. communication - S. Remy/Z. Kipling - nitrates and ammonium are ready in the current model and possibly get activated in the next cycle). Secondly, our forward operator (including mass-to-volume conversion) presently uses particle densities of the pure materials, not taking into account that dry atmospheric particles are often porous (sponge-like, even fractal) with entrapped air owing to coagulation and variable internal mixing, and thus exhibit reduced bulk density. A high-biased particle density results in low-biased equivalent volume, and a corresponding underestimation of all optical properties, because these depend strongly on the particle size. Density reductions for accumulation mode particles, composed of hydrophilic and hydrophobic materials may be as high as a factor 1.5 (~1.3 for surface). Thirdly, the capping transport barrier at the PBL top is less effective in the model, diluting high PBL concentrations with clean FT air. Geometrically, however, the PBL height on average seems reasonable (cf. next section).

Monthly mean bsc profiles in the model roughly follow observations, except that the PBL top is too smooth (Fig 7.3.3) and the PBL too clean. The monthly mean bsc profiles suggest that the aerosol mass, added to the whole column by the assimilation (run 0001), results in overall higher aerosol load than in the control run (gsyg), but the assimilation fails to introduce a realistic step at the top of the PBL to lower values in the free troposphere (FT) as in the ceilometer profiles. Rather, the FT background is too high due to adding an assimilated portion there. This aerosol mass is missing in

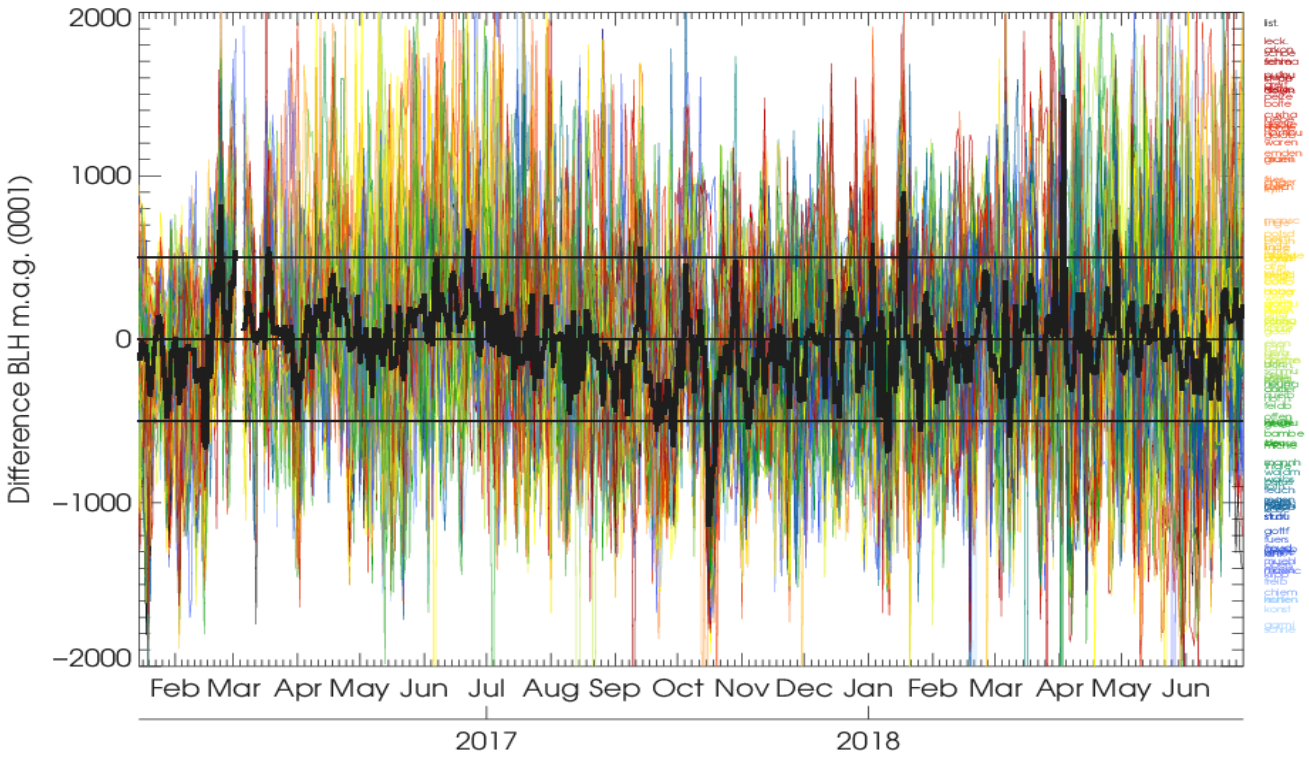

Fig. 7.3.4: Upper panel: Composite of ceilometer 2D time-height sections of attenuated backscatter over Germany and inferred daily maximum planetary boundary layer heights (color bullets) overlayed to model contour map of parameter z. Bottom: bias of daily maximum Aerosol-BLH vs model-BLH since Jan 2017, inferred from >100 German ceilometer stations.

the PBL, yielding a too low amplitude (coded in the standard deviation) of the model compared to observations (reference) in the Taylor plots, too. Strong SD events in the model in April 2018 cause a high bias of the mean bsc profile while the median profiles (background) fit better. Higher backscatter observations in May 2018 are not captured by the model.

Planetary boundary layer height (BLH)

Owing to different definitions, determination and evaluation of the BLH is challenging and still controversially discussed. Thus we compare (not evaluate) only daily maximum Aerosol-BL and model-BL heights at the German ceilometer stations as proxies for the representation of the planetary BLH, archived in MARS as parameter '159.128'. As explained in WP 8.1 report, the information is coded in the measured aerosol gradient respective the modelled Richardson number (Ri > 0.25), which do not necessarily refer to the same atmospheric feature. In Fig. 7.3.4, the model-observation difference ($z_{mod} - z_{obs}$) of the daily maximum BLH at all stations (color coded) and their median confirms that BLH in the model are realistic, but a tremendous variability at individual stations points to issues with artifact filtering in the BLH observations, much of which, we expect, will be removed, when in future improved filtering algorithms are available. Presently, inapplicable multiple layers, clouds, fog, precipitation, and profiles with missing aerosol gradients (e.g during Saharan dust events) limit the analysis at single stations. The median, however, eliminating all outliers, indicates reasonable BLH and a seasonal variation with high bias in summer and low bias in winter.

7.4 Aerosol validation over the Mediterranean

Three-hourly aerosol optical depth (AOD) and surface concentration (PM10 and PM2.5) from o-suite experiment and control experiment have been validated for the period 1 March 2018 – 31 May 2018 against AERONET direct-sun cloud-screened observations.

Aerosol optical depth

CAMS o-suite can reproduce the daily variability of AERONET observations. In Western, Central and Eastern Mediterranean, the correlation coefficient increase from 0.70, 0.75 and 0.73 to 0.74, 0.79 and 0.75, respectively for control and o-suite during spring (see the correlation coefficient by sites in Figure 7.4.1). Both CAMS experiments show high overestimations in the Central Mediterranean as a consequence of high desert dust activity in Tunis-Libya region during the period of analysis (see Section 7.2). Underestimations observed in the Western Mediterranean Basin in control are corrected in o-suite introducing overestimations in the whole Mediterranean Basin. This results in an increase of MB from -0.02, 0.05 and 0.03 for control to 0.03, 0.06 and 0.04 for o-suite. The highest peaks on CAMS AOD simulations are linked to desert dust intrusions (see Barcelona, Rome Tor Vergata, Thessaloniki and Cairo EMA AERONET sites in Figure 7.4.2).

Surface aerosol concentrations

For spring, PM10 results of CAMS o-suite and control show similar skill scores in comparison with EIONET observations despite (see Figure 7.4.3). For PM2.5, CAMS o-suite shows some improvement in northwestern Mediterranean sites (see Figure 7.4.4). From March to May, the overestimations observed in the comparison against EIONET cause that the o-suite over predict the number of exceedances of the EU PM10 daily threshold (i.e. 50 µg/m^3; see Zorita and Villar Arzobispo in Spain in late-April in Figure 7.4.5). Most of these exceedances were associated to desert dust intrusions with origin in Libya that the CAMS model tends to overestimate in magnitude (see Section 7.2). Differences between in the PM10 observed in the Spanish sites of Zorita and Villar Arzobispo are linked to the difference in the altitude of these sites (619 and 430 m above sea level, respectively) and the altitude of the arrival dust plume that was localised between 1 and 4 km over Western Mediterranean.

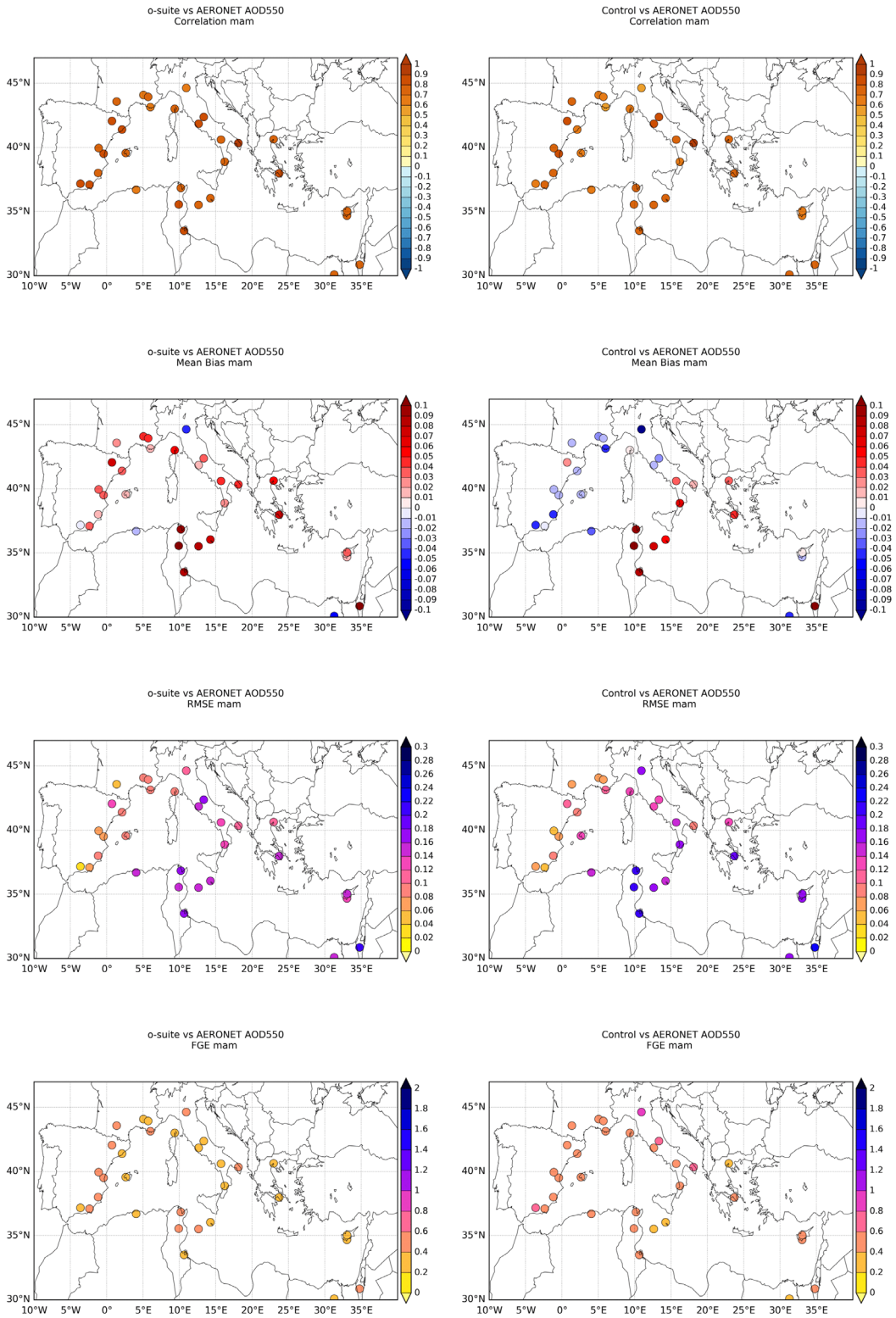

Figure 7.4.1: Skill scores (correlation coefficient, MB, RMSE and FGE) for 24-hour forecasts of CAMS o-suite and control for the study period. AOD from AERONET is the reference.

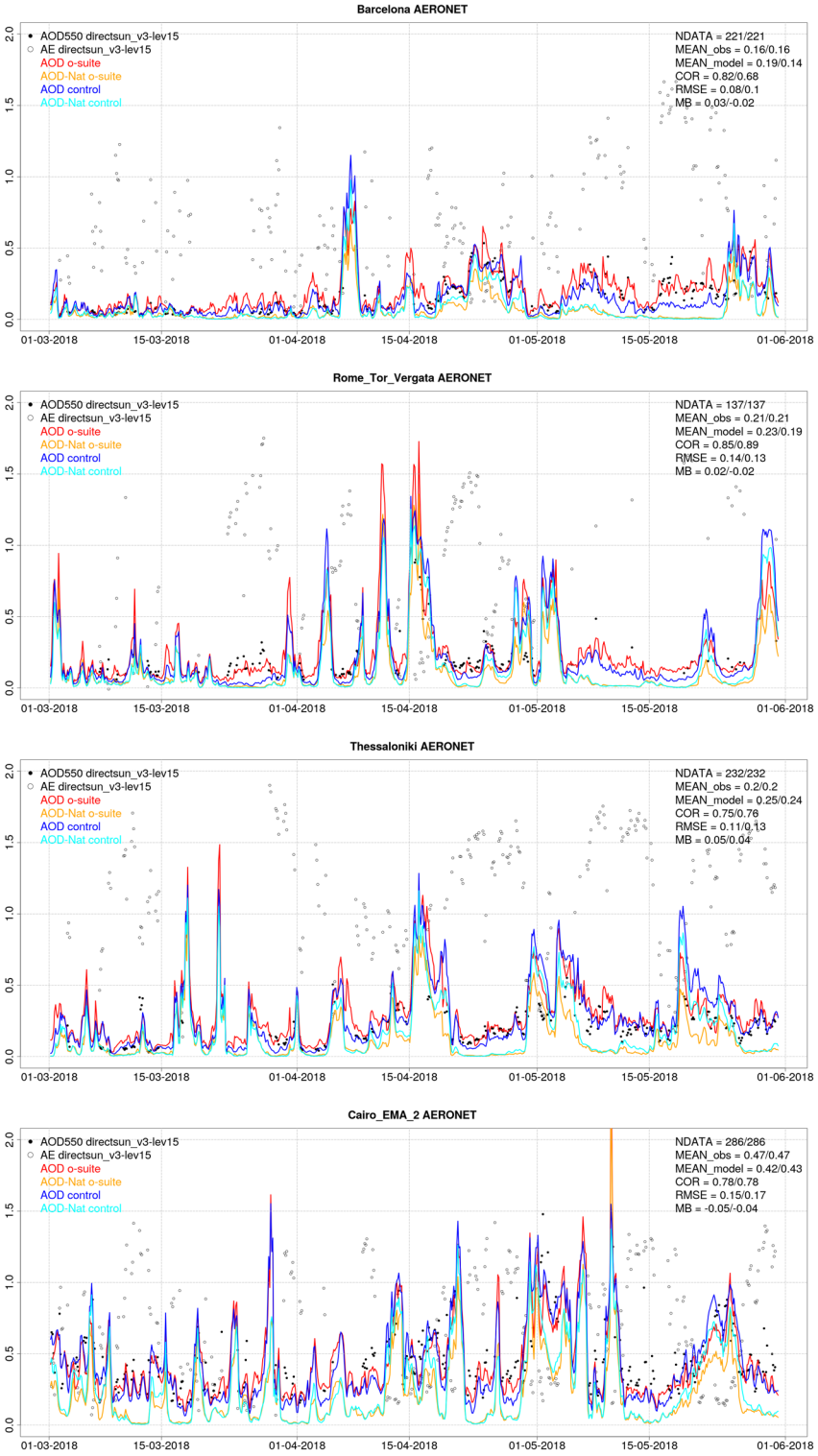

Figure 7.4.2: AOD from AERONET (black dot), AOD o-suite (red line), AOD control (blue line), AOD-Nat o-suite (orange line), AOD-Nat control (cyan line), for the study period over Barcelona (Spain), Rome Tor Vergata (Italy), Thessaloniki (Greece) and Cairo EMA 2 (Egypt). AOD-Nat corresponds to the natural aerosol optical depth that includes dust and sea-salt. Skill scores per each individual site and model (o—suite/control) are shown in the upper right corner (NDATA: available 3-hourly values used for the calculations, MEAN observations, MEAN_model, COR, RMSE, MB).

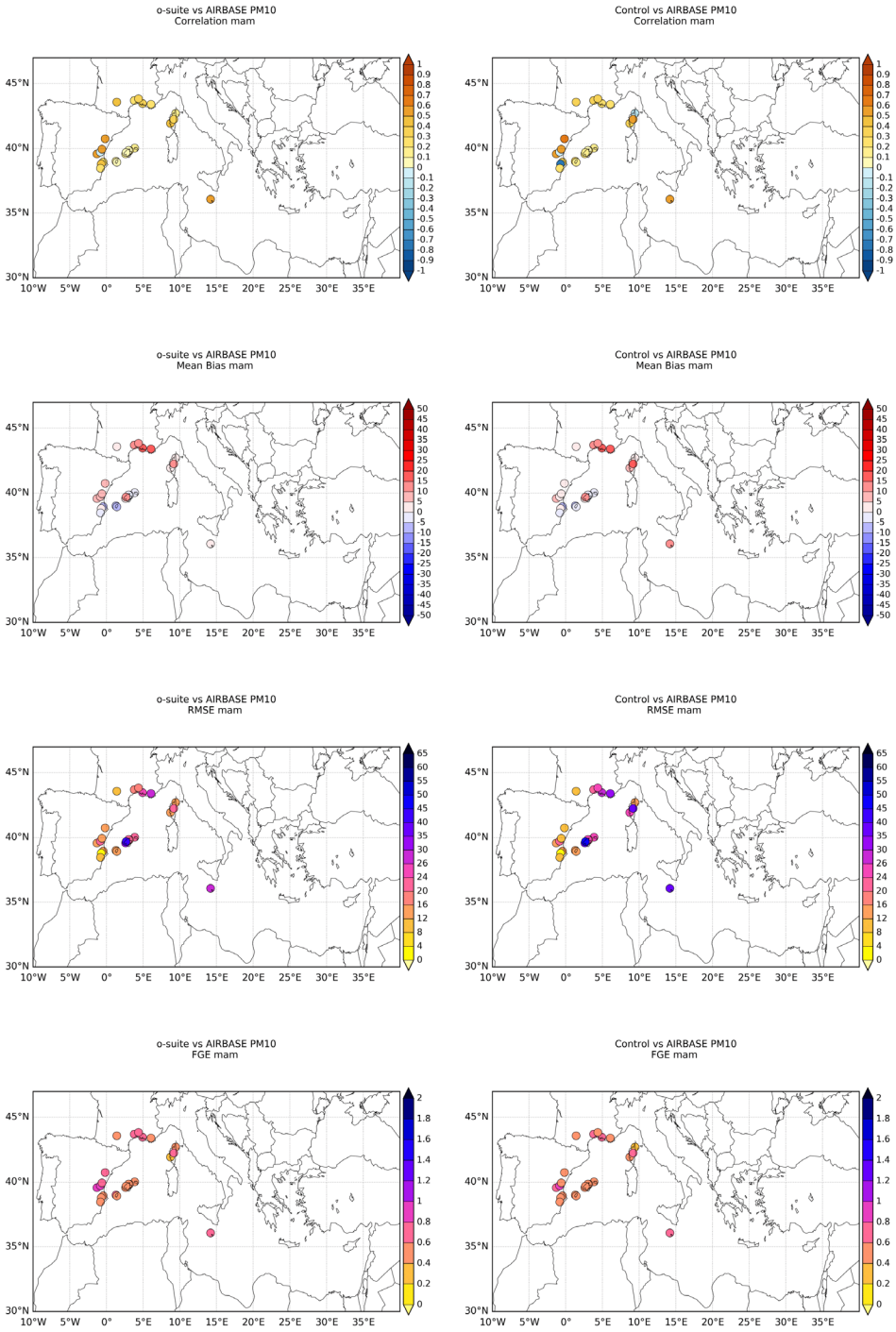

Figure 7.4.3: Skill scores (correlation coefficient, MB, RMSE and FGE) for 24-hour forecasts of CAMS o-suite and control for the study period. PM10 from EIONET are the reference. Only background suburban and rural available stations are displayed.

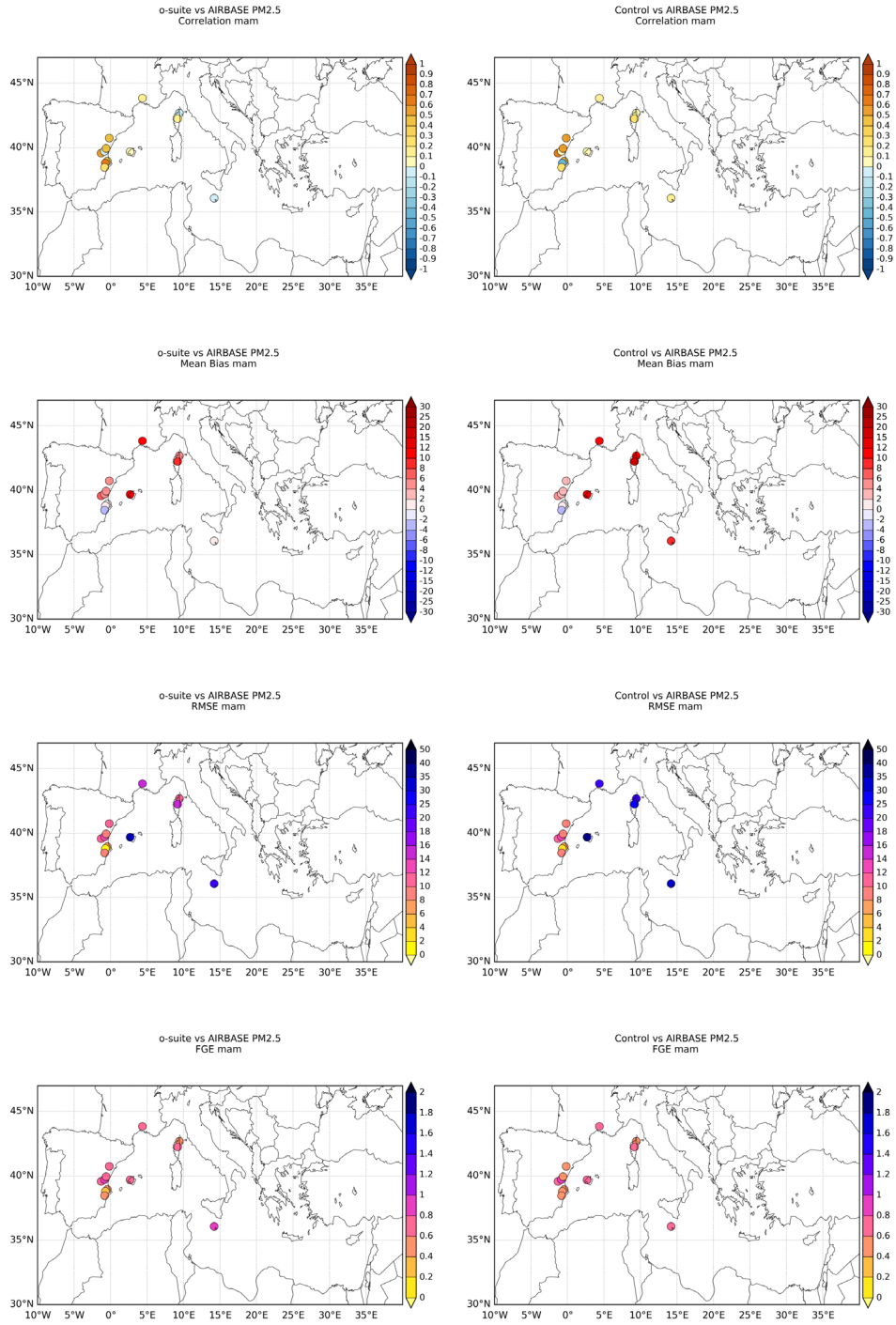

Figure 7.4.4: Skill scores (correlation coefficient, MB, RMSE and FGE) for 24-hour forecasts of CAMS o-suite and control for the study period. PM2.5 from EIONET are the reference. Only background suburban and rural available stations are displayed.

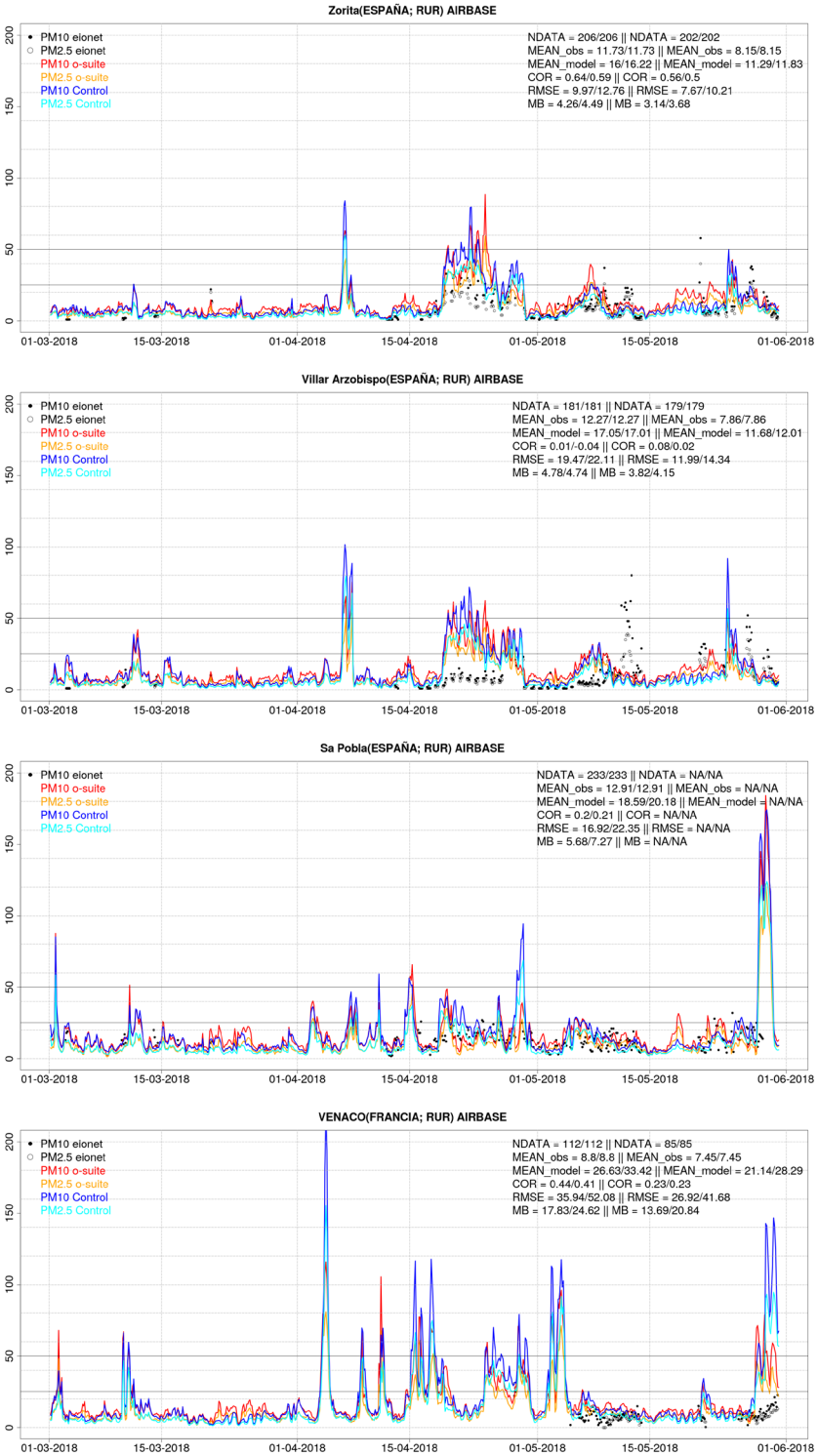

Figure 7.4.5: PM10 and PM2.5 Airbase observations (black and grey dots, respectively), PM10 and PM2.5 o-suite (red and orange lines, respectively) and PM10 and PM2.5 control (blue and cyan lines, respectively) for the study period over Zorita and Villar Arzobispo (Western Iberian Peninsula, Spain) as well as Sa Pobla (Balearic Islands, Spain) and Venaco (Corse, France). Skill scores per each individual site, model (o—suite/control) and PM10/PM2.5 are shown in the upper right corner (NDATA: available 3-hourly values used for the calculations, MEAN observations, MEAN_model, COR, RMSE, MB).

8. Stratosphere

8.1 Validation against ozone sondes

In this section, we present the results of the stratospheric ozone evaluation against ozone soundings from the NDACC, WOUDC, NILU and SHADOZ databases. The sondes have a precision of 3-5% (~10% in the troposphere for Brewer Mast) and an uncertainty of 5-10%. For further details see Cammas et al. (2009), Deshler et al. (2008) and Smit et al (2007). Model profiles of the o-suite are compared to balloon sondes measurement data of 44 stations for the period January 2013 to May 2018 (please note that towards the end of the validation period fewer soundings are available). As C-IFS-CB05 stratospheric composition products beyond O_3 in the o-suite is not useful we provide only a very limited evaluation of the control experiment. A description of the applied methodologies and a map with the sounding stations can be found in Eskes et al. (2016). The o-suite shows MNMBs within the range ±12%, for all regions and months (some exceptions with MNMBs of up to ±18% for single months in the high latitude regions). Figure 8.1.1. shows the results for the period May 2017 to May 2018.

Fig. 8.1.2 compares the averaged profiles in each region during March 2018. The vertical distribution of stratospheric ozone is quite well represented for all regions by the o-suite, with little overestimation in all latitude bands (MNMBs between 1 to 9% for MAM).

The control run shows a strong overestimation of stratospheric ozone in the upper stratosphere, and an underestimation between 40hPa (Arctic 100 hPa) and 300 hPa in the Arctic and the Northern Midlatitudes. In the Tropics, the underestimation is between 80 and 30 hPa. The Antarctic profile shows an underestimation between 300 and 30 hPa. Above, O_3 partial pressures are overestimated.

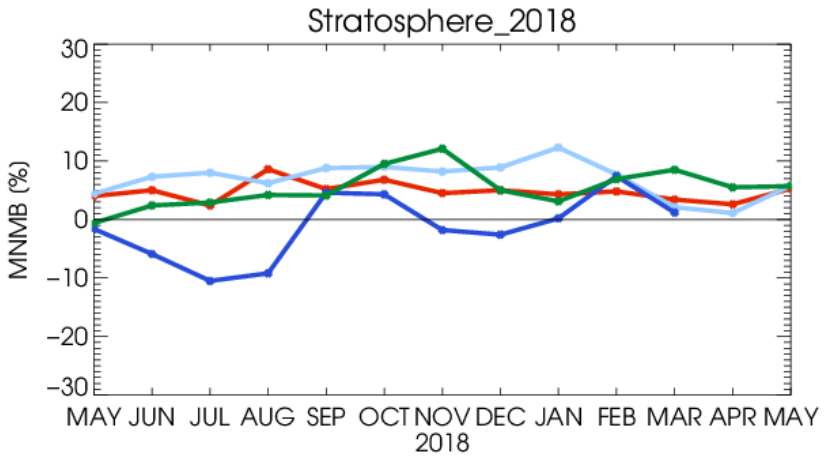

Figure 8.1.1: MNMBs (%) of ozone in the stratosphere from the o-suite against aggregated sonde data in the Arctic (light blue), Antarctic (dark blue) northern midlatitudes (red) and tropics (green).

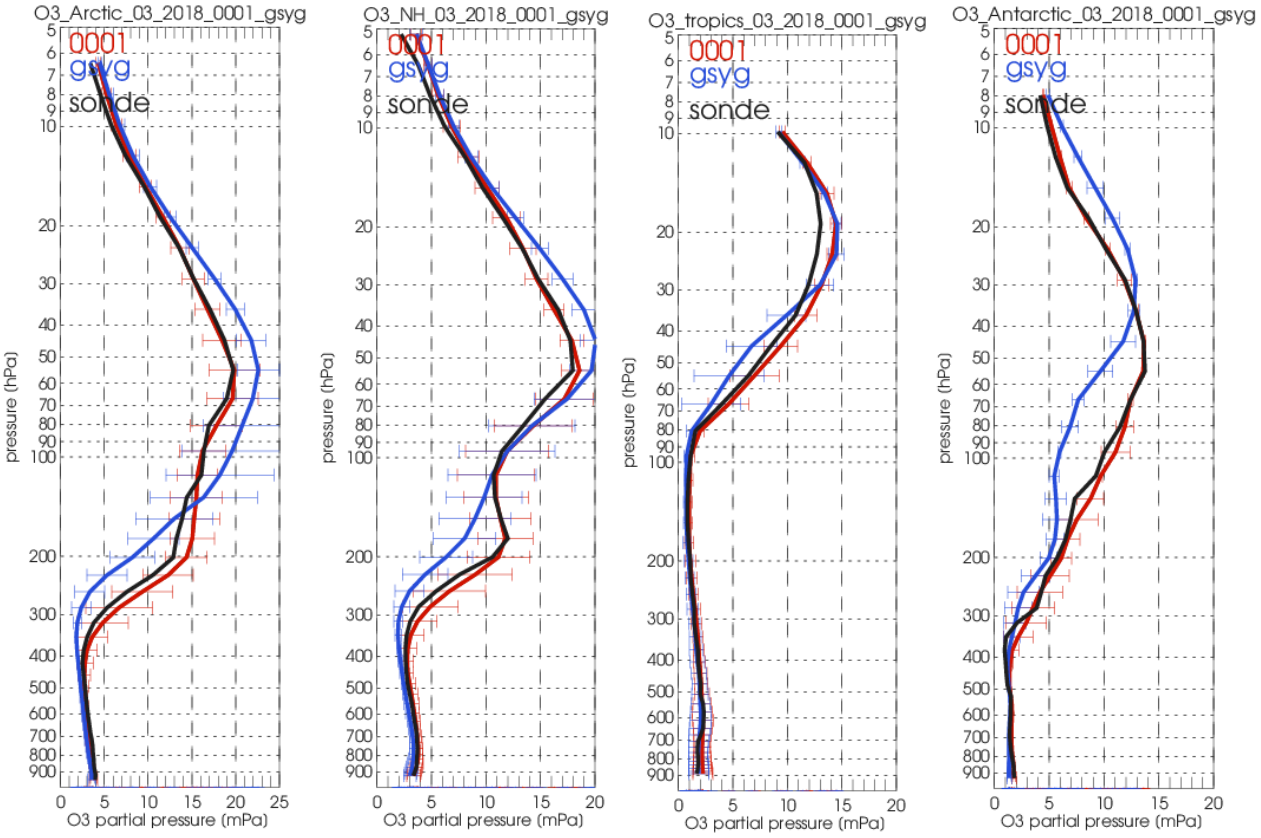

Figure 8.1.2: Comparison between mean O_3 profiles (units: mPa) of o-suite (red), and control (blue) in comparison with observed O_3 sonde profiles (black) for March 2018 for the various latitude bands: Arctic, NH-mid latitudes, Tropics and Antarctic.

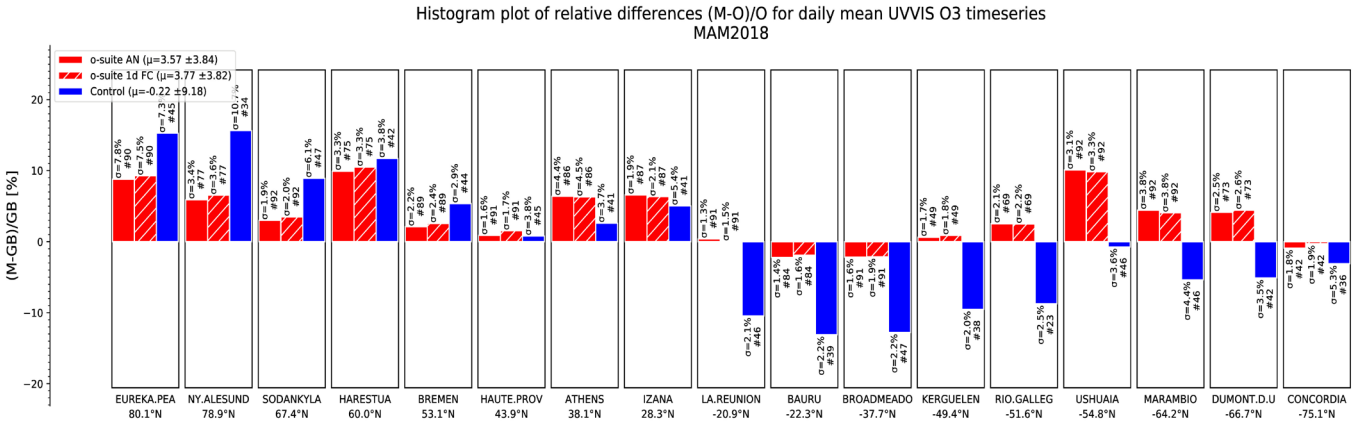

Figure 8.2.1 Relative biases during quarter MAM 2018 for 17 UVVIS stations measuring stratospheric ozone columns with ZENITH measurement geometry (stations sorted with decreasing latitude). The relative bias of the control run is reversed when transitioning from the Northern to the Southern Hemisphere.

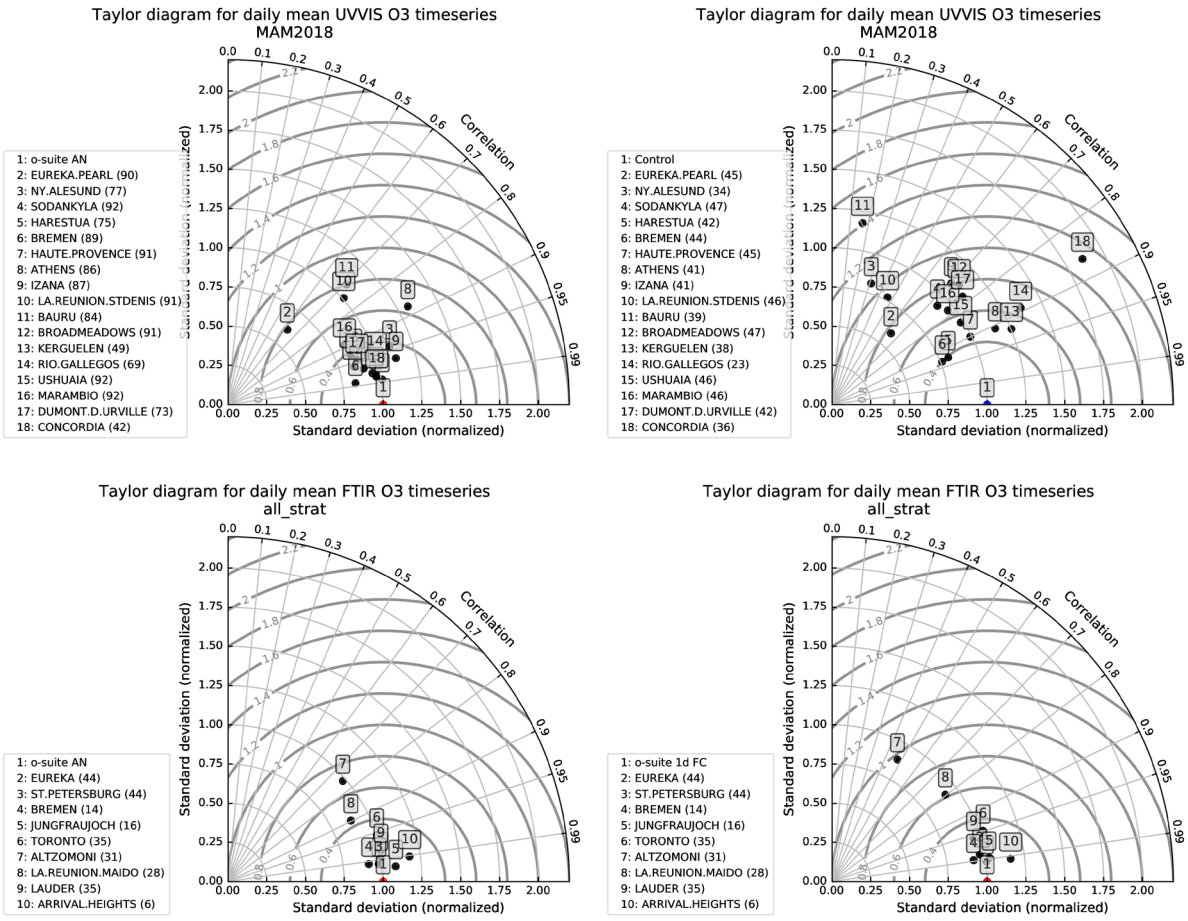

Figure 8.2.2 Taylor diagrams relating the standard deviations for the model and GB time series and their correlation. All time series are normalized such that the std of the model is 1. The increased correlation of all sites between control and o-suite (top row, using UVVIS) and between o-suite 1d FC and o-suite AN (bottom row, using FTIR) shows the positive effect of assimilation.

8.2 Validation against ozone observations from the NDACC network

UVVIS and FTIR stratospheric ozone columns

Since the start of the CAMS27 project, the number of UVVIS Zenith ozone measurements have increased on NDACC. Currently seventeen sites provided data in the recent quarter allowing for a representative picture on the latitude dependence of the model data.

The systematic uncertainty of the UVVIS measurements is typically 5%, hence the relative biases for all sites for the o-suite (AN and 1d FC) are within the uncertainty ranges. The control run shows a sign change of the bias between the northern and southern hemisphere, see Figure 8.2.1.

In Figure 8.2.3 depicts the FTIR stratospheric columns showing a slight positive trend in the observed relative differences which is more pronounced in the 1day o-suite forecast compared to the o-suite AN.

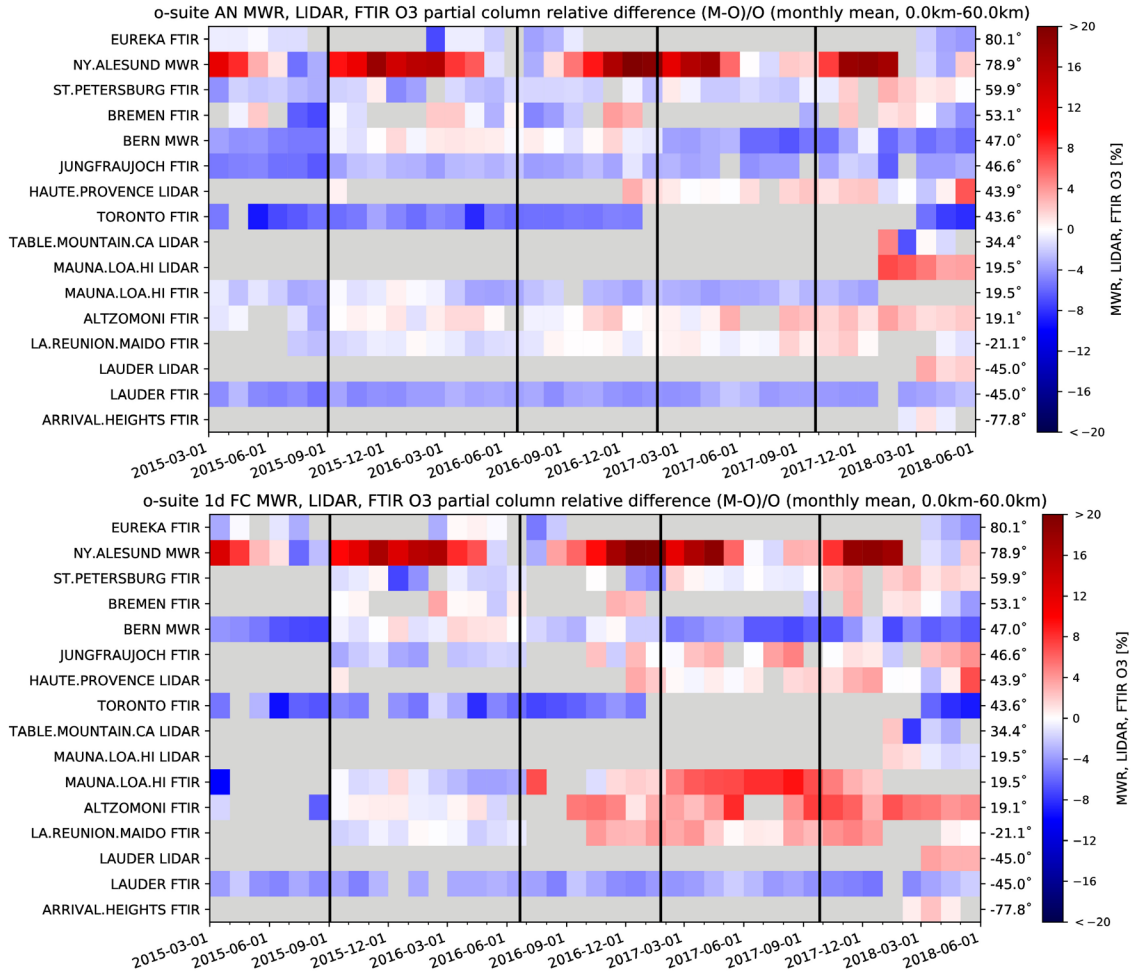

Figure 8.2.3 Time series of monthly mean relative differences for stratospheric columns (FTIR and LIDAR) and mesospheric (MWR) columns along with model cycle updates (black vertical lines) (o-suite AN top, o-suite 1d FC bottom). The stratospheric FTIR columns at St Peterburg, Jungfraujoch, Altzomoni and La Reunion show a slight positive trend in the relative differences.

The correlations between the sites and the model are presented in the Taylor diagrams in Figure 8.2.2. Comparing the Taylor diagrams of the control and o-suite AN model shows the positive effect of assimilation. From the Taylor diagram for the o-suite (left), the UVVIS (Izana, Reunion and Baura) and FTIR (Reunion and Altzomoni Mexico) tropical sites are the stations whose correlation with the o-suite AN model is lowest (≤.9, left diagram) and where the std of the difference between model and measurement is highest (>0.6*std(model)). This is probably due to a numerical artefact because the ozone concentration is much less variable at the tropics which has an impact on the numerical interpretation of the computation of the correlation and the difference relative to the std of the model time series.

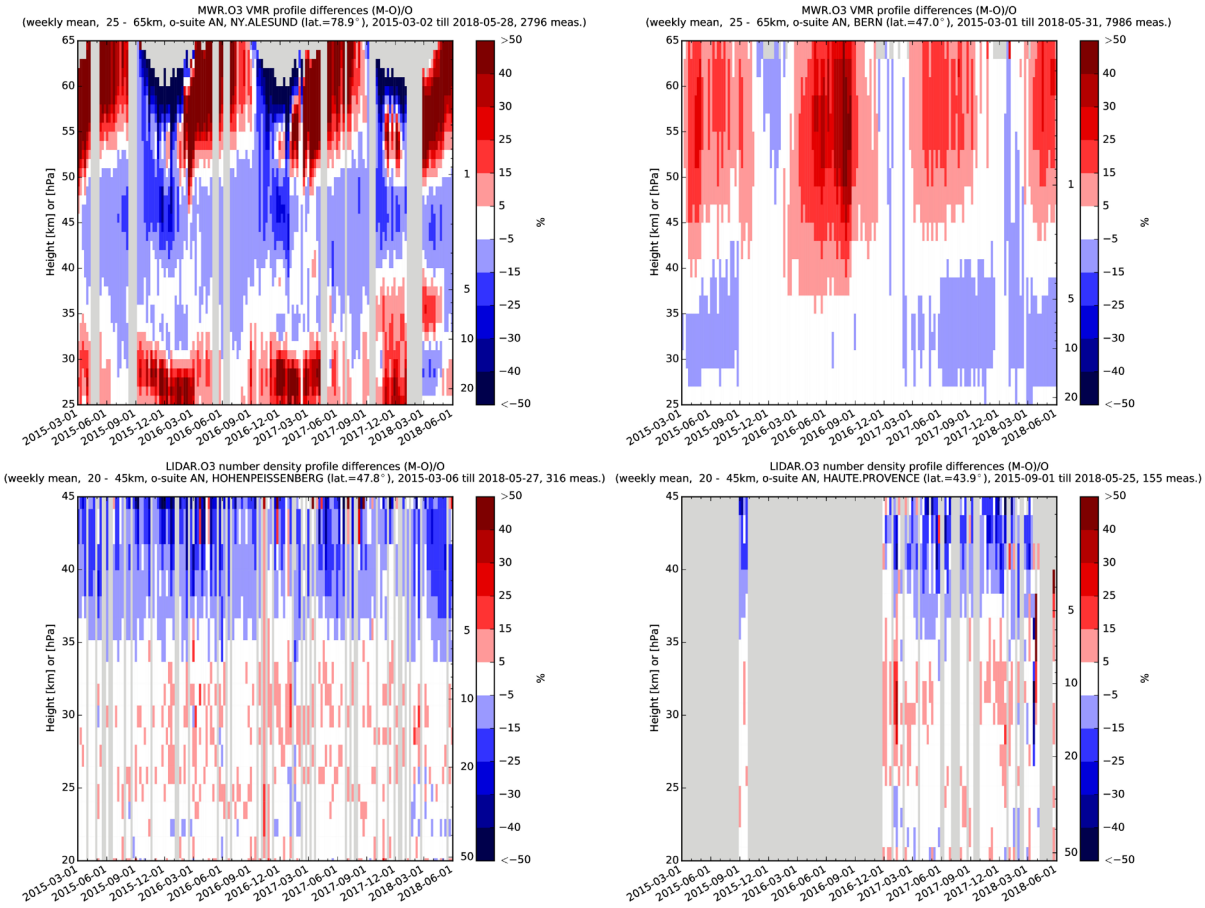

Figure 8.2.4: Comparison of the weekly mean profile bias between the O_3 mixing ratios of o-suite and the NDACC station at Ny Alesund, Bern, Hohenpeissenberg and OHP. For the LIDAR stations, the measurement uncertainty above 35km is comparable to the observed profile bias.

Ozone profile comparison using LIDAR and MWR

In this section we present a comparison between the CAMS o-suite and control run models against MWR and LIDAR observations from the NDACC network. A detailed description of the instruments and applied methodologies for all NDACC instruments can be found at http://nors.aeronomie.be. MWR (microwave) at Ny Alesund (79°N, 12°E, Arctic station) and Bern (47°N, 7°E, northern midlatitude station). LIDAR at Observatoire Haute Provence (OHP), France (43°N, 5.7°E, altitude 650m) and Hohenpeissenberg, Germany (47°N, 11°E, altitude 1km)

From Figure 8.2.3 at Ny Alesund the o-suite overestimates the stratospheric ozone concentration with more than 10% during SON/DJF/MAM and the bias vanishes during summer JJA. Between the model upgrades from September 2015 and January 2017 the relative bias at Bern nearly vanishes.

In MAM-JJA 2015-2017, both MWR stations observe a significant (i.e. comparable to the measurement uncertainty) overestimation of the upper stratospheric/mesospheric ozone content, and the converse is seen during autumn and winter SON-DJF, underestimating up to -30% (Ny Alesund), see also Figure 8.2.4. At BERN the difference between osuite and MWR at 25-35km is negligible since Sept 2015 (compared to the MWR profile uncertainty).

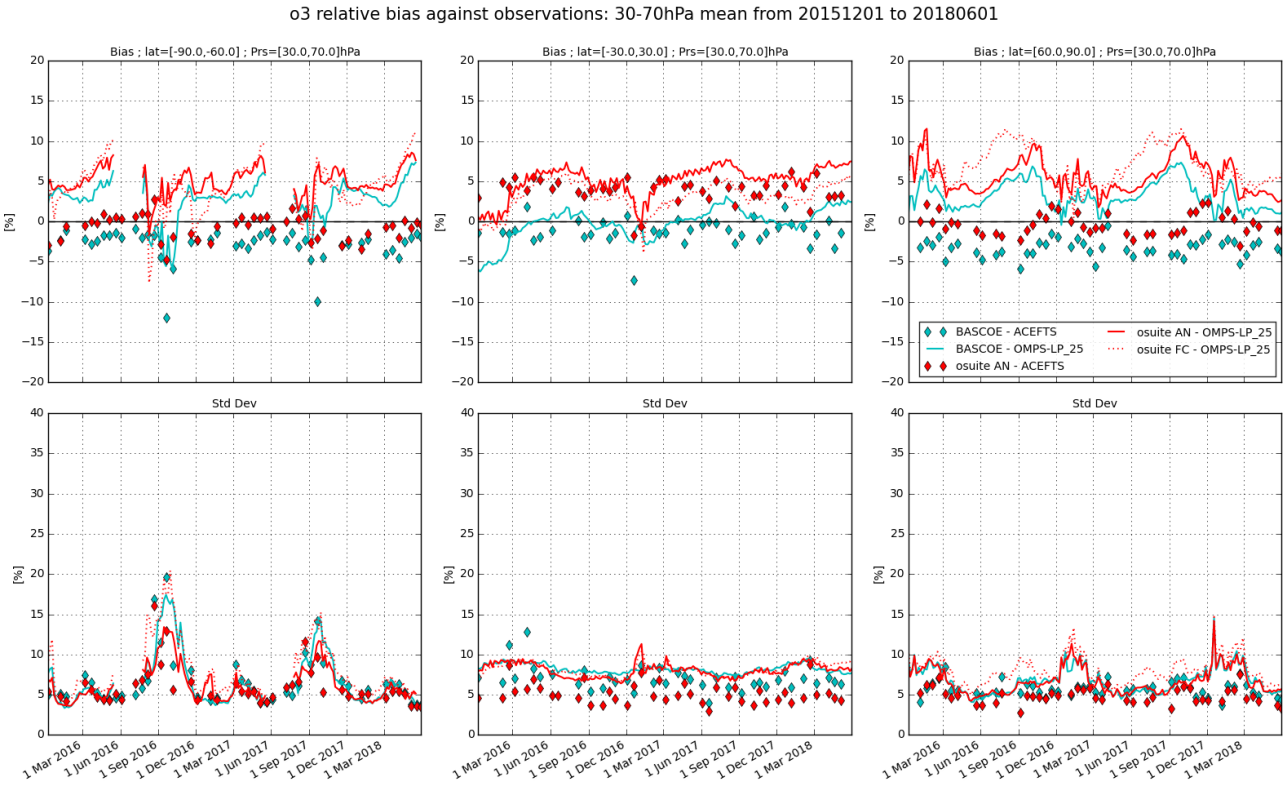

Figure 8.3.1: Time series comparing models to observations for the period 2015-12-01 to 2018-06-01 in the middle stratosphere (30-70hPa averages): o-suite analyses vs OMPS-LP (red, solid), o-suite forecasts 4th day vs OMPS-LP (red, dotted), o-suite analyses vs ACE-FTS (red markers), BASCOE vs OMPS-LP (cyan, solid) and BASCOE vs ACE-FTS (cyan markers). Top row, normalized mean bias (model-obs)/obs (%); bottom row, standard deviation of relative differences (%).

At OHP and Hohenpeissenberg (LIDAR), the o-suite slightly overestimates the observed ozone (<10%) between 25km and 35km. The uncertainty on the LIDAR concentration increases with altitude and above 35km the observed differences are comparable to the measurement uncertainty (>10%, see http://nors.aeronomie.be/projectdir/PDF/NORS_D4.2_DUG.pdf)

8.3 Comparison with dedicated systems and with observations by limb-scanning satellites

This section compares the output of the o-suite for the last period with observations by limb-scanning satellite instruments, using the methodology described by Lefever et al. (2015). We also include the comparisons for the o-suite 4th day forecasts (96h to 120h) of stratospheric ozone. These forecasts are represented by dotted lines in the figures.

All datasets are averaged over all longitudes and over the three most interesting latitude bands for stratospheric ozone: Antarctic (90°S-60°S), Tropics (30°S-30°N) and Arctic (60°N-90°N). In order to provide global coverage, the two mid-latitude bands (60°S-90°S and 60°N-90°N) are also included in some comparisons with satellite observations.

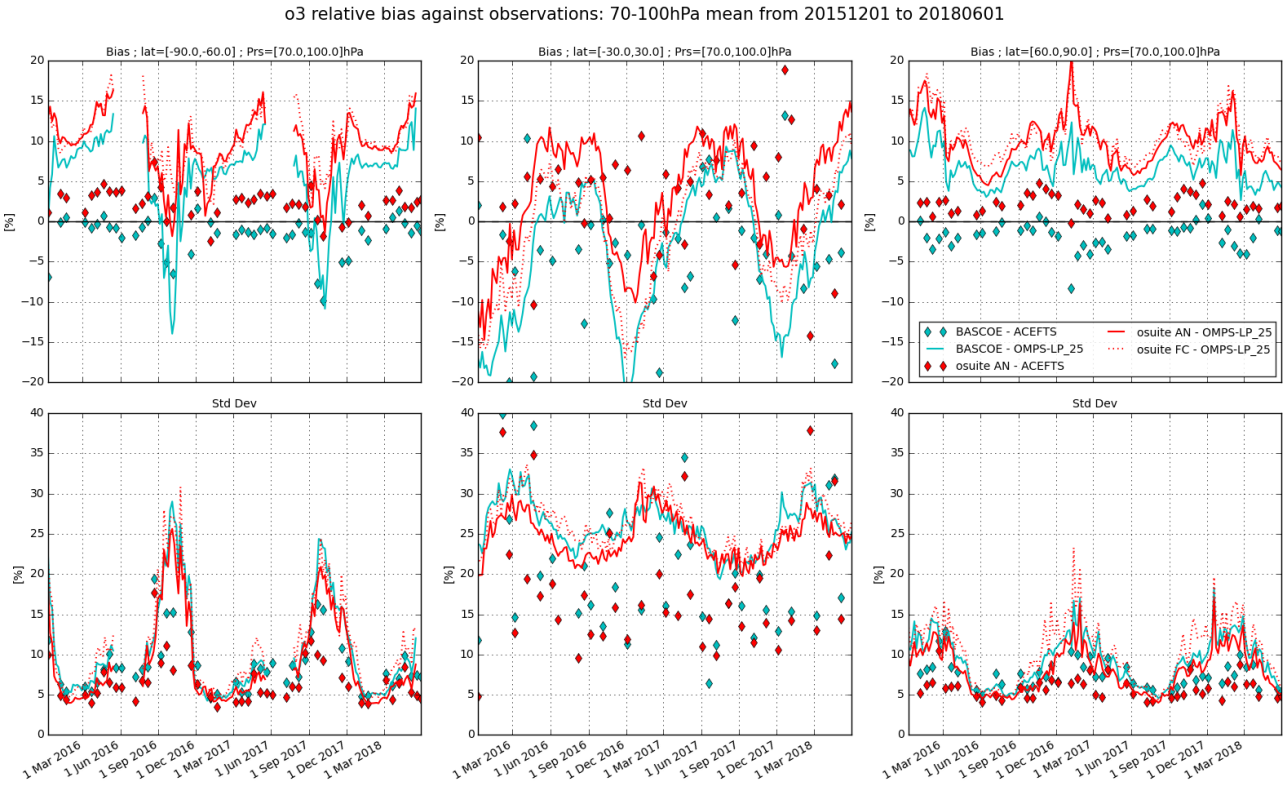

Figure 8.3.2: Time series comparing models to observations for the period 2015-12-01 to 2018-03-01 in the lower stratosphere (70-100hPa averages): o-suite analyses vs OMPS-LP (red, solid), o-suite forecasts 4th day vs OMPS-LP (red, dotted), o-suite analyses vs ACE-FTS (red markers), BASCOE vs OMPS-LP (cyan,solid) and BASCOE vs ACE-FTS(cyan markers). Top row, normalized mean bias (model-obs)/obs (%);bottom row, standard deviation of relative differences (%).

In this section, we use on one hand the version 2.5 of OMPS-LP (i.e. the Limb Profiler) and the version 3.6 of ACE-FTS. For reference, we include also the BASCOE analyses which are very constrained by the AURA MLS offline profiles.

Figure 8.3.1 and Figure 8.3.2 present, in the upper row, the timeseries over the last 30 months of the bias of the o-suite against the two satellite measurements for respectively two regions of the lower stratosphere and UTLS (30-70hPa and 70-100hPa); the bottom row of the figures shows the standard deviation of the differences and can be used to evaluate the random error in the analyses.

Compared to OMPS-LP in the 30hPa to 70hPa region, there is a systematic overestimation by the o-suite: up to 8% in the South polar region and in the tropics and up to 12% in the North polar region. Compared to OMPS-LP in the 70hPa to 100hPa region, the North polar bias increases up to 20% at various periods, while the variability of the bias is much stronger in the South polar region; the tropics exhibits a strong seasonal variation for the bias, with a high variability indicated by the standard deviation.

The agreement with ACE-FTS is much better: the bias is generally within ±5%, except in the tropics for 70hPa to 100hPa region, where the standard deviations indicate less reliable results.

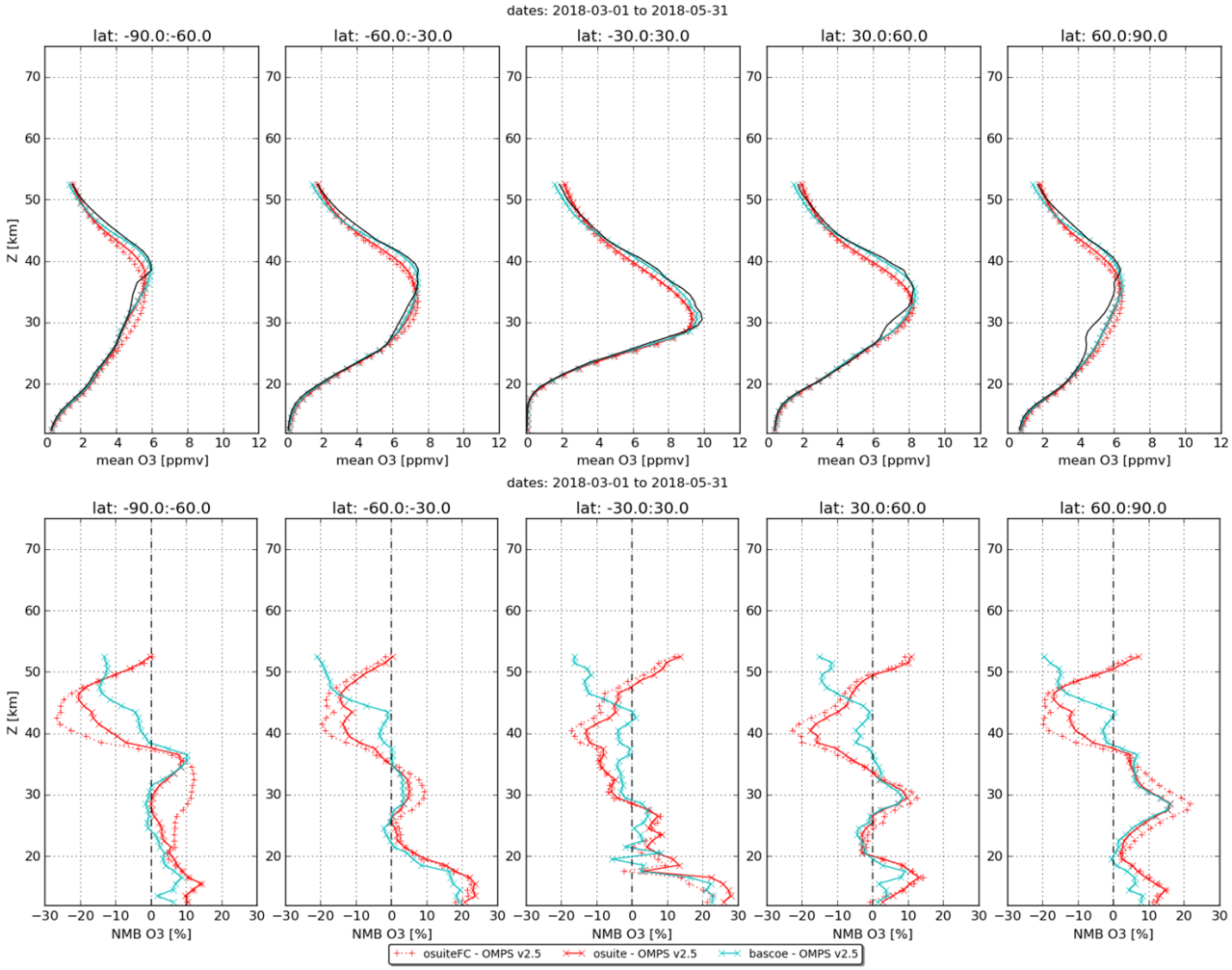

Figure 8.3.3: Mean value (top) and normalized mean bias (bottom) of the ozone profile between o-suite analyses (red, solid), o-suite forecasts 4th day (red, dotted) and BASCOE (cyan line) with OMPS-LP v2.5 observations for the period March to May 2018.

The bias of BASCOE against the satellite observations for the considered regions is systematically lower, but follows a similar evolution as the o-suite.

Figure 8.3.3 and Figure 8.3.4 display vertical profiles of the relative biases between the o-suite or BASCOE and the satellite measurements. The difference is averaged over the most recent 3-month period considered in this validation report, i.e. March to May 2018.

The OMPS-LP profiles are much more irregular than the ACEFTS or MLS profiles, e.g. a notch at around 30km for the north midlatitude and north polar region. Outside these anomalous zones, the relative bias between o-suite and OMPS-LP is <±10% between 20km and 35km.

The negative bias above 40km is confirmed by the ACEFTS profiles, otherwise there is a good agreement in the middle and lower stratosphere.

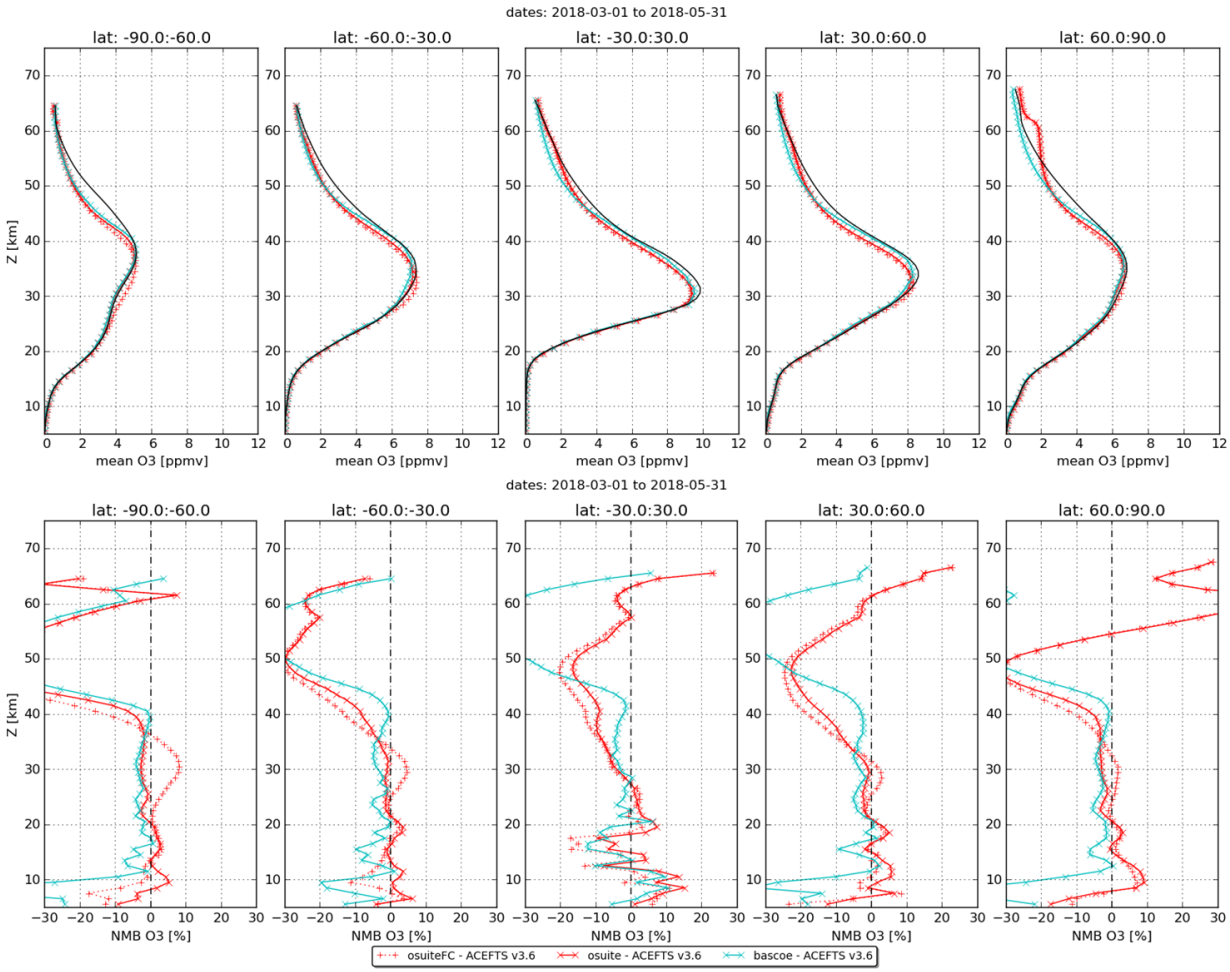

Figure 8.3.4: Mean value (top) and normalized mean bias (bottom) of the ozone profile between o-suite analyses (red, solid), o-suite forecasts 4th day (red, dotted) and BASCOE (cyan line) with ACE-FTS observations for the period March to May 2018.

It must be noted that the different instruments have a variety of spatial and temporal coverage: for a 3 month period and over the latitude bands considered, OMPS and Aura MLS (not shown) provide daily data with more than 40000 valid profiles, while ACE-FTS provides around 750 profiles in the polar region and 150 profiles in the tropics.

8.4 Stratospheric NO_2

In this section, nitrogen dioxide from SCIAMACHY/Envisat satellite retrievals (IUP-UB v0.7) and GOME-2/MetOp-A satellite retrievals (IUP-UB v1.0) are used to validate modelled stratospheric NO_2 columns. Monthly mean stratospheric NO_2 columns from SCIAMACHY and GOME-2 have relatively small errors on the order of 20% in the tropics and in mid-latitudes in summer and even lower errors at mid-latitudes in winter. As the time resolution of the saved model files is rather coarse and NO_x photochemistry in the stratosphere has a large impact on the NO_2 columns at low sun, some uncertainty is introduced by the time interpolation at high latitudes in winter.

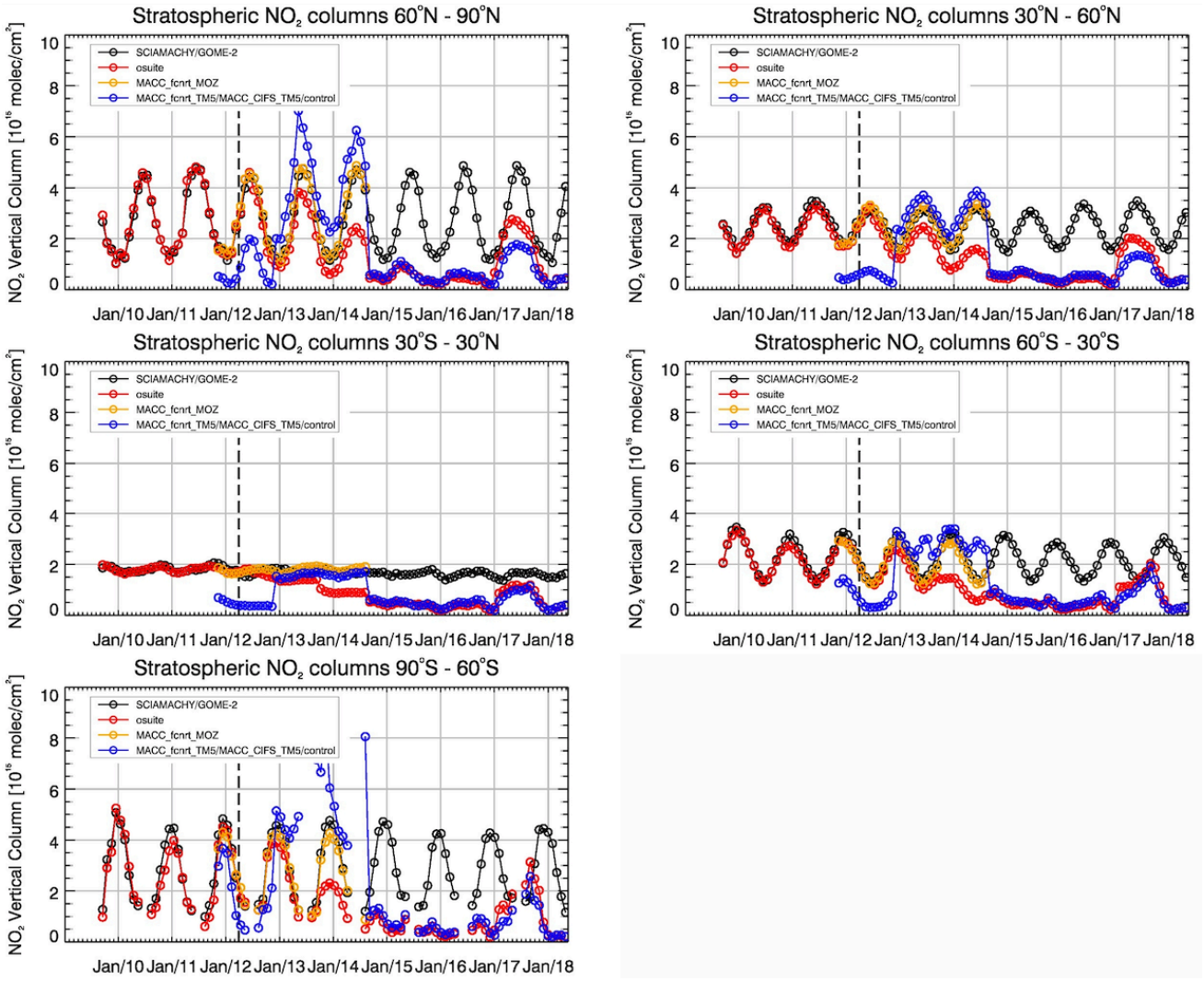

Figure 8.4.1: Time series of average stratospheric NO2 columns [1015 molec cm-2] from SCIAMACHY (up to March 2012) and GOME-2 (from April 2012) compared to model results for different latitude bands. See text for details. The blue line shows MACC_fcnrt_TM5 from November 2011 to November 2012, MACC_CIFS_TM5 results from December 2012 until August 2014 and control results from September 2014 onwards (the model run without data assimilation is termed control since Sep 2014). The vertical dashed black lines mark the change from SCIAMACHY to GOME-2 based comparisons in April 2012.

In this section, nitrogen dioxide from SCIAMACHY/Envisat satellite retrievals (IUP-UB v0.7) and GOME-2/MetOp-A satellite retrievals (IUP-UB v1.0) are used to validate modelled stratospheric NO_2 columns. Monthly mean stratospheric NO_2 columns from SCIAMACHY and GOME-2 have relatively small errors on the order of 20% in the tropics and in mid-latitudes in summer and even lower errors at mid-latitudes in winter. As the time resolution of the saved model files is rather coarse and NO_x photochemistry in the stratosphere has a large impact on the NO_2 columns at low sun, some uncertainty is introduced by the time interpolation at high latitudes in winter.

As shown in Figure 8.4.1, amplitude and seasonality of satellite stratospheric NO_2 columns are poorly modelled with CB05-based chemistry runs including the more recent versions of the o-suite. The significant differences between observations and CB05 chemistry runs, i.e. a strong

underestimation of satellite retrievals by models, can be explained by the missing stratospheric chemistry for these model versions. The only constraint on stratospheric NO_x is implicitly made by fixing the HNO_3/O_3 ratio at the 10 hPa level. This assumption, in combination with the changing model settings for stratospheric O_3 for control compared to MACC_CIFS_TM5, may explain some of the jumps we see in stratospheric NO_2. In any of these runs the stratospheric NO_2 is poorly constrained. It clearly indicates that stratospheric NO_2 in the latest versions of the o-suite is not a useful product and should be disregarded. However, model simulated values increased with the last upgrade of the osuite in February 2017, so that simulations are closer to the satellite observations for 2017 only, especially for northern hemisphere latitude bands where seasonality seems to be reproduced (in contrast to the Southern Hemisphere where seasonality is not reproduced) by the o-suite apart from the pronounced underestimation. O-suite values are larger than the control in2017 at all latitude bands. However, the better agreement found for 2017 does not continue for 2018, values decreased again to the magnitute of 2015-2016 runs at all latitude bands.

Comparison of the o-suite from July 2012 until August 2014 with the other model runs and satellite observations shows that the previous version of the o-suite stratospheric NO_2 columns have a systematic low bias relative to those from MACC_fcnrt_MOZ and satellite observations for all latitude bands. For example, o-suite values are a factor of 2 smaller than satellite values between 60°S to 90°S for October 2013. Best performance was achieved with the MOZART chemistry experiments without data assimilation (MACC_fcnrt_MOZ, running until September 2014), especially northwards of 30°S. Details on the NO_2 evaluation can be found at:
http://www.doas-bremen.de/macc/macc_veri_iup_home.html.

9. Validation results for greenhouse gases

9.1 CH4 and CO2 validation against ICOS observations

This section describes the NRT validation of the pre-operational, high resolution forecast of CO_2 and CH_4 from 1st January 2017 to 25 March 2018 based on observations from 20 surface stations, mostly located in Western Europe. Compared to the previous reports, five stations have been added: Jungfrauhoch (JFJ, Switzerland), Hohenpeissenberg (HPB, Germany), Gartow (GAT, Germany), Hyytiala (SMR, Finland), Kresin U Pacova (KRE, Czech Republic). First one is a mountain site, whereas the four others are tall towers with multi-levels sampling. We have also switched to the new high resolution forecast experiment *gqpe* (previous reports were using the experiments *ghqy*). The same experiment is used for the validation of CO_2 and CH_4 simulations using ICOS surface data and TCCON total column data (TCCON evaluation is available until the end of May).

Figures 9.1.1 and 9.1.2 show the CO_2 and CH_4 comparisons at four stations in South hemisphere (Amsterdam I.), North hemisphere (Mace Head, Trainou tall tower) and in the tropics (Lamto). The best agreement is obtained at the two north hemisphere sites for both CO_2 and CH_4. This is due particularly to the good representation of the wintertime pollution events observed regularly at MHD and TRN. The timing of those synoptic events are very well simulated even if their amplitudes are generally underestimated by 1 to 3% for CO_2. At the remote station of AMS, in South hemisphere, the model overestimates the amplitude of the seasonal CO_2 variation by ±1 ppm (±0.25%). At the same station, the amplitude and phase of the CH_4 concentrations are well represented. The only mismatch is a bias of +0.8% in early 2017, which decrease close to 0 in March 2018. This is a clear improvement compared to the previous *ghqy* experiment which underestimated the CH4 concentrations by -2% (-40 ppb) in early 2017. At the tropical station of Lamto, the model shows a very poor correlation coefficient for CO_2 (r^2=0.13) due to an overestimation of the concentrations in January-March 2017, and even more important from October to December 2017. For CH_4 we observe a better correlation (r^2=0.6) but the model systematically underestimates the observed variabilities at synoptic and seasonal scales with a bias between 0% and -6%.

The figure 9.1.3 presents the annual metrics for all surface stations based on comparisons of the daily means mole fractions, with a distinction between observed and simulated data obtained for daytime (12-16hr local time) and nighttime (00-04hr local time). There is a significant improvement of the performance of the model when looking exclusively at daytime time series, especially for CO_2. Some common features are emerging from the 20 sites.

First, for CO_2 we see a clear improvement of the correlation coefficient with the sampling heights of the tall towers, especially during the nighttime. During the day the correlation coefficients are greater than 0.75 for all sampling levels, a performance which is also reached in nighttime for sampling levels higher than 100m. We observe a convergence of the correlation coefficient, RMSE and biases (mostly negative during the night and positive during the day) with the elevation of the sampling lines. Below 50m from the ground the CO_2 biases are +2.3 ppm and -2.2 ppm respectively during day and night, whereas above 100m they are down to +0.8 and -0.6 ppm. At tropical sites the correlation coefficients are significantly poorer, ranging from 0.3 to 0.6.

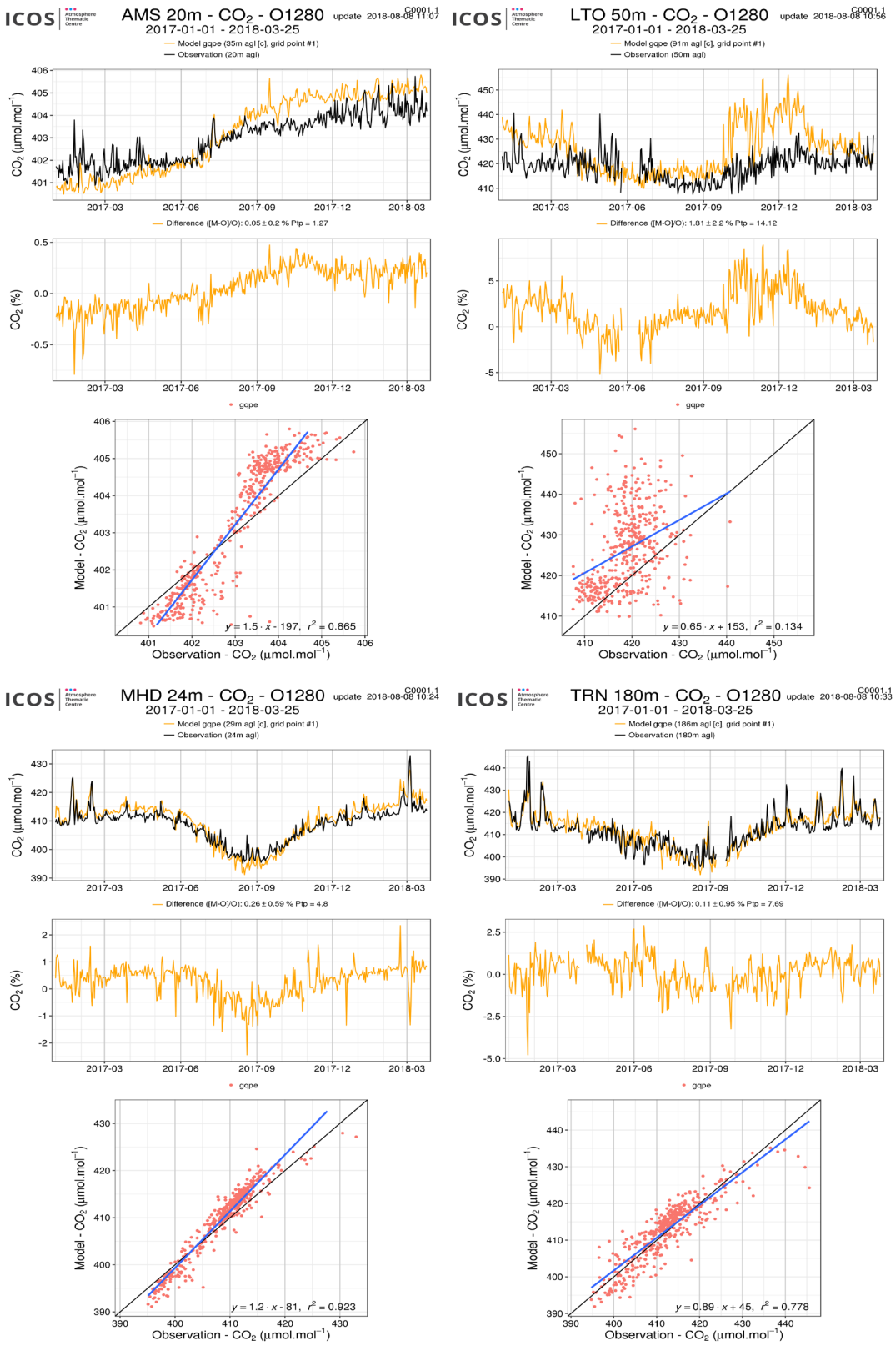

Figure 9.1.1: Above: Comparison of CO_2 daily means observed (black) and simulated (orange) at four stations (Amsterdam I., Mace Head, Lamto and Trainou tall tower). Middle: differences of the observations minus the simulations. Below: Linear fit between observations and simulations.

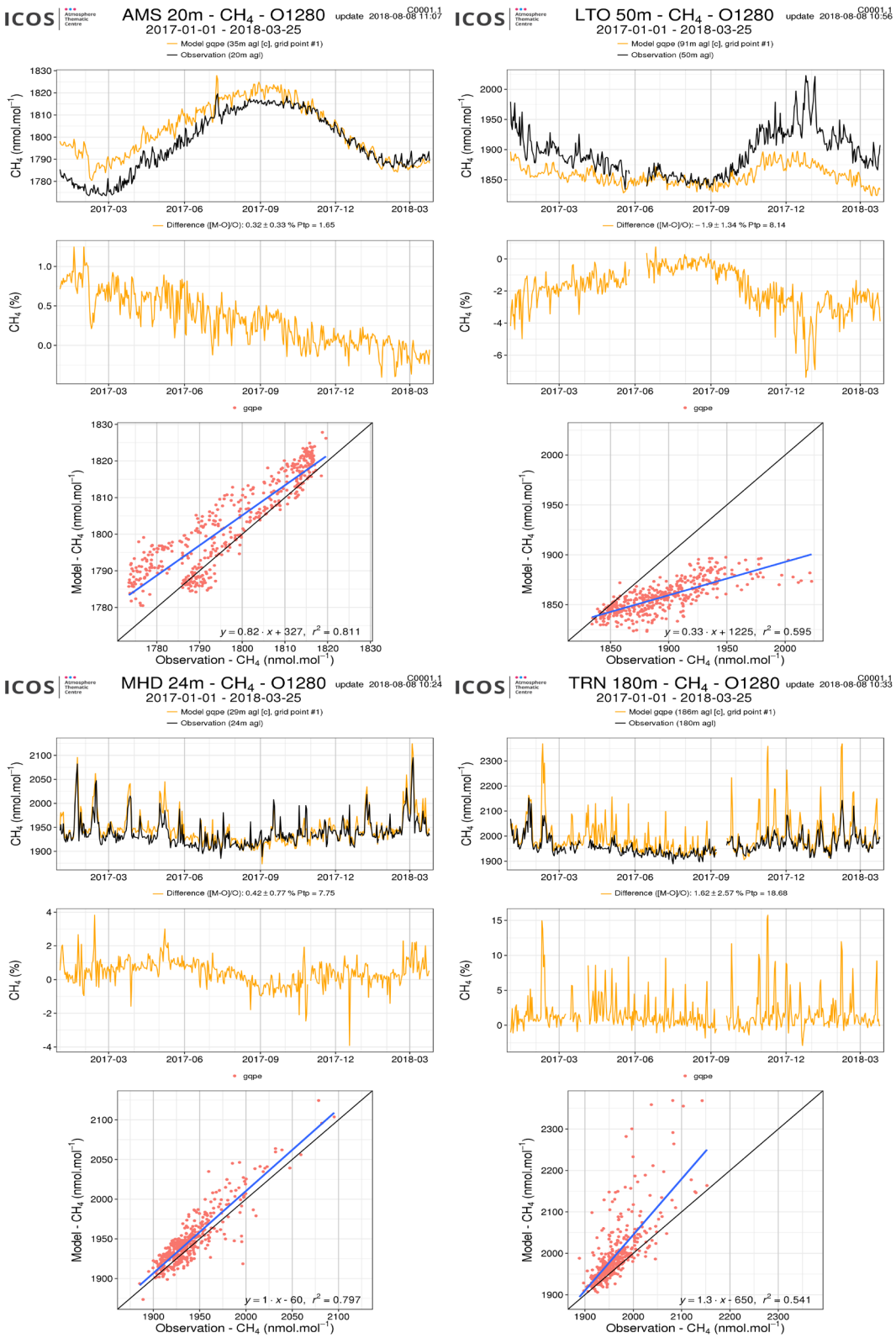

Figure 9.1.2: Same as figure 4.1.1, but for CH_4.

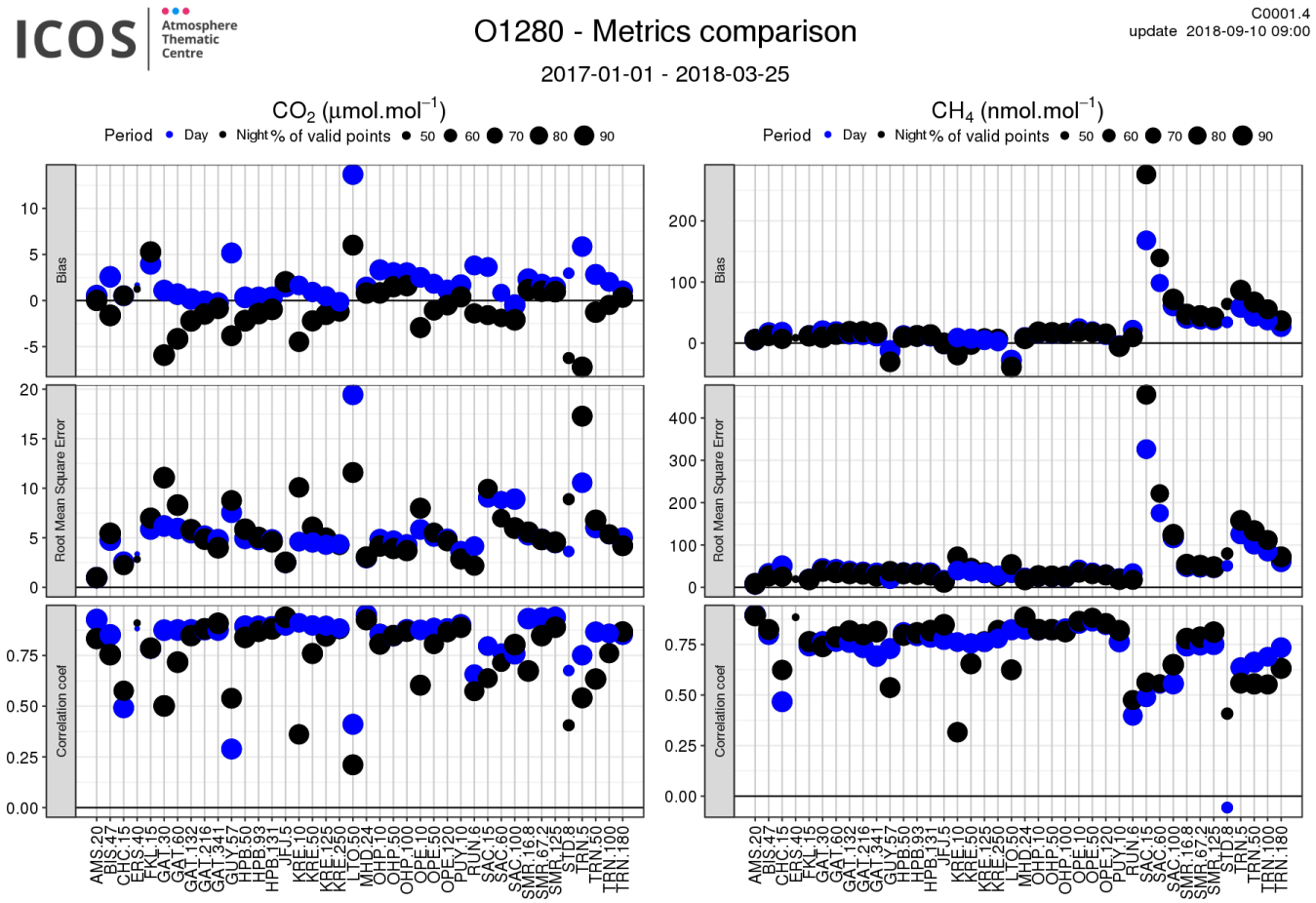

Figure 9.1.3: Annual metrics (bias, RMSE and coefficient correlation) calculated from the model-data comparison for daily means of CO2 (left) and CH4 (right) at the 20 sites (with multiple sampling heights at 8 tall towers). The size of each point relates to the percentage of available data. This figure uses GQPE experiment from 1st January 2017 to 25 March 2018. Daytime data (12-16 hr local time) are shown in blue, and nighttime data (00-04 hr local time) in black.

For CH_4, there is much less difference of the model performance between day and night. The coefficient of correlations are generally higher than 0.75 with few exceptions. In North hemisphere the model has more difficulty to represent the variability observed at Saclay and Trainou tall towers. The model strongly overestimates the synoptic events associated to the emission from Paris area, located at 20 and 100 km respectively from the two stations. Apart from those two stations the mean biases in North hemisphere are 16, 11 and -3 ppb respectively for tall towers, coastal and mountain sites. At Amsterdam Island in South Hemisphere the mean bias is +6 ppb. All tropical sites appear as outliers compared to the North hemisphere stations, illustrating the difficulty of the model to represent those stations.

We have also compared two high resolution forecast experiments *gqpe* and *gxk8*. The latter, which will take over *gqpe*, was started on January 2018, enabling for a three months comparison. The main difference is a correction applied to the CO_2 surface model which should result in a better seasonal cycle, particularly in the northern hemisphere. As shown above the *gqpe* experiment was indeed overestimating the amplitude of the seasonal cycle by ±1%.

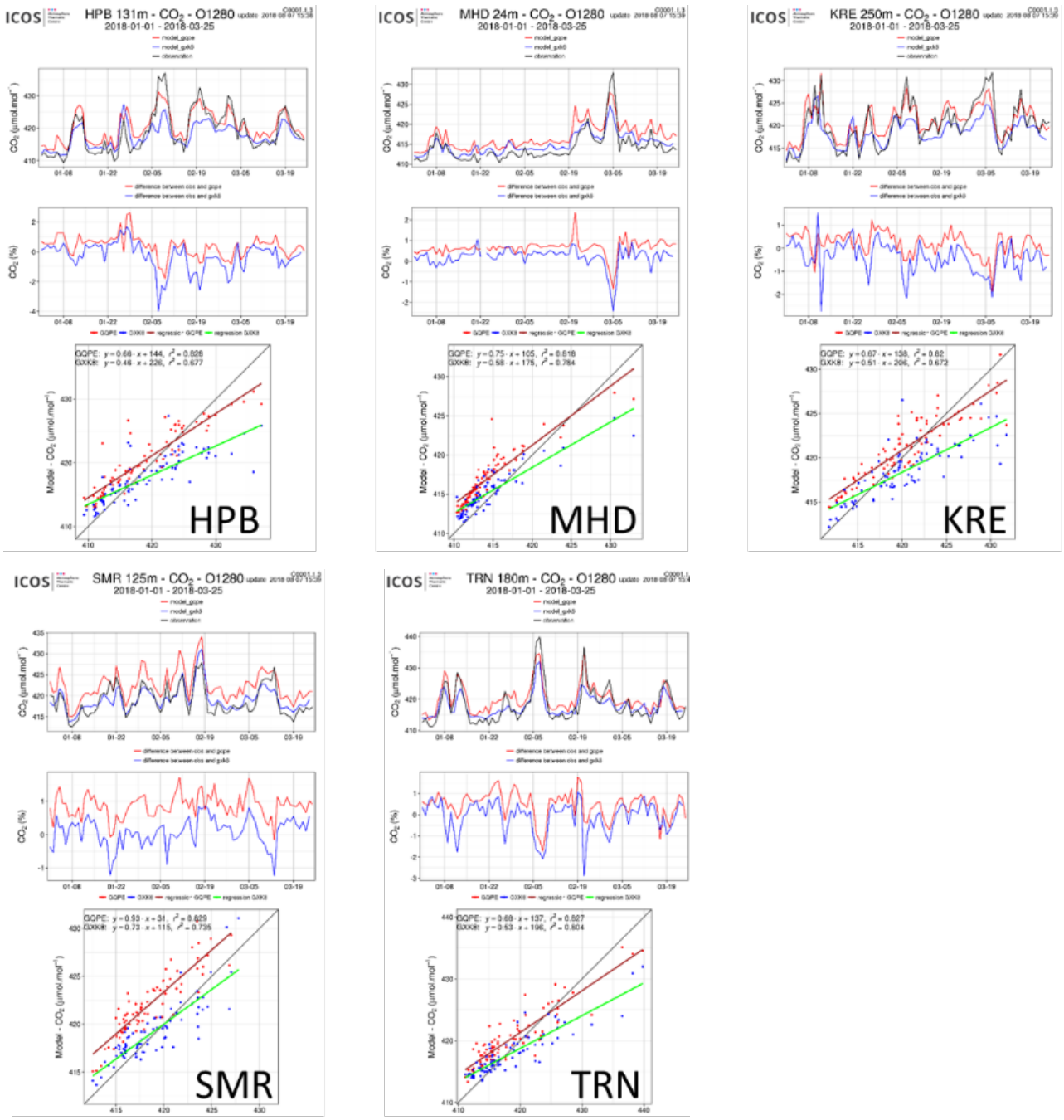

Figure 9.1.4: Above: Comparison of CO_2 daily means observed (black) and two simulations: GQPE (red) and GXK8 (blue), at five stations in North Hemisphere. Middle: differences of the observations minus the two simulations. Below: Linear fit between observations and simulations.

Figure 9.1.4 shows a clear improvement of the background CO_2 level at stations in Western Europe. The decrease of the background CO_2 level in winter by about 0.5% should contributes to reduce the mismatch of the seasonal cycle. We will need a longer period to assess this improvement. This decrease of the background level is also highlighting the overestimation of the amplitude of synoptic events. No significant changes are observed for CO_2 at tropical & south hemisphere sites, neither for CH_4 simulation.

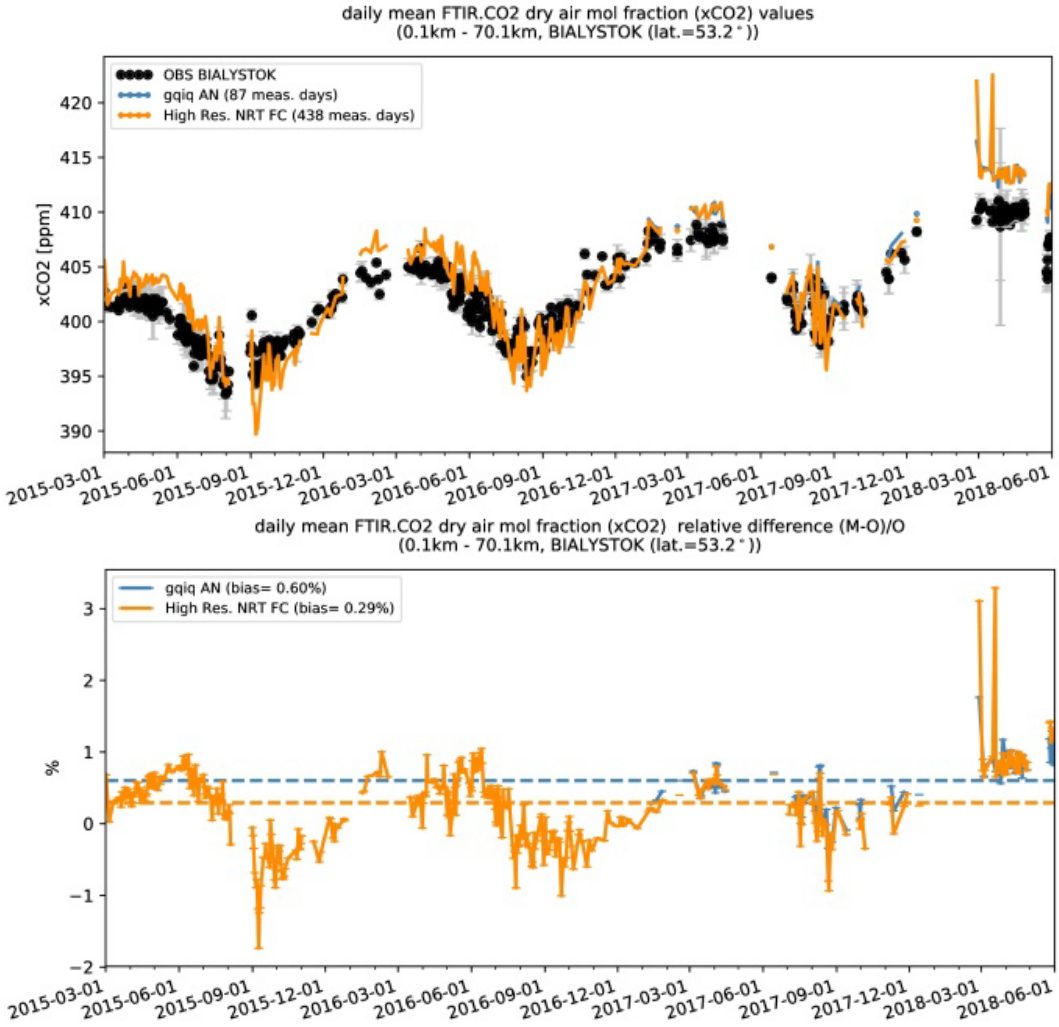

Figure 9.2.1: Time series of column averaged mole fractions (top) and relative difference (bottom) of carbon dioxide (CO_2) at the TCCON site Bialystok compared to model data.

9.2 CH4 and CO2 validation against TCCON observations

For the validation column averaged mole fractions of CO_2 and CH_4 (denoted as XCO2 and XCH4) from the Total Carbon Column Observing Network (TCCON) are used. Column averaged mole fractions provide different information than the in situ measurements and are therefore complementary to the in situ data. For example if models suffer from problems in vertical transport, the combination of TCCON and surface in situ measurements will provide a means to detect this.

For the model validation the official TCCON data cannot be used due to its availability of typically one year after the measurement. Some TCCON sites are providing rapid delivery data (RD-TCCON data), which is available at least one month after the measurement. TCCON sites that deliver RD-TCCON data currently include Trainou (France, close to Orléans), Bialystok (Poland) and Reunion (France). Over the course of the project more TCCON sites might contribute. This largely depends on funding for the fast data product.

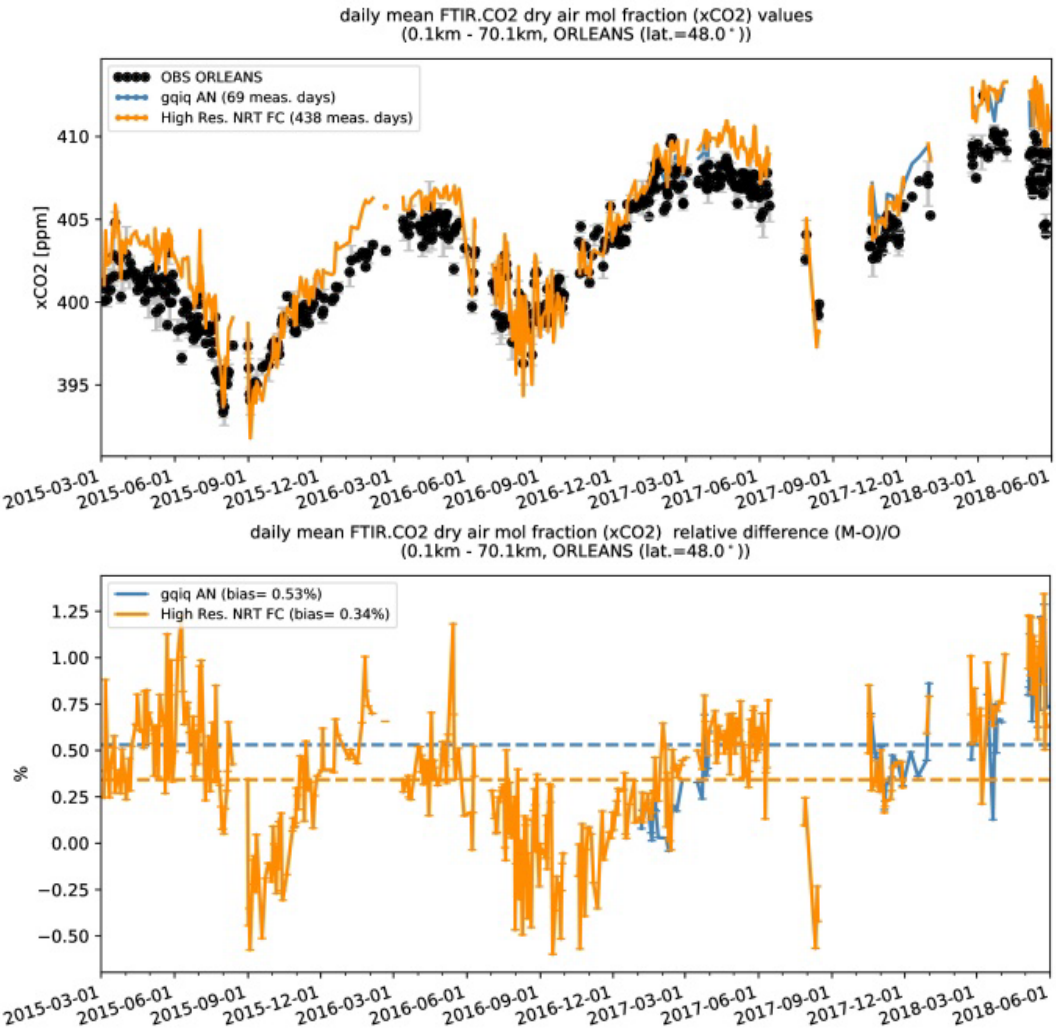

Figure 9.2.2: Time series of column averaged mole fractions (left) and relative difference (right) of carbon dioxide (CO2) at the TCCON site Orléans compared to the high resolution runs (orange) and analysis (blue).

At the time this report was prepared only the TCCON sites Bialystok and Orleans were available for the reporting period. At Reunion a problem with the solar tracker resulted in the lack of measurements. It should be noted that some of the gaps in data at Orleans and Bialystok existing in previous reports have been filled. These gaps were the result of instrumental problems and careful work was required to correct the spectra. This work has now been carried out and the data is presented in this report.

The validation routines used for TCCON data are the same as used for the NDACC network and are documented in Langerock et al. (2015). The routines have been adapted to use the TCCON data format. Only measurements within 2.5h around local noon have been used for the comparison.

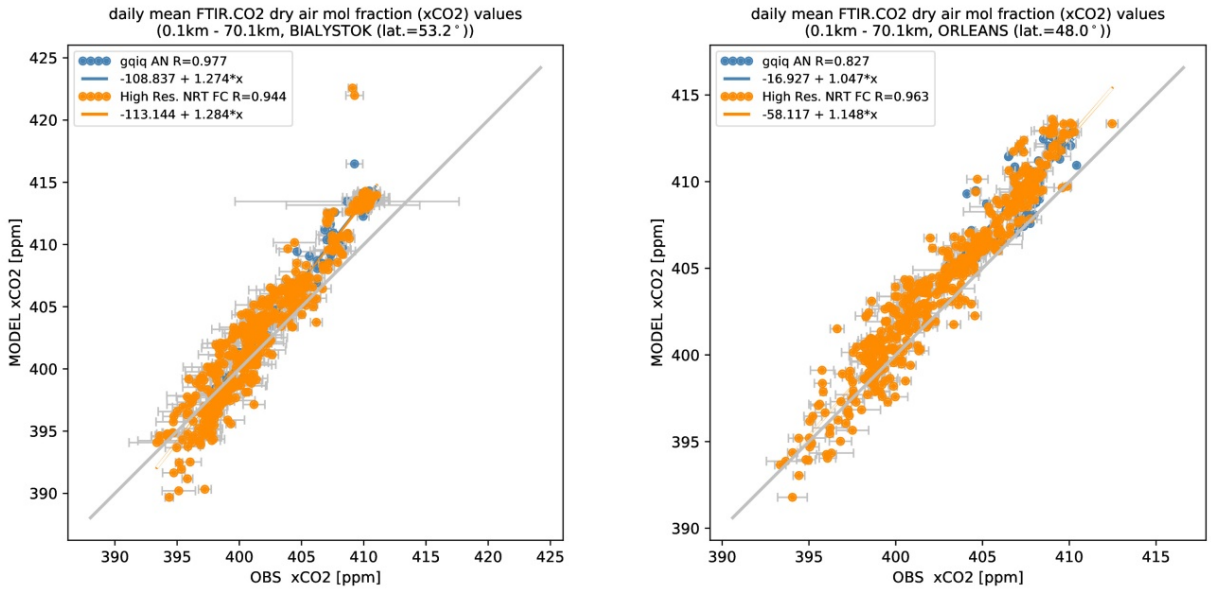

Figure 9.2.3 Scatter plots for the measured CO_2 column averaged mole fractions and model data for the TCCON sites Bialystok (left) and Orleans (right).

9.2.1 Evaluation against TCCON CO2

The data presented in the Figures 9.2.1-9.2.2 show a comparison for the time period March 2015 – June 2018. The gqiq AN model starts in January 2017. The high resolution FC is a concatenation of the ghqy model and the gqpe model from March 2018. At Bialystok (Fig. 9.2.1) and Orleans (Fig. 9.2.2) the difference between the model and the measurement shows a very similar seasonal pattern. The models predict slightly higher CO_2 during the maximum of the CO_2, which is also clearly visible in Fig. 9.2.3.

9.2.2 Evaluation against TCCON CH_4

At Bialystok and Orleans the gqiq AN model compares very good with the measurements. As far as it can be judged from the limited time of comparison it also captures the seasonality well.

For the high res NRT model one can clearly see the improved comparison from March 2018 onwards. This is the point when the gqpe replaces the ghqy model. The previous high resolution model underestimated the XCH4 by about 1-1.5%. The o-suite underestimate the XCH4 by 3-4% at Bialystok and Orleans.

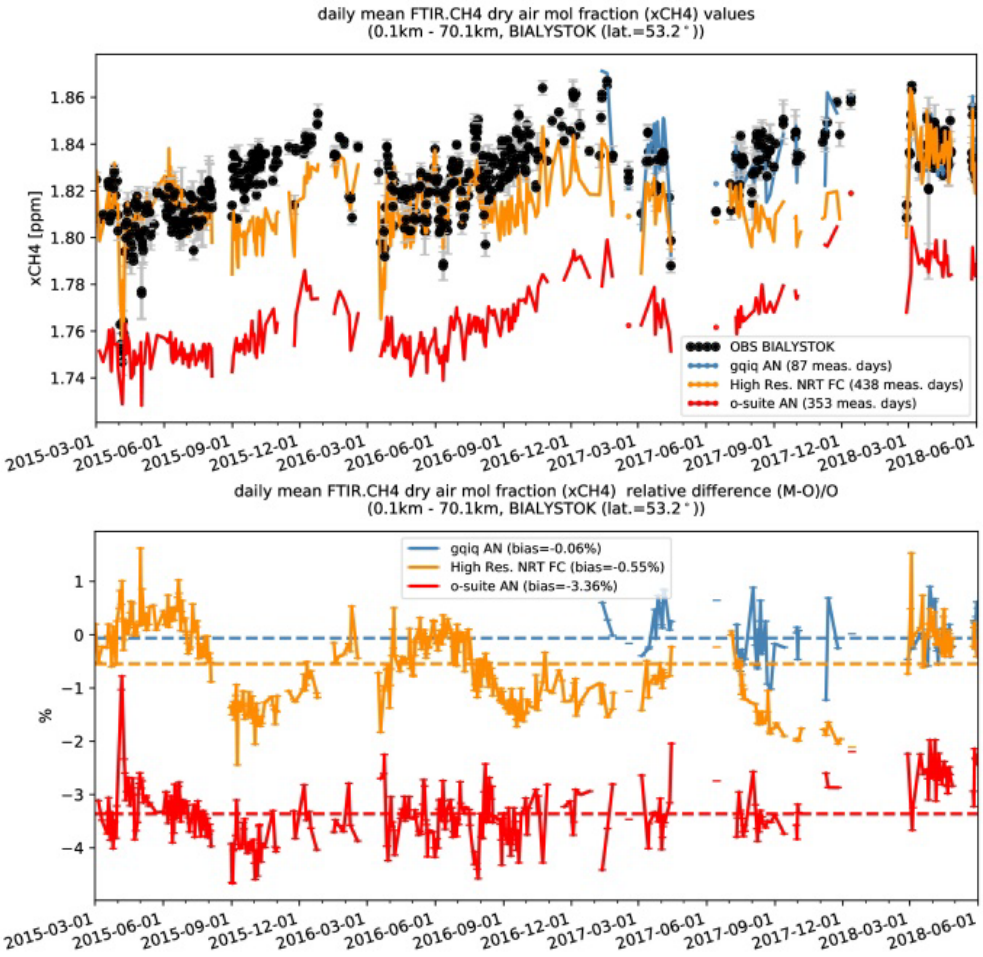

Figure 9.2.4: Time series of column averaged mole fractions (left) and relative difference (right) of methane (CH_4) at the TCCON site Bialystok compared to model data.

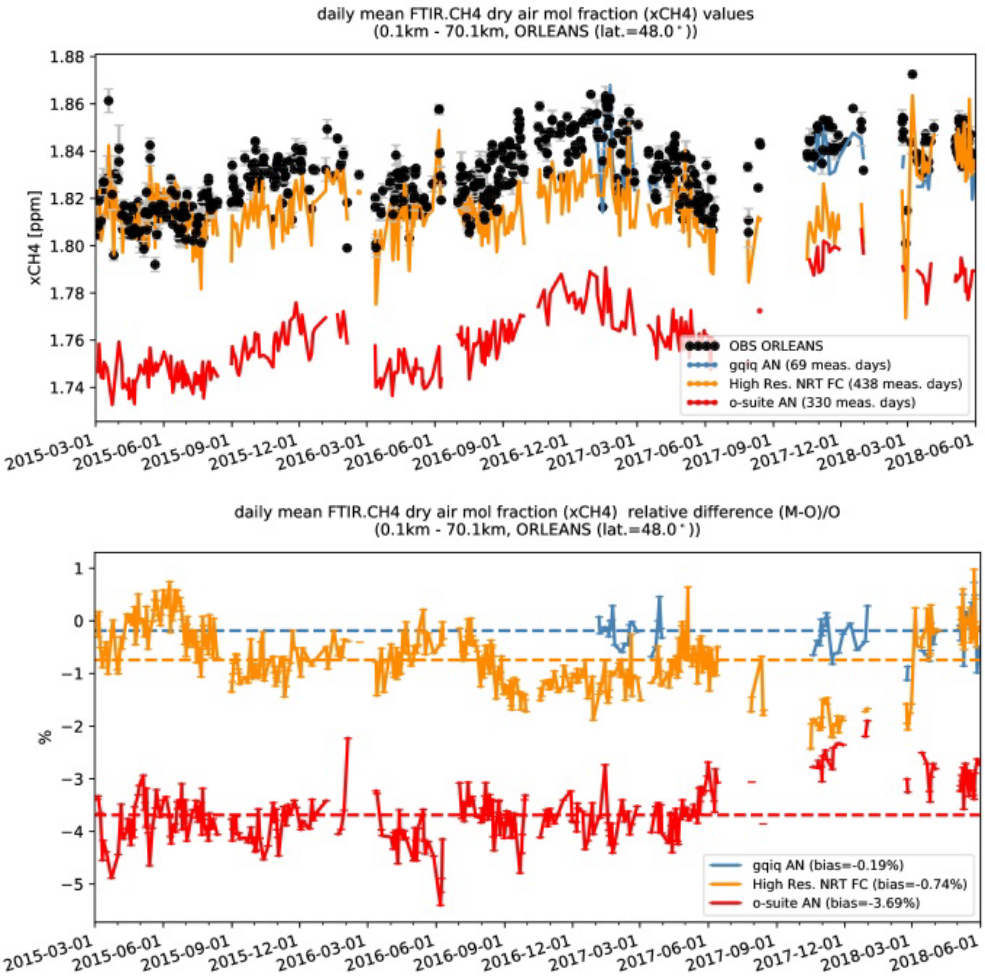

Figure 9.2.5: Time series of column averaged mole fractions (left) and relative difference (right) of methane (CH_4) at the TCCON site Orleans compared to model data.

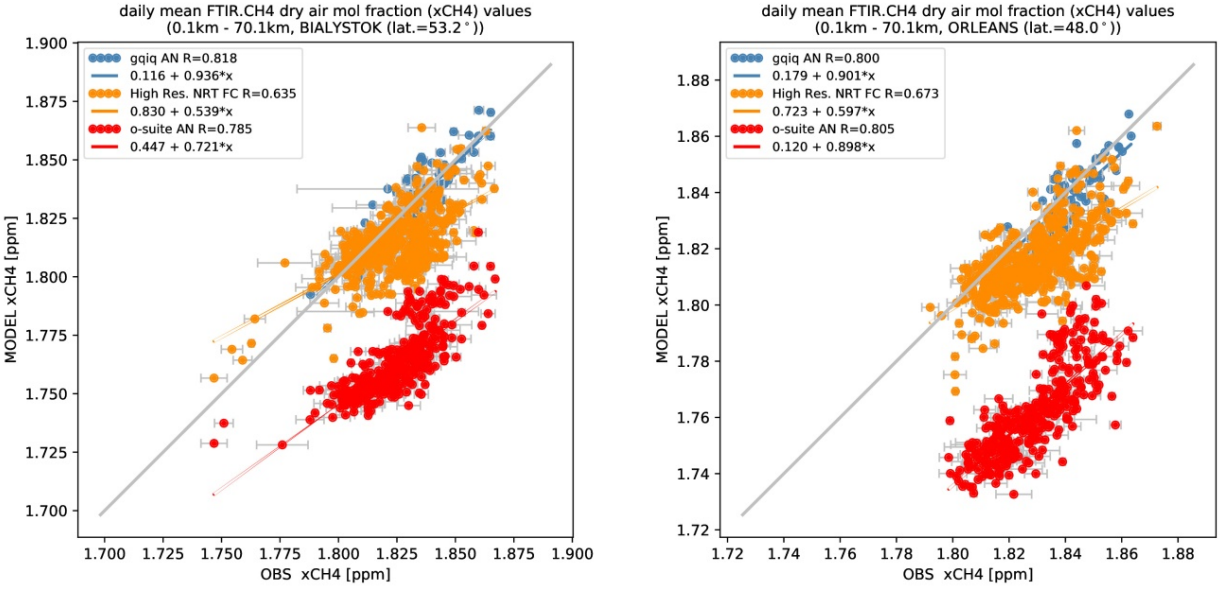

Figure 9.2.6 Scatter plots for the measured CH_4 column averaged mole fractions and model data for the TCCON sites Bialystok (left) and Orleans (right).

10. Event studies

10.1 Dust over the Arabian and Iberian Peninsulas: late April 2018

A dense wall of dust pushed across the Arabian Peninsula in late April 2018. The intensified north-westerly wind caused dust to rise from the Iraq Desert area and move in a south-easterly direction affecting Iraq, Kuwait, Bahrain, Qatar, Kingdom of Saudi Arabia, United Arab Emirates (UAE), and to reach Yemen the next days achieving AOD up to 7.3 and reducing drastically the visibility less than 300 m in sites in the Persian Gulf.

Massive dust storm lashed Riyadh city and its suburbs in the late afternoon on 23rd April, rendering traffic disruptions due to low visibility on the roads as it was reported in different media channels. The large storm stretched roughly 500 km across the Arabian Peninsula. When the Visible Infrared Imaging Radiometer Suite (VIIRS) on Suomi NPP captured this image on April 23, 2018, dust had nearly reached Riyadh, Saudi Arabia's capital and most populous city (see Figure 10.1.1). Large sand storms in this region are often fueled by strong northwesterly winds known as the Shamal.

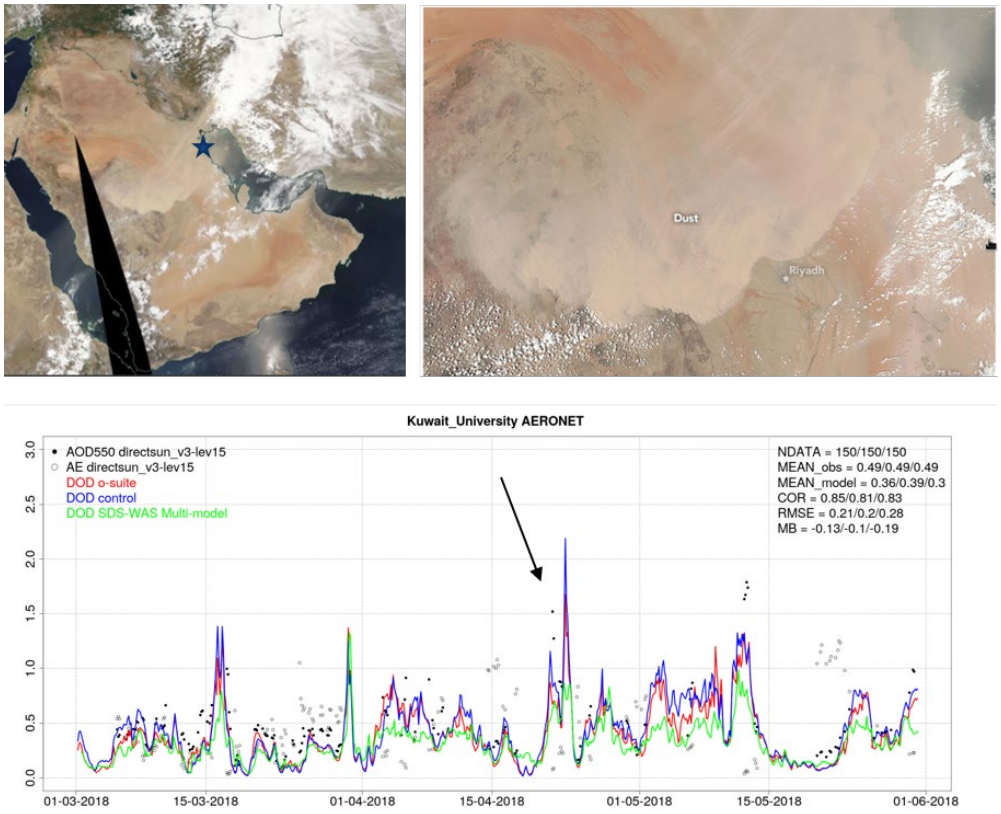

Figure 10.1.1: Upper panels. NASA MODIS/Aqua (right) and Suomi NPP — VIIRS (left) image on 23rd April 2018. LANCE/EOSDIS Rapid Response. Lower panel: Model vs AERONET observations over Kuwait University (its location is indicated in the MODIS/Aqua image). AOD from AERONET (black dot), AOD o-suite (red line), AOD control (blue line), AOD-Nat o-suite (orange line), AOD-Nat control (cyan line). Skill scores per each individual site and model (o—suite/control/SDS-WAS Multi-model) are shown in the upper right corner (NDATA: available 3-hourly values used for the calculations, MEAN observations, MEAN_model, COR, RMSE, MB).

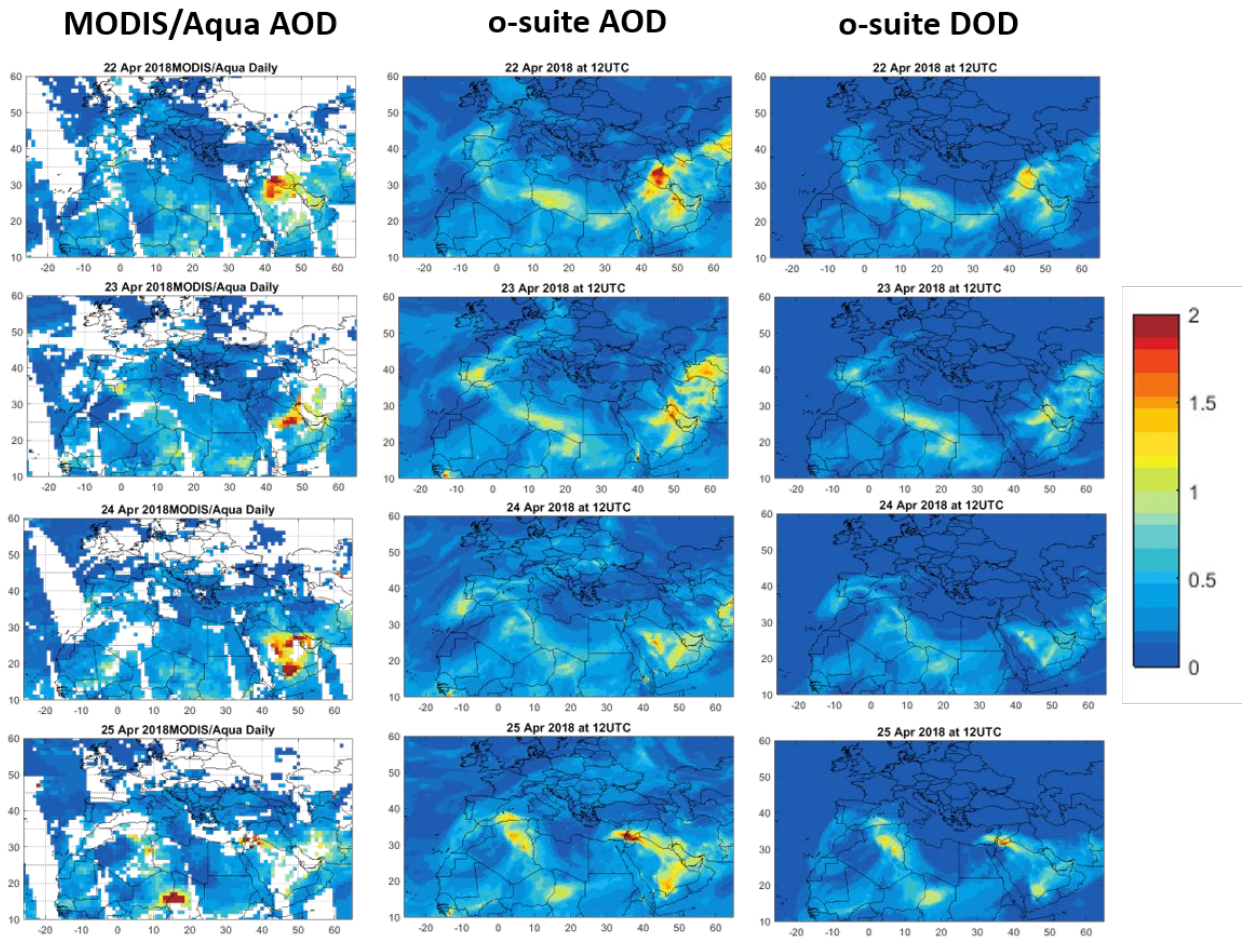

Figure 10.1.2. AOD and DOD at 12UTC from o-suite (central and right column) and AOD from MODIS-Aqua combined Dark Target and Deep Blue aerosol products (left column), from April 22 to April 25, 2018. MODIS-Aqua overpasses are around 12UTC over the study period.

CAMS AOD o-suite can timely reproduce the spatial distribution of the dust plume over the Arabian Peninsula in comparison with AERONET over Kuwait University (see Figure 10.1.1 bottom panel) and MODIS/Aqua (see Figure 10.1.2) despite the model tends to underestimate the observed maximum values during the whole event. At surface levels, CAMS models are also able to reproduce the spatial evolution of the dust transport showing a correspondence with a reduction of the visibility (see Figure 10.1.3).

During the same period, it is observed some hot spots of dust in Libya (on 22-23 April) and Algeria (on 25th April). These events affected the Iberian Peninsula giving one week of high AOD (up to 1.2 in Madrid, Figure 10.1.4) and PM10/PM2.5 (up to 60 µg/m^3 in Villar Arzobispo and Zorita in Figure 7.4.5). The comparison with the visibility observations (Figure 10.1.3) also shows a reduction of the visibility associated to the dust from 22 to 25 April indicating the ability of the CAMS model to predict the extension and timing of the event. This intrusion over the Iberian Peninsula is well predicted by the CAMS model although it overestimates its magnitude as it is shown in comparison with AERONET and EIONET observations.

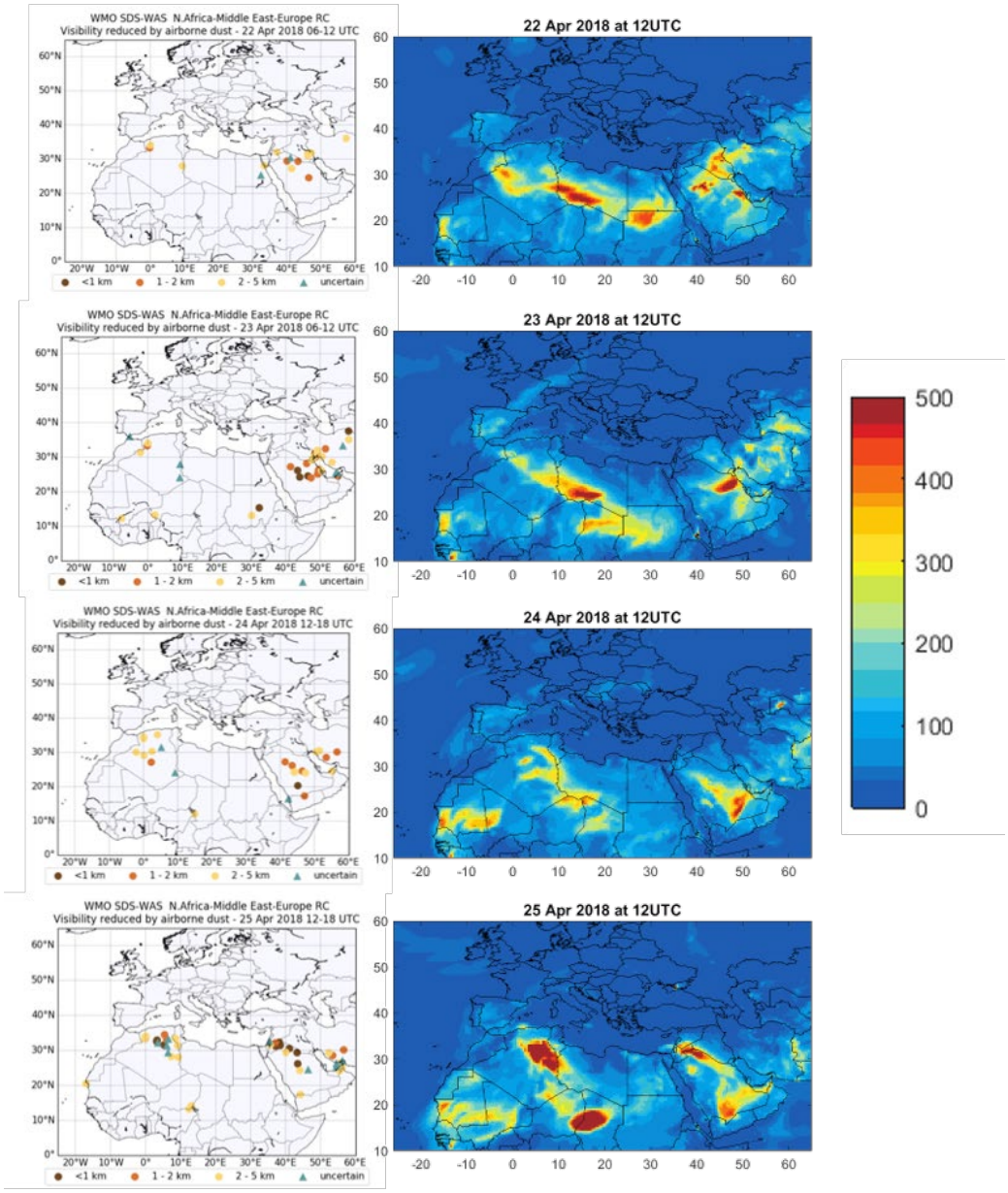

Figure 10.1.3. PM10 (in µg/m^3) at 12UTC from o-suite (right column) and visibility (in km) from METAR reports (left column), from April 22 to April 25, 2018.

As it is pointed out in Sect 4.4, higher dust concentrations predicted by the CAMS model over this spring season are linked to an increase of the magnitude of the predicted gusts winds that consequently causes an enhancement of the dust emissions over desert dust source regions. Consequently, the transported dust to long-range regions as Europe is increased during this season.

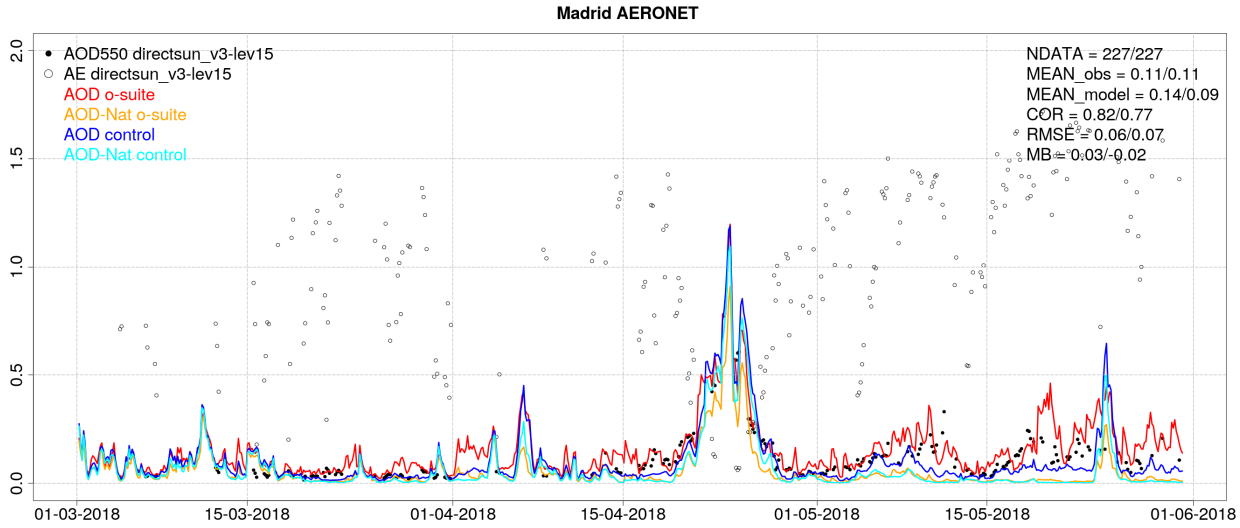

Figure 10.1.4: AOD from AERONET (black dot), AOD o-suite (red line), AOD control (blue line), AOD-Nat o-suite (orange line), AOD-Nat control (cyan line), for the study period over Madrid (Central Spain). AOD-Nat corresponds to the natural aerosol optical depth that includes dust and sea-salt. Skill scores per each individual site and model (o—suite/control) are shown in the upper right corner (NDATA: available 3-hourly values used for the calculations, MEAN observations, MEAN_model, COR, RMSE, MB).

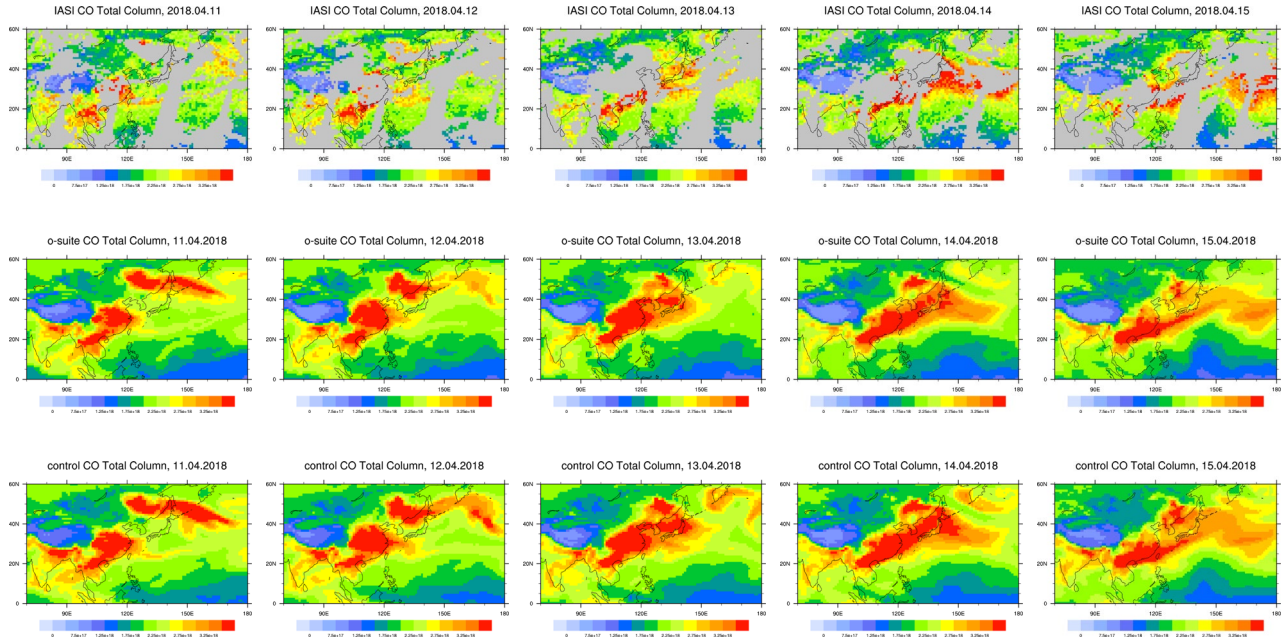

Fig. 10.2.1. CO total column from IASI (top), o-suite (middle) and control runs (bottom) from 11-15.04.2018 over the of Indochinese.

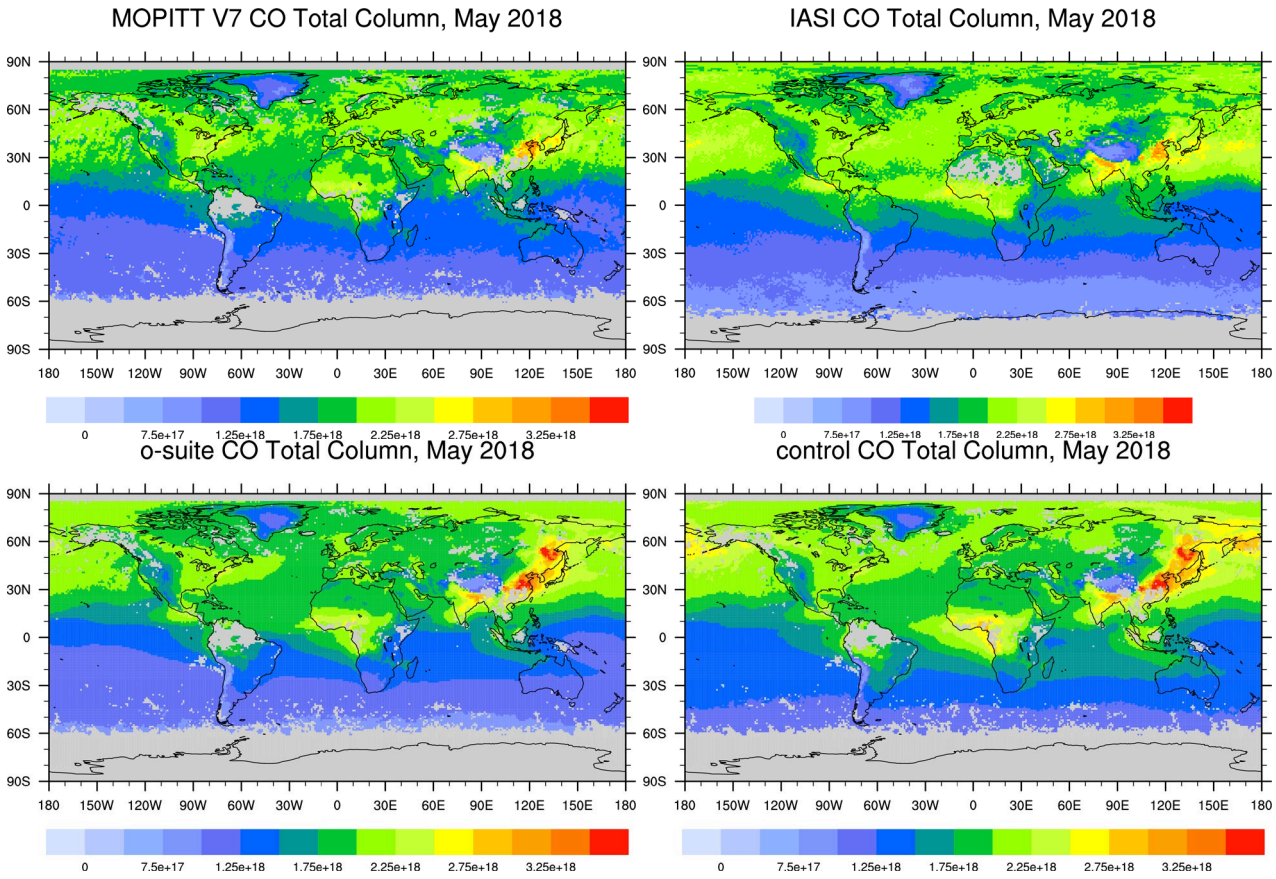

Fig. 10.3.1 CO total columns for MOPITT v7 (left), o-suite (middle) and control (right) runs for May 2018.

10.2 Fire events in Indochina in April 2018

Large number of fire events were detected during April in the area of Indochina. Fig. 10.2.1 represents some cases in mid- April. IASI shows an increase of CO emissions over East Asia on 11.04 with following outspread and transport of the high concentration plume to the east on 14 and 15.04. Both runs capture locations of the emission plumes and transportation pathway. Both runs overestimate emissions over some source regions, e.g. over India and underestimate CO values over the Pacific Ocean along the transportation pathway.

10.3 Rapid increase of modelled CO columns in May 2018 in Alaskan and Siberian fire regions

In May 2018, both, MOPITT and IASI instruments show high CO values over East China and Northern India (more pronounced in IASI), Fig. 10.3.1. Additionally to these plumes the modelled data from the both runs indicate a high CO spot over the Siberian fire region which is not represented in the satellite data. The control run has also high CO values over Alaskan fire region and along the transportation pathway towards North America.

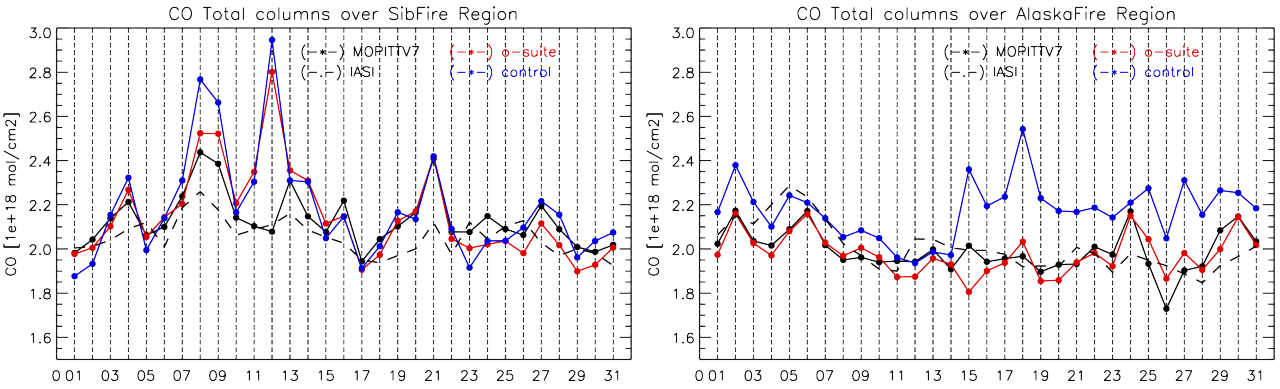

Fig. 10.3.2. Time series of CO total columns during May 2018 over Siberian (left) and Alaskan (right) regions from: MOPITT v7 and IASI (black), o-suite (red) and control (blue) runs.

Time series of CO total columns during May (Fig. 10.3.2) show that both model runs have a rapid increase in 8-9, 12 and 21 May over the Siberian fire region, which is inconsistent with the satellite observations. Over the Alaskan fire region, the o-suite is in good agreement with the satellite data, while the control run shows a rapid increase of CO starting from 15 May with continuously high values till the end of May.

11. References

Agusti-Panareda, A., Monitoring upgrades of analysis/forecast system, MACC-III Deliverable D44.04, June 2015.

Bergamaschi, P., Frankenberg, C., Meirink, J. F., Krol, M., Villani, M. G., Houweling, S., Dentener, F., Dlugokencky, E. J., Miller, J. B., Gatti, L. V., Engel, A., and Levin, I.: Inverse modeling of global and regional CH4 emissions using SCIAMACHY satellite retrievals, J. Geophys. Res., 114, D22301, doi:10.1029/2009JD012287, 2009.

Benedetti, A., J.-J. Morcrette, O. Boucher, A. Dethof, R. J. Engelen, M. Fisher, H. Flentjes, N. Huneeus, L. Jones, J. W. Kaiser, S. Kinne, A. Mangold, M. Razinger, A. J. Simmons, M. Suttie, and the GEMS-AER team: Aerosol analysis and forecast in the ECMWF Integrated Forecast System. Part II : Data assimilation, J. Geophys. Res., 114, D13205, doi:10.1029/2008JD011115, 2009.

Boussetta, S., Balsamo, G., Beljaars, A., Agusti-Panareda, A., Calvet, J.-C., Jacobs, C., van den Hurk, B., Viterbo, P., Lafont, S., Dutra, E., Jarlan, L., Balzarolo, M., Papale, D., and van der Werf, G.: Natural carbon dioxide exchanges in the ECMWF Integrated Forecasting System: implementation and offline validation, J. Geophys. Res.-Atmos., 118, 1–24, doi: 10.1002/jgrd.50488, 2013.

Braathen, WMO Arctic Ozone Bulletin No 1/2016, DOI:10.13140/RG.2.1.4929.6403, 2016.

Cammas, J.P., Brioude J., Chaboureau J.-P., Duron J., Mari C., Mascart P., Nédélec P., Smit H., Pätz H.-W., Volz-Thomas A., Stohl A., and Fromm M., Injection in the lower stratosphere of biomass fire emissions followed by long-range transport: a MOZAIC case study. Atmos. Chem. Phys., 9, 5829-5846, 2009

Cariolle, D. and Teyssèdre, H.: A revised linear ozone photochemistry parameterization for use in transport and general circulation models: multi-annual simulations, Atmos. Chem. Phys., 7, 2183-2196, doi:10.5194/acp-7-2183-2007, 2007.

Dee, D. P. and S. Uppala, Variational bias correction of satellite radiance data in the ERA-Interim reanalysis. Quart. J. Roy. Meteor. Soc.,135, 1830-1841, 2009.

Deeter, M. N., Emmons, L. K., Edwards, D. P., Gille, J. C., and Drummond, J. R.: Vertical resolution and information content of CO profiles retrieved by MOPITT, Geophys. Res. Lett., 31, L15112, doi:10.1029/2004GL020235, 2004.

Deeter, M. N., et al. (2010), The MOPITT version 4 CO product: Algorithm enhancements, validation, and long-term stability, J. Geophys. Res., 115, D07306, doi:10.1029/2009JD013005.

Dentener, F., et al., 2006: Emissions of primary aerosol and precursor gases in the years 2000 and 1750 prescribed data-sets for AeroCom, Atmos. Chem. Phys., 6, 4321 – 4344.

Deshler, T., J.L. Mercer, H.G.J. Smit, R. Stubi, G. Levrat, B.J. Johnson, S.J. Oltmans, R. Kivi, A.M. Thompson, J. Witte, J. Davies, F.J. Schmidlin, G. Brothers, T. Sasaki (2008) Atmospheric comparison of electrochemical cell ozonesondes from different maufacturers, and with different cathode solution strengths: The Balloon Experiment on Standards for Ozonsondes. J. Geophys. Res.113, D04307, doi:10.1029/2007JD008975

Douros, J., S. Basart, A. Benedictow, A.-M. Blechschmidt, S. Chabrillat, Y. Christophe, H. Clark, E. Cuevas, H.J. Eskes, H. Flentje, K. M. Hansen, J. Kapsomenakis, B. Langerock, K. Petersen, M. Ramonet, A. Richter, M. Schulz, A. Wagner, T. Warneke, C. Zerefos, Observations characterisation and validation methods document, Copernicus Atmosphere Monitoring Service (CAMS) report, CAMS84_2015SC2_D.84.8.1.1-2017_observations_v2.pdf, October 2017. Available from: http://atmosphere.copernicus.eu/user-support/validation/verification-global-services.

Dupuy, E., et al.: Validation of ozone measurements from the Atmospheric Chemistry Experiment (ACE), Atmos. Chem. Phys., 9, 287-343, doi:10.5194/acp-9-287-2009, 2009.

Elbern, H., Schwinger, J., Botchorishvili, R.: Chemical state estimation for the middle atmosphere by four-dimensional variational data assimilation: System configuration. Journal of Geophysical Research (Atmospheres) 115, 6302, 2010.

Emmons, L. K., D. P. Edwards, M. N. Deeter, J. C. Gille, T. Campos, P. Nédélec, P. Novelli, and G. Sachse, Measurements of Pollution In The Troposphere (MOPITT) validation through 2006 Atmos. Chem. Phys., 9, 1795-1803, 2009

Errera, Q., Daerden, F., Chabrillat, S., Lambert, J. C., Lahoz, W. A., Viscardy, S., Bonjean, S., and Fonteyn, D., 4D-Var Assimilation of MIPAS chemical observations: ozone and nitrogen dioxide analyses, Atmos. Chem. Phys., 8, 6169-6187, 2008.

Errera, Q. and Ménard, R.: Technical Note: Spectral representation of spatial correlations in variational assimilation with grid point models and application to the belgian assimilation system for chemical observations (BASCOE), Atmos. Chem. Phys. Discuss., 12, 16763-16809, doi:10.5194/acpd-12-16763-2012, 2012.

Eskes, H., Wagner, A., Schulz, M., Christophe, Y., Ramonet, M., Basart, S., Benedictow, A., Blechschmidt, A.-M., Chabrillat, S., Clark, H., Cuevas, E., Flentje, H., Hansen, K. M., Im, U., Kapsomenakis, J., Langerock, B., Petersen, K., Richter, A., Sudarchikova, N., Thouret, V., Warneke, T., and Zerefos, C.: Validation report of the CAMS near-real time global atmospheric composition service December 2016 - February 2017, CAMS84_2015SC2_D84.1.1.7_2017DJF_v1.1, June 2017. Available from: http://atmosphere.copernicus.eu/user-support/validation/verification-global-services

Eskes, H. J., T. Antonakaki, S. Basart, A. Benedictow, A.-M. Blechschmidt, S. Chabrillat, Y. Christophe, H. Clark, E. Cuevas, K. M. Hansen, U. Im, J. Kapsomenakis, B. Langerock, K. Petersen, A. Richter, M. Schulz, N. Sudarchikova, V. Thouret, A. Wagner, C. Zerefos, Upgrade verification note for the CAMS near-real time global atmospheric composition service, Copernicus Atmosphere Monitoring Service (CAMS) report, CAMS84_2015SC2_D84.3.1.3_201706_esuite_v1.pdf, July 2017.

Eskes, H. J., S. Basart, A. Benedictow, Y. Bennouna, A.-M. Blechschmidt, S. Chabrillat, Y. Christophe, H. Clark, E. Cuevas, K. M. Hansen, U. Im, J. Kapsomenakis, B. Langerock, K. Petersen, M. Schulz, A. Wagner, C. Zerefos, Upgrade verification note for the CAMS near-real time global atmospheric composition service, Copernicus Atmosphere Monitoring Service (CAMS) report, CAMS84_2015SC3_D84.3.1.5_201802_esuite_v1.pdf, February 2018; Eskes et al., Upgrade verification note for the CAMS near-real time global atmospheric composition service, Addendum July 2018, CAMS84_2015SC3_D84.3.1.5_201802_esuite_v1.pdf.

Flemming, J., Huijnen, V., Arteta, J., Bechtold, P., Beljaars, A., Blechschmidt, A.-M., Diamantakis, M., Engelen, R. J., Gaudel, A., Inness, A., Jones, L., Josse, B., Katragkou, E., Marecal, V., Peuch, V.-H., Richter, A., Schultz, M. G., Stein, O., and Tsikerdekis, A.: Tropospheric chemistry in the Integrated Forecasting System of ECMWF, Geosci. Model Dev., 8, 975-1003, doi:10.5194/gmd-8-975-2015, 2015.

Flemming, J., Benedetti, A., Inness, A., Engelen, R. J., Jones, L., Huijnen, V., Remy, S., Parrington, M., Suttie, M., Bozzo, A., Peuch, V.-H., Akritidis, D., and Katragkou, E.: The CAMS interim Reanalysis of Carbon Monoxide, Ozone and Aerosol for 2003–2015, Atmos. Chem. Phys., 17, 1945-1983, doi:10.5194/acp-17-1945-2017, 2017.

Franco, B., et al., Retrievals of formaldehyde from ground-based FTIR and MAX-DOAS observations at the Jungfraujoch station and comparisons with GEOS-Chem and IMAGES model simulations, Atmos. Meas. Tech., 8, 1733-1756, 2015

Gielen, C., Van Roozendael, M., Hendrick, F., Pinardi, G., Vlemmix, T., De Bock, V., De Backer, H., Fayt, C., Hermans, C., Gillotay, D., and Wang, P.: A simple and versatile cloud-screening method for MAX-DOAS retrievals, Atmos. Meas. Tech., 7, 3509-3527, doi:10.5194/amt-7-3509-2014, 2014.

Granier, C. et al.: Evolution of anthropogenic and biomass burning emissions of air pollutants at global and regional scales during the 1980–2010 period. Climatic Change (109), 2011

Holben, B. N., Eck, T. F., Slutsker, I., Tanré, D., Buis, J. P., Setzer, A., Vermote, E., Reagan, J. A., Kaufman, Y. J., Nakajima, T., Lavenu, F., Jankowiak, I., and Smirnov A.: AERONET – a federated instrument network and data archive for aerosol characterization, Remote Sens. Environ., 66, 1–16, 5529, 5533, 5537, 5544, 1998.

Hommel, R., Eichmann, K.-U., Aschmann, J., Bramstedt, K., Weber, M., von Savigny, C., Richter, A., Rozanov, A., Wittrock, F., Khosrawi, F., Bauer, R., and Burrows, J. P.: Chemical ozone loss and ozone mini-hole event during the Arctic winter 2010/2011 as observed by SCIAMACHY and GOME-2, Atmos. Chem. Phys., 14, 3247-3276, doi:10.5194/acp-14-3247-2014, 2014.

Huijnen, V., et al.: The global chemistry transport model TM5: description and evaluation of the tropospheric chemistry version 3.0, Geosci. Model Dev., 3, 445-473, doi:10.5194/gmd-3-445-2010, 2010.

Inness, A., Blechschmidt, A.-M., Bouarar, I., Chabrillat, S., Crepulja, M., Engelen, R. J., Eskes, H., Flemming, J., Gaudel, A., Hendrick, F., Huijnen, V., Jones, L., Kapsomenakis, J., Katragkou, E., Keppens, A., Langerock, B., de Mazière, M., Melas, D., Parrington, M., Peuch, V. H., Razinger, M., Richter, A., Schultz, M. G., Suttie, M., Thouret, V., Vrekoussis, M., Wagner, A., and Zerefos, C.: Data assimilation of satellite-retrieved ozone, carbon monoxide and nitrogen dioxide with ECMWF's Composition-IFS, Atmos. Chem. Phys., 15, 5275-5303, doi:10.5194/acp-15-5275-2015, 2015.

Janssens-Maenhout, G., Dentener, F., Aardenne, J. V., Monni, S., Pagliari, V., Orlandini, L., Klimont, Z., Kurokawa, J., Akimoto, H., Ohara, T., Wankmueller, R., Battye, B., Grano, D., Zuber, A., and Keating, T.: EDGAR-HTAP: a Harmonized Gridded Air Pollution Emission Dataset Based on National Inventories, JRC68434, EUR report No EUR 25 299–2012, ISBN 978-92-79- 23122-0, ISSN 1831-9424, European Commission Publications Office, Ispra (Italy), 2012.

Jaross, G., Bhartia, P.K., Chen, G., Kowitt, M., Haken, M., Chen, Z., Xu, Ph., Warner, J., Kelly, T. : OMPS Limb Profiler instrument performance assessment, J. Geophys. Res. Atmos 119, 2169-8996, 2014.

Kaiser, J. W., Heil, A., Andreae, M. O., Benedetti, A., Chubarova, N., Jones, L., Morcrette, J.-J., Razinger, M., Schultz, M. G., Suttie, M., and van der Werf, G. R.: Biomass burning emissions estimated with a global fire assimilation system based on observed fire radiative power, Biogeosciences, 9, 527-554, doi:10.5194/bg-9-527-2012, 2012.

Kramarova, N. A., Nash, E. R., Newman, P. A., Bhartia, P. K., McPeters, R. D., Rault, D. F., Seftor, C. J., Xu, P. Q., and Labow, G. J.: Measuring the Antarctic ozone hole with the new Ozone Mapping and Profiler Suite (OMPS), Atmos. Chem. Phys., 14, 2353-2361, doi:10.5194/acp-14-2353-2014, 2014.

Lahoz, W. A., Errera, Q., Viscardy, S., and Manney G. L., The 2009 stratospheric major warming described from synergistic use of BASCOE water vapour analyses and MLS observations, Atmos. Chem. Phys. 11, 4689-4703, 2011

Lambert, A, et al., Aura Microwave Limb Sounder Version 3.4 Level-2 near real-time data user guide, http://disc.sci.gsfc.nasa.gov/Aura/data-holdings/MLS/documents/NRT-user-guide-v34.pdf

Langerock, B., De Mazière, M., Hendrick, F., Vigouroux, C., Desmet, F., Dils, B., and Niemeijer, S.: Description of algorithms for co-locating and comparing gridded model data with remote-sensing observations, Geosci. Model Dev., 8, 911-921, doi:10.5194/gmd-8-911-2015, 2015.

Lefever, K., van der A, R., Baier, F., Christophe, Y., Errera, Q., Eskes, H., Flemming, J., Inness, A., Jones, L., Lambert, J.-C., Langerock, B., Schultz, M. G., Stein, O., Wagner, A., and Chabrillat, S.: Copernicus stratospheric ozone service, 2009–2012: validation, system intercomparison and roles of input data sets, Atmos. Chem. Phys., 15, 2269-2293, doi:10.5194/acp-15-2269-2015, 2015.

Liu, Z., et al., Exploring the missing source of glyoxal (CHOCHO) over China, Geophys. Res. Lett., 39, L10812, doi: 10.1029/2012GL051645, 2012

Massart, S., Flemming, J., Cariolle, D., Jones, L., High resolution CO tracer forecasts, MACC-III Deliverable D22.04, May 2015, available from http://www.gmes-atmosphere.eu/documents/macciii/deliverables/grg

Morcrette, J.-J., O. Boucher, L. Jones, D. Salmond, P. Bechtold, A. Beljaars, A. Benedetti, A. Bonet, J. W. Kaiser, M. Razinger, M. Schulz, S. Serrar, A. J. Simmons, M. Sofiev, M. Suttie, A. M. Tompkins, and A. Untch: Aerosol analysis and forecast in the ECMWF Integrated Forecast System. Part I: Forward modelling, J. Geophys. Res., 114, D06206, doi:10.1029/2008JD011235, 2009.

Richter, A., Burrows, J. P., Nüß, H., Granier, C, Niemeier, U.: Increase in tropospheric nitrogen dioxide over China observed from space, Nature, 437, 129-132, doi: 10.1038/nature04092, 2005

*Richter, A., Begoin, M., Hilboll, A., and Burrows, J. P.: An improved NO2 retrieval for the GOME-2 satellite instrument, Atmos. Meas. Tech. , **4**, 1147-1159, doi:10.5194/amt-4-1147-2011, 2011*

Sindelarova, K., Granier, C., Bouarar, I., Guenther, A., Tilmes, S., Stavrakou, T., Müller, J.-F., Kuhn, U., Stefani, P., and Knorr, W.: Global data set of biogenic VOC emissions calculated by the MEGAN model over the last 30 years, Atmos. Chem. Phys., 14, 9317-9341, doi:10.5194/acp-14-9317-2014, 2014.

Smit, H.G.J., W. Straeter, B.J. Johnson, S.J. Oltmans, J. Davies, D.W. Tarasick, B. Hoegger, R. Stubi, F.J. Schmidlin, T. Northam, A.M. Thompson, J.C. Witte, I. Boyd: Assessment of the performance of ECC-ozonesondes under quasi-flight conditions in the environmental simulation chamber: Insights from the Juelich Ozone Sonde Intercomparison Experiment (JOSIE), J. Geophys. Res. 112, D19306, doi:10.1029/2006JD007308, 2007.

Solomon, S., Haskins, J., Ivy, D. J. and Min, F.: Fundamental differences between Arctic and Antarctic ozone depletion, PNAS 2014 111 (17) 6220-6225, doi:10.1073/pnas.1319307111, 2014.

Stavrakou,T., First space-based derivation of the global atmospheric methanol fluxes, Atm. Chem. Phys., 11, 4873-4898, 2013.

Strahan, S.E., A.R. Douglass, and P.A. Newman, The contributions of chemistry and transport to low arctic ozone in March 2011 derived from Aura MLS observations, J. Geophys. Res. Atmos., 118, 1563–1576, doi:10.1002/jgrd.50181, 2013.

Taha, G.; Jaross, G. R.; Bhartia, P. K.: Validation of OMPS LP Ozone Profiles Version 2.0 with MLS, Ozone Sondes and Lidar Measurements, American Geophysical Union, Fall Meeting 2014, abstract #A33J-3322, 2014.

Taylor, K.E.: Summarizing multiple aspects of model performance in a single diagram. J.Geophys. Res., 106, 7183-7192, 2001.

van der A, R. J. , M. A. F. Allaart, and H. J. Eskes, Multi sensor reanalysis of total ozone, Atmos. Chem. Phys., 10, 11277–11294, doi:10.5194/acp-10-11277-2010, www.atmos- chem-phys.net/10/11277/2010/, 2010

van der A, R., M. Allaart, H. Eskes, K. Lefever, Validation report of the MACC 30-year multi-sensor reanalysis of ozone columns Period 1979-2008, MACC-II report, Jan 2013, MACCII_VAL_DEL_D_83.3_OzoneMSRv1_20130130.docx/pdf.

van der A, R. J., Allaart, M. A. F., and Eskes, H. J.: Extended and refined multi sensor reanalysis of total ozone for the period 1970–2012, Atmos. Meas. Tech., 8, 3021-3035, doi:10.5194/amt-8-3021-2015, 2015.

*Vrekoussis, M., Wittrock, F., Richter, A., and Burrows, J. P.: GOME-2 observations of oxygenated VOCs: what can we learn from the ratio glyoxal to formaldehyde on a global scale?, Atmos. Chem. Phys., **10**, 10145-10160, doi:10.5194/acp-10-10145-2010, 2010*

Wittrock, F., A. Richter, H. Oetjen, J. P. Burrows, M. Kanakidou, S. Myriokefalitakis, R. Volkamer, S. Beirle, U. Platt, and T. Wagner, Simultaneous global observations of glyoxal and formaldehyde from space, Geophys. Res. Lett., 33, L16804, doi:10.1029/2006GL026310, 2006

WMO (2010), Guidelines for the Measurement of Atmospheric Carbon Monoxide, GAW Report No. 192, World Meteorological Organization, Geneva, Switzerland, 2010.

WMO (2013), Guidelines for the Continuous Measurements of Ozone in the Troposphere, GAW Report No. 209, World Meteorological Organization, Geneva, Switzerland, 2013.

Annex 1: Acknowledgements

Listed below are the authors contributing to the sections in this report. The authors contributing to the model description are also provided, as well as acknowledgements to the validation datasets.

Tropospheric reactive gases reactive gases

Annette Wagner, MPG (editor, O3 sondes, GAW data)
Yasmine Bennouna, Valerie Thouret, CNRS-LA (IAGOS)
Harald Flentje, DWD (O3 sondes, GAW data)
Anne Blechschmidt and Andreas Richter, IUB Bremen (GOME-2 NO2, HCHO)
John Kapsomenakis, Christos Zerefos, AA (ESRL)
Natalia Sudarchikova, satellite IR observations (MPG)
Kaj Hansen, Ulas Im, AU (Arctic theme)
Bavo Langerock, BIRA (NDACC)

Tropospheric aerosol

Michael Schulz, MetNo (editor, Aerocom, Aeronet)
Anna Benedictow, Jan Griesfeller, MetNo (Aerocom, Aeronet)
Sara Basart, MTeresa Pay, Oriol Jorba, BSC-CNS (Aeronet, MODIS, AirBase, SDS-WAS NAMEE RC)
Emilio Cuevas, AEMET (Aeronet, MODIS, AirBase, SDS-WAS NAMEE RC)
Harald Flentje, DWD (Backscatter profiles)

Stratospheric reactive gases

Yves Christophe, BIRA (editor, model-satellite intercomparisons)
Simon Chabrillat, BIRA (model intercomparisons)
Annette Wagner, MPI-M (O_3 sondes)
Bavo Langerock, BIRA (NDACC FTIR, MWR, UVVIS DOAS, LIDAR)
Anne Blechschmidt and Andreas Richter, IUB-UB Bremen (SCIAMACHY/GOME-2 NO_2)

Greenhouse gases

Michel Ramonet, IPSL (ICOS)
Olivier Jossoud and Leonard Rivier, LSCE (ICOS)
Thorsten Warneke, UBC (TCCON)
Bavo Langerock, BIRA (TCCON)

Reactive gases and aerosol modeling

Johannes Flemming (ECMWF), Antje Inness (ECMWF), Angela Benedetti (ECMWF), Sebastien Massart (ECMWF), Anna Agusti-Panareda (ECMWF), Johannes Kaiser (KCL/MPIC/ECMWF), Samuel Remy (LMD), Olivier Boucher (LMD), Vincent Huijnen (KNMI), Richard Engelen (ECMWF)

Acknowledgements for the validation datasets used

We wish to acknowledge the provision of NRT GAW observational data by: Institute of Atmospheric Sciences and Climate (ISAC) of the Italian National Research Council (CNR), South African Weather Service, National Centre for Atmospheric Science (NCAS, Cape Verde), National Air Pollution Monitoring Network (NABEL) (Federal Office for the Environment FOEN and Swiss Federal Laboratories for Materials Testing and Research EMPA), Atmospheric Environment Division Global Environment and Marine Department Japan Meteorological Agency, Chinese Academy of Meteorological Sciences (CAMS), Alfred Wegener Institut, Umweltbundesamt (Austria), National Meteorological Service (Argentina), Umweltbundesamt (UBA, Germany)

We are grateful to the numerous operators of the Aeronet network and to the central data processing facility at NASA Goddard Space Flight Center for providing the NRT sun photometer data, especially Ilya Slutker and Brent Holben for sending the data.

The authors thank to all researchers, data providers and collaborators of the World Meteorological Organization's Sand and Dust Storm Warning Advisory and Assessment System (WMO SDS-WAS) for Northern Africa, Middle East and Europe (NAMEE) Regional Node. Also special thank to Canary Government as well as AERONET, MODIS, U.K. Met Office MSG, MSG Eumetsat and EOSDIS World Viewer principal investigators and scientists for establishing and maintaining data used in the activities of the WMO SDS-WAS NAMEE Regional Center (http://sds-was.aemet.es/).

We wish to acknowledge the provision of ozone sonde data by the World Ozone and Ultraviolet Radiation Data Centre established at EC in Toronto (http://woudc.org), by the Data Host Facility of the Network for the Detection of Atmospheric Composition Change established at NOAA (http://ndacc.org), by the Norwegian Institute for Air Research and by the National Aeronautics and Space Administration (NASA).

We wish to thank the NDACC investigators for the provision of observations at Ny Alesund, Bern, Jungfraujoch, Izaña, Xianghe, Harestua, Reunion Maido, Uccle, Hohenpeissen, Mauna Loa, Lauder and Haute Provence.

The authors acknowledge the NOAA Earth System Research Laboratory (ESRL) Global Monitoring Division (GMD) for the provision of ground based ozone concentrations.

The MOPITT CO data were obtained from the NASA Langley Research Center ASDC. We acknowledge the LATMOS IASI group for providing IASI CO data.

SCIAMACHY lv1 radiances were provided to IUP-UB by ESA through DLR/DFD.

GOME-2 lv1 radiances were provided to IUP-UB by EUMETSAT.

The authors acknowledge Environment and Climate Change Canada for the provision of Alert ozone data and Sara Crepinsek – NOAA for the provision of Tiksi ozone data. Surface ozone data from the Zeppelin Mountain, Svalbard are from www.luftkvalitet.info. Surface ozone data from the Villum Research Station, Station Nord (VRS) were financially supported by "The Danish Environmental Protection Agency" with means from the MIKA/DANCEA funds for Environmental Support to the Arctic Region. The Villum Foundation is acknowledged for the large grant making it possible to build VRS in North Greenland.

We acknowledge the National Aeronautics and Space Administration (NASA), USA for providing the OMPS limb sounder data (http://npp.gsfc.nasa.gov/omps.html) and the Aura-MLS offline data (http://mls.jpl.nasa.gov/index-eos-mls.php).

We thank the Canadian Space Agency and ACE science team for providing level 2 data retrieved from ACE-FTS on the Canadian satellite SCISAT-1.

The TCCON site at Orleans is operated by the University of Bremen and the RAMCES team at LSCE (Gif-sur-Yvette, France). The TCCON site at Bialystok is operated by the University of Bremen. Funding for the two sites was provided by the EU-project ICOS-INWIRE and the University of Bremen. The TCCON site at Réunion is operated by BIRA-IASB, in cooperation with UReunion and is funded by BELSPO in the framework of the Belgian ICOS program.

We acknowledge the provision of CO_2/CH_4 data from SNO-RAMCES/ICOS network coordinated by LSCE/OVSQ (CEA-CNRS-UVSQ, Université Paris-Saclay), as well as Laboratorio de Física de la Atmósfera (UMSA, Bolivia), Environmental Chemical Processes Laboratory (ECPL/UoC, Greece), Station Géophysique de LAMTO, Ivory Coast), C-CAPS/NUIG/EPA (Ireland), BIRA-IASB (Belgium) and the following research institutes in France: LaMP/OPGC, P2OA/LA/OMP, OPE/ANDRA, OHP/PYTHEAS, OPAR/LACY/OSUR, UMR EcoFoG, IPEV, IRD.

The European Environment Information and Observation Network (Eionet) Air Quality portal provides details relevant for the reporting of air quality information from EU Member States and other EEA member and co-operating countries. This information is submitted according to Directives 2004/107/EC and 2008/50/EC of the European Parliament and of the Council.

Copernicus Atmosphere Monitoring Service

ECMWF - Shinfield Park, Reading RG2 9AX, UK

Contact: info@copernicus-atmosphere.eu